UNIVERSITAT POLITÈCNICA DE CATALUNYA BARCELONATECH

Identifying and managing hotspots to extreme events: application to NW Mediterranean conditions

Marc Sanuy Vázquez

UNIVERSITAT POLITÈCNICA DE CATALUNYA BARCELONATECH

PhD program in Civil Engineering

Identifying and managing hotspots to extreme events

Application to NW Mediterranean conditions

Doctoral thesis by:

Marc Sanuy Vázquez

Thesis supervisor:

José A. Jiménez

Laboratori d'Enginyeria Marítima – Faculty of Civil Engineering

Barcelona, September 2019

Acknowledgements

Todo lo bueno se acaba..., o no. Esta tesis representa el final de una larga etapa de mi vida, que ha resultado ser sorprendentemente interesante y completa, con sus dificultades y recompensas. Por ello no es sorprendente que sea particularmente complejo agradecer a todas aquellas personas que de una manera u otra han formado parte de ella, contribuyendo de manera positiva, ya sea en lo científico como en lo personal.

Para empezar, a quin más debo agradecer es a mi profesor, supervisor y compañero de trabajo Jose A. Jiménez. Por un lado, él me ha propuesto iniciarme en el campo de la investigación, cuando *a priori* no entraba en mis planes trabajar en éste. Por otro, su supervisión durante todos estos años ha sido loable por lo exhaustiva e instructiva, de las que consiguen dar forma a tu modo de pensar y escribir, de las que realmente sirven para aprender. Gracias por el tiempo dedicado y por la seriedad de dicha dedicación Prof.

Junto con la supervisión de Jose, otro factor que me ha llevado a disfrutar de la tesis ha sido el poder viajar, y el haber estado involucrado en un proyecto europeo (RISC-KIT) des del primer momento. Por el trabajo compartido, por las experiencias vividas, por los intercambios de ideas, me siento muy agradecido con todo el equipo investigador del proyecto RISC-KIT, y afortunado de haber podido asistir a todas las reuniones en diferentes países europeos.

A raíz del trabajo en RISC-KIT surge una col·laboración y, sobretodo, gran amistad, con el Dr. Enrico Duo, a quien debo también mención especial en estos agradecimientos. Són ya numerosas las veces que él ha venido a Barcelona o que yo he ido a Ferrara, para trabajar juntos, al mismo tiempo que descubrimos uno el entorno del otro, lengua, costumbres, hobbies…, y todas y cada una de ellas han sido un auténtico placer. Por su culpa he aprendido italiano y he descubierto mi pasión por el mundo del Agility Dog. Por mi culpa él se ha comprado una moto… Y entre medias tenemos alguna que otra publicación juntos, y alguna más que esperamos ir haciendo en el futuro.

No puedo dejarme de agradecer al Prof. Paolo Ciavola su hospitalidad cada vez que he visitado la Universidad de Ferrara, ni a mis amigos Mirko, Nico, Chiara y Marci (hasta Gogo) que me han abierto sus puertas y me han hecho sentir como en casa. Grazie a tutti, siete fantastici.

Otra colaboración facilitada por el proyecto RISC-KIT me llevó 3 meses a Saint Petersburg, Florida, donde tuve la oportunidad de trabajar en el USGS con el Dr. Nathaniel Plant. Nunca antes había absorbido tanto en 3 meses, tanto en lo personal como en lo profesional. Agradezco especialmente la hopitalidad de Nathaniel y su fantástica familia, a Anne de Beer por compartir conmigo coffee breaks y almuerzos cuando nadie más salía de sus cubículos (será la sangre europea) y al resto de colegas del USGS con los que finalmente (aunque costó) empezamos a compartir experiencias juntos.

Pero no todo es trabajo, y todo lo anterior se sustenta gracias también a la parte personal. Es ahí donde indudablemente debo especial gratitud a mi compañera de vida, Vero, que me ha acompañado desde

bastante antes de empezar la tesis hasta su finalización, pasando por todas las fases, e incluso acompañándome en mis estancias en EEUU e Italia. Ella me da equilibrio cuando mi cabeza se va por donde no debe, y me entiende como ninguna otra persona. Vero, pasar esta etapa a tu lado ha sido extremadamente fácil, y eso dice mucho teniendo en cuenta todo lo que hemos vivido estos años.

Finalmente llega el turno a mi familia y a los amigos de toda la vida (la otra familia), ese "background" que está ahí siempre y sin el cuál todo se vería muy diferente. A mis padres Silvia y Xavi, porqué se lo han currado toda la vida y porque gracias a ellos, yo soy yo (para lo bueno y para lo malo), y a mi hermano Pol por enseñarme que bajo el mismo techo uno puede llegar a ser muy diferente. A los "Disléxicos" por incontables cervezas de viernes noche (que ahora hecho de menos), y al resto de personas que han estado cerca recientemente como si lo hubieran estado siempre.

Por último, y no menos importante, a mi pequeña border collie Brisca, que es capaz de convertir un dia horrible en uno normal solo con saludarme al entrar en casa.

Funding and data

The thesis period was directly financed for four years by a predoctoral fellowship FPU14/05021 from the Spanish Ministry of Education, Culture and Sport (MECD). Additionally, the PhD candidate has been supported with two travel and accomodation grants for international internships: EEST17/00560 also from MECD (3-month internship in Florida) and the KA103 Erasmus+ EU program 2017/2018 (2-month internship in Italy).

This thesis was conducted in the framework of the following projects: the RISC-KIT (FP7, Grant No 603458) international project, funded by the EU; and the PairisClima (CGL2014-55387-R) and the M-CostAdapt (CTM2017-83655-C2-1-R) national projects, funded the Spanish Ministry of Economy and Competitiveness (MINECO/AEI/FEDER).

The PhD candidate expresses his gratitude to Generalitat de Catalunya, Puertos del Estado and IH-Cantabria for supplying wave and water level data, to the Spanish Ministry for Ecological Transition and Ministry of of Agriculture, Fish, Food and Environment for the bathymetric data, and to the Institut Cartogràfic i Geològic de Catalunya by for the LIDAR data used in this thesis.

Once again, the author aknowledges the USGS institution (and specially Nathaniel Plant) and the University of Ferrara (and specially Paolo Ciavola) for welcoming the PhD candidate during the corresponding international internships.

Contents

SUMMARY

The impact of coastal storms is one of the costliest forms of natural disaster, as it affects a particularly valuable fringe both from the socioeconomic and ecologic perspectives. In addition, storm-induced erosion and inundation risks are expected to rise in the near future due to changing conditions related to climate change combined with current trends on urbanization and population growths and beach losses associated with long-term erosion. The assessment of the hazard component is complex, due to the multidimensionality of the processes involved, the inherent uncertainties of the analysis and the multiple scales in which the hazard characterization must be performed. In this context, there is a need for providing risk assessment methodologies allowing coastal managers integrated decision making based on the analysis of present and future conditions

The present PhD thesis focuses on the development of such methodologies, both at regional scale with the purpose of hotspot identification and at local scale with the aim of providing detailed hazard or risk assessments. The work starts with the study of two main sources of uncertainty involved in hazard assessment: the assignment of probabilities of occurrence to given hazard magnitudes and the definition of the shape of the storm to assess induced hazards. Applying lessons learned from these uncertainty studies, different hazard and risk assessment approaches are proposed based on the use of Bayesian Networks (BNs). They have been selected due to their efficiency in combining multiple variables and characterizing their dependency relations to predict system behaviour while explicitly including uncertainties.

Obtained results highlight the importance of characterizing the hazard probabilities focusing the statistical assessment at coastal response (the so called response approach), especially if detailed hazard estimation (e.g. inundation maps) are to be produced. The use of the alternative approach (event approach, assigning probabilities to event characteristics to later estimate hazards from that event) produces only similar results when assessing simple variables such as run-up or total water levels at the coast, and only in locations with high correlations between involved storm variables. Results also indicate that detailed hazard estimation, as pursued with process-based modelling, may be affected by significant errors when using synthetic triangular events, i.e. design storms with assumed triangular evolution over their duration. These errors are observed to be significant for a wide range of tested conditions, involving different morphologies (dissipative to intermediate-reflective), wave climates (NW Mediterranean and N Adriatic) and storm energy contents.

The proposed methodology at regional scale (~100 km) consists of simple hazard and exposure indicators calculated at ~1 km coastal sectors and has been successfully applied for hotstpot detection at the Maresme coast. The Tordera Delta is identified as a significant hotspot to both erosion and inundation risks. This framework has been improved with the use of BNs to account for intra-sector morphological variability and model uncertainties. Results from the BN regional assessment highlight the importance of a fully stochastic hazard characterization with the inclusion of model errors to avoid

under-predictions. This BN approach also allowed a detailed assessment of the conditional dependencies between hazards and both storm and morphological characteristics giving deeper insight on system response and useful information for the development of coastal adaptation plans.

The proposed methodology at the hotspot local scale (~1-10 km) consists of different BN set-ups following the Source-Pathway-Receptor-Consequences model and trained with large datasets of simulated hazards. They are applied to the Tordera Delta to analyse risk reduction measures and to stochastically obtain the risk profile under present and future scenarios. Hazard simulations are performed though detailed process-based modelling. A XBeach set-up is specifically developed for conditions at the Tordera Delta and validated with an historical extreme event (the Sant Esteve 2008 storm) obtaining a BSS of 0.68 for the morphological response at the subaerial beach. Local scale results show a high sensitivity of the Tordera Delta to incoming wave direction, with associated changes on induced hazards comparable to those of worst-case SLR scenarios (e.g. RCP 8.5, 2100). When assessing the efficiency of risk reduction measures, it is obtained that increasing beach height through an artificial dune is the most efficient action against inundation while managed receptors retreat is the only efficient option against erosion, as beach nourishment is very ephimeral even under mild storm conditions due to background erosion. The method also permits to define probabilistic setbacks for different hazards and risk levels, and characterizes hazardous storm characteristics under different scenarios.

Finally, the BN approach is tested as storm-induced retreat predictive model based on simple storm parameters. Once fed with a large number of storm simulations, results show a great potential to perform as surrogate of simple parametric models at complex study sites where their applicability is limited, e.g. curvilinear coasts with high alongshore morphological variability and beach-structure interactions.

Overall, the use of BNs to characterize hazards and risks associated to coastal storms at different scales has been proved robust, as it can include many natural variabilities and problem uncertainties by efficiently assimilating large datasets. It is a flexible and communication-friendly approach that can be adapted to other specific problems related to coastal evolution, or other natural hazards. The method can be potentially imporved with larger datasets and/or used in combination with other machine learning techniques.

RESUMEN

El impacto de temporales en la costa es uno de los fenómenos naturales más costosos, dado que afecta a un litoral de gran valor tanto des del punto de vista socioeconómico como ecológico. Además, se espera un aumento de los riesgos de erosión e inundación durante los episodios de tormenta, debido a las condiciones climáticas cambiantes, así como a las tendencias actuales de urbanización, aumento de población en las costas y a la pérdida progresiva de playas asociada a la erosión a largo plazo. La multi-dimensionalidad de los procesos involucrados, las incertidumbres inherentes en los análisis y las múltiples escalas para abordar el problema hacen que la erosión e inundación costera sean complejas de evaluar. Por ello, se requieren metodologías de evaluación de riesgo que permitan una gestión integrada basada en el análisis de condiciones presentes y futuras.

Esta Tesis Doctoral se centra en el desarrollo de dichas metodologías, tanto a escala regional, con el objetivo de identificar "hotspots" (zonas sensibles), como a escala local con el propósito de proporcionar evaluaciones detalladas de riesgo o amenaza. El trabajo empieza por el estudio de dos de las principales fuentes de incertidumbre en el análisis de amenazas: la asignación de probabilidades a las magnitudes de erosión e inundación y la adopción de formas de tormenta sintéticas para la estimación de las mismas. De los resultados de dichos estudios se desprenden las metodologías propuestas, que se basan en el uso de Redes Bayesianas (RBs). Éstas se han seleccionado por su eficiencia para predecir el comportamiento de sistemas, combinando múltiples variables y evaluando sus inter-dependencias, permitiendo al mismo tiempo la inclusión de incertidumbres de forma explícita.

Los resultados obtenidos destacan la importancia de basar el análisis estadístico en la respuesta costera a la hora de de asignar probabilidades a las amenazas (el llamado método de la respuesta), en especial si se requiere la obtención de resultados detallados como mapas de inundación. El uso del método alternativo (el método del evento, que asigna probabilidades a características de tormenta para luego estimar su impacto) lleva a resultados parecidos solo cuando se analizan variables simples como el remonte o el nivel total de mar en la costa, y únicamente en lugares con una alta correlación entre las variables de tormenta implicadas. Los resultados también indican que la adopción de tormentas sintéticas triangulares, i.e., tormentas diseñadas con forma triangular a lo largo de su duración, puede llevar a errores significativos si se pretende una estimación detallada de la respuesta costera frente a las tormentas, como por ejemplo la que se busca con el uso de modelos numéricos basados en la física de los procesos. Dichos errores se han observado para un amplio rango de condiciones analizadas, incluyendo diferentes morfologías (disipativas y reflejantes), climas de oleaje (Noroeste Mediterráneo o Adriático Norte) y energía de las tormentas.

La metodología propuesta a escala regional (~100 km) consiste en el uso de indicadores simples de amenaza y de exposición, calculados para sectores de ~1 km. Se ha aplicado con éxito en la costa del Maresme, donde el delta de la Tordera ha sido identificado como principal hotspot para el riesgo tanto de erosión como de inundación. La metodología ha sido posteriormente mejorada con el uso de las RBs,

permitiendo tener en cuenta tanto la variabilidad morfológica intra-sector como la incertidumbre asociada a los modelos usados. Los resultados obtenidos con la RB regional destacan la importancia de caracterizar estocásticamente las amenazas junto con la consideración de los errores de los modelos para evitar sub-predicciones. La RB también ha permitido la caracterización de las correlaciones entre magnitudes de amenaza y características de tormenta o de morfología, dando mayor información sobre la respuesta del sistema, de gran utilidad para el desarrollo de planes de adaptación costera.

La metodología propuesta a escala local (~1-10 km) consiste en diferentes esquemas de RB siguiendo el modelo "Source-Pathway-Receptor-Consequences" y usando largas series de datos simulados de erosión e inundación. Las RBs se han aplicado al delta de la Tordera para analizar la eficiencia de algunas medidas de protección frente al impacto de tormentas, así como para caracterizar estocásticamente el perfil de riesgo en condiciones actuales y futuras. La estimación de amenazas se ha realizado usando un modelo numérico basado en la física de los procesos, el XBeach. Éste se ha configurado y ajustado para el delta de la Tordera, y se ha validado con datos de un evento extremo (tormenta de Sant Esteve 2008) para el que se obtiene un BSS de 0.68 para la respuesta morfológica de la parte emergida de la playa. Los resultados a escala local muestran una alta sensibilidad del delta a la dirección del oleaje incidente, con cambios en la estima de amenazas de magnitud similar al esperado para escenarios pesimistas de subida del nivel del mar (e.g. RPC 8.5, 2100). En cuento a las medidas de protección, la construcción de una duna artificial para incrementar la cota de la playa ha resultado la medida más eficiente contra la inundación, mientras que el retranqueo de receptores resulta ser la única medida efectiva contra la erosión. Esto es debido a que las alimentaciones de playa resultan ser muy efímeras, incluso bajo tormentas suaves. La metodología permite la definición de retranqueos de forma probabilista para diferentes amenazas y niveles de riesgo, así como la caracterización de condiciones de tormenta relacionas con diferentes niveles de riesgo y bajo diferentes escenarios.

Finalmente, la RB se ha probado como modelo para la predicción del de retroceso de playa frente a temporales, basado en parámetros de tormenta simples. Una vez alimentada con un gran conjunto de datos simulados, los resultados de la RB muestran un gran potencial de la misma para actuar como sustituta de modelos paramétricos en casos de estudio complejos donde éstos tienen una aplicabilidad limitada, como en el caso de costas muy curvilíneas con gran variabilidad morfológica, y con presencia de estructuras que generan procesos locales.

En su conjunto, el uso de RBs para la caracterización de riesgos y amenazas asociados al impacto de temporales usa grandes conjuntos de datos para incluir múltiples variabilidades e incertidumbres, dotando al análisis de gran robustez. Es un método flexible, aplicable a otros problemas científicos ya sean costeros o relacionados con otros fenómenos naturales, y que facilita la comunicación de resultados. La metodología puede ser potencialmente mejorada con el uso de mejores conjuntos de datos y/o usada en combinación con otras técnicas del campo del machine learning.

RESUM

L'impacte de temporals a la costa és un dels fenòmens naturals més costosos, atès que afecta un litoral de gran valor tant des del punt de vista socioeconòmic com ecològic. A més, s'espera un augment dels riscos d'erosió i inundació durant els episodis de tempesta, a causa de les condicions climàtiques canviants, així com de les tendències actuals d'urbanització, augment de població a les costes i de la pèrdua progressiva de platges associada a la erosió a llarg termini. La multi-dimensionalitat dels processos involucrats, les incerteses inherents en les anàlisis i les múltiples escales per abordar el problema fan que l'erosió i inundació costanera siguin complexes d'avaluar. Per això, es requereixen metodologies d'avaluació del risc que permetin una gestió integrada basada en l'anàlisi de condicions presents i futures.

Aquesta tesi doctoral es centra en el desenvolupament d'aquestes metodologies, tant a escala regional, amb l'objectiu d'identificar "hotspots" (zones sensibles), com a escala local, amb el propòsit de proporcionar avaluacions detallades de risc o amenaça. El treball comença per l'estudi de dues de les principals fonts d'incertesa en l'anàlisi d'amenaces: l'assignació de probabilitats a les magnituds d'erosió i inundació, i l'adopció de formes de tempesta sintètiques per a l'estimació de les mateixes. Dels resultats d'aquests estudis es desprenen les metodologies proposades, que es basen en l'ús de Xarxes Bayesianes (XBs). Aquestes s'han seleccionat per la seva eficiència a l'hora de predir el comportament de sistemes, combinant múltiples variables, evaluant-ne les inter-dependències, i permetent al mateix temps la inclusió d'incerteses de manera explícita.

Els resultats obtinguts destaquen la importància de basar l'anàlisi estadística en la resposta costanera a l'hora de d'assignar probabilitats a les amenaces (l'anomenat mètode de la resposta), especialment si es requereix l'obtenció de resultats detallats com ara mapes d'inundació. L'ús del mètode alternatiu (el "mètode de l'esdeveniment", que assigna probabilitats a característiques de tempesta per després estimar el seu impacte) porta a resultats semblants només quan s'analitzen variables simples com el run-up o el nivell total de mar a la costa, i únicament en localitzacions amb una alta correlació entre les variables de tempesta implicades. Els resultats també indiquen que l'adopció de tempestes sintètiques triangulars, i.e., tempestes dissenyades amb forma triangular al llarg de la seva durada, pot portar a errors significatius si es pretén una estimació detallada de la resposta costanera causada per tempestes, com ara la que es busca amb l'ús de models numèrics basats en la física dels processos. Aquests errors s'han observat per a un ampli rang de condicions analitzades, incloent diferents morfologies (dissipatives i reflectants), climes d'onatge (Nord-oest Mediterrani o Adriàtic Nord) i energia de les tempestes.

La metodologia proposada a escala regional (~100 km) consisteix en l'ús d'indicadors simples d'amenaça i d'exposició, calculats per sectors de ~1 km. S'ha aplicat amb èxit a la costa del Maresme, on el delta de la Tordera ha estat identificat com a principal hotspot pels riscos tant d'erosió com d'inundació. La metodologia ha estat posteriorment millorada amb l'ús de les XBs, permetent tenir en compte tant la variabilitat morfològica intra-sector com la incertesa associada als models usats. Els resultats obtinguts

amb la XB regional destaquen la importància de caracteritzar estocàsticament les amenaces juntament amb la consideració dels errors dels models per evitar sub-prediccions. La XB també ha permès la caracterització de les correlacions entre magnituds d'amenaça i característiques de tempesta o de morfologia, donant major informació sobre la resposta del sistema, de gran utilitat pel desenvolupament de plans d'adaptació costanera.

La metodologia proposada a escala local (~1-10 km) consisteix en diferents esquemes de XB seguint el model "Source-Pathway-Receptor-Consequences" i usant llargues sèries de dades simulades d'erosió i inundació. Les XBs s'han aplicat al delta de la Tordera per analitzar l'eficiència d'algunes mesures de protecció enfront de l'impacte de tempestes, així com per caracteritzar estocàsticament el perfil de risc en condicions actuals i futures. L'estimació d'amenaces s'ha realitzat utilitzant un model numèric basat en la física dels processos, el XBeach. Aquest s'ha configurat i ajustat pel delta de la Tordera, i s'ha validat amb dades d'un esdeveniment extrem (tempesta de Sant Esteve 2008) per al qual s'obté un BSS de 0.68 per a la resposta morfològica de la part subaèria de la platja . Els resultats a escala local mostren una alta sensibilitat del delta a la direcció de l'onatge incident, amb variacions en les amenaces estimades de magnitud similar a l'esperat per a escenaris pessimistes de pujada del nivell del mar (e.g. RPC 8.5, 2100). Respecte a les mesures de protecció, la construcció d'una duna artificial per incrementar la cota de la platja ha resultat la mesura més eficient contra la inundació, mentre que la reculada de receptors resulta ser l'única mesura efectiva contra l'erosió. Això és degut al fet que les alimentacions de platja resulten ser molt efímeres, fins i tot sota tempestes suaus. La metodologia permet la definició de reculades de forma probabilista per a diferents amenaces i nivells de risc, així com la caracterització de condicions de tempesta relaciones amb risc salt i sota diferents escenaris.

Finalment, la XB s'ha provat com a model per a la predicció del retrocés de platja davant de temporals, basat en paràmetres de tempesta simples. Un cop alimentada amb un gran conjunt de dades simulades, els resultats de la XB mostren un gran potencial de la mateixa per actuar com a substituta de models paramètrics en casos d'estudi complexos on aquests tenen una aplicabilitat limitada, com en el cas de costes molt curvilínies amb gran variabilitat morfològica, i amb presència d'estructures que generen processos locals.

En el seu conjunt, l'ús de XBs per a la caracterització de riscos i amenaces associats a l'impacte de temporals fa servir grans conjunts de dades per incloure múltiples variabilitats i incerteses, dotant a l'anàlisi de gran robustesa. És un mètode flexible, aplicable a altres problemes científics ja siguin costaners o relacionats amb altres fenòmens naturals, i que facilita la comunicació de resultats. La metodologia pot ser potencialment millorada amb l'ús de millors conjunts de dades i/o usat en combinació amb altres tècniques del camp del machine learning.

CHAPTER 1.

INTRODUCTION

1.1. Background and research interest

Assessing the impact of coastal storms has become a global need motivated by the concentration of population, infrastructures and assets in coastal areas and the escalation of damages during the last decades (IPCC 2012, 2013; Kron, 2013). This is also applicable for the Spanish coast, where a similar increasing trend has been identified (e.g., Reyes et al. 1999: Rodriguez-Ramirez et al. 2003; Jiménez et al. 2012; Marcos et al. 2012, Toimil et al., 2017).

An example of the importance of this situation can be given by just considering the impact (and their consequenes) of recent extreme events such as Hurricane Katrina in Louisiana in 2005 (Beven II et al., 2008), Xynthia storm in France in 2010 (Bertin et al., 2012; Kolen et al., 2013), Hurricane Sandy in New York in 2012 (Kunz et al., 2013; Van Verseveld et al., 2015), and the Southern North Sea storm in 2013 (Spencer et al., 2015).

The impact of these extreme coastal storms one of the costliest natural disasters (Kron, 2013; Bertin et al., 2014). In heavily urbanized coastal areas, such as the Mediterranean (in general) and the Catalan coast (in particular), where properties, infrastructures and businesses are located close to the shoreline, these events usually result in the damage or destruction of exposed assets (Jiménez et al. 2012). These effects are the integrated consequences of two main storm-induced coastal hazards: inundation and erosion. Moreover, the projections of rising sea levels (IPCC 2012; 2013; 2014; Church et al., 2013; Vousdoukas et al., 2016), the existence of background erosion in many of our coasts (e.g. Luijendijk et al. 2018; Jiménez and Vlademoro, 2019) and other climate change related variations, such as increases in the magnitude and/or frequency of storms (Lionello et al. 2008; Conte and Lionello, 2013; IPCC, 2014) or changes in the directionality of incoming waves (Cases-Prat and Sierra, 2013), may significantly increase the magnitude (and consequences) of these hazards and, consequently, they also need to be considered in robust hazard assessments.

As a consequence, coastal managers must properly deal with coastal risks when designing coastal management plans. A practical example of this need is the programme developed and implemented by the Spanish Ministry for Ecological Transition (MITECO, former Ministry of Environment) to cope with storm-induced damages along the Spanish coasts. This programme is specifically launched the years with a high storm activity to fund restoration works along the coast, and it has to be implemented 4 times the last 5 years with an average budget of about 32 M€ (see e.g. López-Doriga et al. 2019).

As a matter of fact, several initiatives such as the protocol of Integrated Coastal Zone Management (ICZM, UNEP/MAP/PAP, 2008) for the Mediterranean include a specific chapter on natural hazards, and advises signed parties to implement vulnerability and risk assessments. The EU Floods directive (EC, 2007) is another example dealing specifically with floods, and instructs management groups to prepare flood hazard maps for events of given probabilities of occurrence. These risk assessments should also include the analysis under future projections. At the Catalan coast (NW Mediterranean), in particular, coastal risks are included as a specific chapter of the RISKCAT report (Guillen et al., 2008).

Therefore, the scientific community provides integrated and interdisciplinary approaches (e.g. Ciavola et al., 2011a; Ciavola et al., 2011b; Penning-Rowsell et al., 2014; Vojinovic et al., 2014; Oumeraci et al., 2015; Van Dongeren et al., 2018) that can be used in coastal risk assessments at different scales ranging from regional (up to hundreds of km) to local (up to 10 km). Regional methodologies aim to locate coastal sectors more sensitive to impacts, the so-called hotspots (see e.g., Stockdon et al., 2007; Zanuttigh et al. 2014; López-Royo et al., 2016; Viavatterne et al., 2018; Silva, 2019). Local approaches aim to achieve the highest possible level of accuracy for risk evaluation and support to decision making for previously identified hotspots (Van Versevelt et al., 2015; de Winter and Russeing, 2017; Sanuy et al, 2018; Plomaritis et al., 2018). Notably, coastal risk assessments must include physical concepts to characterise physical phenomena (i.e. the source of the hazard) and socio-economic concepts to describe the impact of the physical phenomena on human assets (i.e. the consequences). A conceptual flexible framework that can capture main aspects required for a robust coastal risk assessment is the well known Source-Pathway-Receptor-Consequence (SPRC) model (e.g. Narayan et al. 2014, Zanuttigh et al. 2014 and Oumeraci et al., 2015). This is a conceptual model which describes how a given risk propagates across a given domain from the source to the receptors. The problem is schematized in terms of the source (storms), the pathway (beach or coastal morphology) and receptors (elements of interest) at the coast, where the impact of the storm induces the consequences. Due to the common scarcity of direct observations, hazards are usually assessed by using predictive models which are fed with information on both the source and the pathway

Regional methodologies mainly rely on simple parametric or 1D-numerical models to estimate hazards, due to the large computational effort associated with large scale analyses. Many of existing regional approaches are semideterministic, either regarding the variability of the source (e.g., use of hurricane categories as levels, Stockdon et al., 2007; use of event approach, e.g., Villatoro et al., 2014; Armaroli and Duo, 2018) or the variability of the pathway (Callaghan, 2008; Bosom and Jimenez, 2011; Ballesteros et al. 2018). Hazard estimations through single-profile schemes are quick to apply but frequently stop short of accounting for morphologic variability when the coast is schematized with a low density of profiles. In such a case, hazards are obtained for specific morphologic characteristics.

When addressing the problem at the local scale, it is necessary to accurately predict the impact and reproduce in detail coastal hazards. The analysis of physical impacts is regularly implemented with process-based numerical models providing detailed information for areas prone to multiple hazards (e.g. Roelvink et al., 2009; McCall et al., 2010; Harley et al., 2011; Roelvink and Reniers, 2012; Van Dongeren et al., 2017). However, multiple forcing conditions acting at the site and under different scenarios must be evaluated, leading to high computational costs and large number of hazard results that need to be efficiently assessed.

Considering both the nature of the forcing and processes controlling the response, it is evident that storm-induced hazard assessments entail an inherent uncertainty in various parts of the analysis (e.g., Apel et al. 2004; Hall and Solomatine, 2008; Vousdoukas et al., 2018b), which should be studied to

determine which of them are most influential in the final result and to efficiently utilize resources (e.g., Sayers et al., 2003).

One of these sources of uncertainty is the assignment of the probability of occurrence to hazard magnitudes. Two general methods are mainly used, the so-called event and response approaches (Garrity et al., 2006). The choice of the method usually depends on the quantity and quality of the available data. In the event approach, the starting data are pre-existing marginal distributions of waves and surges, while the response approach uses long time-series of waves to calculate storm-induce hazards and estimate probabilities based on extreme value analysis on the targed variables. According to Divoky and McDougal (2006) the response approach should be the preferred option specially in locations with large variability of the involved storm variables controlling response processes.

The use of models to estimate hazards has also an inherent associated uncertainty (Plant and Stockdon, 2015; Simmons et al., 2017; Vousdoukas et al, 2018b). Additionally, especially when using numerical models, the storm event needs to be properly described, i.e., continuous (observed or hindcasted) storm time-series of waves and water levels are extremely important to capture the evolution of the event and, thus, its dynamic interaction with the beach. When continuous forcing time-series are unavailable, the event is generally described through observed or assessed bulk information, e.g. maximum significant wave height, peak wave period, maximum total water level, duration and main direction. In these cases, the evolution of the storm must be represented by parametric approaches, assuming a synthetic shape of the event. The symmetric triangular synthetic storm is widely applied for coastal studies (e.g. McCall et al., 2010; Corbella and Stretch, 2012). And it's often used to cover all the possible combinations of forcing (including those not previously recorded) in hazard and risk assessment approaches (e.g. Poelhekke et al., 2016; Plomaritis et al., 2018; Sanuy et al., 2018).

Therefore, effective hazard and risk assessments are favored by methodologies that are based statistically on the response (Garrity et al. 2006; Callaghan et al. 2008) due to the nonlinear and multidimensional dependencies involved in the driving processes (see e.g., Hawkes et al., 2002; Masina et al., 2015; Lin-Ye et al., 2016). Moreover, hazard and risk assessment frameworks need to account stochastically for model uncertainties and both source and pathway variability, which will involve the analysis of large datasets in a cost-effective manner. Using real storm shapes by using existing measured or hindcast records avoids the use of synthetic storm shapes and its associated uncertainties. Additionally, all forcing conditions acting at the site must be evaluated under different scenarios, including mid-long term projections due to background erosion and climate change.

All previously identified needs can be effectively managed with Bayesian Networks (BNs). This statistical tools based on acyclic graph theory and Bayes theorem (Pearl, 1988; Jensen, 1996) have demonstrated their versatility and utility in efficiently combining multiple variables to predict system behaviour, for different scenarios and spatial scales, in a number of applications and frameworks, e.g., groundwater flow predictions supporting decision making (Fienen et al. 2013), habitat protection against

natural hazards (Palmsten et al. 2013; Gieder et al. 2014), coastal vulnerability and shoreline evolution to sea level rise (Gutierrez et al. 2011; Plant et al. 2016), postevent hazard and damage assessment (Van Verseveld et al. 2015; Poelhekke et al. 2016) and disaster risk reduction assessments (Plomaritis et al. 2018, Sanuy et al. 2018). BNs can easily handle nonlinear systems, are not computationally expensive, can work with data from different sources (e.g., modeled, observed, or even opinions) explicitly including uncertainties and have a simple and intuitive graphical structure that is easily understood by nontechnical users (Uuscitalo, 2007). Notably, they can be used to represent the SPR scheme through the dependency relations that physically, or even psychologically, exist between the different steps (e.g., Straub 2005, Jäger et al. 2018); thus, they can be adapted to assess many kinds of natural hazards and impacts on many kinds of receptors, for descriptive or predictive applications (Beuzen et al. 2018b).

Identified shortcomings become the main motivation of this Thesis, which has been developed in the framework of previous research on coastal risk and vulnerability developed at LIM/UPC, and following previous Theses of Mendoza (2008), Bosom (2014) and Ballesteros (2017). Those works developed the hazard phase and the vulnerability phase respectively of a first methodology for hotspot detection at the regional scale and its application to the Catalan coast. This was also a shared objective with the EU-PF7 RISC-KIT project (Van Dongeren et al. 2018) where the PhD candidate was involved and which followed the objective of developing a set of tools at both regional (~100 to 1000 km) and local (~10km) scales.

1.2. OBJECTIVES

The main objective of this thesis is to develop a coastal risk assessment framework to extreme events and test it under Mediterranean conditions. To meet this global objective, the following partial objectives were considered:

1. To assesses tow main sources of uncertainty by performing an analysis on factors affecting the estimation of hazards magnitudes induced by the impact of storms on sedimentary coasts.
    1.1. To assess the uncertainty associated with the method used to assign probabilities to hazard magnitudes, particularly the differences between using the so called event and response approaches.
    1.2. To assess the uncertainty associated with the schematization of the storm shape by using synthetic triangular storm-shapes for the purpose of modelling induced erosion and inundation

2. To develop a methodology to identify and characterize hotspots at the regional scale.
    2.1. To develop a methodology to identify hotspots based on parametric hazard models and simple vulnerability indicators

2.2. To include in such methodology a fully probabilistic hotspot characterization explicitly considering model uncertainties and allowing to assess hotspot evolution at different time horizons in relation with mid-long term processes such as background erosion and sea level rise under climate change.

3. To develop a methodology for the integrated assessment of impacts at the local scale (hotspot).
   3.1. To develop a framework allowing the assessment of risk reduction measure efficiency under different scenarios (including present and future conditions) to support decision making.
   3.2. To develop a fully probabilistic method to characterize risk as the local scale and its interrelation with forcing conditions.
   3.3. To develop a method to characterize morphological response at the local scale and predict coastal erosion as proxy of parametric models where these are not applicable.

4. To validate and apply the entire framework to regional or local study sites at the Catalan coast (i.e. under NW Mediterranean conditions).

1.3. STRUCTURE OF THE THESIS

Following the present first introductory chapter, the body of the thesis (chapters 2 to 8) comprises the edited versions of 6 publications in international journals, from which 4 of them are already published, and 2 of them are under review. It also includes 2 papers currently under preparation. Finally, the document is closed by Chapter 9, which contains the overall conclusions and future lines of research derived from the presented work. Figure 1.1 presents the chronological flowchart of the different chapters and studies therein, and its relations between them and with the international projects and internships related with the thesis.

Chapters 2 and 3 present the uncertainty assessments that later justify the developed hazard and risk assessment methodologies. In Chapter 2 the uncertainty associated with the method to assign probabilities to hazard magnitudes is analysed, by comparing the two main adopted approaches: the event and response methods. The analysis covers all different wave conditions of the Spanish coast by using data form 11 nodes along the in Cantabric, Atlantic and Mediterranean coasts. Chapter 3 analyses the impact of using triangular synthetic storms for storm-induced hazard modelling, a common practice in coastal engineering applications when only bulk information of the events is available. The study in Chapter 3 is the result of a specific collaboration with UNIFE (Ferrara, Italy) and was mostly conducted during a 2-month international internship in that university. Notably, obtained results in Chapters 2 and 3 will later motivate the improvement of semi-deterministic methods presented in Chapters 4 and 6 (developed within the RISC-KIT project) into fully probabilistic risk and hazard assessments presented in Chapter 7 and 8.

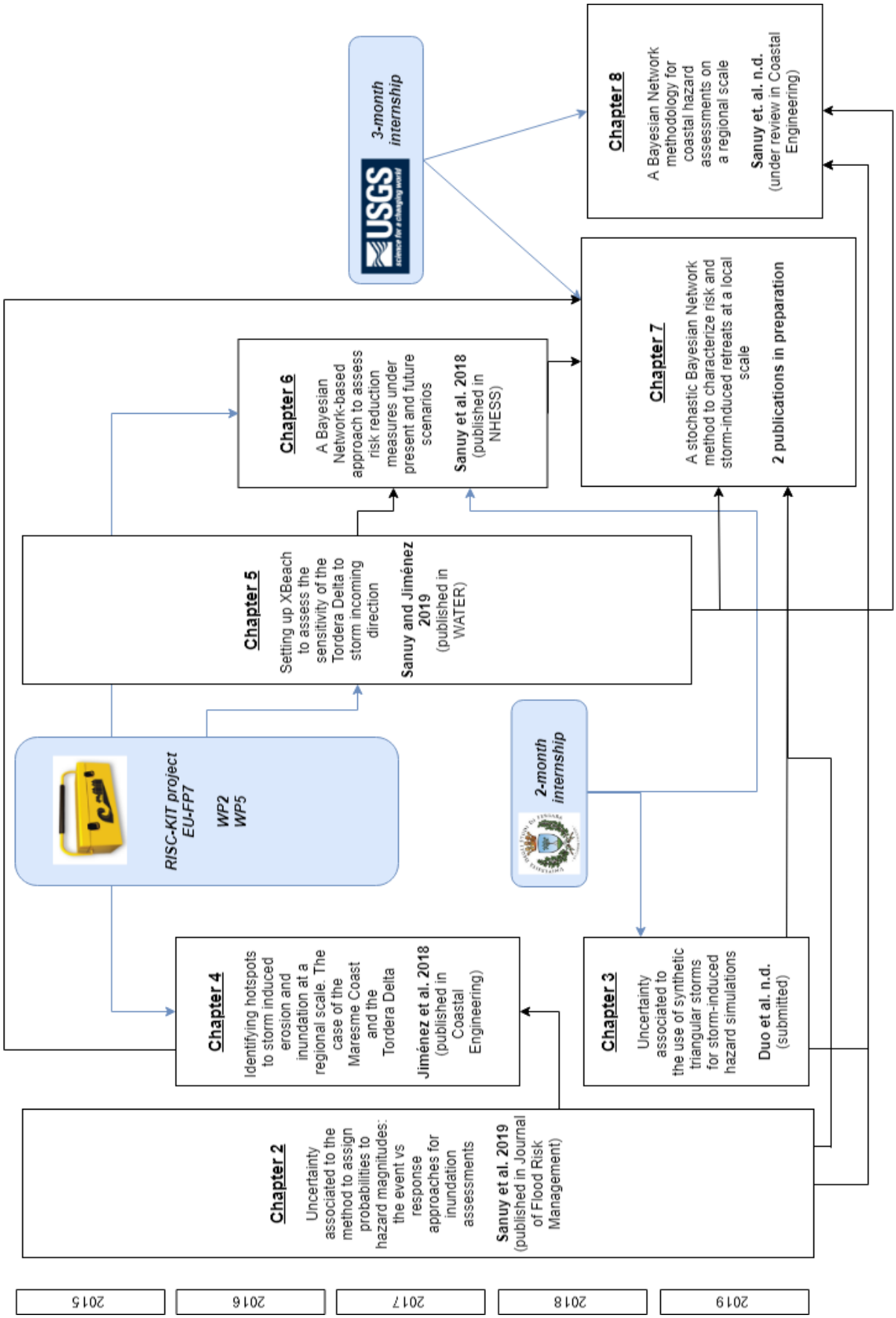

Figure 1.1. Chronological diagram of the research activity and its interconnections.

Chapter 4 presents the regional risk assessment method developed during the RISC-KIT project with the objective of identifying coastal hotspots to the impact of storm-induced erosion and inundation. This is based on simple parametric hazard models and coastal vulnerability indicators. This represents the first step, preceding the detailed local-scale risk assessment method. In this chapter, the Tordera Delta is identified as one of the main hotspots in the NW Mediterranean Catalan coast, and it will be the main study case of the subsequent chapters.

Chapter 5 presents the model set-up and calibration required prior to the implementation of the hotspot risk assessment methodology, which is based in detailed 2DH process-based model simulations. In particular, the chapter presents a SWAN+XBEACH model set-up and its validation using the Sant Esteve 2008 storm (a highest-class historical event from which pre- and post-storm measurements of the subaerial morphology were available). The model set-up is also used to test the sensitivity to storm incoming direction of the Tordera Delta, already stablished as hotspot in Chapter 4.

In Chapter 6, the Bayesian Network-based approach for local detailed risk assessments is presented. This is the second step of the tools developed in the RISC-KIT project, and it is based in the conceptualization and schematization of the Source-Pathway-Receptor-Consequences concept. This chapter describes in detail what this schematization consists of by showing its step-by-step application in two Mediterranean study sites: The Tordera Delta (NW Mediterranean) and the Lidi degli Stensi-Spina (N Adriatic). The BN-model is used to compare the efficiency of risk reduction measures to storm-induced impacts under current conditions and future projections of SLR and its induced coastal accommodation.

Chapter 7 presents two additional BN applications at local scale, using intensive simulations with the model set-up described in Chapter 5. First, in Section 7.2, a fully probabilistic BN-method for local risk characterization following lessons learned after RISC-KIT (Chapter 6) is presented. The RISC-KIT BN-approach (Chapter 6) is designed as semi-deterministic (i.e. event approach in Chapter 2) and includes the use of triangular storms (Chapter 3). As a consequence, it is only used for comparison purposes and cannot be used for probabilistic risk analyses. Thus, Chapter 7 presents a BN application at the Tordera Delta tackling these limitations. Second, Section 7.3 presents the use of a BN-model adapted to characterize morphological response in terms of beach retreat at the Tordera Delta. The BN-model characterizes the relative importance of storm incoming direction, storm multi-peak sequencing and local effects for a proper system response prediction at a highly dynamic study site such as the Tordera Delta. This represents a first attempt to test the performance of the BN-model as surrogate of erosion parametric models used in regional applications (e.g. Chapters 4 and 8).

Chapter 8 presents the development of a BN-based regional assessment tool incorporating lessons learned after the international internship at the USGS-Florida (3 months). This is an evolution of the RISC-KIT regional hotspot detection tool (Chapter 4) incorporating a probabilistic treatment of the

morphology and including parametric model uncertainties to the analysis. The developed approach is tested in 5 small sectors of the Maresme coast (NW Mediterranean), including the Tordera Delta.

Finally, Chapter 9 resumes the global vision of the thesis, summarizes main overall conclusions and explores future research horizons following after the presented work.

Each chapter is designed to be self-contained. Therefore, some repetitions on study site descriptions or parts of common methodologies have been allowed, although reduced to the minimum. The idea is to facilitate the understanding of each chapter without having to constantly skim through the thesis to find all needed key information.

© Copyright disclaimer

performed at local scale. The PhD candidate contributed in the compilation of the erosion and inundation hazard models to be applied at different study sites during RISC-KIT and in the development of model-chain connecting framework for its application at all study sites within the CRAF (WP2) approach. The doctoral candidate facilitated hazard output to be combined with socioeconomic data and vulnerability models by C. Ballesteros to produce final results. The work was first generally conceptualised by J.A. Jimenez and fully supervised and mainly written by him, with the collaboration of all other co-authors.

Chapter 5

Sanuy, M.; Jiménez, J.A., 2019. Sensitivity of Storm-Induced Hazards in a Highly Curvilinear Coastline to Changing Storm Directions. The Tordera Delta Case (NW Mediterranean). Water, 11, 747. doi:10.3390/w11040747.

This work was developed essentially by the doctoral candidate, with the supervision of J.A. Jiménez, who also made important conceptual improvements enriching the final scope of the analysis.

Chapter 6

Sanuy, M., Duo, E., Jäger, W. S., Ciavola, P., and Jiménez, J. A., 2018: Linking source with consequences of coastal storm impacts for climate change and risk reduction scenarios for Mediterranean sandy beaches, Nat. Hazards Earth Syst. Sci., 18, 1825-1847, doi:10.5194/nhess-18-1825-2018.

This work was developed essentially by the doctoral candidate and Enrico Duo (UNIFE), under the supervision of both supervisors, P. Ciavola and J.A. Jiménez, and with the collaboration of W. Jäger in the use of the Bayesian Network to conceptualize the Source-Pathway-Receptor-Consequences framework.

Chapter 7

This chapter will be submitted for publication as 2 differenet papers (one on the morphodynamic BN application and the other on the BN risk characterization). The manuscripts are ready, finalising internal review during the weeks prior to the submission of the present PhD thesis.

Chapter 8

Sanuy, M., Jiménez, J.A., Plant, N. n.d. A Bayesian Network model for coastal hazard assessments on a regional scale: the BN-CRAF. In review (Coastal Engineering).

This work is the result of the 3-month internship of the PhD candidate in the USGS with Dr. Nathaniel Plant. Lessons learned from the application of Bayesian Networks in coastal hazard assessments were later used by the PhD candidate to complement the existing methodologies at UPC, under the supervision of J.A. Jiménez and key feedbacks from Dr. Plant.

CHAPTER 2.

Uncertainty associated to the method to assign probabilities to hazard magnitudes: the event vs response approaches for inundation assessments.

Adapted from: Sanuy M., Jiménez J.A., Ortego MI, Toimil A., 2019. Differences in assigning probabilities to coastal inundation hazard estimators: Event versus response approaches. J Flood Risk Management, e12557. doi:10.1111/jfr3.12557

This chapter assesses one of the sources of uncertainty in coastal storm-induced hazard estimation: the choice of method to assign probabilities (or return periods) to given hazard magnitudes. The analysis focuses on the inundation hazard, at different levels of definition of hazard estimator variables, from run-up to the final inundation maps. The two most commonly used options in coastal hazard assessments, being the choice ususally imposed by data availability, are compared: the event and response methods.

2.1. Introduction

Assessing the impact of coastal storms has become a global need motivated by the increasing number and value of assets located in coastal areas and the escalation of damages during the last decades (IPCC 2012, 2013). This is also true for the Spanish coast, where the same trend has been identified along its littoral front (e.g., Reyes et al. 1999: Rodriguez-Ramirez et al. 2003; Jiménez et al. 2012, 2017; Marcos et al. 2012, Toimil et al., 2017). Among the different storm-induced hazards, inundation is one of the most significant and damaging, and should be considered for its potential to increase in importance over the next decades (e.g., Jongman et al. 2012; Hinkel et al. 2014; Vousdoukas et al. 2018a). The need for proper assessment of inundation is clear when designing coastal management plans, which will require a specific chapter on coastal risks as recognized in the protocol of Integrated Coastal Zone Management in the Mediterranean (UNEP/MAP/PAP, 2008). The European Union (EU) Floods Directive (EC, 2007) instructs management groups to prepare flood hazard maps for events of given probabilities of occurrence. Thus, the scientific community has developed multiple methodologies to assess storm-induced inundation through a variety of estimators (e.g., Sallenger 2000; Stockdon 2007; Ciavola et al., 2011a, 2011b; Tomás et al., 2016; Van Dongeren et al., 2018). Hazard-describing variables of multiple complexities can be used in inundation assessments to provide answers at both regional and local scales. Thus, the literature provides examples of regional parametric methodologies that scale hazard intensity using simple variables such as run-up, surge or total water level (e.g., hurricane impact at US coasts in Stockdon et al. 2007; storm impact along the Emilia-Romagna coast facing the Northern Adriatic described by Armaroli et al., 2012, and Armaroli and Duo, 2018; or storm impact in the northwestern Mediterranean coastline in Chapter 4 and Jiménez et al. 2018). Other approaches exist that assess the inundation at local (or even regional) scales using overtopping/overwash discharges or volumes as hazard estimators (e.g., Chini and Stansby, 2012) or by directly producing inundation maps (e.g., Prime et al. 2016), which can later be used to derive impacts by using receptor vulnerability data, and assess risks for decision support in coastal managing (e.g. Chapters 6 and 7).

Considering both the nature of the forcing and processes controlling the coastal response, it is evident that inundation hazard assessment entails an inherent uncertainty in various parts of the analysis (e.g., Apel et al. 2004; Hall and Solomatine, 2008; de Moel et al., 2012), which should be studied to determine which of them are most influential in the final result and to efficiently utilize resources (e.g., Sayers et

al., 2003). For instance, some studies assess the uncertainty associated with the method to identify the events (storms) or the extreme value distribution function selected for fitting (Arns et al., 2013, Winter el al. 2018). Uncertainty can be categorized into two simple groups, i.e., the variability of nature (e.g. natural randomness of waves and surges) and the uncertainty of knowledge (e.g., numerical models, data analysis, etc). Prior to formal uncertainty analysis, an insight into the expected contributions associated with selected choices can be obtained by making a sensitivity assessment in which the same conditions are simulated when adopting such choices.

Within this context, the main aim of this chapter is to quantify the sensitivity of inundation hazard assessments to the general scheme used to assign probabilities to hazard magnitudes. Two general methods will be compared, the so-called event and response approaches, since they are the two main conceptual schemes used in coastal hazard assessments to estimate probabilities or return periods (Garrity et al., 2006). This will be done with different hazard estimators from wave run-up to final inundation extension maps. The choice of the hazard-describing variable usually depends on the scale, objectives and available data of the studies. The choice of the method usually depends on the quantity and quality of the available data. In the event approach (EV), the starting points are pre-existing marginal distributions of waves and surges. Thus, the statistics are calculated based on the source in a univariate semi-deterministic mode. The response approach (RS) uses a large dataset (when available) of hydrodynamic data to both identify events and perform the statistical calculations directly based on the hazard target variables. The analysis for this chapter has been performed using a large dataset of 11 nodes around the Spanish coast and thus, covering the Cantabric, Atlantic and Mediterranean conditions. All nodes correspond to offshore data, and information on waves and surges are extracted at the same locations from the datasets. This includes the assessment of different wave and surge conditions to obtain results that help provide useful recommendations for different areas, which may be extrapolated to other domains with similar hydrodynamic characteristics.

The structure of the chapter is as follows: section 2.2 presents the data description and assessment locations, section 2.3 describes all the steps of the used methodology and section 2.4 presents the results divided by different levels of hazard estimators which are later discussed in section 2.5. Finally, section 2.6 wraps up the main conclusion of the study.

2.2. Data description

To perform this analysis, data on waves, water levels and coastal morphology are required to characterize the forcing and the receptor respectively. Coastal inundation assessment requires continuous long-term availability of wave and sea level time series with adequate spatial and temporal coverage and such data must have been extensively checked and validated to prove their reliability. This work uses offshore wave and surge data obtained for a series of 11 locations along the Spanish coastal stretch covering the period from 1950-2014 (Figure 2.1).

The offshore waves are obtained from the Global Ocean Waves (GOW) dataset (Reguero et al., 2012) which consists of a hindcast of hourly wave patterns with a spatial resolution of 0.0625° over a span of more than 60 years. These include the information on significant wave height and wave periods used in this work along with information on wave direction and wave spreading. GOW was simulated with the WaveWatchIII model (Tolman et al., 2002) and driven by the NCEP SeaWind I winds (Menendez et al., 2014). The meteorological sea-level component comes from the Global Ocean Surge 1.1 (GOS1.1) database (Cid et al. 2014). GOS1.1 was developed using the Regional Ocean Model System (ROMS) of Rutgers University and forced with NCEP SeaWind I winds, which provided an hourly-basis hindcast of surge levels with a spatial resolution of 0.125° between 1948 and 2014. Both datasets have enough resolution and accuracy to describe the coastal processes at all locations which has been verified using historical records from buoys, tide gauges and open-ocean satellite observations (Reguero et al., 2012 and Cid et al., 2014).

Figure 2.1. Locations of wave and surge data used in this chapter. Data from the Global Ocean Waves (GOW, Reguero et al., 2012) and Global Ocean Surge (GOS, Cid et al 2014) were available for each node.

Since the magnitude of storm-induced flooding depends on the coastal characteristics, we used different types of data to characterize a representative morphology. Thus, on the one hand, for cross-shore inundation estimators (e.g., Ru, overtopping discharges/volumes), the coast is synthetically represented

by different beachface slopes covering dissipative to reflective conditions in the range of 0.025 to 0.2 and elevations from 1.5 to 5 m above mean water level. On the other hand, to illustrate the effects on inundation extent, a low-lying flood-prone area is selected, which is represented by the topography of the Tordera Delta in the northwest Mediterranean (see e.g., Chapter 4). Topographic data were derived from a LIDAR flight performed in 2010 with a 1×1 m resolution and a vertical error of 6 cm provided by the Catalan Cartographic and Geologic Institute.

2.3. Methodology

2.3.1. Inundation hazard estimators

The inundation hazard-describing proxies analysed in this work are the wave-induced run-up (Ru), the total water level at the beach (TWL), the overtopping discharge (Q), the total water volume flowing into the hinterland (TWV) and the inundation maps.

Wave Ru is an important parameter to properly characterize storm-induced coastal inundation and can be used as a hazard estimator to assess coastal vulnerability to flooding in regional-scale approaches (Bosom and Jiménez, 2011; Ferreira et al. 2017; Chapter 4). The accurate prediction of Ru is difficult given the complexity of the processes involved such as the energy dissipation in the surf zone and the interactions between the infragravity and incident wave bands (Ruggiero et al. 2004). There are a number of models that have been derived or specifically calibrated to be applied to beaches (e.g., see Mather et al., 2011). In this work, we use the formula proposed by Stockdon et al. (2006), which has been specifically derived from a large dataset of Ru values measured in field experiments covering different beach characteristics. It is extensively used as a Ru model for open sedimentary coasts and it predicts the $Ru_{2\%}$ magnitude as:

$$Ru_{2\%} = 1.1\left(0.35\tan\beta\,(Hs\,Lo)^{1/2} + \frac{\left[Hs\,Lo\,(0.563\tan\beta^2 + 0.004)\right]^{1/2}}{2}\right), \tag{2.1}$$

and under extremely dissipative conditions ($\xi o < 0.3$) by:

$$Ru_{2\%} = 0.043\,(Hs\,Lo)^{1/2}, \tag{2.2}$$

where Hs is the deepwater significant wave height, Lo is the deepwater wave length associated with the wave peak period (Tp), tanβ is the beachface slope, and ξo is the Iribarren number, which is given by

$$\xi o = \frac{\tan \beta}{\sqrt{Hs/Lo}} \cdot \tag{2.3}$$

Wave induced run-up is usually combined with the storm surge (SU) to derive the TWL at the beach. This corresponds with the stochastic component of the water level and omits the astronomical tide. The TWL is also commonly used as an estimator in coastal inundation assessments when the incidence of the surge component is important (e.g., Benavente et al. 2006, Stockdon et al 2007, Armaroli and Duo, 2018).

When the TWL is significantly higher than the beach elevation, overwash and/or overtopping will occur and this will determine the total volume of water entering into the hinterland. Overtopping (Q) depends on the freeboard during the event, defined as the vertical height of the beach or coastal structure above the still water level, and the level reached by the wave-induced Ru (Pullen et al., 2007).

Different formulations exist to obtain this flow rate from the given wave conditions, and most of them were developed to characterize overtopping at seawalls and breakwaters (see Pullen et al., 2007). In this work, the overtopping discharge Q was evaluated using the semi-empirical model proposed by Hedges and Reis (1998) (hereinafter denoted as H&R) with the coefficients A and B given by Reis et al. (2008):

$$\frac{Q}{\sqrt{gR_{max}^3}} = \begin{cases} A\left(1 - \frac{Rc}{\gamma_r R_{max}}\right)^B & 0 \leq \frac{Rc}{\gamma_r R_{max}} < 1 \\ 0 & \frac{Rc}{\gamma_r R_{max}} \geq 1 \end{cases}, \tag{2.4}$$

where Rmax is the maximum wave run-up value during the storm, γr is a roughness coefficient (γr =1 for sand) and Rc is the beach freeboard relative to the still water level.

Analogously to the analysis performed by Laudier et al. (2011), eq.2.1 and 2.2 are used to estimate the wave Ru which feeds eq.4 after proper transformation.

Once the water levels are known and the flood discharge is calculated, the total water volume (TWV) entering the hinterland during the event can be assessed. This was done by directly integrating each discharge over the time-step (without consideration of the percentage of overtopping waves) and by addition of time-steps over the duration of the storm. This volume can then be used to compute the extension of the inundation of a given area. In this work, the raster-based LISFLOOD-FP inundation model is used, which has been successfully employed to simulate inundations in fluvial and coastal areas (Bates and de Roo, 2000; Bates et al., 2005). The model is used to propagate discharges into the hinterland, and thus, to provide an estimation of the inundation extension over a low-lying flood-prone area given the magnitude of the discharges along the beach. LISFLOOD-FP treats floodplain flows using

a storage cell approach first developed by Cunge et al. (1980), which is implemented for a raster grid to allow an approximation for 2D diffusive wave and momentum equations for each direction. In this model, the flow between cells is calculated according to Manning's law. The model predicts water depths in each grid cell at each time step and simulates the dynamic propagation of waves over the floodplain. The grid is formed by 3 m × 3 m cells obtained from the existing LIDAR, i.e. the original 1m x 1m LIDAR data has been resampled to reduce the computational time while maintaining a high-resolution grid. In this study, a constant value for the Manning's roughness of 0.06 is used throughout the floodplain, according to the recommendations of Arcement and Schneider (1989) for this type of surface i.e., moderate degree of irregularity, minor obstructions and medium to large vegetation.

2.3.2. Storm selection and extreme value analysis

In this chapter, the Peak Over Threshold (POT) approach (see e.g., Coles, 2001; Dupuis, 1998) is used to identify extreme events with a double threshold approach. First, the 98 percentile of the time series (either Hs, SU, Ru or TWL) was used considering only events with durations over 6 h and imposing a 72 h time gap between events to ensure independence. Thus, the first threshold controls the duration of the events and the time of fair-weather conditions between them. Later, the 99.5 percentile is used as the criterion for minimum value at the peak of the event (i.e., only events exceeding the second threshold at the peak are considered extreme).

This approach was adopted to obtain storms in terms of Hs and SU for the event approach (Table 2.1) from the GOW and GOS datasets at the 11 selected nodes. For the response approach, the POT is applied to the Ru and TWL variables previously calculated for the whole length of the datasets (following scheme in Figure 2.2). The double threshold ensures homogeneous statistical criteria to locate extreme events across datasets and has been designed for an output average of ~4-6 events per year. The lower threshold (98 percentile) matches, as a reference, the magnitude of Class 1 events (low energy content) according to Mendoza et. al (2011) for northwest Mediterranean storms (nodes 8 to 11, Table 2.1).

To assign probabilities to the obtained events, an extreme value distribution was fitted to the data. In this work, the Generalized Pareto Distribution (GPD) is used for that purpose (Davison and Smith, 1990). GPD is given by ($\sigma>0$ and $y>0$):

$$F_Y(y;\sigma,\xi) = 1 - \left(1 + \frac{\xi}{\sigma}y\right)^{-\frac{1}{\xi}} \quad , \tag{2.5}$$

where ξ and σ are the shape and scale parameters. The GPD has three domains of attraction, which are $\xi < 0$, $\xi = 0$ and $\xi > 0$ and represent the Weibull (upper-bounded), Gumbel (exponential) and Fréchet (heavy tailed) domains, respectively. Following Egozcue et al. (2006), the storm data is log-transformed before fitting the GPD. Thus, in eq.2.5, $y = \log(X-u)$ where u is the 99.5 percentile threshold (Table 2.1).

The log-scale represents an improved method for positive measurements in which the differences are relative (Tarantola 2006). All of the considered variables in this work describe physical processes that are upper-bounded, and therefore a GPD-Weibull is a suitable model for them.

Table 2.1. Values of the 98 and 99.5 percentiles used as thresholds at each node for all variables under the POT approach and the number of obtained storms per site and variable from 1960 to 2014.

	Hs (m)			SU (m)		
Node	**98%**	**99.5%**	**nº storms**	**98%**	**99.5%**	**nº storms**
1	3.67	4.24	231	0.25	0.29	180
2	4.44	5.12	229	0.26	0.31	162
3	6.65	7.53	231	0.27	0.32	155
4	6.49	7.28	226	0.24	0.28	163
5	3.21	3.81	187	0.18	0.22	170
6	2.66	2.99	252	0.21	0.25	84
7	2.65	3.01	316	0.19	0.23	145
8	2.55	2.98	268	0.20	0.24	153
9	2.40	2.87	246	0.23	0.27	121
10	2.58	2.99	271	0.24	0.28	132
11	2.57	3.08	253	0.24	0.28	174

Table 2.2 presents the fitted parameters for the Hs, SU, Ru and TWL extreme value distributions, along with the modified Anderson-Darling Statistic A* (Stephens, 1977) which illustrates the goodness of fit as follows: at a significance level alpha of 0.01, the GPD is accepted as a good fit for the data for A* values lower than 1.04. As it can be observed, most of the data is correctly represented with a GPD with the following considerations: node 7 presents A* values slightly above the acceptance threshold for all tested variables, and the GPD is less representative for the SU data at most of the Mediterranean locations (nodes 6 to 10). However, it is considered that GPD fits the datasets correctly enough to perform the comparison between event and response methodologies.

Regarding the Q and TWV parameters, the GPD presents poorer goodness of fit results specially for slope-freeboard combinations, due to the nature of eq.2.4, giving a low number of storms producing discharges. In order to include only those cases with better fittings, only combinations with more than one storm per year producing discharges are included in the final comparison assessment.

Table 2.2. Fitted scale (ξ) and shape (σ) parameters for the Hs, SU, Ru and TWL extreme value distributions. The modified Anderson-Darling Statistic A* (Stephens, 1977), denotes a good fit for values lower than 1.04 (at alpha level 0.01).

node	Hs			SU			Ru (slope 0.1)			TWL (slope 0.1)		
	ξ	σ	A*	ξ	σ	A*	ξ	σ	A*	ξ	σ	A*
1	-0.37	0.11	1.17	-0.25	0.10	0.88	-0.37	0.09	0.13	-0.35	0.09	0.31
2	-0.38	0.11	0.58	-0.28	0.10	0.17	-0.38	0.09	0.49	-0.41	0.10	0.40
3	-0.42	0.11	0.35	-0.44	0.13	0.57	-0.38	0.08	0.57	-0.37	0.08	0.88
4	-0.38	0.10	0.63	-0.43	0.13	0.43	-0.28	0.07	0.49	-0.31	0.08	0.45
5	-0.36	0.12	0.33	-0.51	0.16	0.21	-0.26	0.10	0.26	-0.26	0.11	0.38
6	-0.16	0.08	0.43	-1.04	0.37	4.66	-0.19	0.08	0.79	-0.20	0.08	0.97
7	-0.20	0.09	2.01	-0.54	0.20	4.19	-0.15	0.08	1.46	-0.16	0.08	1.62
8	-0.20	0.11	0.50	-0.49	0.18	3.67	-0.14	0.08	0.19	-0.16	0.09	0.25
9	-0.31	0.14	0.24	-0.55	0.21	6.87	-0.22	0.10	0.30	-0.26	0.11	0.20
10	-0.32	0.13	0.48	-0.51	0.19	5.23	-0.24	0.10	0.52	-0.28	0.11	1.16
11	-0.29	0.12	0.36	-0.34	0.13	0.23	-0.22	0.09	0.22	-0.27	0.10	0.34

2.3.3. The event and response approaches

The event approach (EV) (Figure 2.2) is a semi-deterministic methodology, where the starting point is determined by the extreme probability distribution of wave heights and storm surges in addition to some empirical relationships with other storm parameters of interest such as wave period and storm duration. When these are the only available data, it must be assumed that the hazard variables of interest (Ru, TWL, Q, TWV or the inundation map) have the same probability of occurrence than the forcing (wave and storm surge).

In this work, the starting point of the EV corresponds to the fitting of marginal Hs and surge extreme distributions at all nodes (Figure 2.2, Hs and SU as FX(TR); Figure 2.3-a and b). This starting point is usually available in a pre-processed way and provides wave height and storm surge values for a given return period of interest (TR) (Figure 2.2). The remaining parameters required to fully characterize the event, i.e., wave period and storm duration, are calculated by using deterministic relationships (Figure 2.2, Tp= f(Hs) and Dur= f(Hs); Figure 2.3-c and d), since the use of EV is usually imposed by the lack of available data to perform bivariate statistical approximations (as in e.g. Lin-Ye et al. 2016). With this approach each wave height is associated with just one value of the other storm parameters. This implies the loss of significant information regarding the natural variability of the processes (Sánchez-Arcilla et al., 2009, Masina et al., 2015). Obtained Ru is combined with the SU of the same TR of interest to get the TWL (by addition) or Q (with eq.2.4). This is the simplest and most conservative application of the event approach corresponding to situations in which simultaneous datasets of interest are not available. In other cases, bi(multi)-variant statistical distributions could be calculated (e.g., Hawkes et al. 2002,

Masina et al. 2015, Lin-Ye et al. 2016), but this would imply that a large dataset is available and therefore the response approach could be applied as well. In order to estimate discharge evolution during the storm (e.g., to produce inundation maps or to integrate discharges into TWV), an assumption about the shape of the storm development in time must be made. One of the most common hypotheses is imposing a triangular shape with the peak of the event at the centre of the duration (McCall et al. 2010, Poelhekke et al. 2016; Chapter 3); therefore, it is the one adopted here to derive deterministically TWV and inundation maps for the event approach.

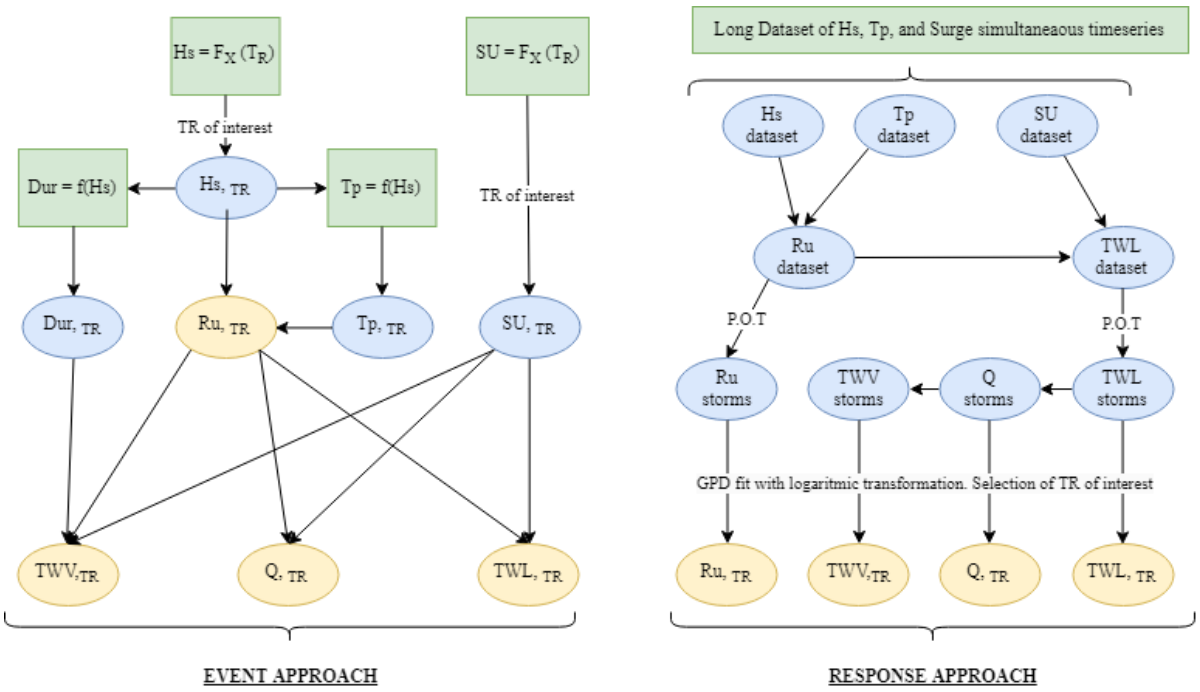

Figure 2.2. A flow chart of the steps and their interdependencies in the analysed methods: event (EV) and response (RS). FX(TR) represents the extreme distribution and f(Hs) the deterministic relationships of a variable with the wave height.

In the response approach (RS), the entire original wave and water level time series are used to establish the hazard parameters of interest. Thus, Ru datasets in all 11 locations are calculated from the available Hs and Tp time series. These are combined with simultaneous SU data to obtain the TWL time series. Then, the POT method is used on both Ru and TWL datasets to identify storms in terms of the target estimator. This permits the proper inclusion in the assessment of the natural variability associated with the simultaneous occurrence of the involved variables without imposing any assumption. From the TWL storm dataset, Q time series and integrated TWVs can be calculated for each event without assumptions on the events' durations and shapes (see Chapter 3). The response method is especially recommended when wave variables during storms (e.g., Hs, Tp and duration) are poorly or partially correlated and it is recommended by the FEMA guidelines for flooding studies (Divoky and McDougal, 2006). However,

it can only be applied if long records (either simulated or measured, covering many years) of the involved variables are available.

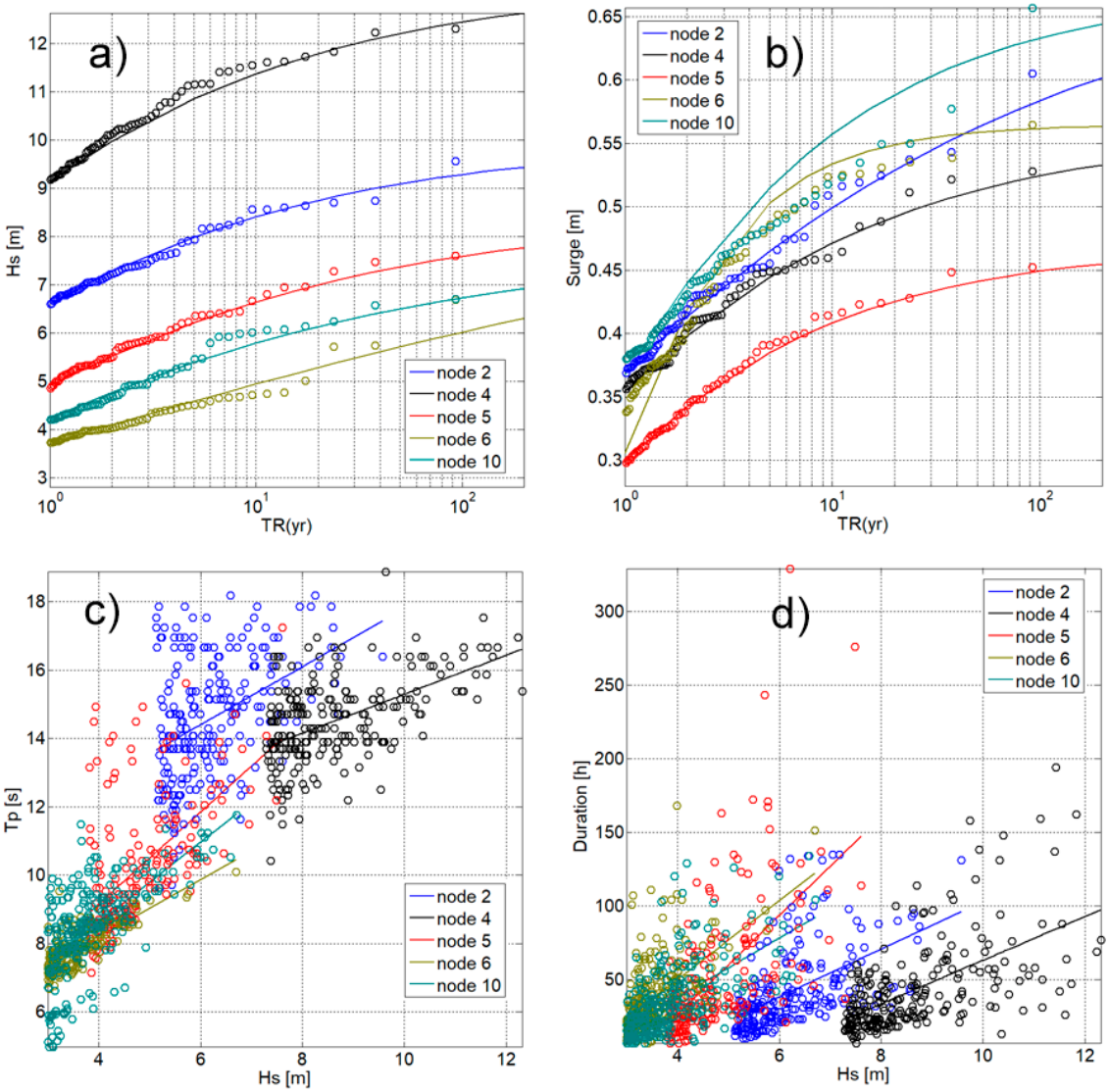

Figure 2.3. Extreme distributions of Hs (a) and SU (b). Tp vs Hs (c) and duration vs Hs (d) relationships for representative nodes covering the different conditions along the Spanish coast (2-Cantabric, 4-N. Atlantic, 5-S. Atlantic, 6-S. Mediterranean and 10-N. Mediterranean).

Figure 2.4 shows an example of the so-obtained extreme distributions of inundation hazard estimators following both approaches for representative nodes along the Spanish coast. The differences in shape of the Q and TWV distributions (Figure 2.4, c-d) are caused by the properties of eq.2.4, and the fact that in the EV approach these are deterministically calculated from the TWL distribution (Figure 2.4, b), while in the RS method a GPD is fitted to maximum Q at the peak and TWV of each storm.

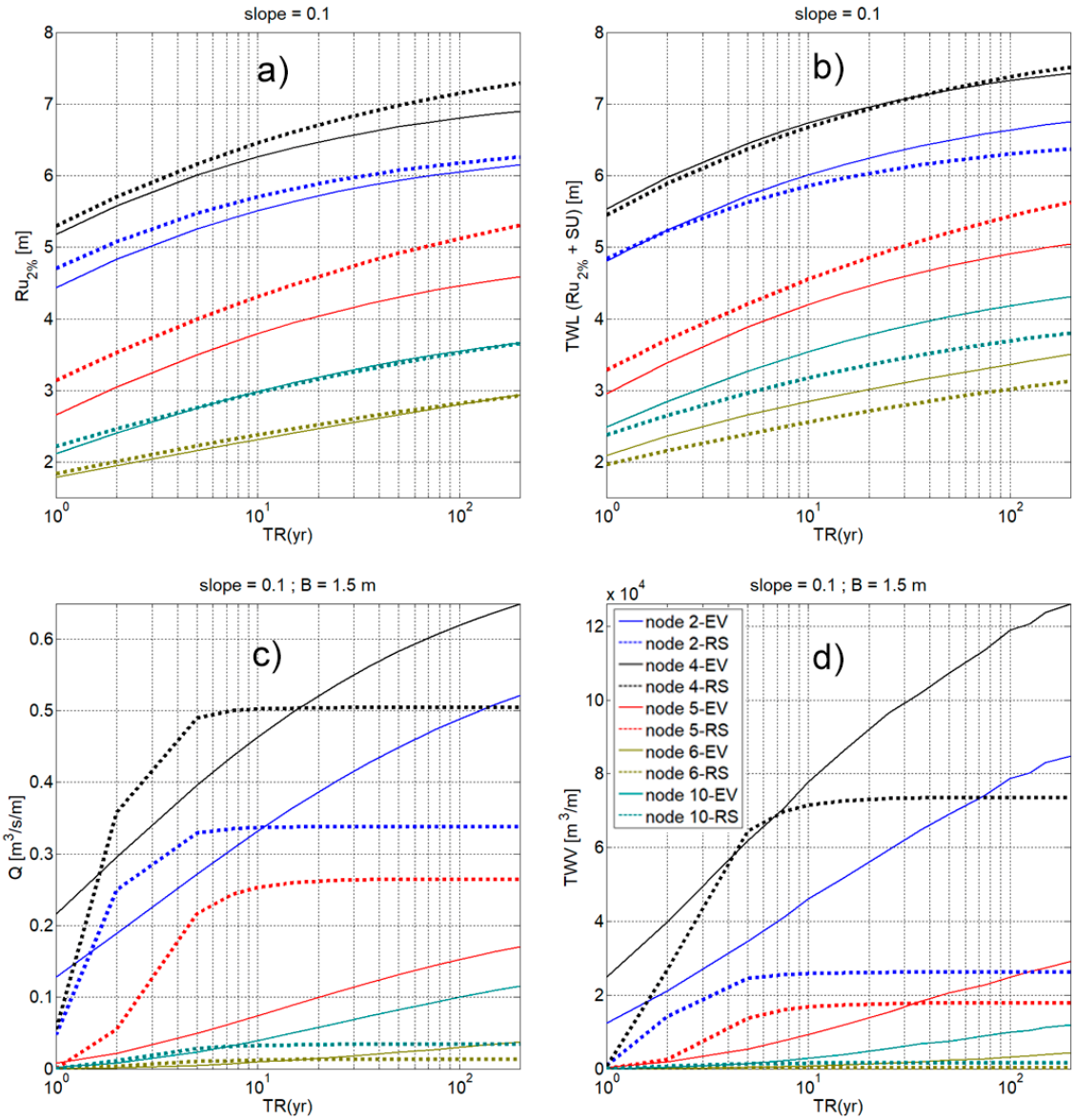

Figure 2.4. Examples of method comparison results for the selected locations (2-Cantabric, 4-N. Atlantic, 5-S. Atlantic, 6-S. Mediterranean and 10-N. Mediterranean) and morphologies (slope = 0.1 and B = 1.5). The selected datasets are presented to illustrate the absolute magnitudes of the involved variables at each of the main oceanic fronts.

2.3.4. The comparative assessment and clustering

The results are calculated at reference return periods (5, 10, 25, 50, 100 and 150 years) for each estimator (Ru, TWL, Q, and TWV), location (node) and approach (EV and RS). The relative differences between EV and RS approaches were calculated as:

$$Diff\% = \frac{RS_{varaible} - EV_{variable}}{RS_{variable}} * 100 \quad (2.6)$$

The Ru and TWL variables were assessed for different slopes (0.025, 0.075, 0.1, 0.14, and 0.2). These are hypothesized slopes that can be present at all 11 locations, except for 0.025, which is characteristic of some deltaic environments. The relative differences in terms of Ru and TWL (per return period and slope) were used as baseline to perform a cluster analysis. The selected clustering method was the inner squared distance (minimum variance algorithm). The aim was to group the 11 locations in representative clusters according to similarities in their differences between EV and RS approaches by using two variables including the wave and surge variabilities at each node (Figure 2.5).

For each variable, the results from all locations within clusters, slopes and freeboards, are integrated by calculating the median of the relative differences, and the 95% probability interval given by the 0.025 and 0.925 quantiles (Figures 2.6, 2.7 and 2.8).

The Q and TWV variables were assessed for slopes higher than 0.05 since this is the lower limit to apply the H&R model according to Reis et al. (2008). Thus, the considered slopes were (0.075, 0.1, 0.14, and 0.2). For each slope, different beach heights were tested ranging from 1.5 m to 4 m with 0.5 m steps. If a combination slope-height was observed to cause less than one discharge event per year, it was not included in the result integration (Figures 2.7 and 2.8).

2.4. Results

2.4.1. Spatial clustering

The obtained dendrogram (Figure 2.5) of the cluster analysis highlights four main groups with differentiated behaviour. The analysis clearly detects 2 big groups corresponding to the Atlantic and Cantabric coasts (nodes 1 to 5) and the Mediterranean Sea (nodes 6 to 11).

Each group is divided into two clusters where different trends of Ru and TWL differences are detected. The area corresponding to the Gulf of Cadiz (CAD, node 5) is clearly differentiated from the rest of N-Atlantic and Cantabric locations (AT-C, nodes 1 to 4). At the Mediterranean front, nodes 8 and 10 are grouped in a different cluster but with higher similarity than the division at the Atlantic-Cantabric front. Hereinafter, the analysis is done by comparing the results for the four clusters.

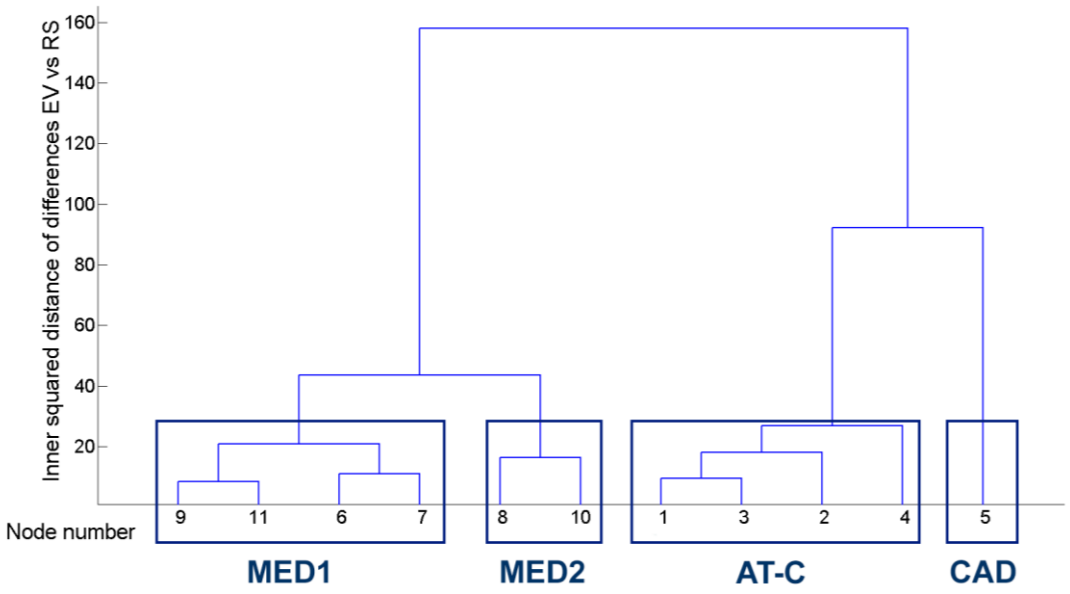

Figure 2.5. Dendrogram of the 11 locations based on Euclidean distance in terms of run-up (Ru) and total water level (TWL). Mediterranean locations (MED1 and MED2) are separated from N-Atlantic-Cantabric locations (AT-C) and Gulf of Cadiz (CAD).

2.4.2. Water level estimators

Figure 2.4 showed the obtained extreme distributions of Ru and TWL for representative nodes of each cluster. As expected, the magnitude of Ru is almost double for AT-C locations (nodes 1 to 4) than for MED1 and MED2 nodes (nodes 6 to 11).

However, when the relative differences in Ru between approaches are analysed, results show that in all locations except for node 5 (CAD), values are low and mainly contained in the 0-5% (Figure 2.6). Notably, at CAD differences are ~10% and can go up to 20% for low slopes and high return periods (100-150 yr).

The general behaviour is an underestimation of Ru by the EV approach except for the locations of MED2 where the RS approach provided values ~0-5% lower than the EV one. Averaged Ru differences for dissipative (tanβ= 0.025) and reflective (tanβ= 0.20) profiles are nearly identical to the median, except for CAD, where differences in dissipative and intermediate slopes (~12%) are higher than in reflective profiles (~0-4%).

When the surge is added to Ru to obtain TWL at the beach, a switch towards overestimation by the EV approach is observed (Figure 2.6). This result is expected due to the adopted approach to combine both components.

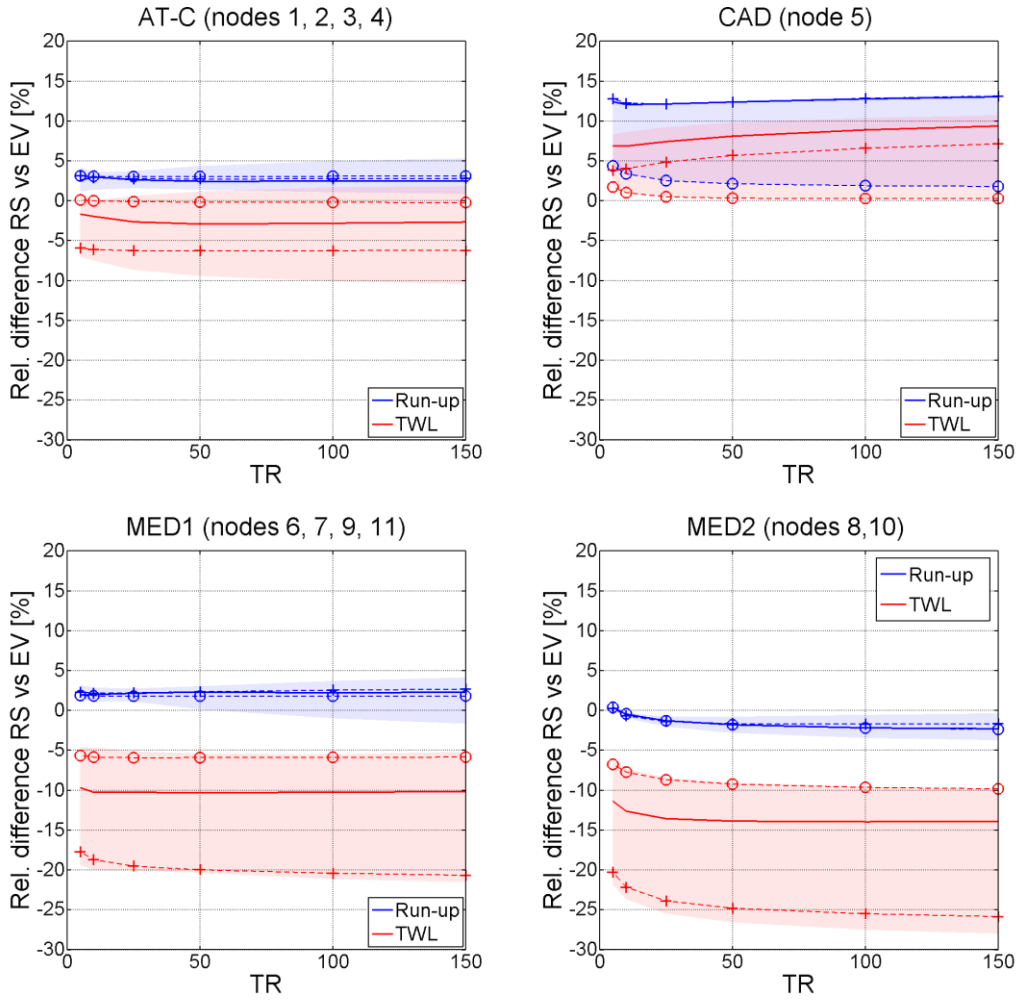

Figure 2.6. Differences between response (RS) and evenet (EV) approaches in run-up (Ru) and total water level (TWL). The solid line represents the median of the corresponding variable from all data nodes and beach slopes. The shaded area represents the 95% probability range. Dashed lines represent average results at tanβ= 0.025 (cross) and tanβ= 0.20 (circle).

The differences in TWL between both methods will depend on the previous differences in Ru and the local dependencies between waves and surges. Thus, at Mediterranean clusters, using the EV approach results in overestimation, with median between 10% and 15%. These differences are significantly higher for dissipative beaches (~20-25%) than for reflective (~5-10%), because the relative contribution of surge to TWL is higher (smaller Ru). The only exception is CAD, where intermediate slopes induce the largest differences. At the AT-C cluster, results also show an underestimation of the EV approach, although of smaller magnitude because of the smaller contribution of SU to the TWL. The exception is the node 5 where TWL values obtained by applying RS are larger. This change in behaviour is associated with the fact that this node presented the largest underestimation by the EV method in Ru values. The addition of the SU to obtain the TWL has a lower impact in CAD and AT-C than in MED1 and MED2.

2.4.3. Water volume estimators

Figure 2.7 shows obtained differences for overtopping discharge at the peak of the storm along the Spanish coast. The first aspect to be highlighted is that the differences and their variability significantly increase due to the properties of eq.2.4. This is illustrated in Figure 2.4, c-d where it can be seen that Q and TWV extreme distributions show a different shape for the EV and RS approaches.

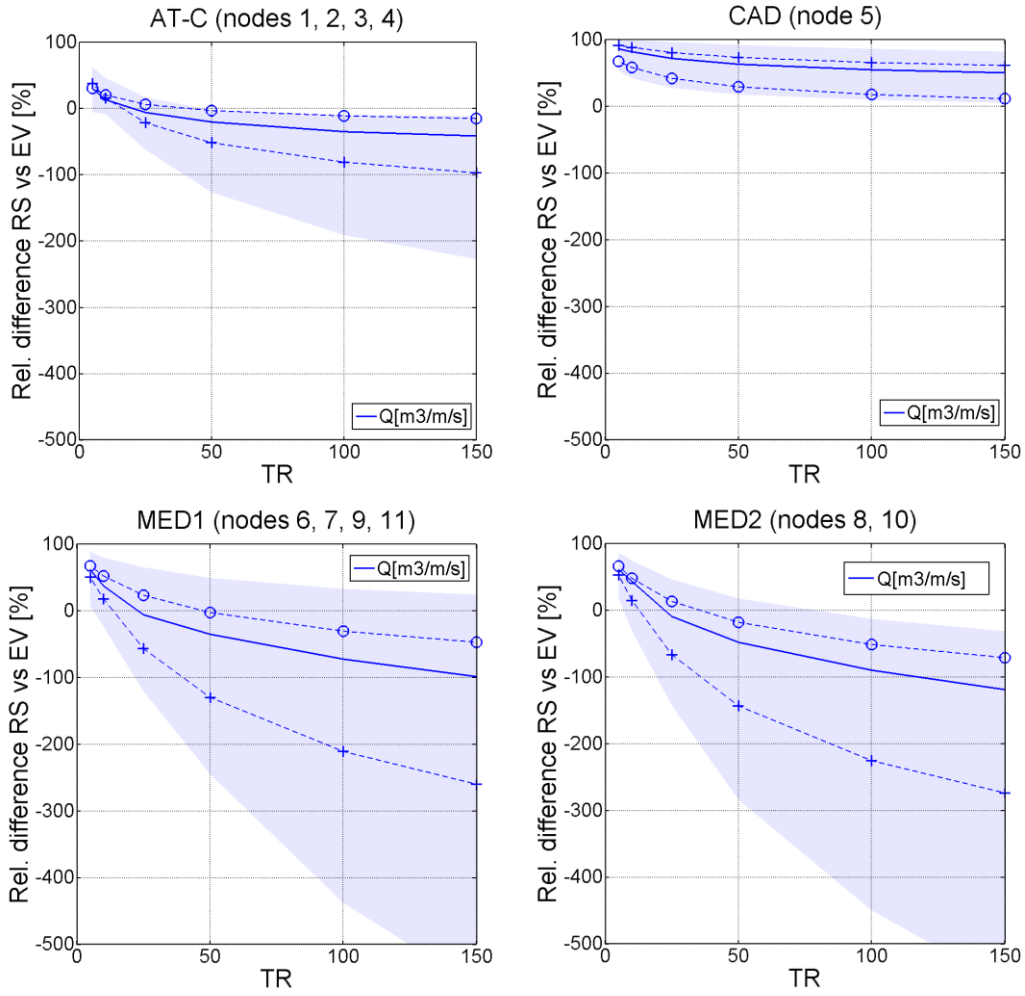

Figure 2.7. Differences between response (RS) and evenet (EV) approaches in overtopping (Q). The solid line represents the median from all of the data nodes and beach slopes-heights within groups. The shaded area represents the 95% probability range. The dashed lines represent average results at tanβ= 0.075 (cross) and tanβ= 0.20 (circle).

The results mimic the ones obtained for the TWL although with larger magnitudes. Thus, at MED1 and MED2, results show an overestimation of Q by the EV approach. The differences increase with TR reaching values up to 120% for TR of 150 yr. As for TWL, AT-C shows a similar response than the observed in the Mediterranean but of lower magnitude, with maximum differences up to 40% for TR of 150 yr. On the other hand, results for the CAD node show larger values of Q when using the RS method

and lower variability than in other locations. In this case, the differences slightly decrease with TR, reaching values of ~50-60% for TR between 100 and 150 yr.

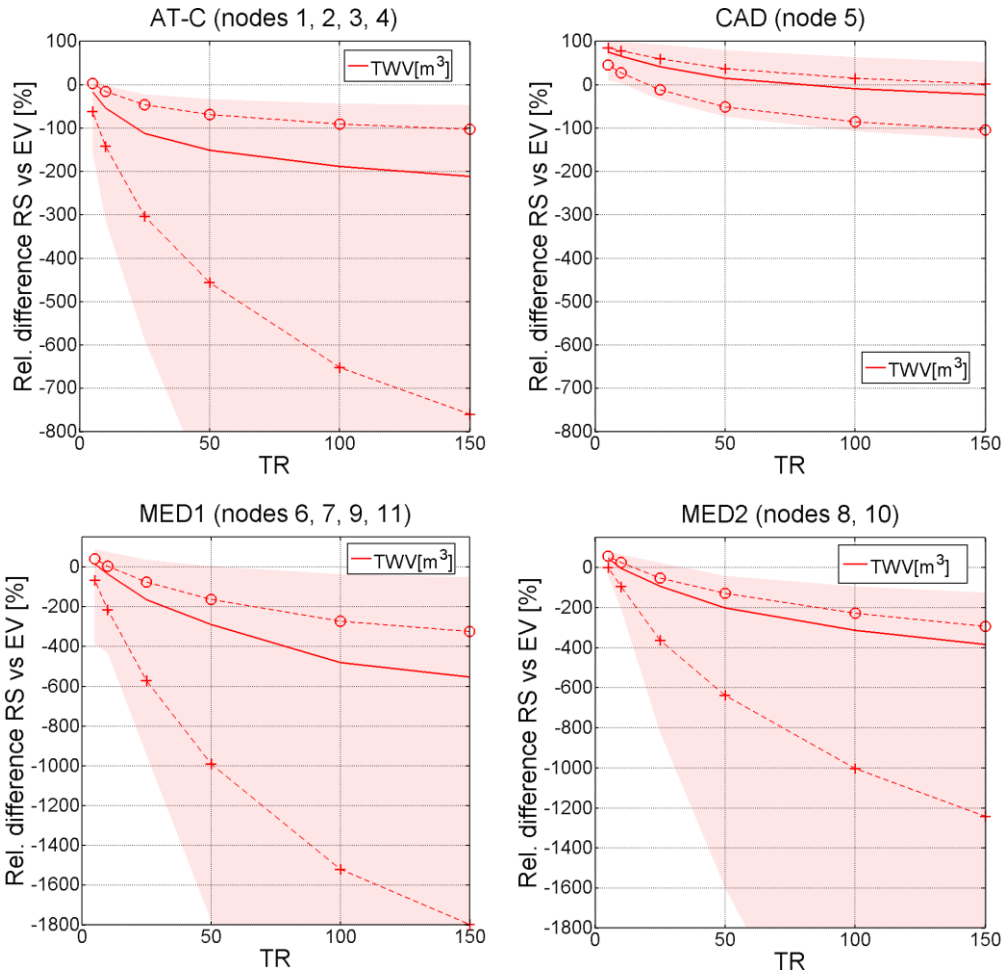

Figure 2.8. Differences between response (RS) and evenet (EV) approaches in total water volume (TWV). The solid line represents the median from all of the data nodes and beach slopes-heights within the groups. The shaded area represents the 95% probability range. The dashed lines represent average results at tanβ= 0.075 (cross) and tanβ= 0.20 (circle). Note that y-axis scale is different between upper and lower graphs.

When Q values are integrated over storm duration to obtain TWV, the calculated differences show the same behaviour than observed for Q (Figure 2.8). The magnitude of computed differences significantly increases at those clusters showing an overestimation of the EV method (i.e. AT-C, MED1 and MED2), reaching up to ~550% for TR of 150 yr. In the CAD node, the previously observed under-prediction by the RS method is reproduced for low-medium TR (10 to 50 yr) and switches towards over-prediction reaching ~25% for TR of 150 yr.

2.4.4. Inundation map estimation

Finally, to illustrate how the differences shown above can propagate to the final step in most of flood hazard assessments, the flood-prone area has been calculated for each cluster under identical conditions of TR, beach morphology (slope of 0.1 and beach height of 2 m) and topography. TWV results for the 100 yr TR are averaged (Table 2.3) and then used as boundary conditions to model inundation with LISFLOOD-FP.

The application of both EV and RS approaches leads to the inundation maps shown in Figure 2.9 and the corresponding inundated areas (Table 2.3).

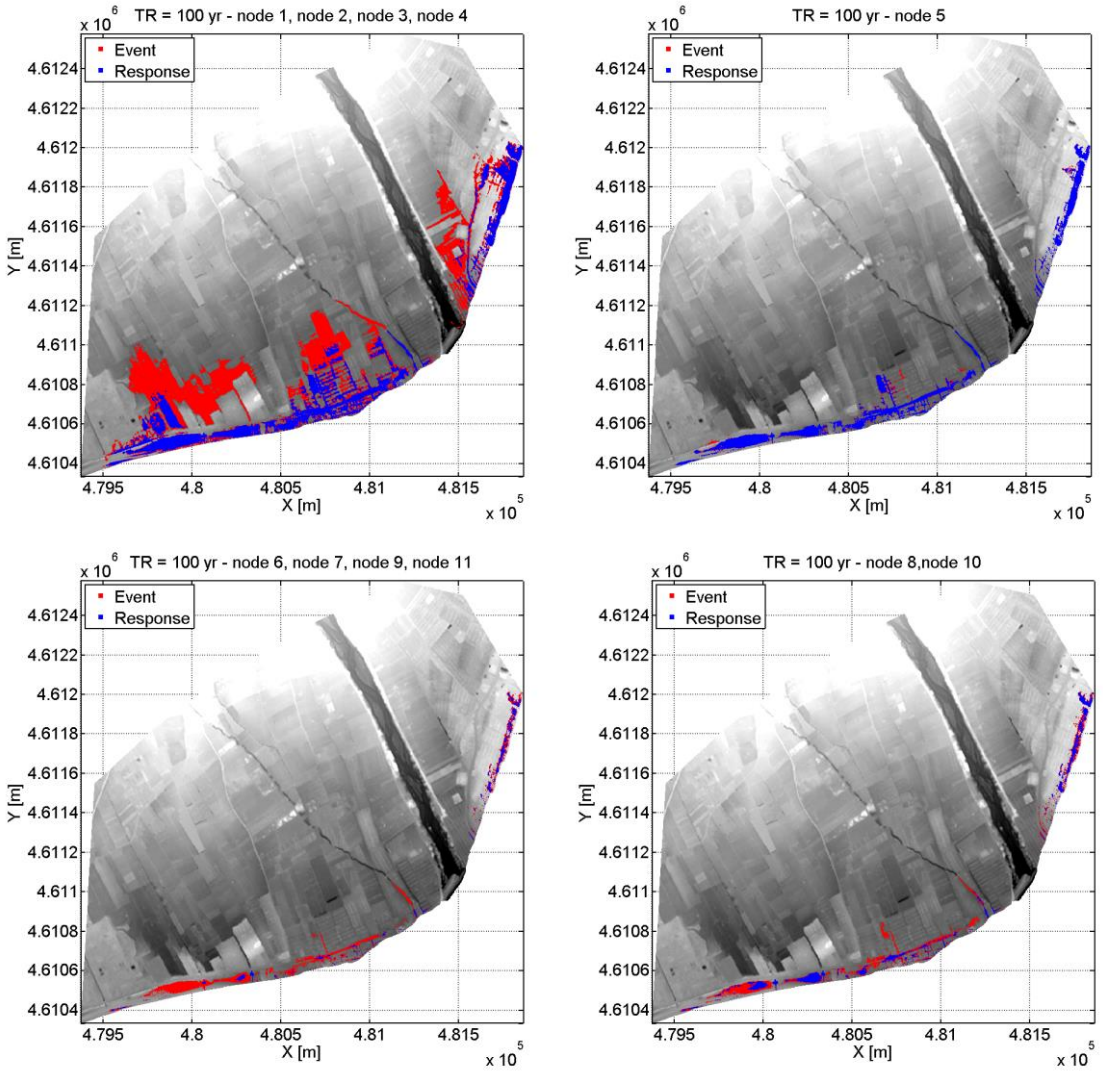

Figure 2.9. Inundation TR= 100 yr maps simulated for beach slope 0.1 and height 2 m over the Tordera Delta floodplain.

The results show, as expected, higher inundation differences in those cases where TWV differences were also greater. The divergence between EV and RS in terms of inundated area depends on the

morphology of the hinterland and the absolute magnitude of the TWV, which is significantly higher for Atlantic-Cantabric hydrodynamics than for Mediterranean conditions for the same beach morphology. The simulated scenarios illustrate different examples of what can be expected in inundation estimation regarding the choice between the EV and RS. For the simulated low-lying floodplain, a high TWV magnitude implies a large inundated area. AT-C (nodes 1 to 4) shows a 112% overestimation of EV in inundation given a TWV difference of 740% at the boundary. Lower TWV provides increasingly shorter inundation surfaces. Mediterranean locations (nodes 6 to 11) show between 75% and 123% EV overestimation, whereas differences were 3 to 5 time larger for the TWV at the boundary. CAD (node 5) presents low differences in both TWV and inundated surface (6 and 9% respectively, Table 3). In other words, the difference in the inundated area is proportional to the relative difference in TWV but highly modulated by the absolute magnitude of the TWV and the shape of the hinterland.

Table 2.3. Synthesis of inundation map results. Total water volume entering the hinterland and inundated surface calculated with the event and response approaches for TR= 100 yr, slope= 0.1 and freeboard= 2 m.

Variable	Case	Response	Event	Diff% (eq. 6)
TWV [m^3]	AT-C	152.420	1.279.800	-740%
	CAD	121.090	127.910	-6%
	MED1	7.924	36.031	-355%
	MED2	18.527	105.080	-467%
INUNDATED AREA [Ha]	AT-C	26.68	56.16	-111%
	CAD	15.34	16.70	-9%
	MED1	4.99	11.12	-123%
	MED2	7.64	13.34	-75%

2.5. Discussion

In this chapter differences resulting from the method to assign probabilities to inundation hazard estimators have been assessed. To this end, the use of the event and response approaches along the Spanish coast has been compared, in order to cover different wave and water level climates. The obtained results highlight the existence of differences between the approaches. The choice of the method, which is usually driven by data availability, can be a significant source of uncertainty in the inundation hazard assessment. The magnitude of the differences depends on the location where the assessment is performed since this determines the exposure to wave and water level conditions. The clustering analysis permitted identification of locations with similar differences in applying both methods. Thus, the results suggest the existence of two main areas along the Spanish coast with a differentiated behaviour, the Atlantic-Cantabric and the Mediterranean This result reflects that

differences in wave and water level climates not only affect the magnitude of induced hazard but also the expected uncertainty to assess their probability of occurrence. In addition to this big spatial division, two subgroups per area were also identified in terms of the quantified differences between methods in run up and total water level probability distributions.

The locations with higher differences when using Ru as hazard estimator can be related with high scatter of the Hs-Tp variables and thus with high variability (Figure 2.10). When assessing TWL, the correlation between SU and Ru is key to how the differences between approaches will propagate. To assess the incidence of this correlation, the Spearman Rho was used (see e.g., Genest and Favre, 2007). Notably, node 5 showed a singular behaviour for both Ru and TWL (Figure 2.6) and it has a high positive Hs-Tp scatter and the largest positive correlation in terms of Spearman Rho between Ru and SU (Figure 10). In contrast, the Mediterranean locations with larger overestimation of TWL with the EV method present negative values of the Spearman Rho. This should indicate that, in such places, the assumption of adding SU and Ru with a certain return level and obtaining a TWL with that same probability is less realistic, specially under conditions where SU mainly dominates the TWL, e.g. in dissipative conditions.

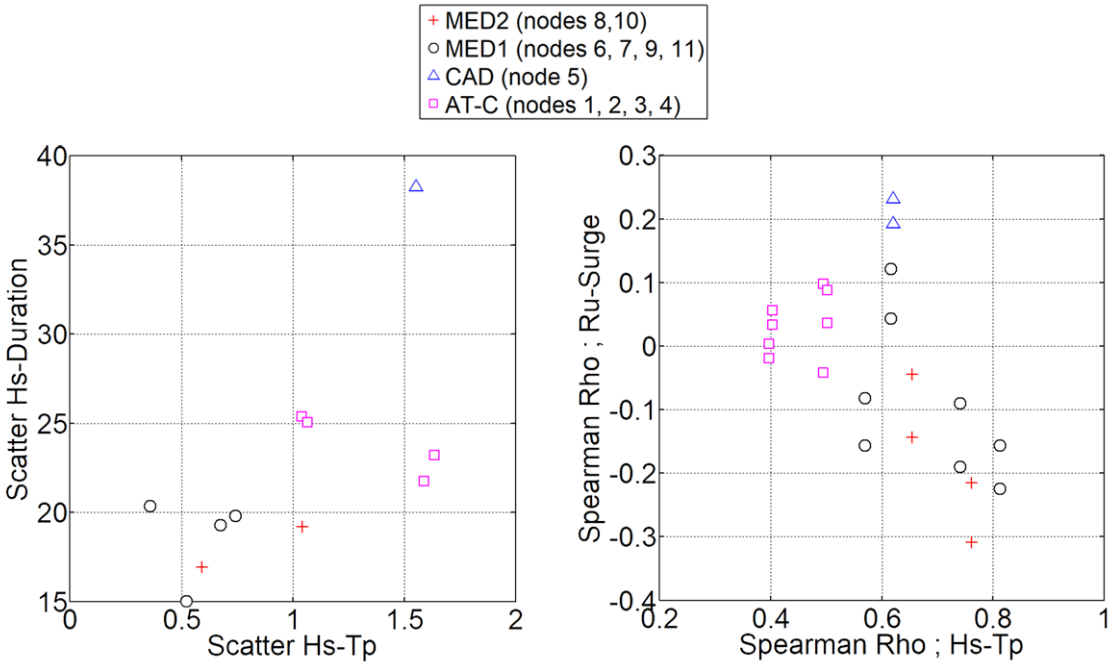

Figure 2.10. Wave height-period-duration scatters (left) and correlation wave height-period and run-up-surge by means of Spearman Rho analysis (right). Double values per node (right) refer to the 2 different Ru formulations in eq.2.1 and 2.2.

When calculating TWV, both the estimation of the duration of the event and the hypothesis about its shape introduces new assumptions in the event approach which lead to the increase of differences between methods. Locations showing a larger scatter of Hs-Dur (AT-C and CAD, Figure 2.10) also

concurrently show lower differences between the event and response in TWV (Figure 2.8). Although these nodes also showed lower differences in Q (Figure 2.7), compared to the Mediterranean locations, their relative increase from Q to TWV is also smaller. Thus, this may also suggest that the errors introduced by the assumption of the triangular shape of the storm evolution in time have a deeper impact (see Chapter 3).

In all cases, the increase in differences and variability from Q (Figure 2.7) to TWV (Figure 2.8) suggests that the assumptions introduced in the EV approach to derive the duration and the shape of the storm have a greater impact on the results than the choice between EV and RS. Differences between approaches, and therefore the degree of performance of the EV approach to approximate the RS one, generally worsen when using detailed hazard variables, i.e., TWV and inundation maps. In addition, variability and divergence between the approaches is observed to be larger in the locations presenting larger variability and less correlation between the involved variables in accordance with the observations of Divoky and McDougal (2006). When assessing the Q and TWV variables, the uncertainty due to the extreme value analysis is also larger, as denoted by a poorer fit by the GPD distributions. Closer attention to this aspect would allow better isolation of this component from the obtained results.

Thus, the event approach is only recommended for large-scale, less-detailed assessments (e.g., Stockdon et al 2007, Armaroli and Duo, 2018) where the target variable may be Ru or eventually TWL if the surge and waves are sufficiently correlated.

Results for TWV and inundated surface showed that differences between methods increase beyond an admissible range with large variability depending on the magnitude of the forcing and beach morphology. This implies that uncertainties are so large that many scenarios can be observed for the same return period: (i) large TWV differences with a large absolute TWV led to a large inundation extent and high differences (over 100% in the inundated area); (ii) similar TWV estimations with medium-large absolute magnitudes led to comparable inundation maps (a difference lower than 10%), but this was only observed in one out of 11 analysed nodes; and (iii) a large difference in TWV with medium-low absolute magnitudes led to a small inundation extent with high differences, which means that one of the approaches may cause a damaging inundation while the other may not cause any flooding beyond the beach itself. These different cases lead to different misleading conclusions in inundation risk assessment and, then, in decision making for coastal management. Thus, if the inundation assessment needs to be more detailed and in a smaller scale with the aim of obtaining discharges or inundation maps (e.g., Chini et al. 2012; Prime et.al 2016), the response approach would be preferable since errors introduced by the event approach may no longer be admissible.

2.6. Conclusions

The event and response approaches to assign probabilities to the intensity of the inundation hazard were compared at 11 locations covering all wave and water level climates around Spain. The magnitude of the differences between methods is location-dependent. Similarities in wave and water level climates influence not only the magnitude of the hazard but also the uncertainty when obtaining their probability of occurrence. Notably, the results highlight that overall relative differences between approaches are higher at the Mediterranean Spanish basin than in the Atlantic and Cantabric locations, due to a milder climate with weak correlation between waves and water levels in the Mediterranean.

Although the response approach is the direct way to obtain the probability of occurrence of coastal inundation hazards due to the multivariate dependence of involved variables, if data availability forces the application of the event approach for inundation assessments, the run-up or total water level (with good correlation between waves and surge) distributions reasonably approximate those of the response approach with lower associated uncertainty. If the inundation assessment aims to create an output for overtopping discharges or inundation maps, observed errors of the event approach suggest that it would produce misleading conclusions in inundation-related coastal management and decision-making.

Thus, the differences between approaches also depend on the estimator used to assess the inundation hazard. The performance of the event approach worsens as the estimator is closer to the inundation maps, where simplifications in the duration and assumptions on the shape of the storm have a great impact. The results indicate that the choice of the method, which is usually driven by data availability, is an important source of uncertainty in the inundation hazard assessment.

CHAPTER 3.

Uncertainty associated to the use of synthetic triangular storms for storm-induced hazard simulations.

Adapted from: Duo, E., Sanuy M., Jiménez, J.A., Ciavola, P., (n.d.). On the Ability of Symmetric Triangular Synthetic Storms to Represent Real Events for Coastal Hazard Modelling. Submitted

This chapter assesses an additional common source of uncertainty in storm-induced impact assessment. When real storm timeseries are not available and only bulk information is accessible, synthetic timeseries are usually built by assuming simplified storm-shapes. One of the most common approaches in coastal studies is the use of symmetric triangular synthetic storm shape (STSS) that is characterized by the assumptions that (i) the peak of the waves occurs in the middle of the storm, and (ii) the forcing varies linearly (see e.g. Chapter 6, where these are used to represent some storm conditions).

3.1. Introduction

The reliability of the quantification of the hazard component is crucial for coastal risk studies. Coastal inundation and erosion hazards must be satisfactorily evaluated, especially when dealing with local assessments on sandy beaches. As an example, the magnitudes of the water discharge inundating the hinterland, or the eroded sediment volume are important for adequately evaluating the associated consequences for exposed elements. Moreover, local managers are interested in quantitative information to design risk reduction measures, such as dikes or nourishments, and to prepare management plans.

Nowadays, hazard assessments largely rely on numerical model simulations. Models are indeed capable of reproducing a large amount of processes affecting the interaction between the beach morphology and the storm event, to provide results from multiple hazards (Roelvink and Reniers, 2012). Nonetheless, these models rely on assumptions and simplifications that may produce unreliable results, when compared with observed coastal hazards. As example, the main factors affecting the simulation of flooding in urbanised coastal areas are linked to the mathematical formulations, the topographic data and the forcing boundary conditions (Gallien et al., 2018). Generally, the degree of robustness of a numerical model is related to the data availability and reliability. This is valid for the information on the morphology of the beach, the characteristics of the sediment, and the hydrodynamics. Therefore, the storm event needs to be suitably described and included in the numerical models as forcing data. Continuous (observed or hindcasted) storm time-series data of waves and water levels (WLs) are important for capturing the evolution of the event and, thus, its dynamic interaction with the beach.

When continuous forcing time-series data are unavailable, the event is generally described through observed or assessed bulk information, e.g. maximum significant wave height (Hs), peak wave period (Tp), maximum WL (mean sea level +surge+tide), duration (Dur) and main direction (Dir). The lack of continuous data leads to the introduction of simplifications and assumptions to proceed with the analysis of the storm hazard impacts. The most simplified approaches calculate impacts directly using statistical bulk information (see Ranasinghe and Callaghan, 2017). However, accounting for wave and WL variations during the storm is necessary for feeding process based numerical models (see e.g. Roelvink et al., 2009). In these cases, the evolution of the storm must be defined by means of a synthetic shape, hereafter called a synthetic storm (SS), with the assumption that it is representative of the real storm (RS). SSs are regularly used to define the shape of probabilistic storm events (i.e. representative of a

given return period). A first attempt to standardise a procedure for SS applications can be found in Carley and Cox (2003), wherein they proposed a synthetically designed storm with exponential-like growth and decay phases and a symmetrical evolution around the peak. This was obtained by assessing Hs exceedances over various durations and associated with different return periods. In contrast, a similar but simpler (linear) approach that is widely applied in coastal studies is the symmetric triangular synthetic storm (STSS) (e.g. McCall et al., 2010; Corbella and Stretch, 2012). It represents the evolution of an event from its bulk characteristics at the peak and in the storm duration. STSSs are often used to cover all of the possible combinations of forcing (including those not previously recorded) when hazard and risk assessment approaches are applied by simulating a large number of realistic storm conditions (e.g. Poelhekke et al., 2016; Plomaritis et al., 2018; Chapter 6).

Thus, the use of any type of SS represents a useful approach for coastal hazard assessments and the use of an SS is recommended for planning purposes by Nielsen and Adamantidis (2007). However, SSs show some inherent limitations and represent an additional source of uncertainty in the analyses. Sánchez-Arcilla et al. (2009) compared computed erosion impacts from RSs and SSs in the Spanish Mediterranean. The study used schematised, linearly-varying Hs and Tp mimicking the shape of the RS, and thus would have had little practical application if only the bulk parameters were known (e.g. as in the case of the STSS). Callaghan et al. (2009) assessed the reliability of the approach proposed by Carley and Cox (2003) for erosion assessments at Narrabeen Beach (Sydney, Australia), by comparing erosion impacts computed from adopting statistical events (i.e. representative of given return periods and simulated with synthetically-designed storms) and statistics of measured impacts. This study found a tendency to underestimate the computed eroded volumes with return periods between three and ten years. However, the results in Callaghan et al. (2009) comprise two different components of the uncertainty: the use of the SS, and the uncertainty of the methodology for assigning probabilities to the hazard (Chapter 2). Therefore, the effect of the synthetic approach on the uncertainty was not isolated. No study has ever assessed the role of commonly used SSs in the propagation of uncertainties when modelling both coastal inundation and erosion hazards.

Within this context, the main aim of this work is to investigate the differences in storm-induced erosion and inundation assessment associated with the definition of storms (i.e. RS versus SS time-series) when using numerical modelling. The focus of this study is on the use of the most common and straightforward way of defining a SS, i.e. the symmetric triangular synthetic storm (STSS). To this end, the magnitude of coastal flooding and erosion is assessed using an extensive dataset of RS data and their equivalent synthetic representations. The obtained variations are analysed and are characterised from the differences observed in the storms. The analysis is performed for real conditions typical of the Northern Adriatic and North-Western Mediterranean coasts (Figure 3.1a). They cover beach profiles ranging from dissipative to reflective, subjected to storm conditions ranging from moderate to extreme. Storm-induced hazards were simulated with the XBeach-1D model (Roelvink et al., 2009), which can be considered as a state-of-the-art model for simulating the impact of extreme events and, which is one of

the most used models for this purpose (e.g. McCall et al., 2010; Vousdoukas et al., 2012; Williams et al., 2015; Harley et al., 2016; Passeri et al., 2018; see Chapter 5).

The inclusion of these two sites permits to increase the robustness of the analysis by anlarging the range of forcing and receptor characteristics aiming to obtain a higher representativity of the Mediterranean conditions.

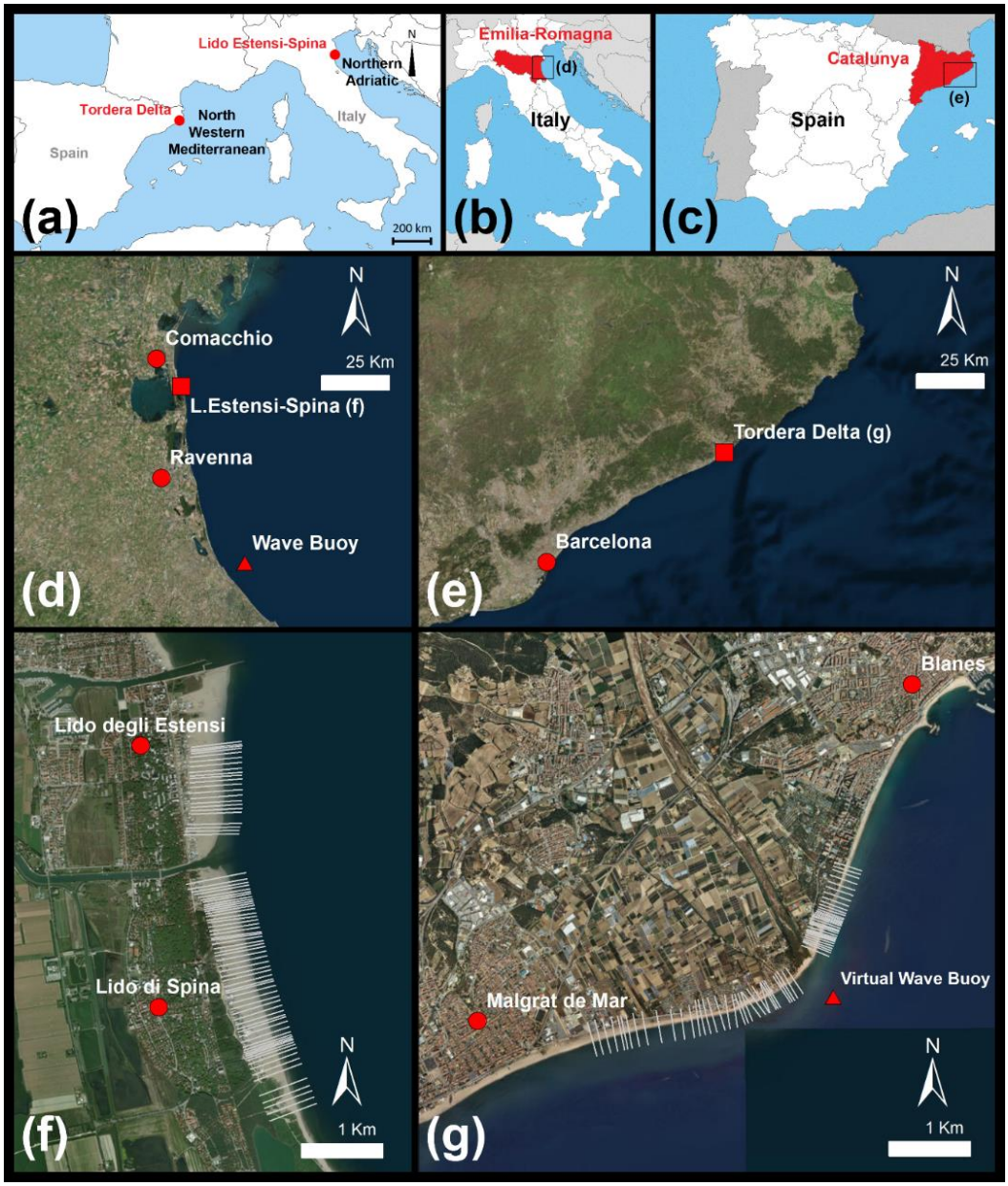

Figure 3.1. (a) Locations of the sites in the Northern Adriatic and North-Western Mediterranean Seas. The site (f), i.e. Lido Estensi-Spina is located on the (b,d) Emilia-Romagna (Italy) coast, whereas the site (g), i.e. the Tordera Delta is on the coast of (c,e) Catalunya (Spain). The main cities and towns are shown in (d), (e), (f), and (g) as circles. The locations of the wave buoys used to retrieve the wave data used in this study are shown in (d) and (e) as triangles. The partial tracks of the profiles used to select the representative data analysed in this study are shown in (f) and (g) as grey lines.

3.2. Methods and data

3.2.1. Study area and data

The study area comprises two coastal stretches: in the Northern Adriatic (hereafter NA), Lido degli Estensi-Spina (Italy); and in the North-Western Mediterranean (hereafter NWM), the Tordera Delta (Spain) (Figure 3.1). These two areas are composed by fine and coarse sandy beaches, respectively. Both have been impacted by coastal storms, and they have already been classified as critical coastal sectors at the regional level (Armaroli and Duo, 2018; Chapter 4). Sun-and-sand tourism is the main coastal economic sector at both sites and, owing to this, the related infrastructures and services (e.g. beach facilities, campsites, restaurants) are directly located on the beach, or in the immediate first part of the hinterland. Thus, these beaches provide space to accommodating beach users during the bathing season, and protection to the hinterland during the storm season. The general characteristics for each site, as well as the main references regarding site conditions can be found in Table 3.1. The main data used in the analysis are shown in Table 3.2.

Table 3.1. General information on the sites (see Figure 3.1) where the datasets were collected.

Site	Sea Basin	Environment	Tidal range (m)	Storm Surge (m)	Waves (m)	Main references for regional and local scales
Lido degli Estensi-Spina (Comacchio, Italy)	Northern Adriatic (NA)	Micro-tidal; Low-energetic; Dissipative.	neap: 0.3-0.4 spring: 0.8-0.9	1-in-10 yrs: 0.72	Mean H_s: ~0.4 Max H_s: 4.6*.	Armaroli et al., 2012; Armaroli and Duo, 2018; Duo et al., 2018; Chapter 6
Tordera Delta (Blanes-Maresme, Spain)	North-Western Mediterranean (NWM)	Micro-tidal; Medium-energetic; Intermediate-reflective.	neap: 0.2-0.25 spring: 0.3-0.4	1-in-10 yrs: 0.51	Mean H_s: ~0.7 Max H_s: 5.4**	Mendoza et al., 2011; Chapter 2 Chapter 4; Chapter 6.

*recorded in February 2015 at the buoy in Figure 3.1f; ** at the virtual node in Figure 3.1g (Camus et al. 2013).

3.2.2. Real storms

The first step in the analysis consists of defining the storms. To this end, similarly to Chapter 2, storms were identified at each site by applying the peak-over-threshold (POT) method with a double threshold for Hs, i.e. the 0.98 and 0.995 quantiles of the respective time-series, and by imposing a minimum Dur based on local experience (see table 3.3). The first Hs threshold (0.98 quantile) was used to calculate Dur and to define the period between consecutive events. Events with shorter durations than the

minimum Dur are not considered. In consecutive peaks, when conditions under the threshold lasted less than the meteorological independence criterion (Table 3.3), peaks were considered as part of the same storm event. The second Hs threshold was applied to identify the most significant storms, which are defined here as extreme events. Table 3.3 summarises main characteristics of the POT analysis for both sites. A total of 227 storms were identified to build the storm dataset (48 and 179 for the NA and NWM basins, respectively). As both wave datasets correspond to different water depths (10 m at NA, 20 m depth at NWM; see Table 3.2), the NA storms were linearly back-propagated to the 20 m depth, to generate a consistent dataset.

Table 3.2. Summary information on the topo-bathymetric and wave datasets.

Site	Dataset	Type	Resolution	Period	Source
IT	Wave time-serie (Hs, Tp, Dir)	Offshore buoy Wave buoy at 10 m depth (see Figure 3.1f)	0.5 h	2007-2018 (83% coverage)	ARPA E-R Available at: https://simc.arpae.it/dext3r/
	Topography (DSM)	Lidar	1 x 1 m	October 2014	National Petrol Company, Eni
	Nearshore Bathymetry	Lidar	1 x 1 m	2012	National Petrol Company, Eni
	Offshore Bathymetry	Multibeam	1 x 1 m	2013	National Petrol Company, Eni
ES	Wave time-serie (Hs, Tp, Dir)	DOW hindcast 20 m depth virtual buoy (see Figure 3.1g)	1 h	1960-2014	IH-Cantabria (Reguero et al., 2012; Camus et al., 2013)
	Bathymetry	Multibeam	1 x 1 m	2010	Ministry of Agriculture, Food and Environment
	Topography (DSM)	Lidar	1 x 1 m	2010	Institut Cartogràfic de Catalunya Available at: www.icgc.cat

Once the storms were identified, each storm was characterised through a set of parameters: Hs at the storm peak (Hs,max), associated Tp, Dir, Dur, energy content (E), and energy at the storm peak (Ep). The energy content (E) is calculated as:

$$E = \int Hs^2 \, dt \tag{3.1}$$

The Ep is calculated at the peak of the storm, which is defined as the period in which Hs > 0.85·Hs,max.

Table 3.3. Summary information on the thresholds applied at the two sites to isolate the extreme events. The thresholds refer to the original wave time-series, no linear (back-)propagation was applied at this stage of the analysis.

Site ID	Sea Basin	Hs 98% Quantile	Hs 99.5% Quantile	Minimum Storm Duration	Meteorological Independence Criterion	Nr. of Isolated Storms
IT	NA	1.85 m	2.6 m	4 h	12 h	48
ES	NWM	2 m	2.6 m	6 h	72 h	179

3.2.3. Synthetic storms

To define a SS representing a real event, a simple shape describing the evolution of wave parameters during the storm must be selected (see e.g. McCall, 2010; Poelhekke et al., 2016; Sanuy et al. 2018). As previously mentioned, this work focuses on the use of STSS, where Hs linearly grows from the threshold value up to a Hs,max halfway through the storm duration. From here, it linearly decreases down to the threshold value (Figure 3.2).

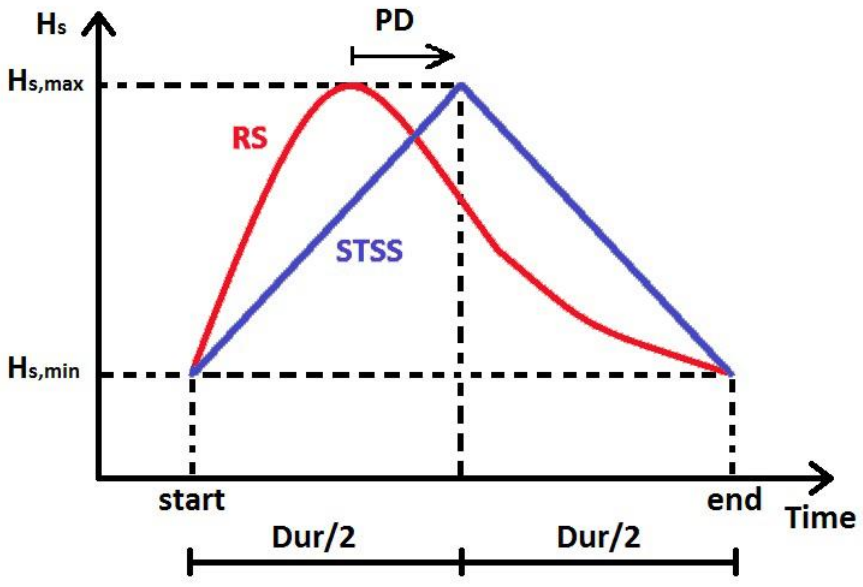

Figure 3.2. Schema of the real storm (RS; in red) and its representation with the symmetric triangular synthetic storm (STSS; in blue). The peak delay (PD) is graphically defined.

To assign the corresponding wave periods to each STSS, an empirically derived Hs-Tp relationship, separately assessed for each storm dataset, is used (see e.g. Mathiesen et al., 1994). It has to be considered that this assumption introduces differences in real and synthetic wave periods which are not caused by the adoption of a given shape. However, this would be a common procedure when the use of a SS is needed, e.g. as it is the case of adopting the event approach to assess coastal hazards (see Chapter 2). The direction of the storm (Dir) would correspond to the mean wave direction during the peak of the event, although in this study it is not considered. This is because in this analysis, the worst-case scenario is considered, which corresponds to normal incidence. This study focuses on the schematization of the wave component, and thus, the effects of time-varying WLs (i.e. MSL+surges + tides) are ignored, and the WL is schematised as a constant for the duration of the storms.

To compare the SSs and RSs, a set of parameters have been selected. These parameters essentially characterise differences in storm shape (storm peak) and E (see table 3.4). The peak delay (PD) is defined as the delay between the peaks of the RSs and SSs (Figure 3.2).

Table 3.4. Summary of the indicators adopted to quantify the comparison between real and synthetic time-series of the storms. The subscripts of the variables in the formulas refers to the real (r) and synthetic (s) storm.

Symbol	Name	Formula
ΔE	Energy relative difference	$100 \cdot (E_s - E_r)/E_r$
ΔEp	Peak energy relative difference	$100 \cdot (Ep_s - Ep_r)/Ep_r$
ΔTp	Peak period relative difference	$100 \cdot (Tp_s - Tp_r)/Tp_r$
ΔPD	Relative peak delay	$100 \cdot [t(Hs, max_s) - t(Hs, max_r)]/(0.5 \cdot Dur)$

3.2.4. Modelling of storm induced hazards

To simulate storm-induced hazards, a process-based morphodynamic model called XBeach (Roelvink et al., 2009) was used here, and was applied in profile mode (1D), similarly to Vousdoukas et al. (2012) and Harley et al. (2016). Beach morphology, WL, waves and water discharge were simulated and stored during the entire simulation of the storms. The parameters of the model were defined as the default values except for morfac (5), D50, D90 (see Table 3.5), and bedfriction (white-colebrook-grainsize). In this way, the friction was calculated as a direct function of the sediment grain size.

In this application, topographic and bathymetric datasets (Table 3.2) of each site were merged to build a coastal digital terrain model, from which a significant number of profiles (i.e. 80 at the site in Italy, Figure 3.1f; and 67 at the site in Spain, Figure 3.1g) were extracted to describe the local morphology of the beach in detail. At each site, the extracted profiles were classified into five groups, covering the range of local beach morphology. Grouping was performed by minimising the variability of all profiles with respect to an average profile, which was used to represent the beach morphology of the sector. This

resulted in five average profiles for each site (Figure 3.3). The basic characteristics of the representative profiles and sediments (D50 and D90) are summarised in Table 3.5.

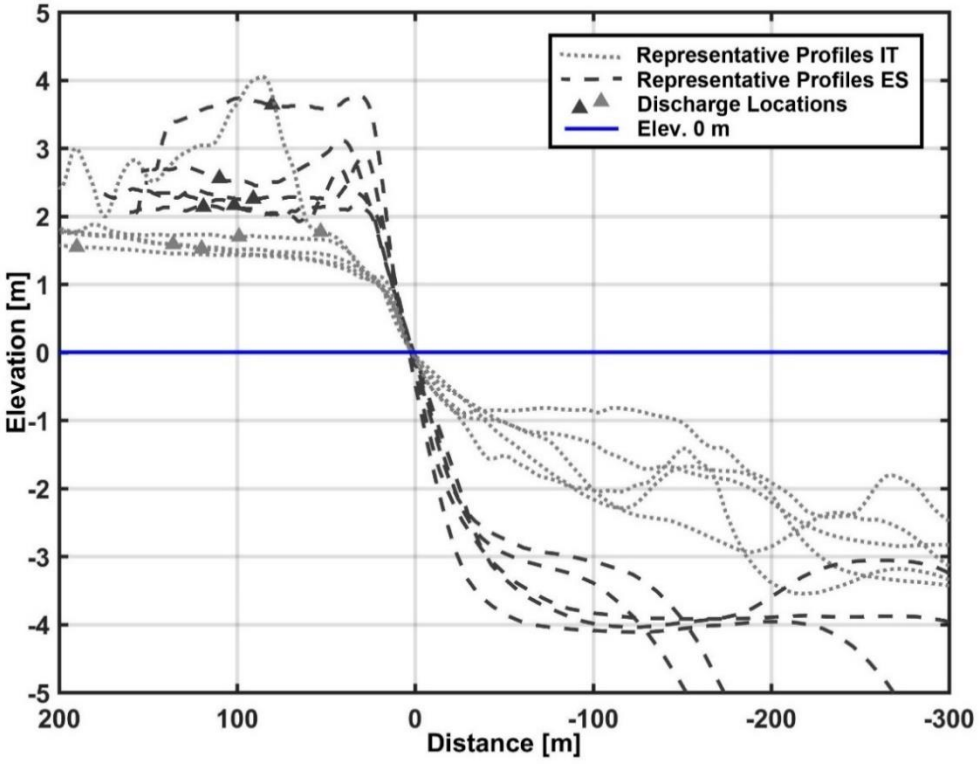

Figure 3.3. Overview of the profile dataset with indication of the discharge positions.

Table 3.5. Summary information on the profile dataset.

Site ID	Grain size [mm]		Representative Average Profile	Berm Elevation [m]	Slope	Dune	Bar
	D50	*D90*					
IT	0.23	0.3	1	1.06	0.013	Yes	Yes
			2	0.79	0.012	No	Yes
			3	1.00	0.012	No	Yes
			4	0.95	0.009	No	No
			5	1.11	0.005	No	Yes
ES	1.3	1.9	1	3.76	0.037	No	No
			2	2.89	0.032	No	No
			3	3.11	0.021	No	No
			4	2.70	0.016	No	No
			5	2.10	0.016	No	Yes

The storm conditions for the simulation consisted of 227 real events (see Section 3.2.2), and their 227 synthetic representations (see Section 2.3). Each real and synthetic event was simulated for each of the 10 profiles. To include the potential variability owing to the mean sea level conditions, three WL scenarios were defined (baseline WL, +0.25 m, +0.75 m). As a result, a total of 13620 simulations were computed.

The obtained results were the morphology and water discharge for each simulation. The water discharge (Q) time-series was extracted for each profile at the locations shown in Figure 3.3. The discharge positions were defined in areas that were not significantly affected by erosion for the entire dataset of simulations, and that were close enough to the shoreline to capture significant floodwater volumes.

3.2.5. Analysis of simulated hazards

The eroded volume (EV) of the emerged beach (i.e. from the shoreline to where erosion ends) was calculated by comparing the initial and post-storm profiles. The maximum and significant (i.e. the average of the highest third, to capture the average magnitude near the peak of the event) water discharges were calculated (as Qmax and Qs, respectively), as well as the total water volume (TWV) inundating the hinterland. These variables give quantitative information on both the peak of the storm (i.e. Qmax) and its event-integrated values (i.e. EV, Qs, and TWV).

For each variable, the differences between the real- and synthetic-driven outputs were assessed through the expressions shown in Table 3.6. Positive values of the comparative variables indicate an over-estimation of the STSS in comparison to the RS, and vice versa. The use of relative differences can, however, generate misleading interpretations of the results for high-intensity events, as important absolute differences are smoothed relative to a large hazard output.

Table 3.6. Summary of the functions adopted to quantify the comparison between real- and synthetic-driven outputs.

Symbol	Name	Formula
ΔQD	Relative Peak Discharge Delay	$100 \cdot [t(Qmax_s) - t(Qmax_r)]/Dur$
ΔQ_s	Significant Discharge Relative Difference	$100 \cdot (Qs_s - Qs_r)/Qs_r$
ΔQ_{max}	Maximum Discharge Relative Difference	$100 \cdot (Qmax_s - Qmax_r)/Qmax_r$
ΔTWV	Total Water Volume Relative Difference	$100 \cdot (TWV_s - TWV_r)/TWV_r$
ΔEV	Eroded Volume Relative Difference	$100 \cdot (EV_s - EV_r)/EV_r$

3.3. Results

3.3.1. Storm characteristics

The application of the POT method to both datasets resulted in a total of 227 storms, 48 in the NA and 179 in the NWM basin. As mentioned before, because the NA wave data were recorded at 10 m depth, the storm Hs values were back-propagated to the 20 m depth, to obtain the corresponding offshore values and thereby generate a consistent dataset. Main characteristics of the identified storms (RS) at each site can be seen in Figure 3.4.

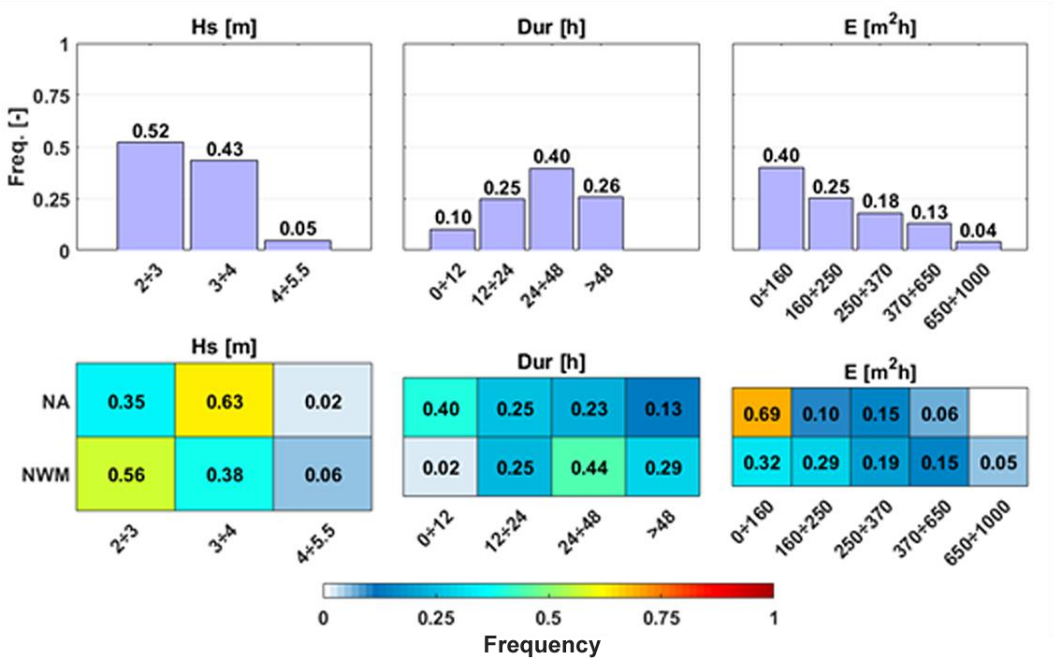

Figure 3.4. Overview of the storm dataset. The distribution of storm characteristics (Hs, Dur, E) is given for the whole dataset (top panels) and for the subset of storms identified at the two Mediterranean sites (bottom panels). NA storms were linearly back-propagated to the 20 m depth to ensure the consistency of the dataset of storms.

The comparison between the normalized shapes of RSs versus its reproduction by means of the use of SSTSs is shown in Figure 3.5, where the median and associated 75% probability range (given by the 0.175 and 0.825 quantiles) of the normalized Hs time series of both storms are represented. As can be seen, the STSS mimics the typical Hs evolution, although some differences also occur. The average RS shows higher growth rates during a shorter Dur as compared to the average STSS. The average shape of the RS presents a plateau indicating a natural variability in the occurrence of the peak during the storm. Differently (and by definition) the average STSS shows a point peak at the middle of the storm. The shadowed areas in Figure 3.5 represent the variability of the Hs evolution during the storm, which as expected, is larger for the RS.

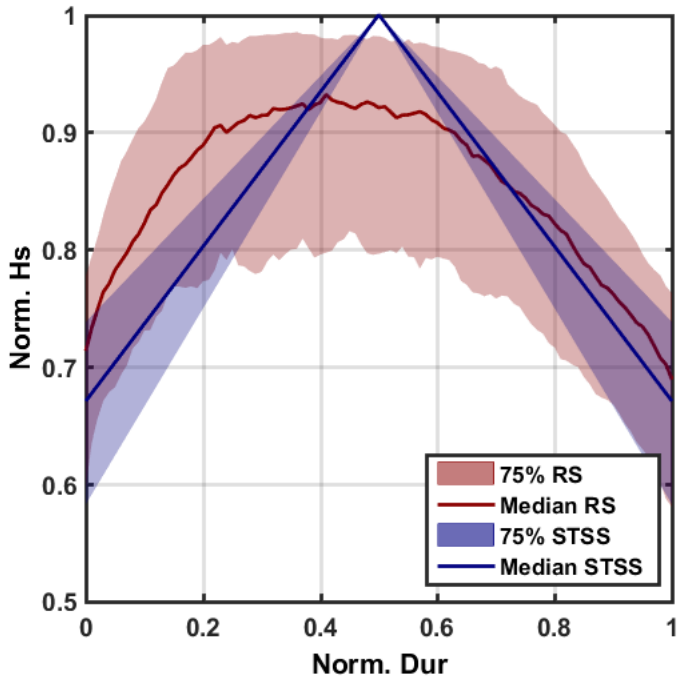

Figure 3.5. Graphical comparison between the normalised real (red) and synthetic (blue) storms calculated for the whole storm dataset. The median is represented through solid lines. The shadow area represents the 75% of the dataset given by the 0.175 and 0.825 quantiles.

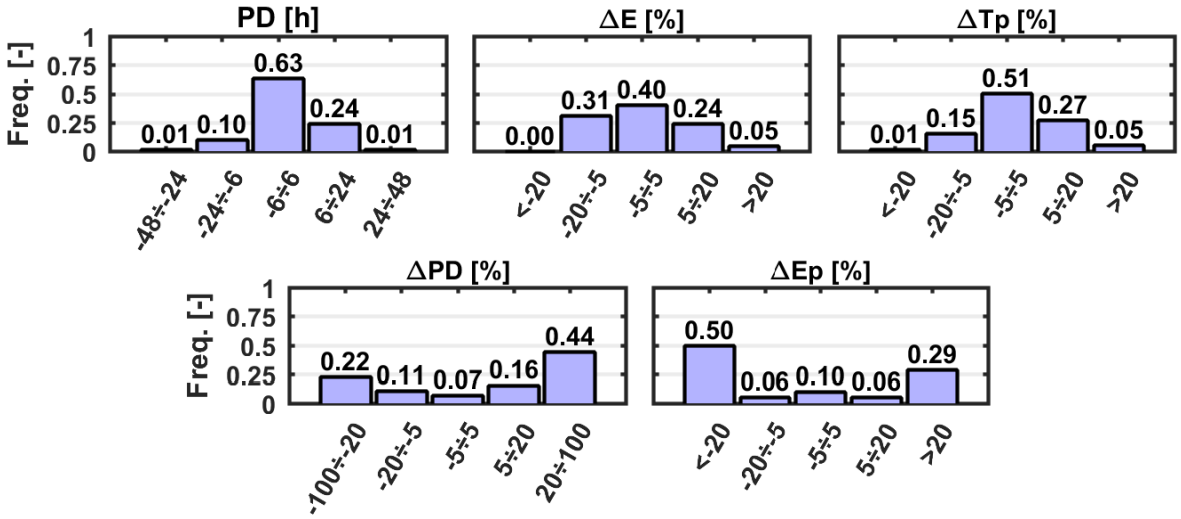

Figure 3.6. Variability in storm properties between STSS and RS according selected control parameters (table 3.4).

Figure 3.6 illustrates a comparison between parameters defining RSs and SSs, in terms of the relative differences in PD, E, Ep and Tp. As can be seen, the timing of the storm peak (PD) is reasonably well

captured, with more than 60 % of the total cases having a phase lag shorter than 6 h. In general terms, the adopted symmetric shape of the SSTS resulted in peaks slightly more frequently delayed with respect to the RS. However, when this parameter is measured in relative terms (ΔPD), the results indicate that 66% of storms present a phase lag of the peak that is longer than 20 % of the storm Dur (as a reference this corresponds to a phase lag of ~10 h on a 2-day storm). With respect to the E, about 40 % of the cases were well reproduced by using the STSS as they presented a relative difference smaller than 5 %. The remaining cases presented both higher and lower energy values with a slight tendency to underestimate E. If we focus on the Ep, the STSS poorly represented the reality, with a clear tendency to underestimate the variable. This can be easily understood by simple inspection of Figure 3.5, i.e. STSSs presents always a single point peak whereas RSs usually have a longer peak Dur. As a consequence, the integration of the E is performed during a longer period. Figure 3.6 also shows the differences in Tp between the STSS and RS. Although not directly related to the adopted shape for the SSs, as it can be seen, results show that the adopted approach reasonably reproduces real wave periods (more than 50 % of the cases presented a difference lower than 5% in Tp). The remaining cases show a slight tendency towards overestimating Tp.

3.3.2. Storm-induced hazards

The previously-obtained differences in storm definition propagate to differences in hazard estimation. Figure 3.7 shows examples of model outputs from integrating the results of all of the performed simulations. The median of the position of the post-storm profile and normalised discharge time-series and the associated 75% probability ranges given by the 0.825 and 0.175 quantiles for the RS and STSS, respectively, are presented for two profiles of the dataset (one intermediate-reflective and one dissipative). The discharge normalization was implemented considering the average value between the real and synthetic Qmax for each combination storm-profile. The normalised discharges in Figure 3.7 provide information on how the STSS and RS compare in different phases of the storm relative to Dur, and cannot be interpreted to compare discharge peaks. This is because all STSSs have their peak in the centre of the storm, whereas only 7% of RSs do.

When assessing results across all profiles, the analysed events induced erosion and inundation hazards covering a large range of values (Figure 3.8). Thus, approximately 60% of the cases induced an inner EV larger than 60 m^3/m (this is equivalent to an average beachface retreat of approximately 30 m, assuming 2 m of beachface height), and more than 10% generated an erosion larger than 120 m^3/m (this is equivalent to an average beachface retreat of approximately 60 m, assuming 2 m of beachface height). With respect to inundation, about more than approximately 25% of the events resulted in a TWV overtopping the beach and larger than 100 m^3/m (as reference, this is an average discharge of ~0.001 m3/s during 24 h of storm).

The use of the STSS to represent the RS resulted in a general underestimation of storm-induced EVs (Figure 3.8), with approximately 20% of the cases underestimating EV by more than 20%. With respect to the inundation hazard, analysed variables were not properly simulated by using the STSS. As it can be seen in Figure 3.7, the differences in the flood-related hazards are larger. In general, and independently of the beach type, the use of the STSS results in an under-prediction of the water discharge during most of the event, except during the central phase of the storm, when the discharge tends to be overestimated. This agrees with the obtained phase lags for the peak discharge (ΔQD, Figure 3.8). Overall, only a few cases resulted in a good reproduction of the maximum and/or significant discharges (Qmax and Qs), or the TWV. Notably, most of cases underestimated or overestimated these variables with relative errors larger than 20%, with a higher tendency towards underestimation (Figure 3.8).

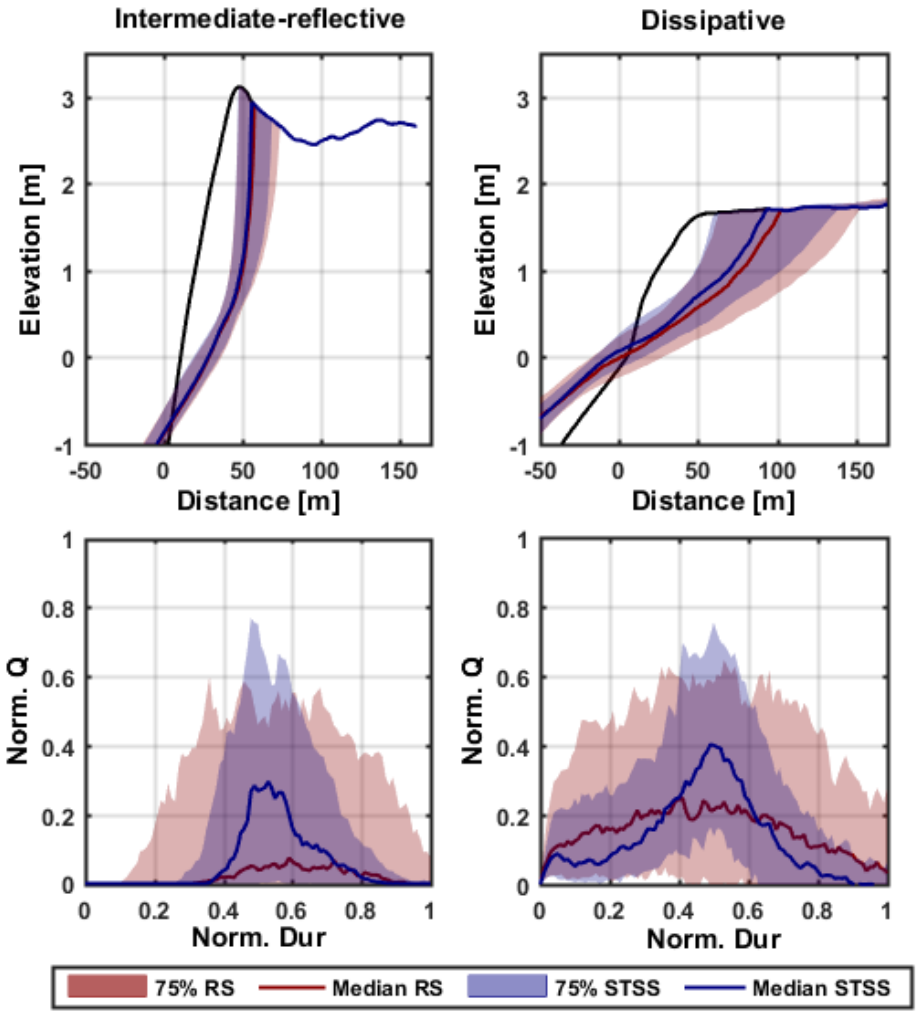

Figure 3.7. Real- (red) and synthetic-driven (blue) post-storm profiles calculated for the whole dataset of simulations for a predominantly intermediate-reflective (top-left) and dissipative (top-right) beach profile. Real- (red) and synthetic-driven (blue) normalised discharge time-series calculated for the whole dataset of simulations for a predominantly intermediate-reflective (bottom-left) and dissipative (bottom-right) beach profile. All graphs are represented by the median (solid line) and the 75% of the dataset given by the 0.175 and 0.825 quantiles.

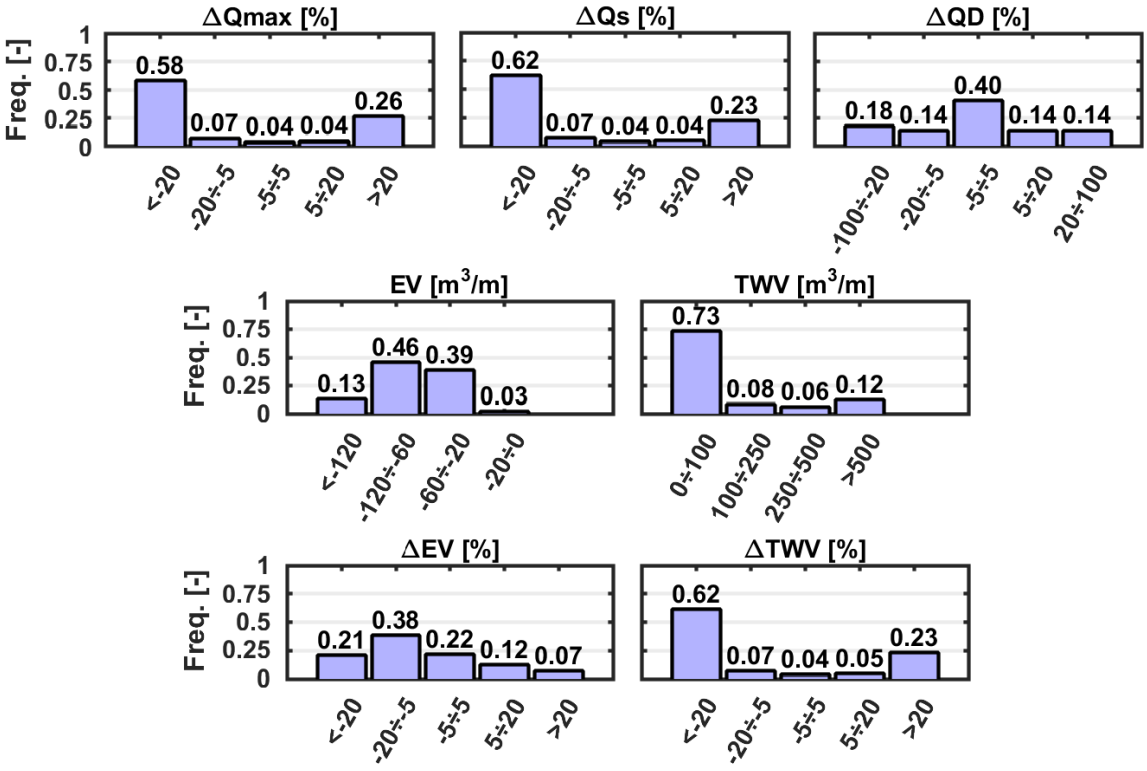

Figure 3.8. Variability in storm-induced hazards between STSS and RS according selected control parameters (table 3.6).

3.4. Discussion

The analysis has shown that, although using the use of a synthetic time-series to represent wave forcing for simulating storm-induced coastal hazards is a widely-used approach (e.g. McCall et al., 2010; Corbella and Stretch, 2012; Poelhekke et al., 2016; Plomaritis et al., 2018; Sanuy et al., 2018), the obtained results can significantly differ than those obtained using the real time-series they are intended to represent. This study represents the first attempt to quantify the uncertainty related to the use of these types of synthetic events in deterministic modelling.

The use of an STSS can be discussed in two different and complementary ways. The first one regards how well this approach represents the characteristics of an RS. The obtained results showed that, for this purpose, the use of an STSS provides a reasonable representation of reality, as it implies a perfect representation of Hs at Hs,max and the Dur of RSs. When the adopted shape has a potential influence on the magnitude of a variable to be characterised, the results begin to differ. Thus, the selected triangular shape determines the PD between both approaches. As has been shown here, even when the analysed storms are retrieved from localised areas (two in this case) where the meteorology presents well-defined and stable patterns, the peak occurs at different phases of the RS development, depending on specific conditions. This results in a relatively wide area along the storm duration where the peaks can be verified, as contrasted with a single fixed point in the STSS. This prevents the proper representation of the storm growth and relaxation phases and, in consequence, potentially affects any

process depending on these characteristics. Moreover, although the total E during the storm is statistically well-captured by the STSS, the adopted shape affects (mostly underestimates) the Ep. This is a direct result of the width of the area for integrating E, i.e. a very narrow one (STSS) and a wide one (RS).

The second consideration regards how changes in storm properties are transferred to storm-induced hazards. As opposed to the previous parameters, according to the obtained results, the adopted STSS has important effects on the reproduction of the induced hazards. Indeed, the storm-induced erosion was properly captured in just 22% of cases, whereas the TWV inundating the hinterland was properly captured in only 4% of cases. The better representation of the erosion hazard is a consequence of the morphodynamic feedback taking place during the impact of the storm, where the modifications of the beach morphology affect beach overtopping. In consequence, errors in beach morphology reproduction will propagate (and expand) to beach inundation.

Sánchez-Arcilla et al. (2009) also compared the use of RSs and SSs to assess beach erosion using the Sbeach model (Larson and Kraus, 1989). In their study, they used simplified Hs and Tp time-series in linear segments following the evolution of the RSs, and thereby captured storm peaks. This resulted in an average over-estimation of the E of approximately 15% (with a maximum of approximately 60%), whereas in the present study, E is well-captured in most of cases, with similar frequencies of under- and over-estimations (~5% with $|\Delta E|>20\%$; Figure 3.6). Their study also showed an over-estimation of EVs and shoreline erosion when using a synthetic event, possibly owing to the over-estimation of the E. The present study, however, evidenced a general under-estimation of the EV as shown in Figure 3.8, which was linked to the more frequent under-estimation of Ep with the STSS. Such differences between both studies reflect the use of a different approach to represent the storm evolution. Despite this, the differences between real- and synthetic-based outputs were smaller in Sánchez-Arcilal et al (2009) than those found in this study. However, to apply that approach, the shape of the event must be known a priori to mimic the storm evolution, whereas the STSS approach only requires storm bulk information. In addition to this, the number of cases simulated here to obtain a robust statistic of errors is much larger, and covers a wider range of conditions than in Sánchez-Arcilla et al (2009).

In this chapter, the differences in the EV (ΔEV) showed some relation to the variables describing the differences between the real and triangular time-series (i.e. ΔEp, ΔTp, and ΔPD) (see Figure 3.9). It is important to recall that the differences in wave period are mainly caused by the adopted empirical relation Hs-Tp, and they are not related to the applied shape. The under-estimation of the EV ($\Delta EV<-5\%$) was linked, as expected, to the under-estimation of the E at the peak ($\Delta Ep<-20\%$) and the PD ($\Delta PD>20\%$). In this case, $\Delta EV<-5\%$ is also moderately linked to a slight under-estimation of the Tp. In contrast, the over-estimation of the EV ($\Delta EV>5\%$) is related to the over-estimation of the Tp ($\Delta Tp>5\%$) and storm peak anticipation ($\Delta PD<-20\%$).

This apparent trend highlighted for the ΔEV-ΔEp and ΔEV-ΔTp relationships agrees with the findings of McCall et al. (2010). In that work, these authors performed a sensitivity analysis of a 2D XBeach model of the barrier island of Santa Rosa (FL, US), varying by the symmetric triangulas Hs by 30% and varying the Tp time-series of the Hurricane Ivan event (the base case). Notably, since the introduced variation did not influence its symmetric triangular shape, a relative variation of the energy was equal to the relative variation of the energy at the peak. Therefore, for that study, ΔE was equal to ΔEp. An analysis of the morphological impact on a foredune area showed that, in addition to expected changes in the EV following changes in Hs, the varying Tp conditions (ΔTp=±30%) resulted in the under-estimation (ΔEV~-30%) and over-estimation (ΔEV~18%) of the EV respectively. However, the same study also concluded that the erosion model output was more sensitive to (some) sediment transport parameters than to varying hydrodynamic conditions. This suggests that the differences induced using triangular storms (or SSs, in general) can potentially be compensated for by a calibration process. However, as the results obtained in this study show both under- and over-prediction, deeper investigations are required to verify this hypothesis under a wide range of storm conditions.

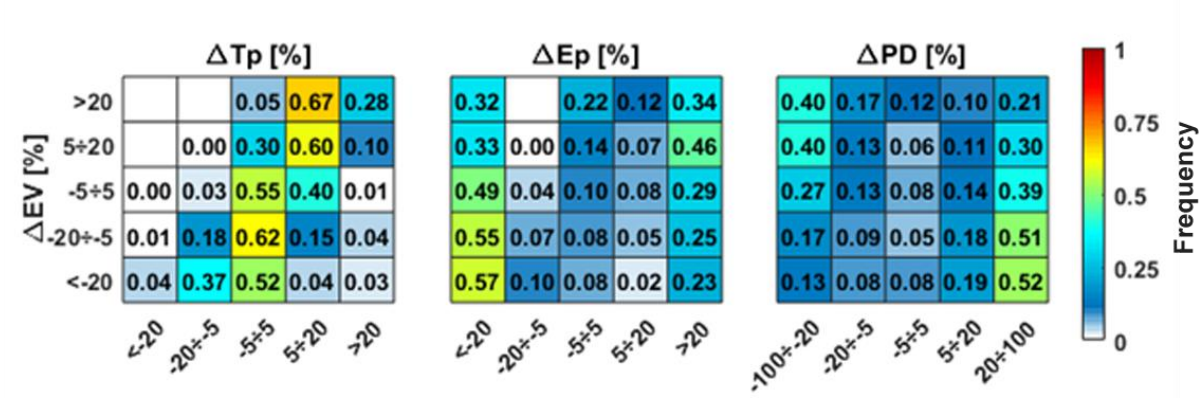

Figure 3.9. Relations between the eroded volume relative difference (ΔEV) with the variables describing the relative differences between the real and triangular time-series. The normalised distributions are shown through coloured tables where each row represents a range of ΔEV. From left to right: peak energy relative difference (ΔEp), peak period relative difference (ΔTp), and relative peak delay (ΔPD).

The obtained results demonstrate the existence of a strong relation between differences in erosion and inundation hazards (see Figure 3.10). The differences in the EV (ΔEV) and the phase lag of the water discharge (ΔQD) are linked, confirming the importance of morphodynamic feedback when simulating coastal inundation. A good/reasonable agreement (between real and triangular storms) on the computed EV (|ΔEV|<20%) leads to a good agreement on the positioning of the peak of the water discharge (|ΔQD|<5%). This should be important when the interest is in accurately timing the peak of the floodwater volume. However, this fine reproduction of the peak timing does not necessarily imply that the total floodwater during the event will be accurately reproduced. In fact, the obtained results showed

that a good reproduction of the EV (|ΔEV|<5%) is not accompanied by a good simulation of the inundation (|ΔTWV|<5%). Despite this, under- or over-estimation of erosion (|ΔEV|>5%) leads to strong under- or over-estimation of inundation (|TWV|>20%), respectively.

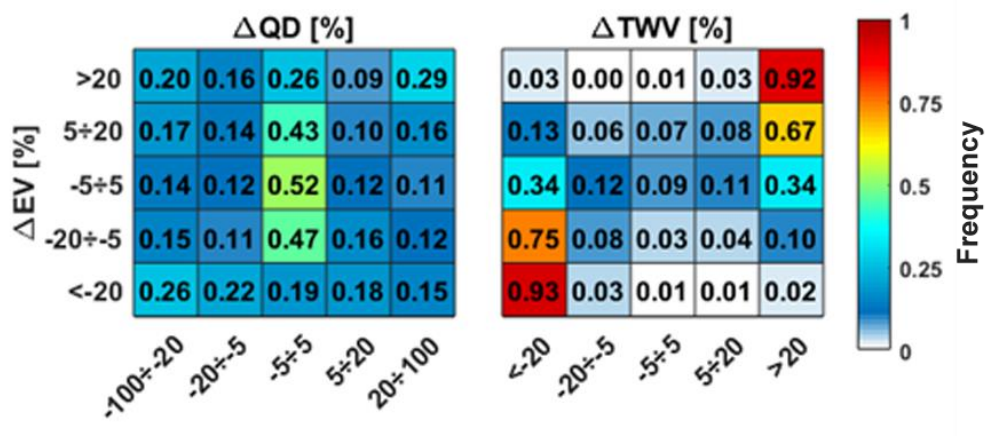

Figure 3.10. Relations between the eroded volume relative difference (ΔEV) with the relative differences in flooding-related variables. The normalized distributions are shown through coloured tables where each row represents a range of ΔEV. On the left: relative peak discharge delay (ΔQD); on the right: total water volume relative difference (ΔTWV).

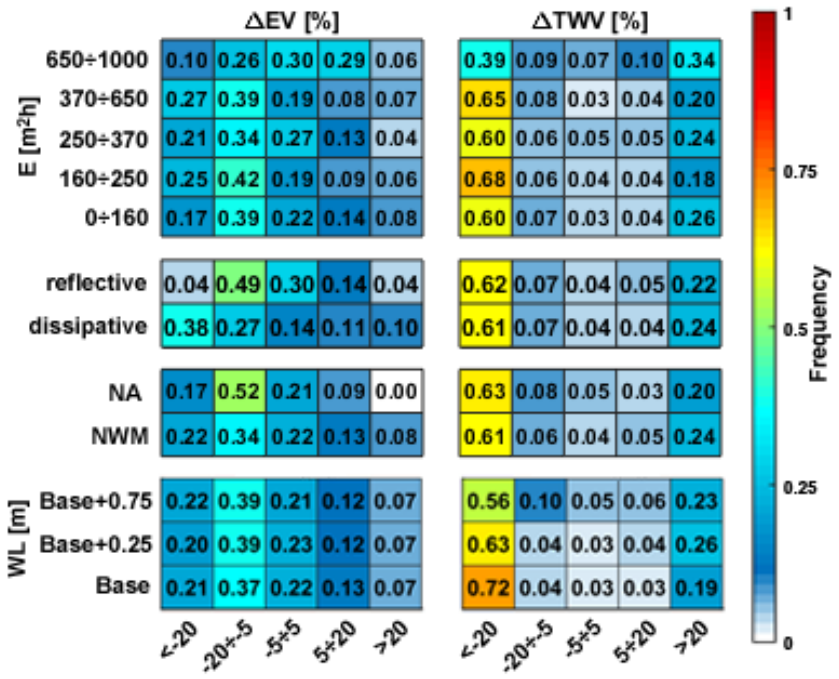

Figure 3.11. Relations between the eroded volume relative difference (ΔEV; on the left) and the total water volume relative difference (ΔTWV; on the right) with (from top to bottom) the storm energy (E) class, the profile conditions, the storm sub-datasets (i.e. Northern Adriatic, NA; North-Western Mediterranean, NWM), and the mean sea level (MSL) scenario. The normalized distributions of ΔEV and ΔTWV are shown through coloured tables where each row represents a different subset of the analysed variables.

To determine if the previously-observed differences are related to the structure of simulated conditions, they were further analysed according to the energy of the storm, the profile conditions (dissipative or reflective), location (storm dataset), and WL (Figure 3.11). Focusing on the -20% to +20% range of uncertainty in the hazard estimation, the results presented in Section 3 are not strongly conditioned by any of the analysed conditions. Although a slightly better estimation of EVs is obtained for reflective conditions and extremely energetic storms, the obtained results are consistently homogeneous throughout the dataset, especially when looking at the relative differences between -5% and +5%.

3.5. CONCLUSIONS

This chapter investigated the differences generated when simulating the hazard impacts of coastal storms using a STSS of waves, instead of the real data. It was demonstrated that the synthetic (or designed) method leads to highly uncertain and misleading hazard assessments, strongly limiting the reliability of the modelling approach.

After analysing the computed differences in reproducing storm-induced hazards by using STSSs, it can be concluded that they hardly reproduce the real magnitude with independence from the structure of storms or profiles. This is applicable to the range of simulated conditions, and permits one to conclude that although the use of STSSs adequately reproduces the main bulk variables defining the storm, they only reasonably reproduce the storm-induced hazard magnitude, i.e. accepting uncertainty in the order of (or greater than) +20% and -20%.

This highlights the need for further investigations towards a generalised synthetic approach that can optimise the simulation of coastal hazards, while minimizing the uncertainty related to the use of design events.

CHAPTER 4.

Identifying hotspots to storm induced erosion and inundation at a regional scale. The case of the Maresme Coast and the Tordera Delta.

Adapted from: Jiménez, J.A., Sanuy, M., Ballesteros, C., Valdemoro, H.I., 2018. The Tordera Delta, a hotspot to storm impacts in the coast northwards of Barcelona (NW Mediterranean). Coast. Eng. 134, 148–158. doi.org/10.1016/j.coastaleng.2017.08.012.

This chapter presents the risk characterization at the regional scale developed during the RISC-KIT project. This was dsone by applying the coastal risk assessment framework (CRAF) which is a screening methodology based on parametric models to estimate storm-induced erosion and inundation hazards combined with receptor exposure indicators with the objective of comparing coastal sectors.

The present chapter presents the application of CRAF to the Maresme coast using the response approach (Chapter 2) and a detailed description of the Tordera Delta as main detected hotspot to both erosion and inundation risks. Note that numerical modelling results of the Tordera Delta are introduced in this chapter, as they are used as complementary information to the CRAF method and the existing knowledge of the impact of historical events to fully characterize the situation at the Tordera Delta. However, the numerical model set-up and validation exercise will be formally presented in Chapter 5.

Finally, it has to be stressed that this is the starting point for the indentification of regional hotspots to storm impacts which will be further extended and improved with Bayesian Networks (Chapter 8)

4.1. Introduction

The progressive concentration of urban settlements in coastal zones has increased the exposed values and this, together with the nearly worldwide erosive trend of our coastlines (Bird, 2000; European Comission, 2004), has led to an increase in the associated risks, even under a steady-storm climate (e.g., Zhang et al., 2000; Jiménez et al., 2012). Moreover, it is expected that under a climate change scenario, these risks will increase in the near future (Hallegate, 2013; Wong et al., 2014). In this context, there is an increasing number of existing practical approaches ranging from vulnerability to risk assessments (e.g., Ferreira, 2004; Bosom and Jiménez 2011; Villatoro et al., 2011; Cirella et al., 2014; Rangel-Buitrago and Anfuso 2015) to assess natural hazards in coastal zones. In this line, recently in the framework of the RISC-KIT research project, a set of tools and approaches have been developed to support storm-induced risk management in coastal areas (Van Dongeren et al., 2018).

When this risk management is going to be implemented for very large spatial scales, one of the first steps to be done is the identification of hotspots. In simple terms, a coastal hotspot can be defined as a coastal stretch that is more sensitive to a given hazard (and within the context of this work, an associated risk) than surrounding areas. This is a screening process that allows for the delimitation of sensitive stretches along the coast to storm impacts, where a further and -more refined risk assessment analysis will be implemented at a later time.

Within this context, the main aim of this chapter is twofold: (i) to identify hotspots to the impact of storms along the coast northwards of Barcelona (NW Mediterranean) by applying the methodology developed within the RISC-KIT project (Viavattene at al., 2018); and (ii) to analyse the importance of storm-induced risks in the most highly-sensitive hotspot of the area, namely, the Tordera Delta.

The structure of the remainder of this chapter is as follows: (i) the section 4.2 describes the study area and the data used; (ii) section 4.3 presents the identification of hotspots at the regional scale along the Maresme coast; (iii) section 4.4 analyses in detail risk assessment and management at the hotspot scale in the Tordera Delta; and finally, (iv) the summary and general conclusions of this work are presented in the 4.5 section.

4.2. Study area and data

4.2.1. Study area

Maresme is the coastal region of Catalonia (Spain, NW Mediterranean), extending from the city of Barcelona to the south to the Tordera river to the north (Figure 4.1). It originally was an interrupted coast composed by about 45 km of straight, coarse, sandy beaches. Today it is segmented into five coastal cells due to the presence of five marinas. The combination of relatively high net longshore sediment transport rates directed toward the SW, and the presence of these barriers has induced a typical alternating shoreline evolution pattern, with upcoast accreting beaches and downcoast eroding ones.

From an administrative standpoint, the coastal fringe extends along 16 municipalities, which are the most densely-populated areas of the region (IDESCAT, 2014). The region can be divided into two different areas in terms of socio-economic and territorial dynamics. Southern municipalities are strongly influenced by the presence of the city of Barcelona, and have a large residential development, while the northern ones have largely based their economies on tourism. This area supports an important transport link composed of a coastal railway and a national road. The coastal railway is located very close to the shoreline, and in many sections is only separated from the sea by a revetment protecting the infrastructure against direct wave impact. The large urban and infrastructure development in the coastal fringe makes this region particularly vulnerable to extreme marine events, having experienced significant damage during the past decades (Jiménez et al., 2012).

The northern end of the study area is formed by the Tordera Delta coast (Figure 4.1). This is a highly dynamic zone, currently in retreat due to the net result of the littoral drift and the decrease of the Tordera River sediment supplies. As a result of this, beaches surrounding the river mouth, traditionally stable or accreting, have experienced significant erosion during the last 20 years, with a measured shoreline retreat of about 120 m at the point of maximum erosion (Jiménez et al., 2011; Jiménez et al., 2016). The hinterland of this area is composed by the deltaic plain, which is occupied in its outer part by different campsites which are solely protected from wave action by existing beaches, with the exception of a few spots where small revetments exist.

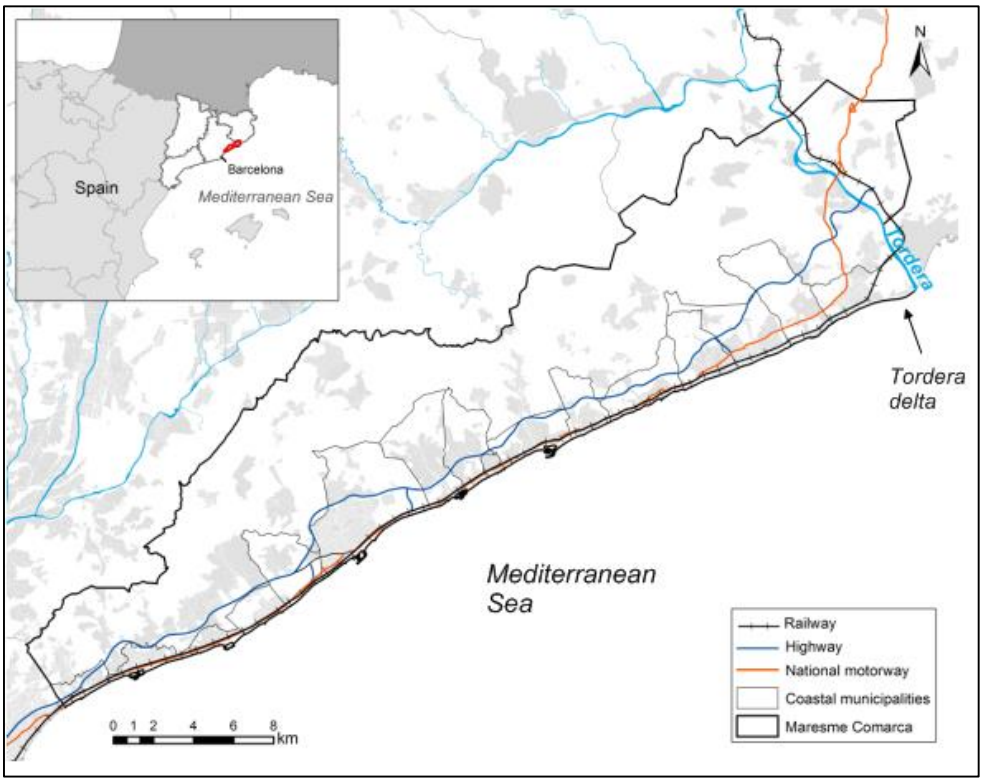

Figure 4.1. Maresme coast and Tordera Delta. Location, main administrative divisions and transport infrastructures.

4.2.2. Data

The topography of the study area has been characterized by using a 2 m x 2 m Digital Elevation Model obtained from Lidar flights performed between 2008 and 2011 by the Cartographic and Geologic Institute of Catalonia. Sediment sizes along the coast have been obtained from data supplied by (CIIRC, 2010).

Wave and water level data have been derived from the extended SIMAR dataset obtained by Puertos del Estado (Spanish Ministry of Public Works) for the Spanish coast. This dataset originally consisted of a 44-year (1958-2001) time series of wave and water level data obtained within the Hipocas project (Guedes-Soares et al., 2002; Ratsimandresey et al., 2008), which has been extended until 2016. Waves were generated by using the third-generation wave model WAM forced by wind fields, whereas sea level data were obtained by means of the baroclinic HAMSOM model. This database has been widely used (Bosom and Jiménez, 2011; Gomis et al., 2008; Alvarez-Ellacuria et al., 2009; Casas-Prat and Sierra, 2010) and has been extensively validated in the Mediterranean (Ratsimandresey et al., 2008; Sotillo et al., 2005; Musić and Nicković, 2008). Although some extreme events are underestimated, the data have been used without further calibration. A similar approach was also used by Casas-Prat and Sierra (2010) in analysing storminess along the Catalan coast.

To characterize existing land uses in the coastal zone we have used the last version of the land-use map of Catalonia developed by CREAF for the Government of Catalonia (Ibàñez and Burriel, 2010). Socio-

economic data have been obtained from the official information provided by the Statistical Institute of Catalonia (IDESCAT, 2014).

4.3. Regional assessment of hotspots

The first step in the analysis consisted of the identification of coastal hotspots to the impact of extreme events in the area. It essentially consists of assessing storm-induced risks, in terms of flooding and erosion hazards associated to a given probability of occurrence and their potential consequences along the coast to identify sectors with higher risks than surrounding areas. This is done by evaluating a risk index along the coast, CI, which is composed by a hazard (i_h), and an exposure (i_{exp}) indicator and it is given by

$$CI_{hazard} = [\![(i_h * i_{exp})]\!]^{1/2} \quad (4.1)$$

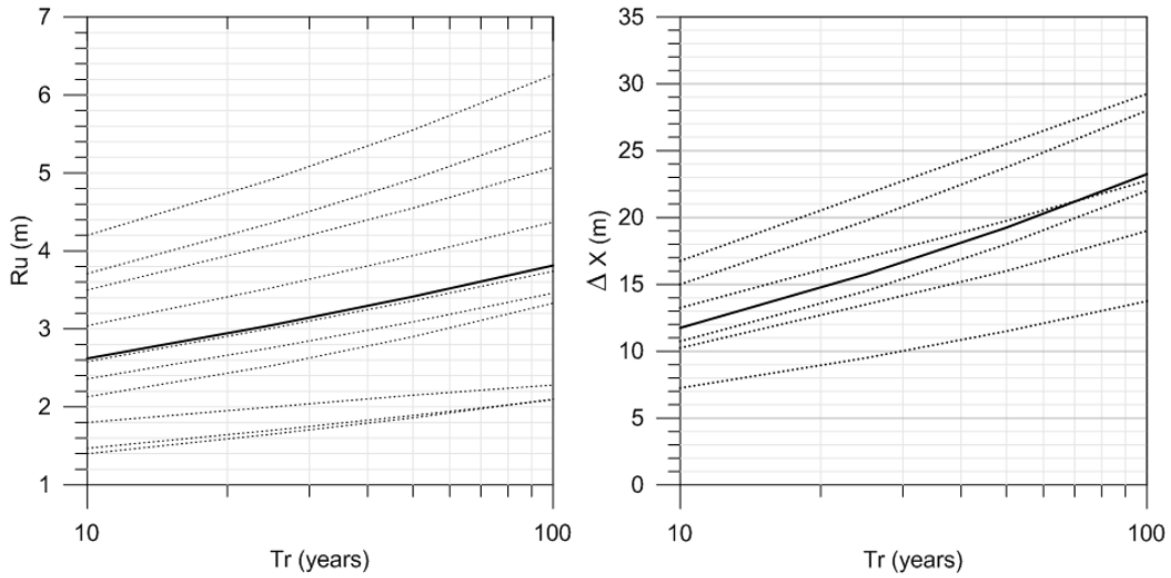

Figure 4.2. Extreme Ru (flooding) and ΔX (erosion) climates along the Maresme coast. Dashed lines correspond to regimes for computed for representative profiles along the coast and the solid line is the regional-averaged climate.

To this end, the area was segmented in 46 sectors of one km length along the coast, each one being defined in terms of a representative beach profile which has been selected by taking the most sensitive one to analysed hazards. Hazards are characterized in each sector by using the response approach (see Chapter 2), which requires computing hazard time series from initial forcing data to directly obtain hazard–probability distributions (see Figure 4.2 in Viavattene et al., 2018).

The magnitude of the flooding hazard was assessed by estimating the water level extreme climate along the coast and the extension of the area to be flooded. Storm surges in the area are relatively small (maximum recorded values up to 0.5 m) and thus, wave-induced runup, Ru, becomes the main contributor to water levels during storms (Mendoza and Jiménez, 2008), and they were calculated by applying the Stockdon et al. (2006) model in each sector along the coast. In the southern part of the study area, there are some stretches where the beach is fully eroded and the coastline is formed by a riprap revetment. In these areas, Ru has been calculated using the EurOtop model (Pullen et al., 2007). Resulting Ru time series calculated for each beach profile (defined in terms of its slope) were fitted by means of a General Pareto Distribution (GPD). Obtained Ru probability distributions for representative beach slopes of the study area are shown in Figure 4.2, together with the representative regional regime, which has been obtained by averaging Ru climates obtained in each one km section.

The extension of the area to be potentially flooded along the coast was calculated using the bathtub approach. Due to the characteristics of the study area, with beach profiles characterized by a monotonous increasing elevation in the landward direction, this approach is a good representation of the maximum area to be (temporarily) potentially affected by inundation. The point where the storm-water level intersects the beach was individually calculated for each profile, taking into account the corresponding water level for selected return periods, TR, and the local beach topography. Computed values were converted to a flooding hazard scale, which was derived by taking into account the local characteristics of the process. These values range from zero (potentially flooded area restricted to the beach) to five (a large area at the hinterland will be affected) (Viavattene et al., 2018).

The magnitude of storm-induced erosion hazard was assessed by estimating the eroded volume from the inner part of the beach and the corresponding shoreline retreat during the impact of the storm in each sector along the coast. This was done by applying the parametric erosion model proposed by Mendoza and Jiménez (2006) which predicts the storm-induced beach profile erosion as a function of storm (wave height, wave period and storm duration) and profile (slope and sediment grain size) characteristics. Since storms need to be defined in order to compute the associated erosion during each event, a threshold criteria given by Hs = 2.5 m and minimum duration of 6 hours was used. This threshold was selected based on previous works on the storm climate in the area (Mendoza and Jiménez, 2008; Mendoza et al., 2011) and adapted to the objective of this work. These authors used a threshold of 2 m and 6 hours, which has been increased to just retain the most significant storms per year (about 3 storms per year) which will be the most hazardous for the coast.

Similarly, in order to compute the extreme beach erosion climate, and resulting eroded-volume, time series calculated for each sector were fitted by means of a GPD. Figure 2.4 shows the calculated shoreline retreat values associated with different return periods for representative beach profiles of the study area.

The next step is to derive the value of corresponding hazard indicators (i_h). This is done by selecting the hazard magnitude associated to the target probability of the analysis and, ranging them from 0 to 5 according to the scale showed in Table 4.1.

Table 4.1. Hazard scales for erosion and flooding along the Maresme coast as a function of the remaining beach width (W) after storm impact and extension of the flooding respectively. ΔX_{10} corresponds to the storm reach associated to a return period of 10 years.

i_h	hazard	
	erosion	**flooding**
	beach width after erosion (m)	**flooding extension (m)**
5	beach fully eroded	> beach width + 60 m
4	$W \leq \Delta X_{10}$	≤ beach width + 60 m
3	$\Delta X_{10} < W \leq 2\ \Delta X_{10}$	≤ beach width + 40 m
2	$\Delta X_{10} < W \leq 3\ \Delta X_{10}$	≤ beach width + 20 m
1	$\Delta X_{10} < W \leq 4\ \Delta X_{10}$	≤ 100 % beach width
0	$\Delta X_{10} < W \leq 5\ \Delta X_{10}$	≤ 50 % beach width

In order to assess the "consequences" component of the risk, exposed values susceptible to the effects of storm-induced hazards were characterized, following the methodology outlined in Viavattene et al., (2018). To do this, an exposure indicator (i_{exp}) which integrates five types of receptors was used: land use ($i_{exp\text{-}LU}$); population ($i_{exp\text{-}SV}$); transport systems ($i_{exp\text{-}TS}$); critical infrastructures ($i_{exp\text{-}UT}$); and business settings ($i_{exp\text{-}BS}$). It is given by

$$i_{exp} = \left[\left(i_{exp-LU} * i_{exp-SV} * i_{exp-TS} * i_{exp-UT} * i_{exp-BS}\right)\right]^{1/5} \quad (4.2)$$

$i_{exp\text{-}LU}$ measures the importance of the different types of land uses susceptible to be affected. $i_{exp\text{-}SV}$ indicates the intangible impacts to the affected population in terms of their socio-economic characteristics by adapting the Social Vulnerability Index (SVI) suggested by Tapsell et al., (2002). i_{exp_TS} and $i_{exp\text{-}UT}$ indicate the existence and importance of transport networks and critical infrastructures respectively. $i_{exp\text{-}BS}$ measures the potential impact on business. Since, tourism is the most representative coastal economic sector involved, we have used the tourist index developed by la Caixa bank (La Caixa, 2013). This indicator measures the relative importance of the tourist sector at municipal level based on the tax rate (Business Activities Tax), and it takes into account local characteristics of tourism establishments (category, number of rooms and annual occupancy). Exposure indicator is calculated and ranked from 1 to 5 following the scale shown in Table 4.2 for each sector along the coast. The exposure

will vary depending on the hazard extent, which will depend on the hazard type (flooding or erosion), which is calculated independently. In the case of flooding, it is computed for a 100 m-wide buffer landwards from the beach, whereas for the case of erosion, it is computed considering only a 25 m buffer behind the beach.

Table 4.2. Scale used to assign values to each component of the exposure indicator.

Exposure indicators	**Consequences**				
	1 Inexistent or very low	**2 Low**	**3 Moderate**	**4 High**	**5 Very high**
Land use (i_{exp-LU})	Barren Riparian buffer/wetland (1.5) Grassland (1.5)	Forest Urban green	Beach and dune Cropland	Campsite Industrial	Urban
Transport system (i_{exp-TS}) *Presence of*	No significant	Local road	National road	Coastal railway	National road + coastal railway
Utilities (i_{exp-UT}) *Presence of*	No significant	Mainly local and small	Moderate of local/ regional importance	High dense / multiple utilities of local / regional importance	High dense / multiple utilities of national / international importance
Business (i_{exp-BS}) *Tourist Index*	<45	45-89	89-133	133-177	>177
Population and social (i_{exp-SV}) *Social Vulnerability Index*	≤ -4.4	]-4.4; -1.8]	]-1.8; -0.2]	]-0.2;1.8]	>1,8

Figure 4.3 shows the computed values for each component of the exposure indicator, as well as for i_{exp}, for flooding along the Maresme coast. With these values, this coastal stretch can be classified as having medium values at exposure, with a more or less homogeneous distribution along the coast with the exception of transport and business. The southern part has important transport elements subjected to exposure and low-business importance (tourism), whereas the northern part has high-business values and fewer transport elements subjected to exposure.

As mentioned before, hazard and exposure indicators are integrated into a Coastal Index for each analysed hazard.

This index can be calculated associated with any probability of occurrence since hazards have been characterized in probabilistic terms (Figure 4.2). The selection of the probability to be used to find

hotspots is a choice of the decision-maker and depends on the safety level to be used in the analysis. As an example, here we use the probability of occurrence given by a TR of 100 years, which is the value used in the EU Flood directive as representative for medium probability events (EC, 2007). Figure 4.4 shows the spatial distribution of flooding and erosion coastal risk indexes obtained for a TR of 100 years along the Maresme coast.

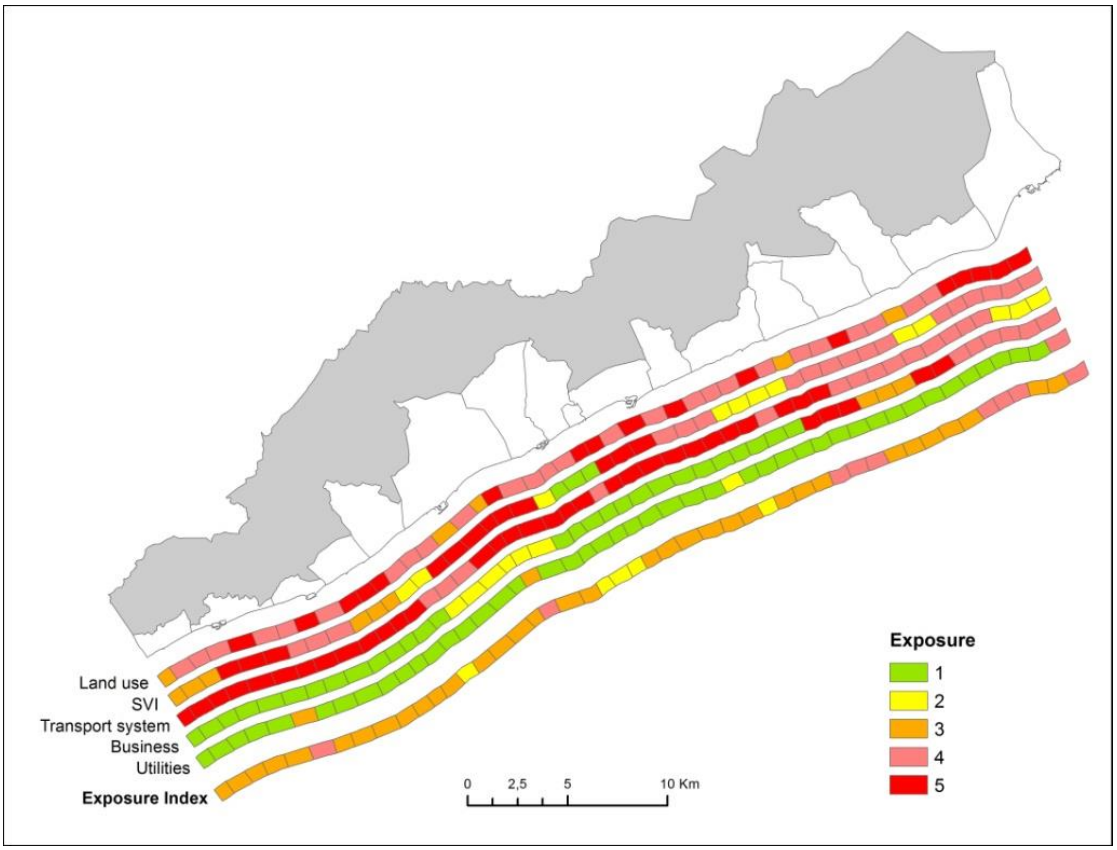

Figure 4.3. Exposure indicator and contributing components along the Maresme coast for flooding risk analysis.

With respect to flooding, the area can be classified as a low-medium risk due to the relatively short extension of inundation reaches, with the exception of two areas. The first exception is the Tordera Delta, at the north, which is composed of relatively narrow and steep beaches protecting a low-lying area. In terms of values at exposure, beaches in this area are used for recreational purposes, being important in economic terms (local scale), supporting various campsites, which are the basis for local tourism. This area has been experiencing systematic storm-induced problems since the end of 90's, which have been aggravated in recent years due to the significant deltaic front retreat and the consequent increase in the level of exposure of the hinterland (Jiménez et al., 2011;2016). The second exception represented by two spots to the south, which are located downcoast to the Balis and Mataró harbours, where the beach has been fully eroded in such a way that currently, the coastal fringe is composed by a riprap revetment protecting the coastal railway from wave action. During the impact of moderate and

extreme storms, wave-induced runup can exceed the height of the revetment, producing overtopping and, as a consequence, affecting the railway traffic. This has been observed several times during the last decades along this coastal stretch (see Figure 4.5).

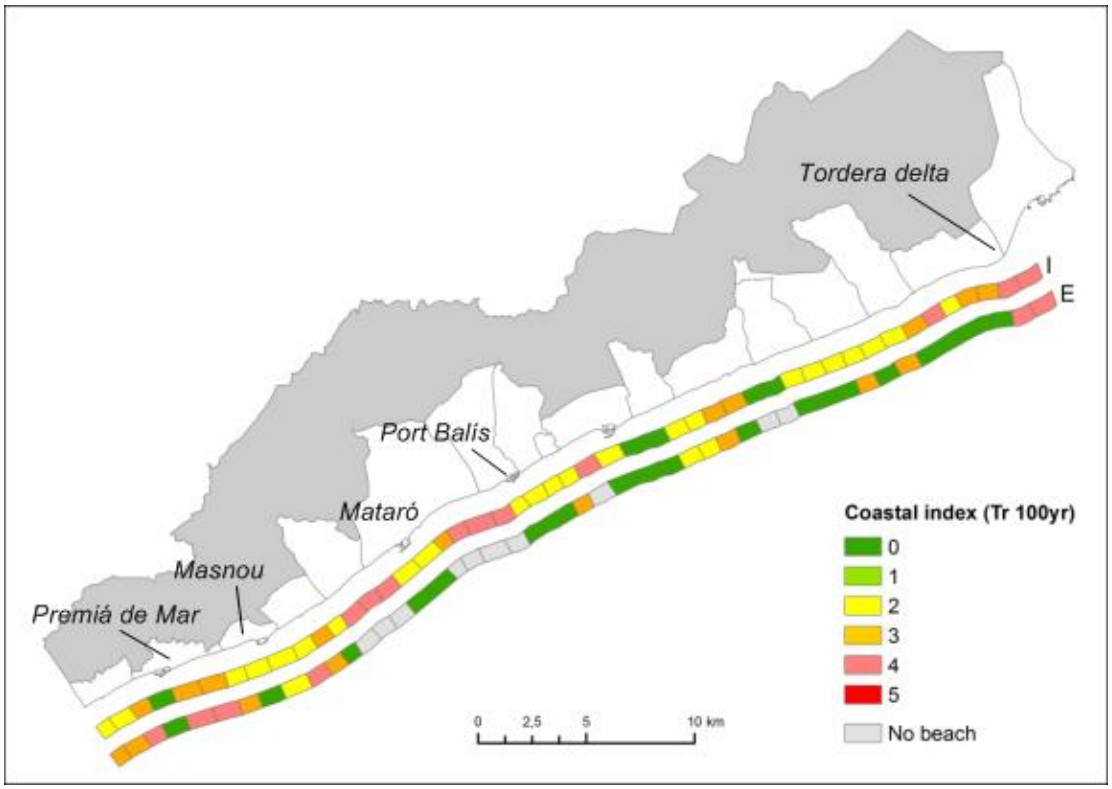

Figure 4.4. Coastal flooding (I) and erosion (E) indexes associated to a probability of occurrence given by Tr = 100 years along the Maresme coast.

With respect to erosion, the obtained coastal risk index reflects the spatial distribution of hazard intensities but is modulated by the spatial distribution of values at exposure, and specifically, by the level of protection of the hinterland (e.g. the coastal railway and the revetment protecting it). In comparison with flooding, the area presents lower risk values due to both lower hazard intensities and values at exposure. In general, the area can be classified as low to medium risk with the exception of two spots: one to the north, which coincides with the one previously identified in the inundation analysis, namely, the Tordera Delta; and one to the south, located between the Premia de Mar and Masnou municipalities. Although beaches upcoast existing marinas are wide, the rest of the coast presents relatively narrow beaches, which can be fully and instantaneously eroded by the impact of storms. It has to be mentioned that the southern hotspot identified in the inundation analysis has not been identified for erosion because the coast was composed of a revetment where no erosion is possible.

Figure 4.5. Affectation of the coastal railway along the Maresme coast during the impact of a storm on March 2003.

4.4. Storm-induced risks at the tordera delta

Among all the identified sensitive areas along the Maresme coast, the Tordera Delta is one of the most significant hotspots for both storm-induced hazards, flooding and erosion. This is a simple cuspate deltaic sandy shoreline where the northern part is composed by a straight beach (s'Abanell) with an orientation of 20° with respect to the East whereas the southern part is orientated from 55° to 70° with respect to the East (Figure 4.6). This configuration and location determines the coastline to be directly exposed to the action of the most energetic storm waves in the area (E-NE storms) as well as to those coming from secondary directions (S) (see details on storms characteristics in the study area in Mendoza et al., 2011).

To analyze in detail the sensitivity of this hotspot, we have used the XBeach model (Roelvink et al., (2009) to simulate storm-induced erosion and flooding hazards (see Chapter 5). First, the model was calibrated using Lidar measurements of the beach before and after the impact of an extreme storm (TR ~ 100 years), the St. Esteve storm, on the 26th December 2008 (Jiménez, 2012; Sánchez-Vidal et al., 2012; Plana Casado, 2013). Pre-storm and post-storm Lidar data were acquired on 16th October 2008 and 17th January 2009 respectively by the Institut Cartogràfic de Catalunya and they have an average vertical error of 8 cm (see also Durán et al., 2016). To select model parameters during the calibration we used the Brier Skill Score (BSS) to assess the model skill by comparing it to the real post-storm LIDAR measurements of the emerged profile. Final calibrated model resulted in a BSS score of 0.651 (Sanuy and Jiménez 2019 – see Chapter 5) which according to Sutherland et al., (2004) can be considered as a very good morphodynamic model performance. Figure 4.7 shows some simulated vs measured beach profiles at both sides of the river mouth obtained during the calibration process.

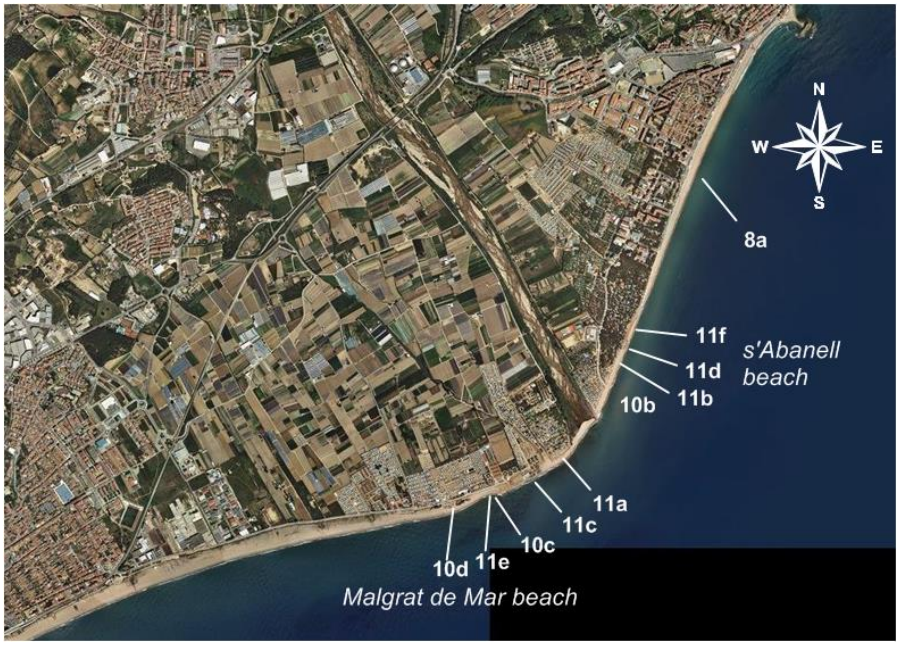

Figure 4.6. The Tordera delta coast. Numbers refer to locations of photos in Figures 4.10 and 4.11.

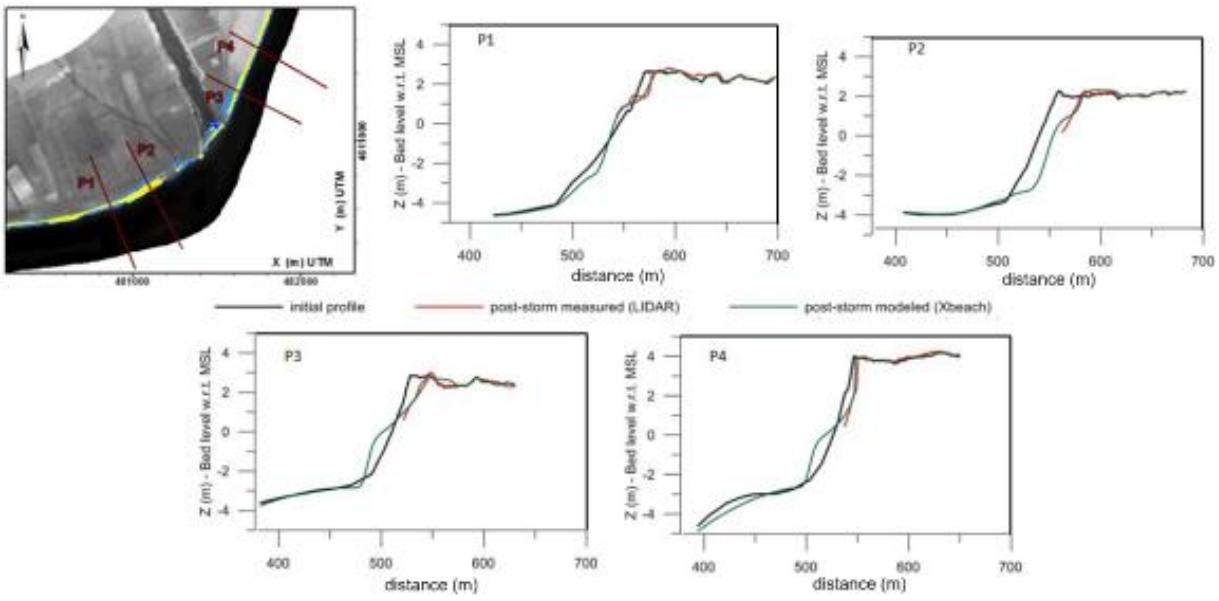

Figure 4.7. Calibration of the XBeach model in the Tordera delta for the 26th December 2008 storm (see Chapter 5 for further detail). Insets show measured (only the subaerial part) vs modelled beach profile changes at both sides of the river mouth.

After that, the model was used to simulate storm-induced hazards for a set of storms covering the full range of potential storm conditions in the area in terms of wave height, direction, and storm duration. This permitted the assessment of the expected magnitude of storm-induced hazards for any condition,

and thus, to assess their possible implications in terms of damages induced in the hinterland (Chapters 6 and 7).

It is out of the scope of this chapter to present the details of the performed numerical analysis. However, to illustrate obtained results, Figure 4.8 shows the simulation of the morphodynamic response of the area to the impact of the previously-mentioned extreme storm of December 2008. This was an ENE storm reaching a Hs of about 4.7 m just in front the Tordera Delta (Jiménez, 2012). As it can be seen in Figure 4.8, the response of the area was different at both sides of the river. See Chapter 5 for more detail on the impact of the Decembre 2008 storm and its numerical simulation with XBeach.

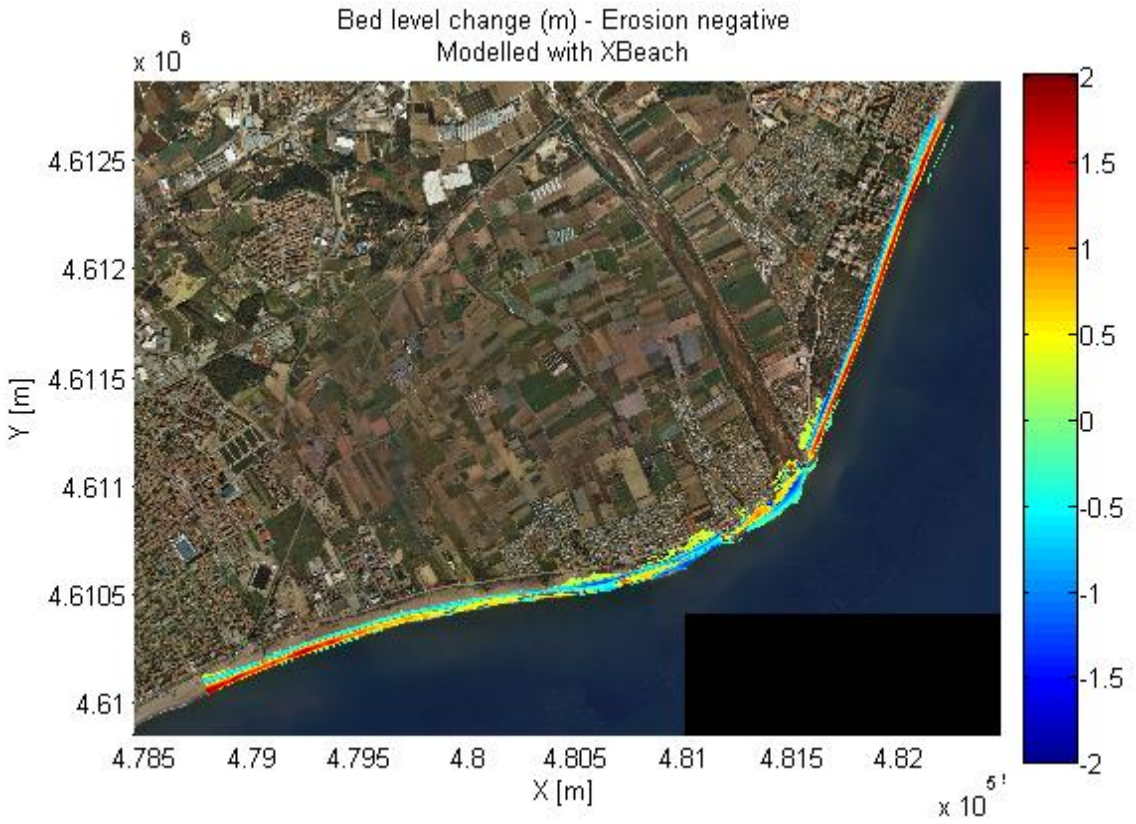

Figure 4.8. XBeach simulation of beach changes in the Tordera delta due to the impact of an extreme storm (TR ~ 100 years) that took place in December 2008.

This spatial variation in hazard magnitude at both sides of the river mouth is also detected in storm-induced flooding. As an example of the analysed potential variations, Figure 4.9 shows XBeach simulations of storm-induced flooding under the impact of an extreme storm (TR > 100 years) with different directions (E and S). As can be seen, whereas the flood-prone area northwards of the river mouth has a similar extension for both storms, the affected area in the southern beach is very sensitive to incident wave direction. Under the impact of an E storm, the extension of the flood prone area, although large, is smaller than under the S storm, due to the orientation of the coastline. Under the impact

of an S storm, the potential extension of the flood prone area significantly increases, because on the one hand, waves impact nearly perpendicular to the coast and, on the other hand, the existing submerged longshore bar is not very efficient in protecting the area.

These results stress the sensitivity of the southern part of the delta to wave direction during storms, which is furtherly analysed in Chapter 5. However, it has to be considered that wave heights during S storms are usually smaller than during E storms (Mendoza et al., 2011). In spite of this, this analysis permits the identification of potential changes in storm-induced flood risk under a scenario of wave climate variations (see, e.g., Casa-Prat and Sierra 2013).

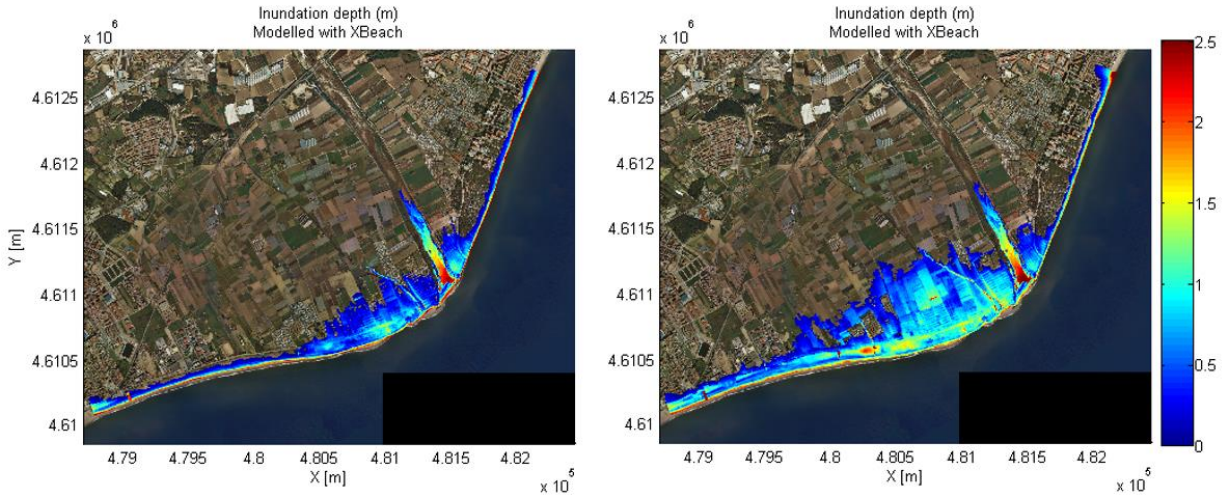

Figure 4.9. Simulation of coastal flooding in the Tordera delta using XBeach under the impact of an extreme storm (TR > 100 years) coming from E (left) and S (right) directions. See chapter 5 for further detail.

The hinterland of this area has been occupied by campsites for over 40 years, which were originally protected from wave action by relatively wide beaches (from 60 m to 100 m, depending on the location). However, as previously mentioned, beaches along the deltaic front on both sides of the river have been retreating during the last 20 years (Jiménez et al., 2011;2016). This resulted in an increasing exposure of values in the hinterland to storm impacts, which has become an alarming situation due to the current high frequency of damages (Jiménez et al., 2011;2012). Moreover, due to the decrease in protection provided by beaches, these situations are beginning to occur under the impact of relatively moderate storms, which reinforce their "hotspotness" to storm-induced hazards. Figure 4.10 shows an example of damages experienced by the area due to storm impacts during the last decade, which include beach promenade collapses at the north, campsite infrastructural damages at both sides of the river, as well as flooding of various campsites with associated damages in their installations.

Figure 4.10. Example of damages induced in Tordera delta beaches during the impact of different storm events in the last decade (see locations in Figure 4.6).

Until now, disaster reduction measures have seldomly been implemented in the area by the responsible Administrations and, when done, they have been met with limited success. As an example, a 180,000 m^3 nourishment was done by the Catalan Water Agency in the northern beach to protect a pumping station of a desalination plant that was directly exposed to wave action (Figure 4.10b) due to a massive shoreline retreat. However, the lifetime of the work was only 1.5 months, since it was fully eroded after the impact of a moderate storm (Jiménez et al., 2011). Under this situation of increasing damages and the perception of being abandoned by the Administration, local private stakeholders have taken action under their own initiative to cope (or to try to) with coastal disasters (Figure 4.11). It should be stressed that these actions are illegal, and they have usually been undertaken without any integrated perspective, in such a way that, some of the implemented measures have affected adjacent neighbours by inducing new problems. The clearest example of these new induced problems is observed downcoast of a revetment that was built to locally protect a building at Les Nacions campsite (point 11 c in Figure 4.6). Once the beach in front of the revetment was fully eroded, the revetment started to affect littoral dynamics and produced the typical flanking effect downcoast accelerating erosion in front of the neighbouring campsite.

In order to test the performance of different risk management strategies, we analysed the behaviour of the system by simulating the same set of storms used to characterize current conditions by including different measures in the southern beach (Malgrat de Mar). The first one was designed to reduce the magnitude of the hazard by increasing the protection provided by the beach (see Chapter 6). This was done by means of moderate beach nourishment to only increase the beach width 40 m along 600 m of

the coastline and, by building a +4 m-high artificial dune at the back of the beach. Obtained results showed that the protection strategy was effective in reducing storm-induced risks, although it behaves as a very ephemeral measure due to erosion of the fill during the impact of the storm. This implies that after each storm season, the beach has to be re-nourished in order to maintain its protective capacity against storms. The effectiveness of this strategy was also tested in the field by analysing the behaviour of a 114,000 m^3 nourishment done to increase the width of a southern beach (Malgrat de Mar) in July 2015. The hinterland remained protected during the impact of two moderate storms (Hs = 3.5 m) in October 2015, although the fill was fully eroded (Jiménez et al., 2016). It has to be mentioned that most of the sediment eroded during the impact of dominant E storms is removed from the site and alongshore transported towards the south. The most efficient conditions to promote local beach recovery correspond to the action of S waves which bring sediment to the area, which are the least frequent.

The second strategy consisted of reducing the damages by managed realignment, which implies the redefinition of the public domain limit and the removal of all values at exposure between the new limit and the shoreline (see Chapter 6). To this end, we tested the effects of imposing three different setbacks: 25 m, 50 m, and 75 m. As expected, this strategy was also effective in reducing risks, with larger reductions for larger retreats (see Sano et al., 2011 for discussion on setbacks and coastal erosion). As in the previous case, if additional action is not taken, this will also be an ephemeral strategy due to the existing background erosion, although at a longer timescale.

Finally, risk management strategies in the area were consulted with local stakeholders in a Multi-Criteria Analysis as described in Barquet and Cumiskey (2018). Strategies were scored taking into account three different criteria, i.e. feasibility, acceptability and sustainability, where corresponding weights were agreed by stakeholders (3/8, 1/8 and 4/8 respectively). Obtained results showed that the most valued strategy was the one based on beach nourishment and the artificial dune. This was essentially due to the fact that, in addition to solving the problem, it permits the maintenance of the economic activity (campsites) as they are at present, while providing a beach for sustaining coastal tourism. With respect to its ephemeral behaviour, stakeholders consider that eroded volumes will positively contribute to the sediment budget of the neighbouring areas, acting as a sediment input. Of course, the acceptance of this strategy is assuming that re-nourishment is granted when necessary.

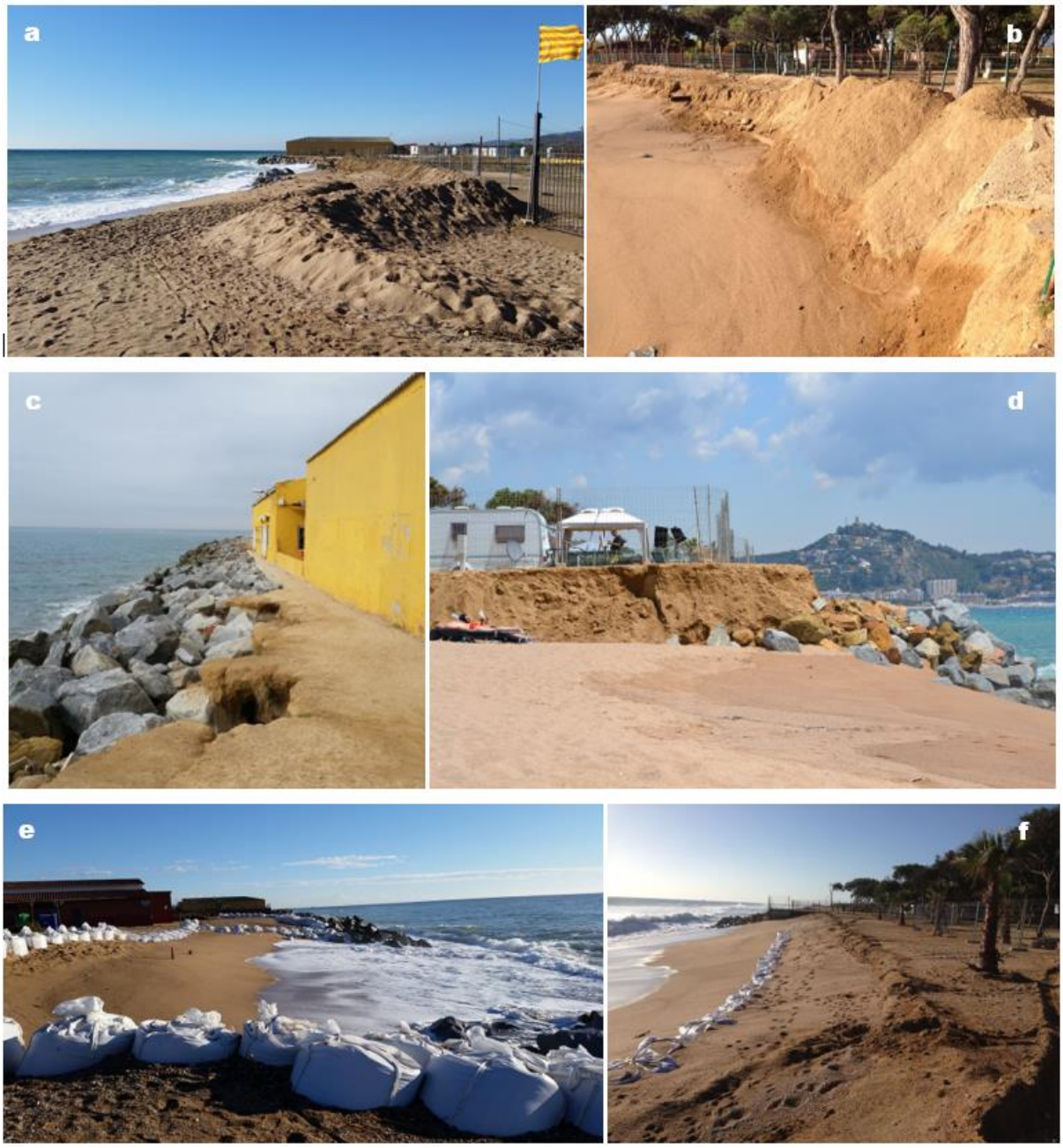

Figure 4.11. "Self-protection" measures against erosion and inundation implemented by campsite owners in the Tordera delta beaches (see locations in Figure 4.6). Left figures correspond to Malgrat de Mar beach (southwards of the river mouth) and right figures correspond to s'Abanell beach (northwards of the river mouth). Top: temporary artificial dunes/dikes to avoid flooding during storms in winter season; middle: revetments to protect exposed camping installations; bottom: sand bags to locally maintain the beach.

On the other hand, setback redefinition was very negatively considered, with rejection increasing the greater the retreat was. Private stakeholders argue that they have already retreated to accommodate to background erosion, and that under this strategy, they bear the brunt of the costs. Moreover, they state that if no further action is taken, new retreats will be required in the near future. In summary, from the perspective of the private stakeholder, this is not a solution. In any case, the selection of any risk

management strategy must be integrated in a general beach management framework, such as the ecosystem-based one proposed by Sardá et al., (2015).

4.5. Summary and conclusions

In this chapter we have tested the methodology developed within the RISC-KIT project for identifying and analysing coastal hotspots to the impact of storms in the Catalan coast. Analysed conditions can be considered as characteristic of the Mediterranean coastline where the influence of waves usually dominates over surges, and where the erosion hazard is, at least, as important as flooding.

Obtained results show that, at a regional scale (several tens of km), the employed methodology has been very efficient in separately identifying hotspots to storm-induced flooding and erosion. The use of the response approach resulted in the direct assessment of the hazards' probability distributions, which permitted the selection of the severity of the hotspots to be identified. This selection will be made by decision-makers as a function of the safety level of the analysis and, in this work, the probability of occurrence associated with TR = 100 years has been used.

The obtained spatial distribution of hazards shows that, although they are related, they are not necessarily coincident. This is due to the different dependence of hazards' magnitude on storm variables and, on the different variables determining the resilient capacity of the coast, i.e., beach width and height. In spite of this, there are few locations behaving as hotspots simultaneously for both hazards, and when present, they become highly sensitive stretches to storm impacts. In the study area, this condition of very high "hotspotness" is the Tordera Delta.

The spatial distribution of risks along the coast will depend on the hazard distribution but modulated by their potential consequences. In this sense, the adopted approach in which these consequences are hypothesised by means of indicating values at exposure, implies to assume a kind of worst-case scenario, i.e., potential damage does not depend on values' vulnerability. In areas as the analysed one, where many of the exposed values present a more or less homogeneous distribution along the coast, local variations can determine a significant relative increase in the assessed risk. This is important because it will permit an improved discrimination of sensitive coastal stretches. In the study area, existing values at exposure in the identified Tordera Delta hotspot, have been significantly affected during the past decades, with most of the damages affecting campsite installations (tourist use).

When the analysis is done at the hotspot scale (few kms), the adopted approach in which storm-induced processes are simulated in detail for the full range of storm conditions permit the testing of the associated risk under any risk reduction strategy. In our case, this small-scale approach has been used to test the efficiency of two typical strategies based on protection and retreat. In both cases, they efficiently cope with storm-induced damages, but both are temporary solutions. This is due to the medium-term coastal behaviour in the area, where existing erosion rates determine a continuous shoreline retreat. Thus, any

beach nourishment-based solution needs to consider an adequate re-nourishment scheme to compensate such erosion. Otherwise, the capacity to protect the hinterland will progressively decrease until its total disappearance in a relative short period. Similarly, to design a long lasting retreat-based solution, the setback definition must consider not only the storm-induced erosion but the background shoreline retreat to avoid the need of further retreat in a relatively short period. The absence or the non-application of a storm-induced risk analysis (from identification, quantification, and proposal of solutions) in the study area has led to non-regulated operations by private stakeholders to protect their assets. Of course, they have not solved existing problems and, even worse, they have been aggravated in some locations. These experiences highlight the need to include these types of risk management frameworks in coastal planning, as well as to promote a participatory process that involves the affected stakeholders.

CHAPTER 5.

Setting up XBeach to assess the sensitivity of the Tordera Delta to storm incoming direction.

Adapted from: Sanuy, M., Jiménez, J.A., 2019. Sensitivity of Storm-Induced Hazards in a Highly Curvilinear Coastline to Changing Storm Directions. The Tordera Delta Case (NW Mediterranean). Water, 11, 747. doi.org/10.3390/w11040747.

This chapter presents the set-up and validation of the XBeach model at the Tordera Delta. Model settings and grid were adapted to properly represent the conditions at the study site, characterized by steep slopes, coarse sediment and a strongly curved shoreline. A first application of the model is also presented here to assess the sensitivity of the delta to different incoming storm direction in terms of changes in storm induced erosion and inundation. A sneak peak of obtained results was already presented in Chapter 4, and the process based model will be extensively used to simulate storm-induced hazards in Chapters 6 and 7

5.1. Introduction

An accurate assessment of the magnitude, location and extension of these hazards is becoming an essential part of the risk management process (e.g., Ciavola et al. 2011a, 2011b; Van Dongeren et al. 2018, Jimenez et al. 2018; Plomaritis et al. 2018, Harley et al. 2017) and, in this sense, the use of process-oriented models to forecast storm-induced morphodynamic changes under given scenarios is now standard (e.g., Roelvink et al., 2009; McCall, 2010; Van Dongeren et al. 2017 and references therein, Dissanayake et al. 2014). Most of the studies on testing state-of-art morphodynamic process-based models have addressed cases characterized by straight coastlines and gentle slopes (i.e., conditions close to the comfort zone of the models) (e.g., McCall, 2010; Harter and Figlus 2017). However, applications to estimate costal hazards in hihgly curvilinear environments (e.g., deltaic cuspate coasts) have seldom been tested (e.g., Roelvink et al., 2010; Valchev et al., 2018; and Dissanayake et al. 2014). Furthermore, the effect of testing models based on surf-beat (i.e., the infragravity wave band) on steep slopes and coarse sediment has been recently undertaken mainly in 1D applications (e.g., Vousdoukas et al. 2012; Elsayed and Oumeraci 2017) but rarely so in fully 2DH (2-dimensional, depth-averaged) simulations.

Within this context, the magnitude of storm-induced hazards on a highly curvilinear coast by using XBeach is assessed in the present study. The relevance and main aim of this chapter is twofold: first, from a general standpoint, to test the use of Xbeach on a highly curvilinear coast characterized by coarse sediment reflective beaches, and second, from the local standpoint, to analyze the sensitivity of an already identified hotspot, the Tordera Delta (NW Mediterranean) (Chapter 4), to assess storm impacts for different storm direction scenarios. Thus, the largest recorded storm in the area is used as base case scenario. It occurred in December 2008 and had the typical incoming direction of current climate conditions where eastern (E) incoming storms dominate (e.g., Mendoza et al. 2011). Existing storminess projections under climate change scenarios for the Western Mediterranean do not predict any increase in wave height (e.g., Lionello et al. 2008; Conte and Lionello 2013), but some projections identify potential changes in wave direction (Cases-Prat and Sierra 2012, 2013). Due to this and to the great sensitivity of cuspate coastlines to wave direction resulting from their curvature (e.g., Slott et al. 2006; Johnson et al. 2015), the study aims to assess the potential effects of changing wave direction on extreme storm-induced hazards for the Tordera Delta. The hypothesis to be tested is that changes in wave

direction may cause large variations in the magnitude of storm-induced hazards. Other studies have included the sensitivity to incoming storm direction in their assessments, such as those by Mortlock et al. 2017 in Australia, or de Winter and Ruessink 2017 in Holland.

The chapter is arranged as follows: the section 5.2 introduces the study site and the data used, describes the Sant Esteve 2008 event, which is used as the base case storm-scenario, and presents the methodological part, i.e., the used morphodynamic model and the comparative assessment framework descriptions; the section 5.3 presents obtained results; and finally, the discussion and concluding remarks are presented in section 5.4.

5.2. Materials and methods

5.2.1. Study area

The Tordera Delta is located in the NW Mediterranean Sea approximately 60 km northwards of Barcelona (Figure 5.1). It is a coarse sand delta (i.e., sediment in the range between 0.8 and 1.6 mm) with an aerial surface of approximately 4.2 km2 at the end of a small river basin of approximately 879 km2 (Vila and Serra 2015). The Tordera river is dry during most part of the year, with long dry summers and episodic discharges after heavy rainfall (Martin-Vide and Llasat, 2000). Coastal storms and heavy rainfall events are usually uncorrelated at the area and, in fact, during the simulated storm, significant river outflow was present after the storm peak, with a phase delay of 1 day (Sanchez-Vidal et al. 2012). It has a cuspate configuration with two well differentiated parts at each side of the river mouth (Figure 5.1). The northern part is fronted by the S'Abanell beach, which is oriented towards the E. It has a steep nearshore bathymetry without any relevant geomorphological features in shallow waters The northern hinterland presents a higher topography, except for the zone closest to the river mouth outlet. The southern part is fronted by the Malgrat de Mar beach and is oriented towards the S, which serves as natural protection of a lower hinterland. Shallow water bathymetry is characterized by the presence of a longshore bar running parallel to the coast from the river mouth to the SW, which encloses a plateau at 4 m water depth.

The delta coastline has been eroding during the last several decades as the net result of the littoral drift and the decrease of the Tordera river sediment output, with maximum measured retreats of approximately 120 m Jiménez et al. (2011). The combination of a progressively narrowing beach protecting a low-lying hinterland and this being mainly occupied by campsites makes this area a hotspot for storm-induced hazards (Chapter 4) with different consequences depending on storm characteristics and beach morphology at the time of impact (see e.g., Chapter 6 and 7). As Jiménez et al. (2011) noted, under former accretive-stable deltaic conditions only extreme storms were able to exceed the capacity of protection provided by wide beaches, but under present medium/long-term erosion conditions,

smaller storms have become able to exceed the dissipation capacity of the narrower beaches, increasing the frequency of storm-induced problems (e.g., Jiménez et al. 2012; Chapter 7, Section 7.2).

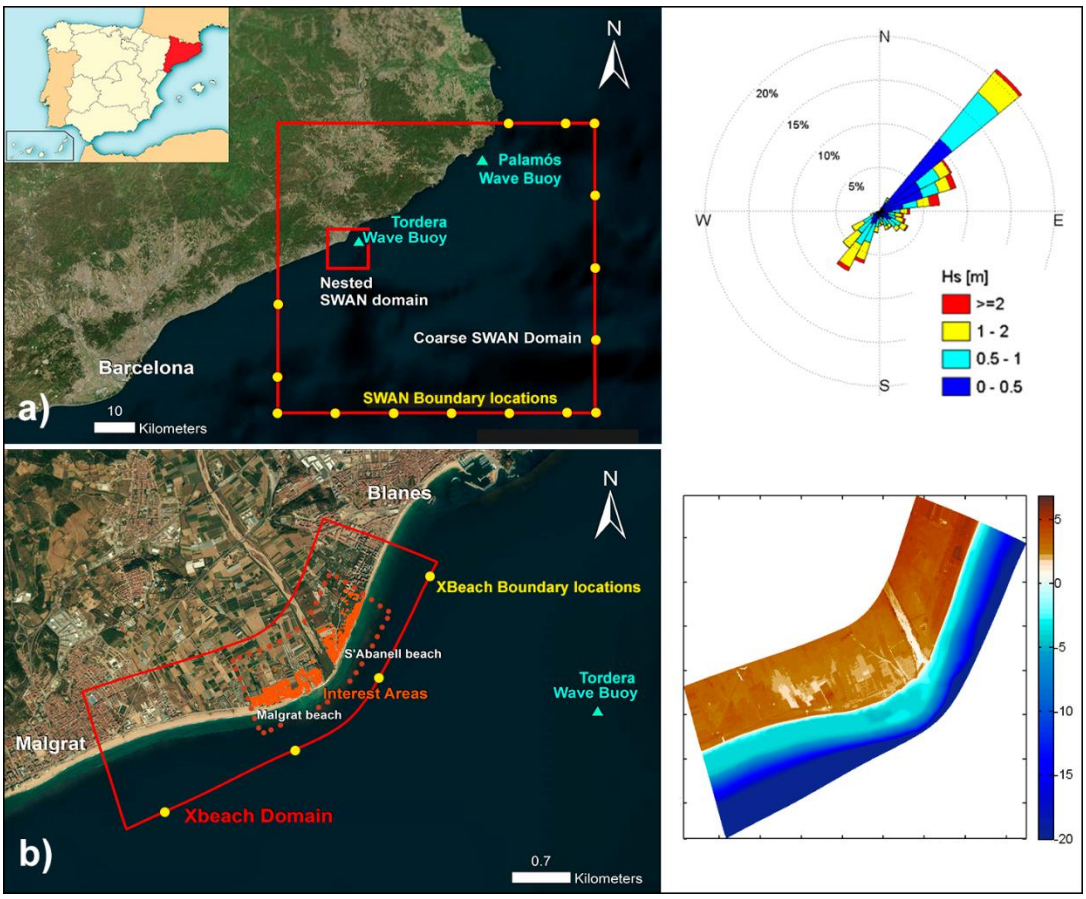

Figure 5.1. Tordera Delta study area, location and model set-up. (a) SWAN (Simulating Waves Nearshore) grids (red) with boundary wave-spectrum nodes (yellow), wave buoys (blue triangles), and significant wave height wave rose for the period 1948–2009 (Global Ocean Waves, GOW, Reguero et al. 2012) at the Tordera wave buoy location. (b) XBeach set-up, curvilinear grid domain (red) and interest areas (orange) and pre-storm topobathymetry.

Wave climate at the NW Mediterranean is characterized in the wave rose in Figure 5.1 (Global Ocean Waves, GOW dataset hindcast, Reguero et al. 2012). Storm events are defined as events with significant wave height (Hs) exceeding 2 m during a minimum of 6 hours (Mendoza et al. 2011). The main incoming wave direction at the site is NE and E, with some events arriving from the S, especially during spring. Within this two main groups, some residual events, can also be found. Thus, the nearshore area, storm conditions can be characterized with waves in the range NE-S being the two extremes of the range the most frequent situations. Nonetheless, some studies rise concerns at the Catalan coast about future climate-induced changes in storm direction, particularly a frequency transfer from the current main cluster (NE-E) towards the secondary one (S) (Casas-Prat et al. 2012, 2013). The area is micro-tidal, with storm surges having a limited role in storm-induced processes due to its relative weight when compared to the wave component. Notably, surges are uncorrelated with waves, are most frequently

under 25 cm, with some extreme events showing maximum recorded surges around 50 cm (Mendoza and Jiménez, 2008).

5.2.2. Data

The wave data used in this analysis were measured by a directional wave buoy located off the Tordera Delta at approximately 70 m water depth (Figure 5.1) belonging to the XIOM (Xarxa d'Instruments Oceanogràfics i Meteorològics) network, which is no longer operative (Bolaños et al. 2009). The Tordera Buoy was a Datawell waverider, sampling during 20' every hour, and thus providing sea states and statistics with an hourly time-step. It covers the period from 1984 to 2013.

Wave spectra from deepwaters and wind fields used to force the model chain were provided by Puertos del Estado, from the WAM (WAve Model, version 4, European Centre for Medium-Range Weather Forecasts, Reading, UK) and HIRLAM-AEMET (HIgh Resolution Local Area Modelling version 7, Agencia Estatal de METeorología, Madrid, Spain) models respectively. Both datasets have a temporal time-step of 1 h. Nearshore water levels were obtained from the same source, provided by the HAMSOM model (HAMburg Shelf Ocean Model, barotropic version, Center for Marine and Atmospheric Sciences. Institute of Oceanography, Hamburg, Germany) with the same temporal resolution.

Storm-induced topographic changes have been quantified by using LIDAR-derived topographies obtained before (16 October 2008) and after the storm impact (17 January 2009) by the Institut Cartogràfic i Geológic de Catalunya. The data were provided as high-resolution digital elevation models (DEMs) with a 1-m grid step, a maximum vertical precision of 2–3 cm and overall RSME of 6 cm (Ruiz et al. 2009).

The bathymetry of the study area has been obtained by combining an offshore grid with a spatial resolution of 0.28' derived from the GEBCO (General Bathymetric Chart of Oceans, 2014), and a finer inner topography while nearshore bathymetry was built by combining the LIDAR-derived topography and multi-beam bathymetric data provided by the Ministry of Agriculture, Fish, Food, and Environment, covering the whole area from the +2 to the −50 m with a 5 × 5 m resolution. Multiple bathymetries were available from different years, including 2006 and 2010, and these information was merged to properly fit the 2008 LIDAR shoreline and link the emerged topography with the submerged bed.

5.2.3. The sant esteve 2008 storm

The storm of reference used in this study was a V-class (extreme) event, according to the classification of storms in the NW Mediterranean of Mendoza et al. (2011). This storm, known as the Sant Esteve storm, occurred on 26 December 2008 in the northern part of the Catalan Sea. It was created by the presence of a low-pressure center located over the Balearic Sea, with a minimum pressure of 1012 hPa,

along with a high pressure center over northern Europe (1047 hPa). This is one of the typical mechanisms of cyclogenesis in the Mediterranean (e.g., Trigo et al. 2002), and it is the most common situation originating extreme storms along the Catalan coast (Mendoza et al. 2011). Under these conditions, the action of very strong NE winds in the Gulf of Lyon (wind velocities up to 20 m s−1 were recorded at the coast) generated a wave field with a clear spatial pattern, with Hs values and power content decreasing from north to south along the Catalan coast (Jiménez, 2012; Sánchez-Vidal et al. 2012). Thus, according to the data recorded by the Palamós buoy (see location in Figure 5.1), the storm lasted 73 h (Hs > 2 m) reaching a Hs of 7.5 m at the peak of the storm and a maximum wave height (Hmax) of 14.4 m. The associated return period of this storm was approximately 125 years according to the data on extreme climate obtained by Puertos del Estado (2006) for this buoy and in light of data previous to the storm. The storm progressively lost strength as it moved south and, off the study site, the values recorded by the Tordera buoy showed a storm with a duration of 66 h, reaching a Hs at the peak of the storm of 4.65 m and Hmax of 8.0 m. Mean wave direction during the storm was E, which corresponds to the dominant direction during extreme storms in the area (Mendoza et al. 2011). Figure 5.2 shows the recorded values of wave parameters during the storm by the Tordera buoy (see location in Figure 5.1).

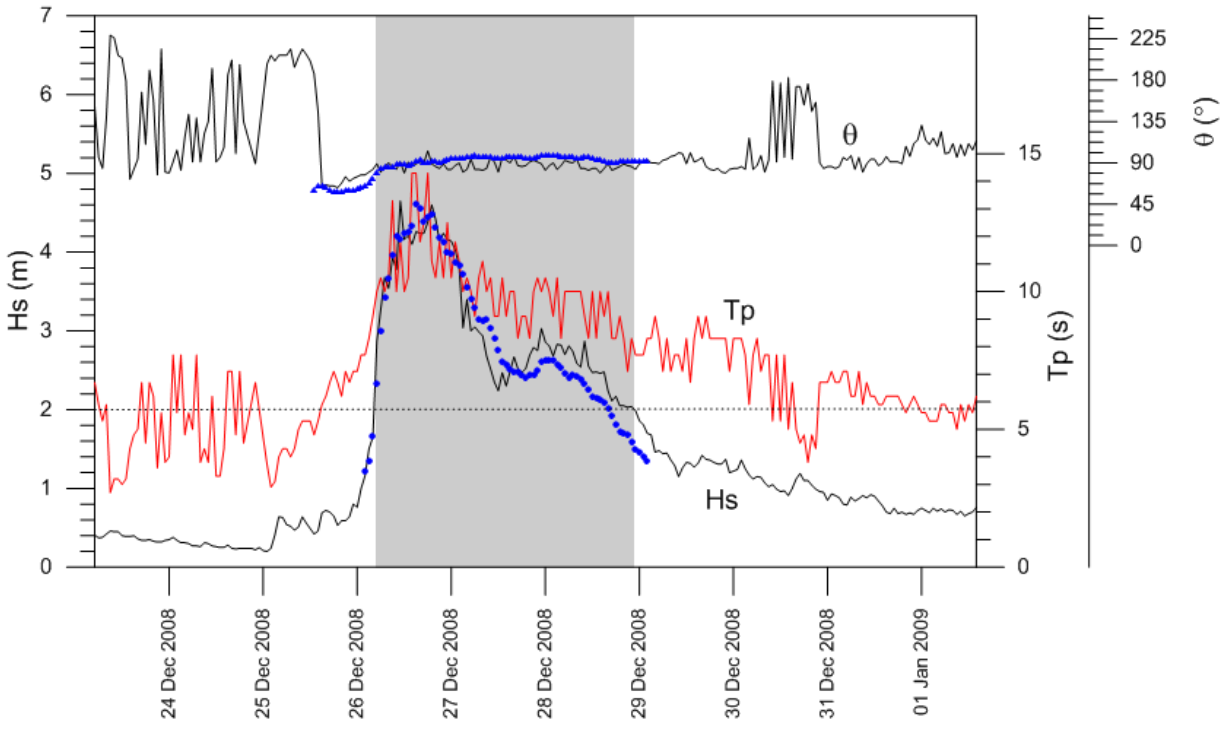

Figure 5.2. Wave records off the study site (Tordera buoy, see Figure 5.1) during the San Esteve storm. Blue dots indicate SWAN output at the same location.

The impact of the storm produced a significant coastal morphodynamic response in the form of erosion and overwash for most beaches along the northern part of the Catalan coast (Plana-Casado, 2016; Jiménez et al. 2014; Durán et al. 2016). Moreover, the magnitude of the storm was so considerable that many benthic ecosystems were also significantly affected (Sánchez-Vidal et al. 2012; Teixidó et al. 2013; Pagès et al. 2013).

Storm-induced topographic changes in the surroundings of the Tordera river mouth are shown in Figure 5.3. The observed response was different on both sides of the river, with the largest erosion taking place in the northern part, the s'Abanell beach. This beach is oriented to the East, nearly perpendicular to storm waves, and thus, the beach presented a generalized erosive behavior along its total extension (2.4 km). The volume of sediment eroded from the subaerial part of the beach was approximately 66,000 m^3, with a beach-averaged erosion rate of approximately 30 m^3/m and a maximum value of approximately 80 m^3/m at its northernmost part (section SB-1 in Figure 5.3). Storm-induced wave overtopping occurred along the entire beach, and in its southernmost part, close to the river mouth, overwash deposits up to 6 m^3/m were detected (section SB-3 in Figure 5.3). These volume changes resulted in a beach-averaged shoreline retreat of 11 m, with a maximum recession of approximately 30 m (Plana-Casado, 2016; Jiménez et al. 2014).

From the river mouth to the south, the coast experienced a different morphodynamic response. This section, the Malgrat de Mar beach, is oriented to the S, resulting in a large obliquity to E incoming waves during the storm. Just south of the river mouth a small post-storm accretion spot of approximately 7000 m^3 was detected. This seems to be related to the alongshore deposition of material eroded from the northern part. South of this area, the coastline shows a nearly generalized moderate erosion together with significant overwash deposits in the subaerial part of the beach (Figure 5.3). The spatially averaged erosion of the emerged beach was approximately 10 m^3/m (one third of that observed for the northern beach) whereas the averaged overwash accumulation was approximately 7.5 m^3/m (Plana-Casado, 2013; Jiménez et al. 2014).

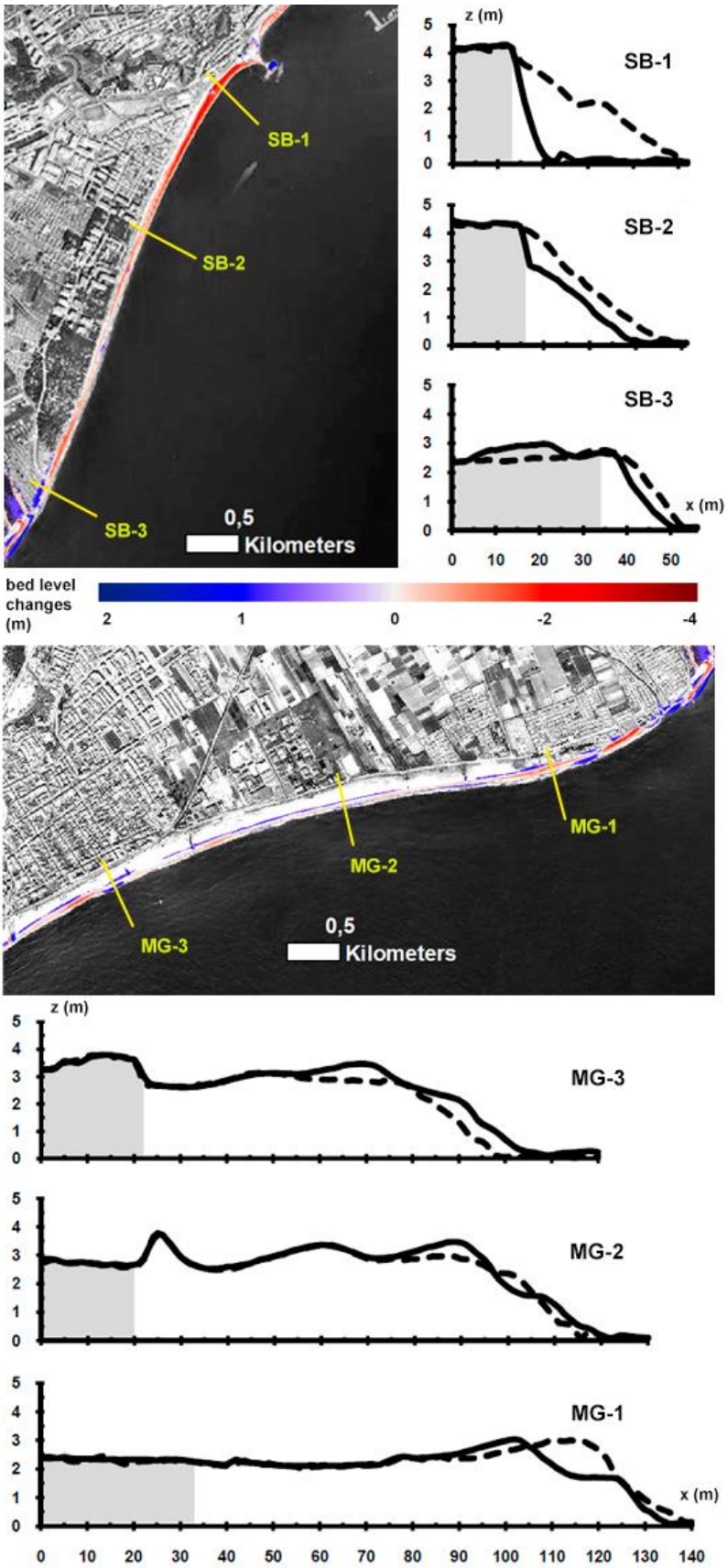

Figure 5.3. Morphologic changes after the St Esteve 2008 storm. Dashed line pre-storm and continuous line post-storm profiles. Grey shaded area represents de position of the promenade (north) or road (south).

5.2.4. Models

Simulations have been done by using a model setup composed of the SWAN model (Simulating Waves Nearshore, version Cycle III v41.01, Delft University of Technology, Deltares, The Netherlands) (Booij et al. 1996,1999; Ris et al. 1999, TU Delft 2016), which propagates waves to the coast, and of the XBeach model (eXtreme Beach behavior, Kingsday version, Deltares, Delft, The Netherlands) (Roelvink et al. 2009), which is used to assess two storm-induced coastal hazards: inundation and erosion.

SWAN (Simulating Waves Nearshore) is a third generation wave model which is based on the wave action balance equation. It simulates short-crested wind generated waves by incorporating wave–water interactions, wind growth and dissipation processes such as whitecapping, bottom friction, and depth-induced breaking. For more detailed insight into these mechanisms controlling energy and wave propagation processes the reader is referred to the SWAN manual and to SWAN scientific technical documents at http://swanmodel.sourceforge.net/. The implemented model version uses the Komen et al. (1984) formulation to calculate whitecapping. This version permits counteracting the previously reported under-predictions of significant wave height and wave period in areas characterized by fetch-limited conditions under the influence of transient winds (see e.g., Bolaños 2004; Pallares et. al 2014), which are typical conditions for the NW Mediterranean coast.

The model has been implemented using a nested grid configuration (Figure 5.1). A coarse grid with a total extension of approximately 80 × 70 km is used to transfer offshore wave conditions to the study area. The bathymetry grid has a spatial resolution of 0.28′ whereas the wind field grid has a spatial resolution of 5′. This coarse setup is fed with wave spectra at 15 positions distributed along the offshore boundaries of the grid (Figure 5.1). The inner fine grid covers a domain of approximately 20 km × 26 km with a spatial resolution of 0.06’. This grid has been generated to properly reproduce the existing sharp changes in the bathymetry between intermediate-shallow waters due to the large steepness of the lower shoreface. This can permit a better simulation of wave propagation in the region close to the XBeach coastal grid (external boundary at 20 m water depth). A limitation of the SWAN model is its inability to simulate storm surges. To characterize storm surges in the study area we use water level predictions obtained with the HAMSOM model implemented by Puertos del Estado (Ratsimandresy, et al. 2008) at three locations close to the study site. The storm surge contribution to the total water level in the study area is of low magnitude and significantly smaller than wave-induced runup during storm conditions (e.g., Mendoza and Jiménez, 2008). The validated SWAN model has been used to propagate waves from deep to shallow waters during the entire storm duration. Since a simultaneous time series of measured wave data was available within the modelled domain, it was possible to obtain transfer coefficients for wave conditions (wave height and direction) for any point in the grid with respect to the buoy location. With this information, the recorded wave conditions at the buoy have been transferred to selected grid points to be used as input data for Xbeach modelling.

Once the forcing conditions during the storm have been propagated from deep water to nearshore, the remaining task is to propagate these conditions to the coast and to assess the magnitude of storm-induced hazards, i.e., erosion, overwash and overtopping, which is done with the XBeach model. XBeach is an open-source 2D depth averaged model which solves wave propagation, flow, sediment transport and bed level changes for varying wave and flow boundary conditions (Roelvink et al. 2009). It solves the time-dependent short wave action balance on the scale of wave groups, which allows for the reproduction of directionally spread infragravity motions (so called surf-beat) along with time-varying currents. The frequency domain is represented by a single representative peak frequency, assuming a narrow banded incident spectrum. Shallow water momentum and mass balance equations are solved to compute surface elevation and flow. Additionally, to solve the contribution of short waves to mass fluxes and return flows, XBeach uses the Generalized Lagrangian Mean formulation (Roelvink et al. 2009).

Sediment transport rates are calculated from the spatial variations in depth-averaged concentration, which are calculated from advection-diffusion equations with a source-sink term based on an equilibrium sediment concentration. The equilibrium concentration takes into account both the contribution of the suspended and bed loads by means of the Soulsby-Van Rijn formulation (Soulsby, 1997) with a limitation of the maximum stirring velocity based on the Shields number at the start of the sheet flow (McCall et al. 2010). For deeper insight into the XBeach description, setup and equations, see Roelvink et al. (2009).

The model has been implemented by using a curvilinear grid with variable cell size in both alongshore and cross-shore directions (see Figure 5.4). The extension of the mesh is approximately 1.5 km in the cross-shore direction, with cell size ranging from 5~6 m at the offshore boundary (20 m depth) to 0.7–0.8 m at the swash zone. In the alongshore direction the model has an extension of 4.5 km and the cell size ranges from 25 m at the lateral boundaries down to 2–3 m around the river mouth. The grid was obtained by means of the Delft3D-RGFGRID module, imposing consecutive maximum cell-size changes ~5–10% to ensure proper smoothing, while maintaining valid orthogonalisation. The final result has 669 alongshore by 568 cross-shore nodes. The model wave boundary conditions consist of wave characteristics specified at four different locations along the offshore boundary (see Figure 5.1), with a time-step of 1 h, which is the same resolution of the original data used to force SWAN. The use of four different locations aims to capture the difference in wave conditions on both sides of the river due to the different coastline orientation. Water level variations during storms to be simulated are directly introduced in the model from HAMSOM simulations, also with a time-step of 1 h. XBeach model computations (i.e., hydrodynamics and morphodynamcis) are performed with a temporal resolution of 1 second (dtbc = 1).

The morphology of the study area, characterized by coarse sand and steep reflective beaches, makes XBeach modelling a demanding exercise in terms of predicting beach morphodynamic response during storms (see e.g., Vousdoukas et al. 2011, 2012). Notably, coarse sediment environments are characterized by a lower frequency of the avalanching processes, a greater importance of the bed load

over the suspended transport, and higher importance of mechanisms such wave asymmetry, or water infiltrations and groundwater effects. All these are by default configured in XBeach to work for fine sand environments, and must be revised and modified for its application at the study site, modelled with a D50 of 1.3 mm and a D90 of 1.9 mm.

To properly reproduce morphodynamic changes, both the surf-beat and the non-hydrostatic modes of the XBeach model were initially tested. The surf-beat model was observed to under-predict overwash when using typical XBeach-grid resolution for straight and mild-slope coasts. This under-prediction is also caused by the lower contribution of infragravity waves to the total run-up in steep profiles (Wright and Short, 1984). However, the surf-beat model accurately reproduced the alongshore patterns of erosion in the entire domain. In contrast, the non-hydrostatic model was observed to have better performance in reproducing wave-by-wave run-up but lower accuracy in reproducing the alongshore morphodynamic patterns of erosion and deposition, with a quite higher computational cost (since it requires denser grids). An additional difficulty was using XBeach with a curvilinear grid to properly reproduce alongshore processes driven by the change of coast orientation at both sites of the river mouth. The final adopted approach was to use the surf-beat model with a higher resolution than the typically used in straight and gentle-slope coasts, which considerably improved the overwash prediction. The average cross-shore resolution of 5.2 m (typically 20~25 m) at the offshore boundary, going down to 0.7 at the swash zone, ensured a better reproduction of wave propagation. This setting aimed to properly capture the abrupt changes in the bathymetry from the 20 m to the 5 m depth by using a larger number of cells. In addition, the average alongshore resolution around the river mouth, where the largest alongshore gradients are present, was increased up to 2.3 m (typically 5~10 m) (Figure 5.4).

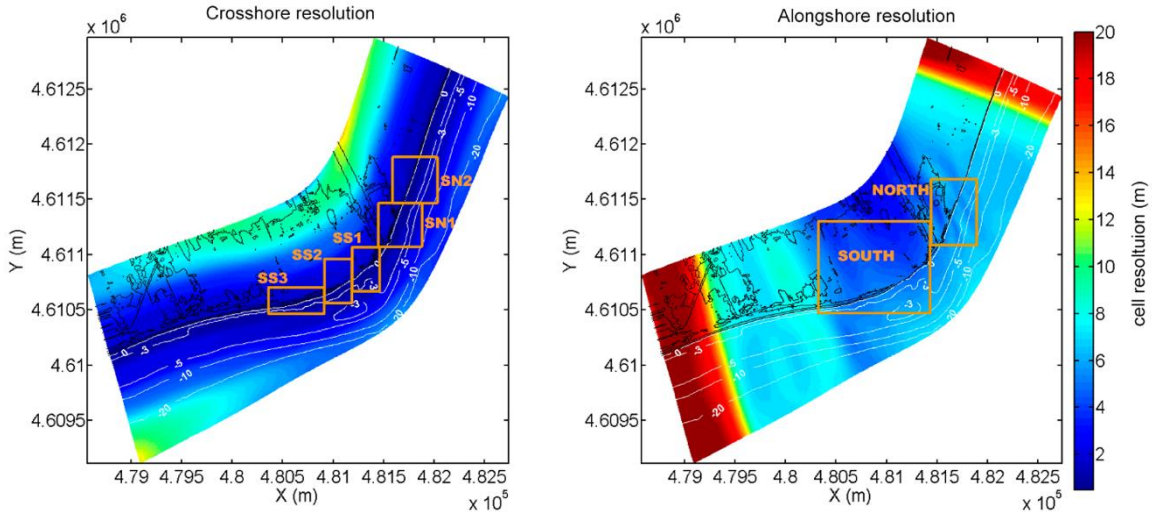

Figure 5.4. Distribution of cross-shore and alongshore grid resolution over the XBeach domain. Orange boxes show the location of post-processing subdomains, being SN and SS sectors (left) for the morpholodynamic analysis and NORTH, SOUTH sectors (right) for the inundation assessment.

5.2.5. Scenario testing

Since the recorded Sant Esteve 2008 event had the characteristics of a V-class extreme storm in the area, with the largest recorded Hs and with a typical E direction, it was used as base case scenario (C0). From this, six additional scenarios were defined to test the effect of different incoming wave directions. The procedure consisted of simulating the exact same wave time series as the Sant Esteve 2008 storm (keeping the same Hs, Tp, and directional spreading) and only changing the mean wave direction. This approach permits maintaining the same storm wave intensity as the validated reference case. The tested conditions were two scenarios where wave direction was shifted 20° and 40° counter-clockwise to the North (C20− and C40−) and four scenarios shifting 20°, 40°, 60°, and 80° clockwise to the South (C20+, C40+, C60+, and C80+). Thus, seven different scenarios, including the baseline condition, were simulated and compared to assess the differences in storm-induced hazards under incoming directions ranging from ~60° N (C40−) to ~180° N (C80+). The scenarios have been chosen to cover the tipical range of incoming conditions at the −20 m depth with directional spans of 20°.

The magnitude of storm–induced hazards was quantified in different control sectors along the study area to capture main factors potentially affecting the beach response to different incoming directions. Thus, the morphodynamic response was analyzed in five sectors: two 250 m long sectors northward of the river mouth (SN1, SN1), and three sectors southward of the river mouth (Figure 5.4). These S sectors are as follows: (i) SS1, a 200-m-long stretch between the river mouth and an existing rigid structure at the shoreline; (ii) SS2, a 200-m-long sector, southward of the mentioned existing structure; and (iii) SS3, a 500-m-long stretch at the southernmost end. At each sector, three variables are used to characterize morphodynamic changes: erosion volume (m^3/m), overwash volume (m^3/m) and profile retreat (m). All of the variables are calculated from XBeach gridded output, from which sector-averaged values and standard deviations are derived. Erosion volumes are computed in the inner part of the beach, from the subaerial part down to the −2 m level, which roughly determines the water depth where main inner profile changes occur. Overwash volumes are computed as deposited sediment volumes in those parts of the subaerial beach where vertical growth is detected. The profile retreat is measured at three elevations at the beachface (1, 1.5, and 1.75 m above mean water level).

To characterize inundation, just two sectors were selected, one for the region at the north of the river mouth and another to the south (Figure 5.4). The selected variable to characterize inundation was the inundation surface (Ha) over different thresholds of inundation depth: 0.05, 0.25, 0.5, and 1 m.

5.3. Results

5.3.1. Base case scenario (c0). The sant esteve storm

This base case scenario corresponds to the model validation using the recorded Sant Esteve 2008 Storm event. The SWAN model was validated with wave conditions recorded by the Tordera wave buoy and by comparing the measured and modelled wave conditions (Hs, θ), shown in Figure 5.2. As can be seen, the model reproduces well wave parameters during the storm, especially during the peak of the event, when simulated variables almost coincide with recorded ones. The obtained root mean squared error (RMSE) of the model during the entire duration of the storm is 0.53 m in Hs and 12.5 degrees in θ, with the largest contributions to the error taking place during the relaxation phase of the storm (Figure 5.2). Since the largest storm-induced morphodynamic changes occurred during the storm peak, we can accept that the use of the SWAN model to simulate wave propagation in the study area is acceptable for the purposes of this research.

To calibrate XBeach, the model's results were compared with LIDAR measurements of the emerged beach. The calibration of the model was performed by adopting a double approach: (i) by optimizing the Brier Skill Score (BSS), which quantifies model performance by comparing model output to the real post-storm LIDAR measurements of the emerged profile; (ii) by performing a qualitative assessment of the modelled features, such as alongshore and cross-shore patterns of bed level changes, magnitude, and location of the overwash deposits and validation of the inundation reach according to the available qualitative information on the event. The used BSS to characterize model predictive skill takes into account the measurement error (ΔZ_e) as in Harley and Ciavola (2013), and thus, the BSS score is given by:

$$\mathrm{BSS} = 1 - (\sum(|z_{mf} - z_{mod}| - \Delta Z_e)^2 / (\sum(z_{mf} - z_{mi})^2 \qquad (5.1)$$

where z_{mf} is the final LIDAR measured bed level, z_{mod} the final modelled bed level, and z_{mi} the initial bed level. Here, ΔZ_e is considered as the LIDAR measurement error (i.e., RSME of the overall LIDAR product), which is 0.06 m. According to Sutherland et al. (2004), the classification of models' performance based on the BSS score can be considered to be very good for values over 0.4 and excellent for values over 0.5–0.6. Due to the morphology of the study area, which induces a differentiated morphodynamic response along the coast (Figures 5.5 and 5.6), three BSS were calculated: (i) a global BSS, which is calculated for the entire area; (ii) a local BSS at the north of the river mouth; and (iii) a local BSS southward of the river mouth. Since the BSS assessment can only be performed for the emerged profile (where pre- and post-storm topographic data exist), a qualitative assessment of the modelled submerged profile was also performed. To this end, we analyzed the final shape of the

modelled submerged profile taking into account the expected typical morphodynamic response under storm conditions at the site.

Table 5.1. Calibration parameters. Range of tested values and final parameter setup.

Parameter	Tested Values	Description	Final Set-up[1]
gamma	0.55–0.7	Breaker parameter in Baldock or Roelvink formulation (default = 0.55)	0.7
delta	0–0.5	Fraction of wave height to add to water depth in wave breaking formulations (default = 0)	0.5
facAs	0.2–0.7	Calibration factor time averaged flows due to wave asymmetry (default = 0.1)	0.6
facSk	0.2–0.7	Calibration factor time averaged flows due to wave skewness (default = 0.1)	0.6
wetslp	0.3–0.8	Critical avalanching slope under water (dz/dx and dz/dy) (default = 0.3)	0.7
gwflow	0 and 1	Turn on groundwater flow (default = 0)	1
sedcal	0.1–1	Sediment transport calibration coefficient per grain type (default = 1)	0.1

[1]based on best BSS score and qualitative assessment

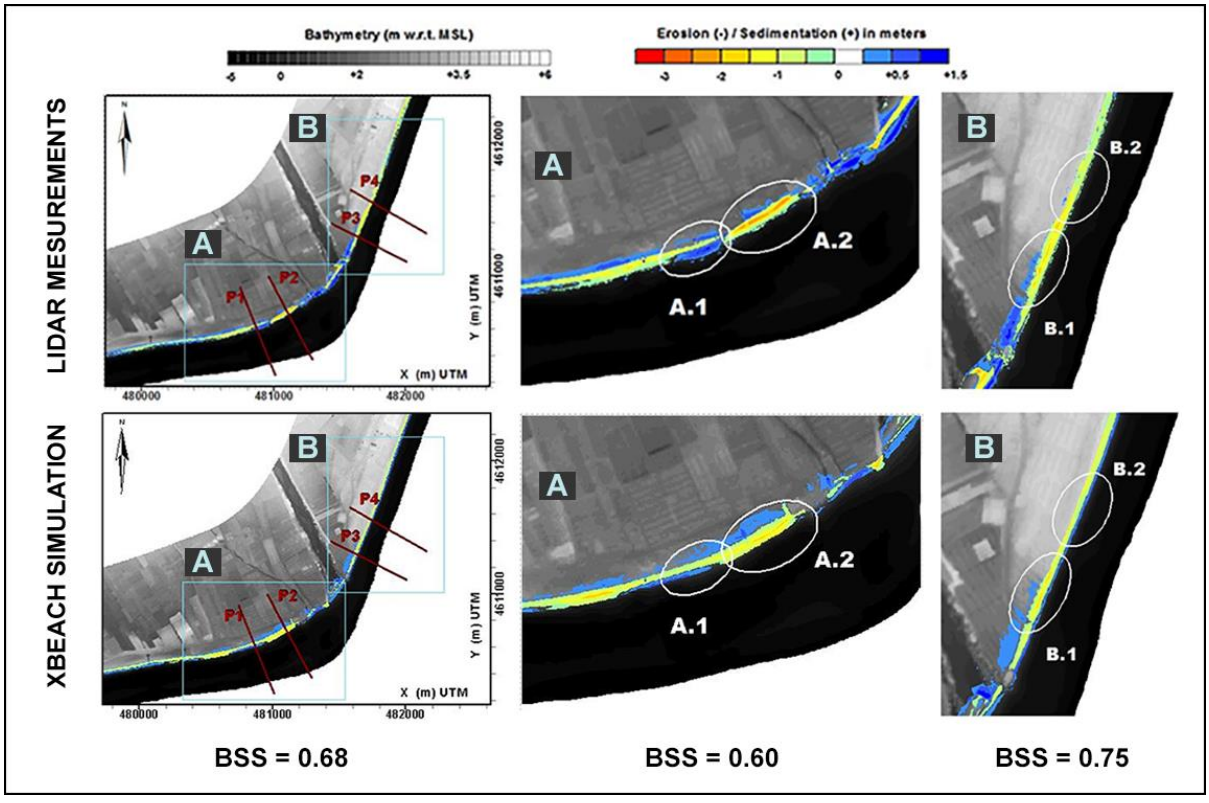

Figure 5.5. XBeach validation with LIDAR measurements of the emerged morphological changes. BSS: Brier Skill Score.

Although different combinations of model parameters resulted in BSS scores over 0.4 for the emerged profile, the qualitative assessment highlighted that some of them produced excessive deposition volumes in the submerged part. The final setup parameters, which resulted in an overall BSS of 0.68 (measured at the northern beach and first 600 m of the southern beach) and a meaningful qualitative simulation of the predicted submerged profile and alongshore bed level change patterns, are shown in Table 1 along with parameter description and tested ranges.

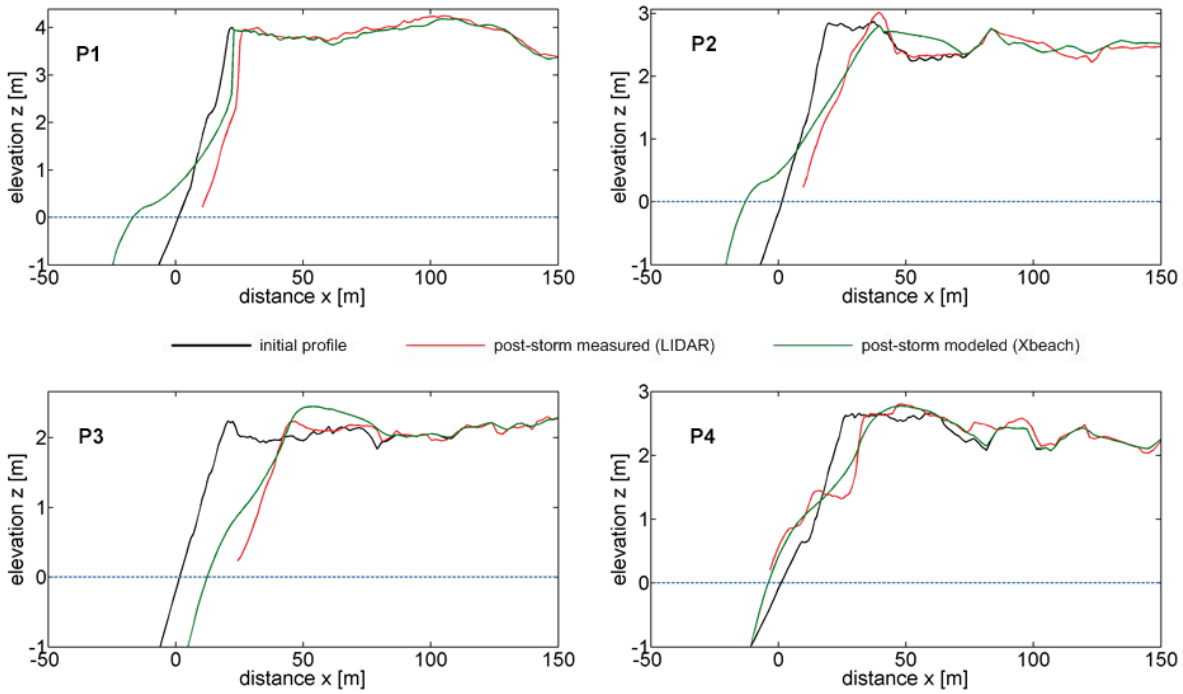

Figure 5.6. Comparison between XBeach simulated and measured beach profiles after the impact of the storm (see profiles location in Figure 5).

The implications of the selected values are as follows. First, the increase in wave-attack on the coast improves the behavior of the model in terms of reproducing observed overwash deposits (gamma and delta). Second, the contribution of avalanching to bed level changes was limited, taking into account the steepness of the site (wetslp). Third, the non-linearity effect on sediment transport for steep profiles (facAs and facSk) may be taken into account as reported in Elsayed and Oumeraci (2017). Fourth, sediment particle mobilization may be limited (sedcal). With respect to this, other authors have already reported an excess of modelled sediment suspension because the shear stress values required to initiate particle motion are higher than those predicted by using the Shields curve, as noted in Elsayed and Oumeraci (2017) or McCall et al., (2010). Fifth and finally, the groundwater module was turned on (gwflow) because the role of infiltration is more significant in coarse sediment environments, such as the Tordera Delta, where grains are close to gravel-size. The value of the permeability factor has been

estimated using the Kozeny–Carman formula as described in Carrier (2003). For the grain size in the study area, the value of the permeability factor was estimated to be 0.0058 m/s. The results of the storm-induced morphological changes simulated with the final adjusted set of model coefficients are shown in Figures 5.5 and 5.6. As it can be seen, the measured changes in beach elevation at both sites of the river mouth are well reproduced by the model, with a BSS of 0.68 when the entire area is considered. The model also properly reproduces the differentiated response at both sites of the river mouth, mimicking the effects of change in coastal orientation with respect to the storm wave direction and the differences in coastal morphology.

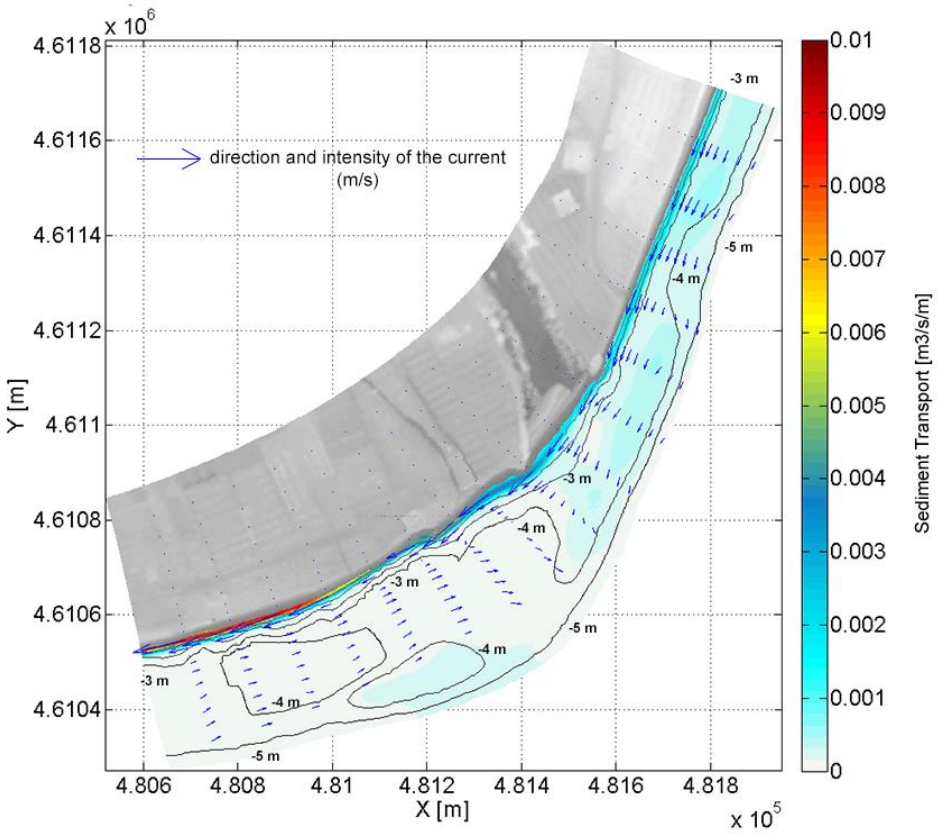

Figure 5.7. Simulated depth-averaged currents and sediment transport. Mean XBeach output at each 1 h time-step is averaged during the 4 h of maximum storm intensity.

Figure 5.7 shows the modelled depth-averaged wave-induced circulation during the peak of the storm, where a different circulation pattern is observed at both sides of the river mouth. Mean XBeach output (average conditions at 1 h output time-step) is used to average the current velocity and sediment transport during 4 h around the maximum peak of the event. At the northern part, where the beach is fully exposed to storm waves (i.e., a relatively small obliquity during the storm) and without any submerged morphological features, wave-induced circulation shows a typical quasi-uniform longshore current structure along the beach until the river mouth at the southern end. At the southern part, the coast is

partially sheltered from storm waves (i.e., a large wave obliquity during the storm) and there is an alongshore bar running parallel to the shoreline with varying crest levels. This bar delimits a shallow shelf of approximately 4 m water depth to the shoreline. In this area, the induced circulation pattern during the peak of the storm shows a longshore current directed towards the south close to the shoreline and a local inversion of the current towards the N over the shallow shelf (Figure 5.7).

With respect to morphodynamic changes (Figures 5.5 and 5.6), the model predicts, for the northern part, a nearly continuous erosion along the beach without significant alongshore gradients in sediment transport, and with significant sediment mobility down to about −5 m depth. The model properly reproduced the observed increase in erosion magnitude from B2 (P4) to B1 (P3), as well as most of the overwash deposits, which increase towards the south as the height of the berm decreases. In summary, the model reproduced well the observed variability in beach erosion and overwash along this northern site with a local BSS of 0.75. Southwards of the river mouth (Malgrat Beach), induced sediment transport and beach erosion present significant alongshore variations, with the largest erosion taking place just southwards of an existing structure located at the northern part of the sector, A2 (P2), which should act as a local boundary condition. This local effect can be seen in Figure 5.7 where a gradient in the longshore sediment transport, starting at the rigid structure north of A2, is detected. Longshore transport rates are larger than in the north, and mainly concentrated down to – 3 m water depth. The model reproduced observed beach topographic changes with large erosion and overwash deposits due to a relatively low beach berm (A2, P2). At the southernmost part, erosion is only taking place at the upper level of the profile, whereas part of the material is deposited around zero level (A1, P1). The obtained local BSS for this sector was 0.60.

5.3.2. The effects of wave direction to storm-induced hazards

As was previously mentioned, once the morphodynamic model was calibrated, it was used to analyze the sensitivity of the area to changes in wave direction during storm impacts. Simulated morphodynamic changes and inundation for cases C20− (~80° N) to C40+ (~140° N) at northern and southern parts of the study area are shown in Figure 5.8, whereas the variation of integrated control variables for each sector can be seen in Figures 5.9 and 5.10 for inundation and morphodynamic changes respectively.

With respect to inundation, the beach northward of the river mouth (Figure 5.9a) experiences an increase of the predicted inundation surface from C40− to C20+, when the surface reaches its maximum extension (5.47 Ha with 1 Ha over 0.5 m depth). Wave direction in this scenario corresponds to a nearly normal wave attack on the local coastline orientation. As incoming wave direction continues shifting towards the south, the predicted inundation surface progressively decreases, reaching values for the C80+ case similar to those observed for the C40− case. At the southern coast, the obtained pattern is significantly different (Figure 5.9b). Thus, for wave direction scenarios dominated by NE components (C40−, C20−) no significant inundation is observed, and this is consistent with a large sheltering from

highly oblique wave incidence. For wave directions shifting from the base scenario to the south (C0 to C80+), the predicted inundated surface increases, reaching a maximum value for scenarios C60+ and C80+ of approximately 74 Ha (for an inundation depth above 0.05 m) and 33 Ha (for an inundation depth of 0.5 m), the C80+ case. Taking into account the total inundation of the study area, we can state that the magnitude of the inundation hazard significantly increases as wave direction shifts to the south. The southern coast is the most affected in terms of the magnitude of expected changes due to the local low-lying topography.

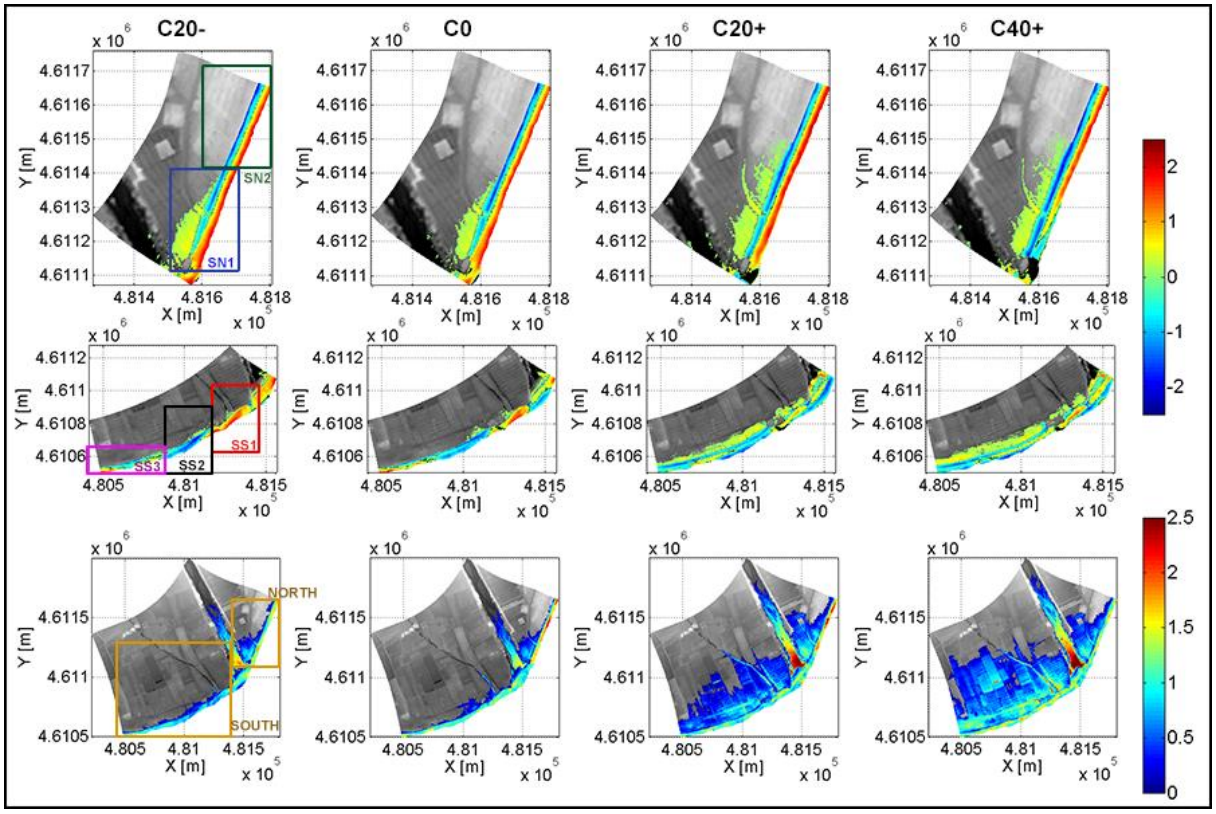

Figure 5.8. XBeach-simulated inundation depth (m) (bottom) and bed level changes (m) northwards (top) and southwards (middle) of the Tordera River.

Regarding morphological changes, the northern beach (S'Abanell) shows a relatively low sensitivity to wave direction for scenarios C40− and C20+ when erosion volumes and profile retreats are considered (Figure 5.10). For this range of wave directions, the local wave-induced circulation is characterized by a southward directed longshore current along the beach (see Figures 5.7 and 5.11) which turns north when the wave direction is C20+ (Figure 5.11). As the incoming wave direction turns southwards, a stronger north-directed alongshore current is induced with velocity increasing along the beach (Figure 5.11) which results in an increasing erosion and profile retreat. Figure 5.11 also shows hatching areas in the velocity field which originate in those areas where wave incidence is orthogonal to the nearshore bathymetry, characterized by a heterogeneous bar in front of the coast. This beach erosion increase is

particularly observed at the southernmost end of the section (SN1), just northwards of the river mouth, where an existing revetment acts as a boundary condition (barrier) for northwards directed transport. This overall modelled behavior is consistent with local field observations, where the northern part of the beach (out of the domain) experiences a significant sediment deposition under the impact of southern storms, bringing sediment from the south.

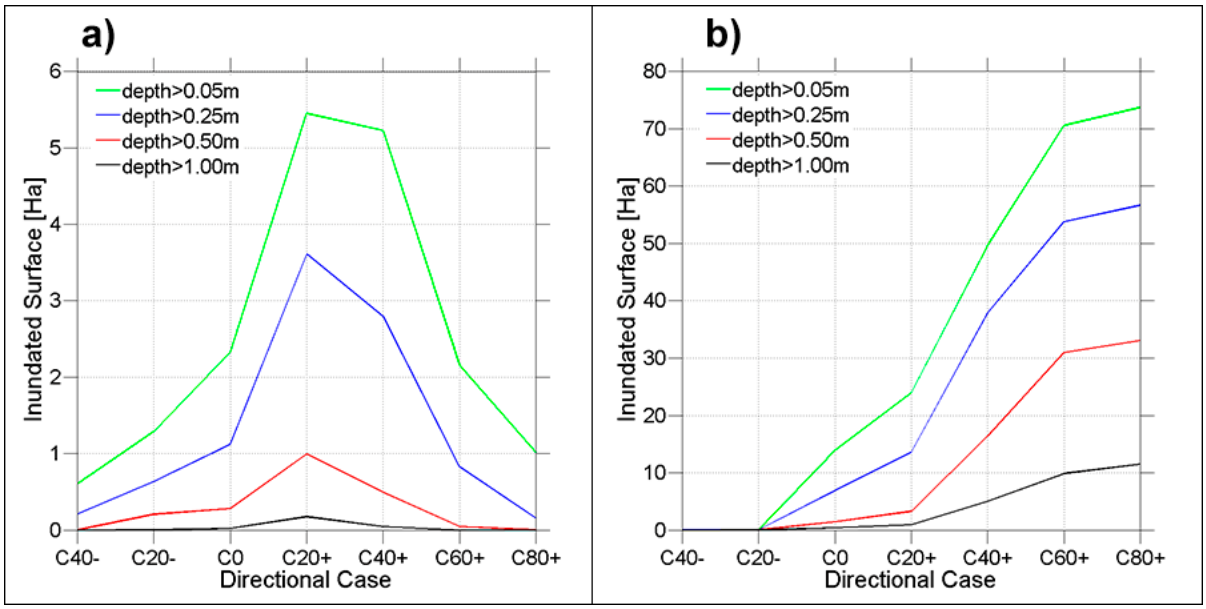

Figure 5.9. Variation of simulated inundated surface for different inundation depths as a function of the simulated storm direction for the northern (a) and southern (b) control areas (see Figure 5.4 or 5.8 for location).

Overwash deposits along the northern section present a variation pattern with wave direction consistent with modelled inundation. The largest overwash verifies in the southern end of this sector (SN1) due to its lower beach berm. Thus, maximum overwash deposition verifies at SN1 under C20+ and C40+, which were the scenarios producing the largest inundations. As wave obliquity increases (scenarios C60+ and C80+), overwash significantly decreases, which is also in agreement with the observed inundation decrease under these conditions.

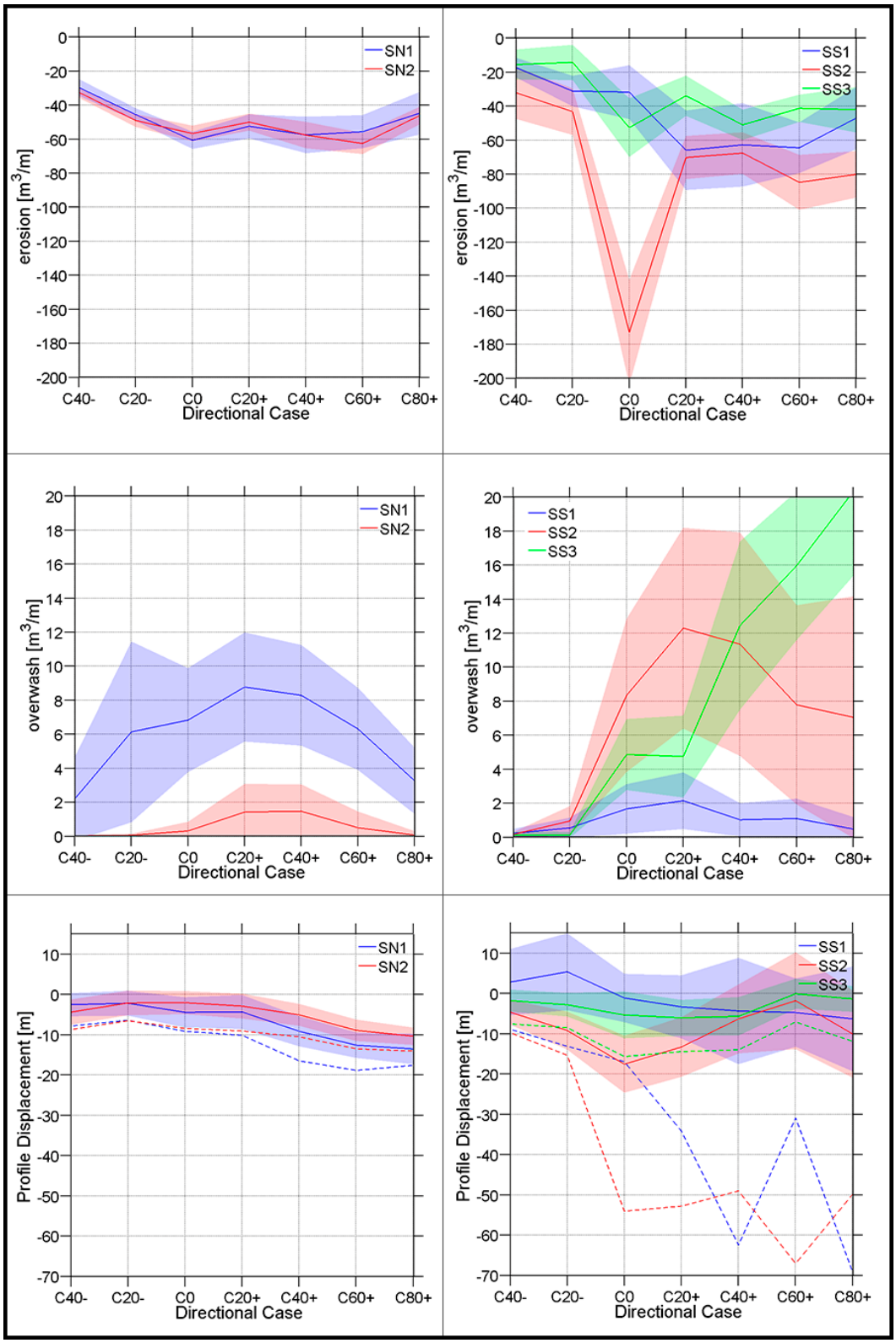

Figure 5.10. Variation of simulated morphodynamic parameters (see text for description) at selected control areas the N (left) and S (right) coasts for tested storm directions (see Figure 5.4 or 5.8 for location). Continuous lines denote variable mean, shaded areas represent standard deviation and dashed lines indicate maximum profile retreat at each sector.

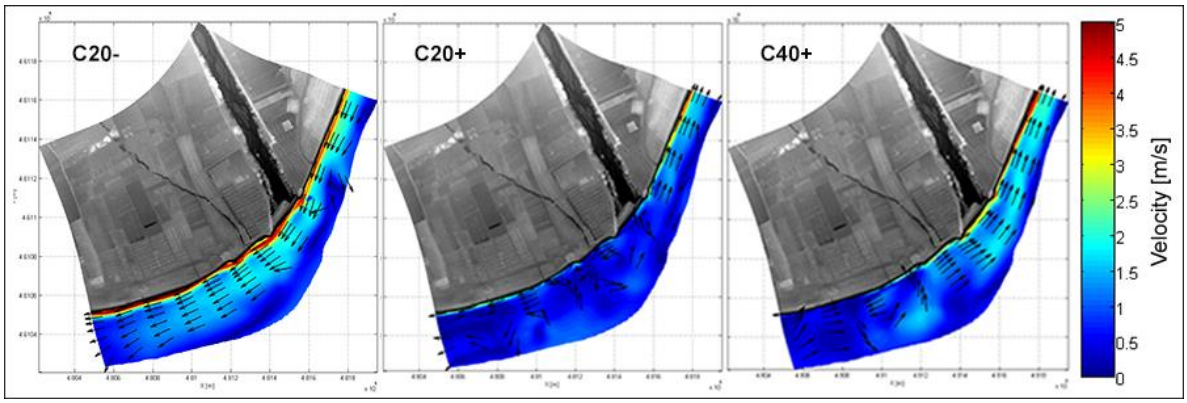

Figure 5.11. XBeach simulated depth-averaged currents. Mean XBeach output at each 1 h time-step is averaged during the 4 h of maximum storm intensity.

5.4. Discussion and conclusions

In this chapter, the potential effects of changing wave direction for the storm-induced hazards on a highly curvilinear coarse sandy coastline have been assessed. This sensitivity test has been selected because although storminess projections under climate change scenarios for the Western Mediterranean do not predict any increase in wave height (e.g., Lionello et al. 2008; Conte and Lionello, 2013), some existing projections identify potential changes in wave direction (Casas-Prat and Sierra 2012, 2013). These changes in wave direction may have significant implications for coastal sediment transport and coastal stability, as has been confirmed for the interannual changes influenced by El Niño (e.g., Barnard et al. 2011). Moreover, regarding cuspate coastlines such as the study area, their greater sensitivity, due to their curvature, results in even more significant implications (e.g., Slott et al. 2006; Johnson et al. 2015).

The tested hypothesis is that changes in wave direction may cause large variations in the magnitude of storm-induced hazards. This effect has also been addressed in other studies such as those by Mortlock et al. (2017) and de Winter and Ruessink (2017), which specifically analyzed the effects of changes in wave direction on the storm-induced hazards in the SE Australian and Holland coasts respectively. To this end and to isolate the influence of wave direction, we used a recorded long-return period storm as a base case scenario and we built test scenarios just by changing wave direction while maintaining the other wave parameters as recorded during the base storm (wave height and period).

In any case, tested conditions have not been designed to be used as climate change induced projections, as that may require the proper forecasting of regional wave conditions under given climate scenarios (e.g., Casas Prat and Sierra, 2013). These have to be considered from the perspective of coastal risk management, in which a set of possible conditions are analyzed to characterize coastal vulnerability and resilience to inform risk management under uncertainty (see e.g., Hinkel et al., 2015 for an application of this perspective to analyze sea level rise). In the study area, the current storm wave conditions depend

on direction, with largest wave height and power being associated with NE-E waves, whereas S storms are less frequent and present a smaller associated power (e.g., Sánchez-Arcilla et al. 2008; Mendoza et al. 2011). To assess the potential variability on storm-induced hazards, tested scenarios were built by just changing wave direction while the remaining recorded parameters (representative of a worst case scenario, according to recorded conditions) were maintained.

This analysis has been performed by using the SWAN and XBeach models to simulate storm-induced hazards. Both models were calibrated by using data recorded during the impact of an extreme storm recorded in December 2008, which is used as the base case scenario. Although it is desirable to use more than one event to properly calibrate/validate the models (e.g., Callaghan et al., 2013; Ranashinge 2016), data availability during storm conditions was restricted to this event. However, on the positive side, it has to be considered that this storm was the largest event recorded in the area and representative of extreme storms with a very long return period (Mendoza et al., 2011) under current climate conditions. The SWAN model was very successful in simulating wave conditions during the development phase of the storm and during its peak, with the larger differences between measured and simulated waves being detected during the relaxation phase of the storm, when most of the induced changes had already occurred. The default parametrization of the XBeach model had to be adapted for application at the side to represent the effects of a coarse-sand environment. Sediment transport was limited by using the sedcal parameter, avalanching was limited by increasing the critical slope, wave asymmetry was increased as suggested in literature for steep slopes (Elsayed and Oumeraci, 2017) and groundwater effects were included. Gamma and delta wave breaking parameters were also tuned (Table 5.1). Calibrated parameters setup for XBeach in the study area led to a BSS score of 0.68 in spite of the out-of-comfort tested conditions (i.e., highly curvilinear coast, steep beach, coarse sediment). Although the predictive skill was very good for the northern and southern beaches, the model performance was better in the northern domain (BSS = 0.75) than in the southern one (BSS = 0.60), since this last area presented a significantly larger obliquity to wave direction during the storm, and a more complex bathymetry.

The obtained results show a very high sensitivity of storm-induced processes, i.e., inundation and erosion, to changes in storm wave direction. With respect to inundation, expected changes in hazard magnitude are very significant, especially in the southern part of the study area, since its morphology is characterized by a lower berm, and its low-lying unprotected hinterland makes this area sensitive to storm flooding (Jiménez et al. 2018 – see Chapter 4). Thus, as storm waves turn from the base case (C0) to the south, the inundated surface along this southern beach dramatically increases due to its direct exposure to that direction. On the contrary, a potential shift of wave direction to the N will have a positive impact on inundation in this area, since it will be more sheltered from wave action. At the northern beach, the largest increase in inundation hazard verifies under C20+ and C40+ scenarios when waves face nearly orthogonally to the coastline, although due to local morphology, the affected surface is much lower than in the southern beach. The hinterland of the study area is mostly occupied by agriculture land and, in the outer fringe just behind the shoreline, by campsites. In this sense, to transfer

the potential change in hazard magnitude to changes in damage risk, it should be important to consider not only the change in direction but also its seasonality. Thus, risk may vary dramatically between the summer season (when the campsite facilities are used by visitors) and the rest of the year when only installations will be affected (e.g., Merz et al. 2007). An analysis of the risk associated with storm-induced inundation for different storm conditions can be seen in Chapters 6 and 7.

Similarly, storm-induced morphodynamic changes are more sensitive to directional changes on the southern beach, where the magnitude of the changes is larger. The beaches at the south of the river mouth present a larger spatial variability than those in the north due to the presence of a local boundary condition in form of a revetment at the shoreline. This revetment, which modifies local longshore transport, significantly enhances downcoast erosion under storm conditions. This induces a southwards directed longshore sediment transport while simultaneously promoting the accumulation of upcoast sediment. This contrasting behavior is particularly observed in the base case scenario which seems to represent the optimum conditions for longshore sediment transport in the area, thus inducing the largest changes in the surroundings of the structure.

In a particular case, under C40− and C20− scenarios, when wave direction turns north, the beach sector just south of the river experiences an important sediment accumulation due to the apparently efficient transfer of sediment from the northern beach across the river mouth and the partial barrier effect of the existing revetment.

The magnitude of the erosional response along the two control sectors in the northern beach is similar, although a higher variability is detected in the area closest to the river mouth. In general, there is a slight increase in erosion rates as wave direction turns south. This variation should be indicative of the role of longshore sediment fluxes during storm conditions. Thus, as the controlled northern area is just besides the river mouth, where there is another structure acting as a boundary condition, the increase in longshore sediment transport as waves turn S (scenarios from C20+ to C80+) will increase sediment losses, which will be transported further to the north. This behavior is currently observed in the northernmost part of this beach (out of the control zone in Figure 5.10) which experiences sediment accumulation under the impact of southern storms.

As expected, changes in the magnitude of overwash deposits follow observed changes in inundation, i.e., they increase as wave direction turns to the south, with maximum values around C20+ and C40+. The exception to this is the predicted changes in the southernmost sector, which present the largest overwash for C80+ conditions. The spatial variability in the northern beach is significantly lower than in the south, with small variations in magnitude across the tested range. Moreover, and reflecting the observed differences in inundation, the magnitude of overwash deposits is much higher in the southern sector.

Finally, and as a concluding remark, this chapter has shown that storm-induced hazards along a highly curvilinear coast are extremely sensitive to changes in wave direction. This means that even under a

climate scenario of relatively steady storminess (wave power and frequency), a potential shift in wave direction may significantly change hazard conditions and, in consequence, need to be accounted for in robust damage risk assessments. To this end, an analysis such as the one presented here also permits an assessment of how coastal geomorphology modulates induced changes. In the study area, the low-lying nature of the southern beach and its orientation with respect to the current dominant storm direction make this area much more sensitive to directional changes. This is especially relevant from the coastal management standpoint because this area has been already identified as a hotspot for storm impacts under current conditions. The use of detailed process-based models has permitted the identification and quantification of the drastic increase in sensitivity when anthropogenic perturbations are present along the coast. These perturbations act as boundary conditions modifying local hydrodynamics and associated transport. For the case study analyzed here, the obtained results clearly identify the hazardous potential of the existing revetment in the southern beach, suggesting that its removal will soften the estimated morphodynamic response.

CHAPTER 6.

A Bayesian Network-based approach to assess risk reduction measures under present and future scenarios.

Adapted from: Sanuy, M., Duo, E., Jäger, W. S., Ciavola, P., Jiménez, J. A., 2018: Linking source with consequences of coastal storm impacts for climate change and risk reduction scenarios for Mediterranean sandy beaches, Nat. Hazards Earth Syst. Sci., 18, 1825-1847, doi.org/10.5194/nhess-18-1825-2018.

This chapter presents the local risk assessment tool developed during the RISC-KIT project, and its application to two study sites in the Mediterranean coast: the Tordera Delta (Catalan Coast, Spain) and Lido degli Etensi-Spina (Emilia-Romagna coast, Italy). This tool followed after CRAF, with the objective of performing a risk assessment at previously identified hotspots (Chapter 4) consisting of the comparison of inundation and erosion risks under different scenarios, comprising future conditions in terms of SLR due to climate change both with and without the presence of pre-selected risk reduction measures. This is the first extensive application of the XBeach model developed in Chapter 5, and represent the first use of Bayesian Networks (BNs) for the analysis of coastal risk during the thesis. Note that the description of the Tordera Delta study site will be repeated here, as it is parallel to that of the Italian case illustrating similarities and differences.

As occurred in Chapter 3, the inclusion of the Italian site permits to increase the robustness of the analysis and to demonstrate its applicability beyond the specificity of the Catalan coast.

6.1. Introduction

The need for integrated decision support systems based on modern approaches for coastal risk assessment is increasing and the scientific community provides integrated and interdisciplinary approaches (e.g. Ciavola et al., 2011a; Ciavola et al., 2011b; Penning-Rowsell et al., 2014; Vojinovic et al., 2014; Oumeraci et al., 2015; Van Dongeren et al., 2018). Notably, coastal risk assessments must include physical concepts to characterise physical phenomena (i.e. the source of the hazard) and socio-economic concepts to describe the impact of the physical phenomena on human assets (i.e. the consequences). A conceptual flexible framework that can capture all aspects of coastal risk assessment is the Source-Pathway-Receptor-Consequence (SPRC) model (e.g. Narayan et al. 2014, Zanuttigh et al. 2014 and Oumeraci et al., 2015). This is a conceptual model which describes how a given risk propagates across a given domain from the source to the receptors. In this particular case, it is applied to storm-induced hazards (erosion and inundation) assessment, and the problem is schematized in terms of a source (storms), the pathway (beach or coastal morphology) and receptors (elements of interest) at the coast. To this end and under the common scarcity of direct observations, hazards are usually assessed by using predictive models which are fed with information on both the source and the pathway.

When addressing the problem at the local scale, it is necessary to accurately predict the impact and reproduce in detail coastal hazards. The analysis of physical impacts is regularly implemented with process-based numerical models providing detailed information for areas prone to multiple hazards (e.g. Roelvink et al., 2009; McCall et al., 2010; Harley et al., 2011; Roelvink and Reniers, 2012). However, multiple forcing conditions acting at the site and under different scenarios must be evaluated. Bayesian Network-based (BN) approaches have demonstrated their versatility and utility in efficiently combining multiple variables to predict system behaviour for multiple hypotheses (e.g. Plant et al. 2016). The data assimilation capacity of BN approaches allows integrating many multi-hazard simulations from

process–oriented models for joint assessment of different scenarios and alternatives (e.g. Gutierrez et al., 2011; Poelhekke et al., 2016), including also socio-economic concepts (e.g. Van Verseveld et al., 2015). This is an advantage compared to classical GIS-based approaches, which are more limited when combining large number of simulations in multiple subsets of scenarios.

Jäger et al. (2018) proposed the conceptual BN framework used in this work, which is based on the integration of the SPRC and was developed in the RISC-KIT EU FP7 project (Van Dongeren et al., 2018), where it was used as a Bayesian-based Decision Network. Plomaritis et al. (2018) applied the framework to test its potential as an Early Warning System and the response of risk reduction measures in Ria Formosa (Portugal). In this paper, the authors describe the application of the framework adapted to select and compare strategic alternatives to reduce coastal risk in current and projected future climate scenarios. The application was conducted at two sedimentary coasts in the Mediterranean environment, namely the Tordera Delta for the Catalan coast (Spain) and the Lido degli Estensi-Spina for the Emilia-Romagna coast (Italy). At both study sites, the tested measures were pre-selected taking into account the outcome of interviews to stakeholders (see Martinez et al., 2018) and obtained results were used in a participatory process to select acceptable measures on the basis of a multicriteria analysis (see Barquet and Cumiskey, 2018).

6.2. Regional contexts and case studies

The two presented case study sites are representative of many other coastal areas in the Mediterranean consisting of sandy beaches where local economic activities are based on the tourist sector. These areas are characterised by urbanisation and infrastructural growth close to the shoreline (limiting natural beach accommodation processes) and economic activities located on the beach and immediate first part of the hinterland (e.g. concessions, campsites, restaurants). The coast keeps offering its recreational function, but loses its protective function against storms. In addition, the hinterland is exposed to storms-induced hazards.

6.2.1. Tordera Delta, Catalunya (Spain)

The Catalan coast is located in the NW Mediterranean Sea (Figure 6.1, A1). It consists of a coastline 600 km long with about 280 km of beaches. Coastal damage has increased during the last decades as a result of the increasing exposure along the coastal zone and progressive narrowing of existing beaches (Jiménez et al., 2012) through dominant erosive behaviour due to net littoral drift (Jiménez et al., 2011). Locations experiencing storm-induced problems are present along the entire coastline, and are especially concentrated in areas experiencing the largest decadal-scale shoreline erosion rates. Among these areas, the Tordera Delta, located about 50 km north of Barcelona, provides a good example (Jiménez et al., 2018 – see Chapter 4) (Figure 6.2).

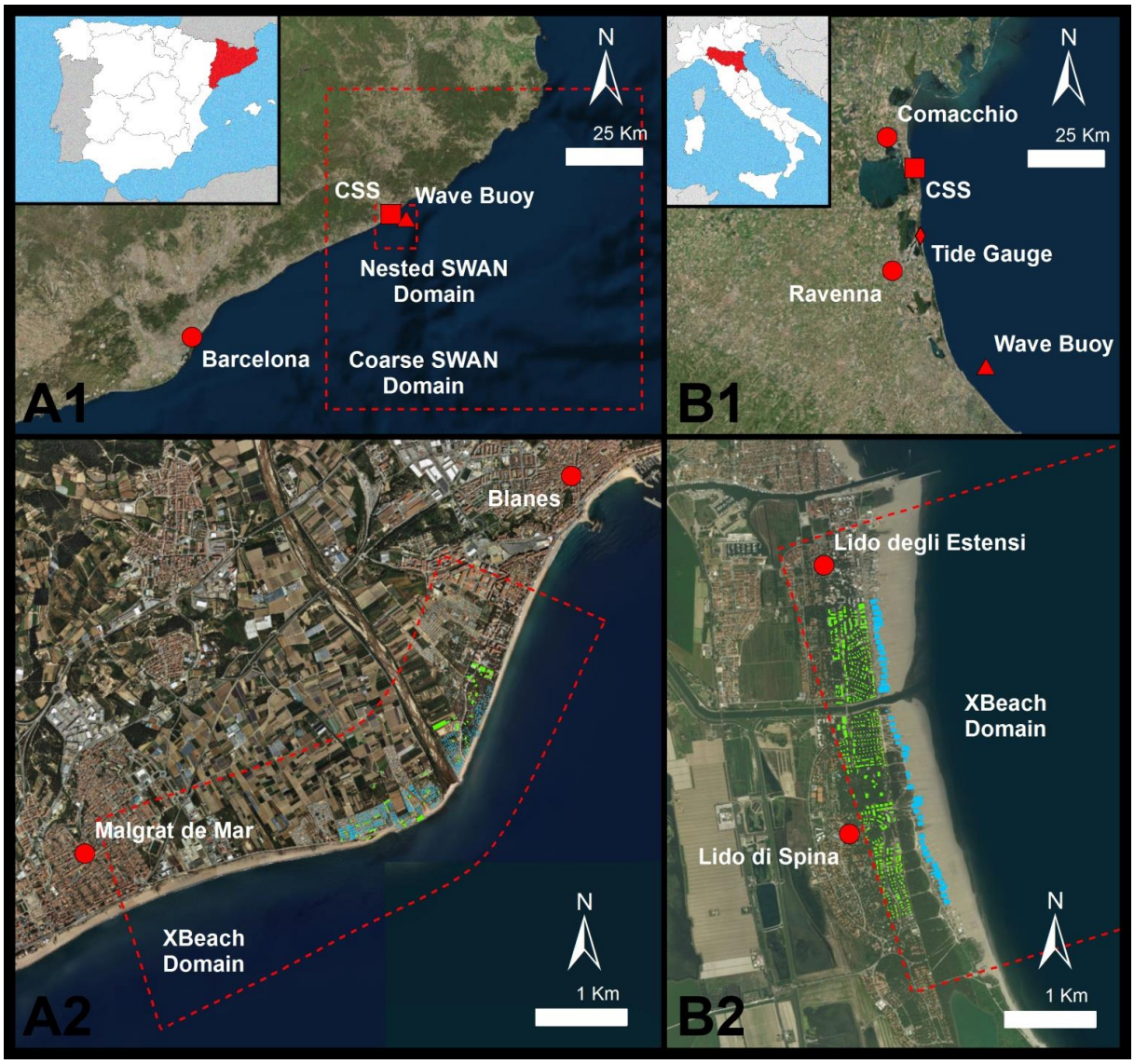

Figure 6.1. Regional and local contexts: A1) central-northern Catalan coast; B1) Emilia-Romagna coast; A2) local hotspot of Tordera Delta; B2) local hotspots of Lido degli Estensi-Spina (2b). The main locations (red dots), wave buoys (red triangles), tide gauge (red diamond), and the case study sites (red squares). The domains of the large-scale and local models (dashed red lines) are highlighted for each box

The deltaic coast is composed of a coarse sandy coastline extending about 5 km from s'Abanell beach at the northern end and Malgrat de Mar beach in the south (see Figure 6.2). This zone is highly dynamic, and is currently in retreat because of the net longshore sediment transport directed southwest and the decrease in Tordera river sediment supplies. Consequently, the beaches surrounding the river mouth, which were traditionally stable or accreting, are being significantly eroded (Jiménez et al., 2011; Sardá et al., 2013). As a result of the progressive narrowing of the beach in the area, the frequency of inundation episodes and damage to existing infrastructure (beach promenade, campsite installations, desalination plant infrastructure, roads) has significantly increased since the beginning of the 90s (Jiménez et al., 2011; Sardá et al., 2013) (Figure 6.2).

Subsequently, existing campsites in the most affected zones have abandoned the areas closer to the shoreline, as in many cases, those are fully eroded or directly exposed to wave action. In other cases, owners have tried to implement local protection measures that in many cases have enhanced existing erosion (Jiménez et al., 2018, see Chapter 4).

Coastal storms in the Catalan Sea can be defined as events during which the significant wave height (Hs) exceeds a threshold of 2 m for a minimum duration of 6 hours (Mendoza et al., 2011). Despite this, not all storms can be considered as hazardous events in terms of induced inundation and/or erosion. Mendoza et al. (2011) developed a five-category storm classification for typical conditions in the Catalan Sea based on their power content. The classification seems to well represent the behaviour of storm events in the Mediterranean, and was successfully employed in the Northern Adriatic (Armaroli et al., 2012). Furthermore, Mendoza et al. (2011) estimated the expected order of magnitude of induced coastal hazards (erosion and inundation) for each class and beach characteristics along the Catalan coast. According to their results, storms from category III (Hs = 3.5 m, duration around 50 hours) to V (Hs = 6 m, duration longer than 100 h) are most likely to cause significant damages. One important aspect to consider is that wave-induced run-up (setup + swash) is the largest contribution to overwash at the beach during storm events, because the magnitude of surges along the Catalan coast is relatively low (Mendoza and Jiménez, 2008).

Figure 6.2. Impacts on the Tordera Delta. Destruction of a road at Malgrat (A); overwash at campsites north of the river mouth (B); destruction of the promenade north of the river mouth (C); beach erosion, and damage to utilities and buildings at Malgrat (D and E).

6.2.2. Lido degli Estensi-Spina, Emilia-Romagna (Italy)

The Emilia-Romagna (Italy) coast is located in the northern part of the Adriatic Sea (Figure 6.1, B1). The coast is about 130 km long and characterized by low-lying, predominantly dissipative sandy beaches. The coastal corridor has low elevations, mainly ranging from -2 to 3m above MSL (Regione Emilia-Romagna, 2010). The area alternates between highly urbanised touristic zones and natural areas with dunes, which are often threatened by flooding and erosion (Regione Emilia-Romagna, 2010). The impact of coastal erosion was emphasised by subsidence due to water and gas extraction over the last century, especially in the Ravenna area (Taramelli et al., 2015), a decrease in riverine sediment transport, because of the strong human influence on rivers and their basins (Preciso et al., 2012), and the reforestation of the Apennines (Billi and Rinaldi, 1997). Touristic activities (accommodation, food service, sun-and-bath) can be considered main drivers of the coastal economy. Beach concessions, which provide sun-and-bath and food services, have grown exponentially in number since the second half of the last century, with negative consequences on natural areas, as in Ravenna Province (Sytnik and Stecchi, 2014). To protect the coast and its assets from the impacts of flooding and erosion, regional managers have constructed hard defences (e.g. emerged and submerged breakwaters, groins, rubble mounds; Regione Emilia-Romagna, 2010) along the entire regional coast (over 60% of the coast is protected), and regularly implement restorative nourishment plans.

During the last decades, several EU projects such as Theseus (www.theseusproject.eu) and MICORE (www.micore.eu) provided a good understanding of hydro-morphodynamics and risks to the coast. These projects and works published in the international literature such as Ciavola et al. (2007), Armaroli et al. (2009, 2012), and Perini et al. (2016) were the product of strong collaboration between scientists and regional managers (Servizio Geologico Sismico e dei Suoli, SGSS). This led to the compilation and implementation of a storm database (Perini et al., 2011) and a regional Early Warning System (Harley et al., 2016). The RISC-KIT project (www.risckit.eu) provided additional knowledge on this coastal area. The areas most exposed to coastal risk are well known, as can be seen in the works of Perini et al. (2016) and Armaroli and Duo (2018).

For a more local perspective, the Lido degli Estensi-Spina coastline (Comacchio municipality, Ferrara province, Italy) area represents a highly touristic stretch of coast with concessions directly facing the sea (Figure 6.1, B2). The littoral drift is northward as confirmed by the width of the sandy beaches, which increases from 20 to 50 m in the southern part of Lido di Spina to 200 to 300 m in the northern part of Lido degli Estensi. Here the sediment is trapped by the groin of the mouth of a navigation canal (Porto Canale). The beach is not protected, and regional managers implement regular nourishment in the southern part of the area (Nordstrom et al., 2015). At the back of the concessions, the villages accommodate restaurants and hotels for tourists, along with residential buildings (mainly holiday houses). In a recent study, Bertoni et al. (2015) analysed aerial photographs of the evolution of the case study area, focusing on the stretch of coast between Porto Garibaldi and the Reno river mouth. The area

was impacted by the event in February 2015 (see Figure 6.3) with limited, but not negligible, consequences for several concessions (Perini et al., 2015; Duo et al., 2018)

The hydrodynamics of the regional domain are well described in terms of storm waves and surges (IDROSER, 1996; Ciavola et al., 2007). The area is micro-tidal (neap tidal range: 0.3–0.4 m; spring tidal range: 0.8–0.9 m); the surge component plays an important role (1-in-2 years storm surge: 0.61 m) and is mainly generated from the SE (Scirocco) winds (according to the orientation of the Adriatic Sea). Furthermore, the wave climate is low energy (mean Hs –0.4 m; 60% of waves are below 1 m). However, extreme events can be energetic, such as the storm of September 2004 (Hs,max=5.65m, estimated by Ciavola et al,. 2007) or the one of 5-6 February 2015 (Hs,max=4.66 m, measured at the Cesenatico buoy shown Figure 6.1, B1; Perini et al., 2015; Duo et al., 2018).

The combination of high waves and storm surges, whose combined probability of occurrence in the area was assessed by Masina et al. (2015), can have strong impacts at the regional level, as demonstrated by Armaroli et al. (2009), Armaroli et al. (2012) and Harley and Ciavola (2013). Notably, based on historical data (Perini et al., 2011), Armaroli et al. (2012) provided a set of critical storm thresholds for natural and urbanised beaches to characterise potentially impacting storms. The thresholds included a combination of offshore Hs and TWL: 1) Hs ≥ 2 m and TWL (surge + tide) ≥ 0.7 m for urbanised zones; 2) Hs≥3.3 and TWL (surge + tide) ≥0.8 m for natural areas with dunes.

Figure 6.3. Impacts of the event in February 2015 on the Lido degli Estensi-Spina case study area. Impacts of erosion and flooding on concessions at Lido di Spina south (A, B) and Lido degli Estensi (C); sandy scarp due to the erosion of the dune in the south of Lido di Spina (D); eroded Winter Dune in Porto Garibaldi (E); damages to the Porto Canale front at the Lido degli Estensi (F).

6.3. Methodology

6.3.1. General approach: from source to consequences

The analysis framework employed in this study follows Jäger et al. (2018) and is based on the use of the SPRC (Source-Pathway-Receptor-Consequence) model (FLOODsite, 2009; Oumeraci et al., 2015), as shown in Figure 6.4. This model is widely used in coastal risk management (e.g. Narayan et al., 2014) and permits a clear representation of all risk components and their links from source to consequence.

The source includes the forces determining coastal response to the impact of extreme storms, which in this case are essentially a set of events representative of the storm climates of the study sites over the entire intensity range (from moderate to extreme). These storms propagate through the pathway, causing erosion at the coast and inundation on the hinterland. Both hazards are the main focus of the analysis. The pathway is solved through a process-oriented model chain to propagate storms and quantify induced processes. These are assessed for the entire coastal domain where receptors are present, characterised by their location and typology, which define their exposure and vulnerability to each hazard. Finally, consequences are evaluated by combining the vulnerability and exposure of each receptor with the magnitude of the hazards.

Since the main objective of the analysis is to test risk reduction strategies to help decision makers in future planning, the framework is applied under current conditions (CUS) which define the baseline scenario and climate change conditions (CCS) to define a plausible future projection. Finally, the analysis is repeated considering different risk reduction measures.

The Bayesian Network-based (BN) approach reproduces the steps of the SPRC model through dependency relations between variables. This affects the application of the steps of the SPRC model, as explained in the following sections. At the same time, the BN data assimilation capabilities are used to integrate large amounts of simulations, i.e. results from multiple sources at multiple receptors. The BN integrates dependency relations between source-hazard-consequences, at the receptor scale, for all available incoming conditions and scenarios.

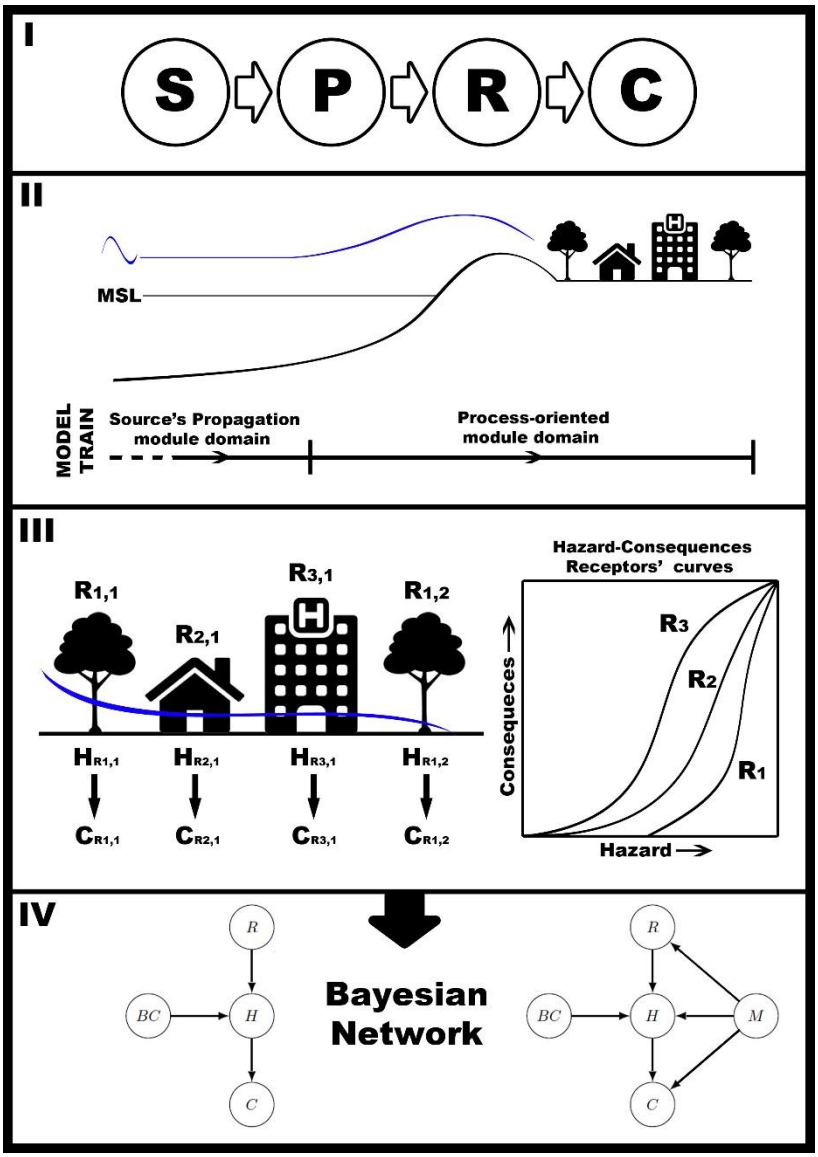

Figure 6.4. General methodology. (I) The SPRC conceptual framework is implemented through (II) a model chain, which consists of a propagation module of the source (S) and a process-oriented module for the coastal area reproducing the pathway (P). Then, (III) the consequences (C) are calculated based on the computed hazards (H) at the receptor (R) scale by using vulnerability relations (i.e. hazard-consequences functions). In the last step (IV), all variables including source boundary conditions (BC) are fitted in a BN, as well as impacts and the implementation of measures (M).

6.3.2. Source: identification and design

To properly characterise storms, all relevant variables controlling the magnitude of induced hazards (erosion and inundation) must be considered, in other words, Hs, wave period (Tp), wave direction, storm duration, and water level. In this approach, source characteristics are defined in terms of a set of representative storms that cover the typical conditions at each study site. This information is obtained from existing wave time series or bulk data of the events (recorded or modelled), usually in deep waters, propagated towards the coast to characterise storm conditions at the nearshore of the study areas. Probable combinations that cannot be covered using existing records are represented by synthetic design

storms (e.g. Poelhekke et al., 2016; Plomaritis et al., 2018; Jäger et al., 2018). The storm events were selected based on the information available for each study site through the RISC-KIT WEB-GIS impact-oriented database (Ciavola et al., 2018; http://risckit.cloudapp.net/risckit/#/), which provided storm characteristics and socio-economic impacts of the events. In addition, time series of waves (either bulk Hs, Tp and mean direction or spectrum) and water levels during each storm event were used when this information was available. In order to be used in a BN approach, storm characteristic variables must be discretized in ranges which define the resolution of the source description. In this application, used simulations cover uniformly all variable combinations, assuming no prior knowledge of their statistics.

Table 6.1. Source characterization. Variable discretization applied at the study sites. NC denotes a variable not considered in a study case, and therefore not divided in ranges.

	Hs (m)	**Storm Duration (h)**	**Incoming direction (ºN)**	**TWL(tide+surge) (m)**	**Mean Sea Level (MSL)**
TORDERA DELTA	2 to 3 3 to 4 4 to 5	6 to 30 30-65	30-135 (E) 135-220 (S)	0 to 0.6 m NC	Current Current +0.73 m Morph. response included
LIDO DEGLI ESTENSI-SPINA	2 to 3 3 to 4 4 to 5 5 to 6	12 – 68 NC	60 to 135 NC	0.65 to 1.05 1.05 to 1.45 1.45 to 1.85	Current Current+0.30 m No morph. response

For the Tordera Delta case, the selected variables to define storm scenarios were Hs at the peak of the storm, total storm duration, and incoming storm direction. Tp does not significantly vary during storms in the study area (see Mendoza et al., 2011) and was not included as a characteristic variable. Due to the coastline configuration and morphology, the area is sensitive to storm incoming direction (Sanuy and Jiménez, 2019 – see Chapter 5). Thus, the main directions in terms of dominant (E) and secondary (S) storms needed to be considered separately. Finally, the position of the mean sea level (MSL) during the event was included to reproduce hypothetical future projections of sea level rise (SLR) due to climate change. The selected bins for each variable can be seen in Table 6.1. These lead to 12 combinations defining the source under current MSL and 12 under future MSL (given by a SLR scenario). Each combination of states is represented by two simulations of slightly different storms to account for potential variability within variable ranges, leading to a total of 24 simulations under the current MSL and 24 under SLR. Of the 24 simulations under current MSL, 16 correspond to historic (recorded) events including the two largest, which occurred in November 2001 and December 2008. These were classified as extreme storms (category V) according to the Mendoza et al. (2011). To include the full range of cases, the remaining 8 storms were completed by using combinations of Hs-duration-direction not previously recorded. These events were modelled assuming they follow a triangular-shaped evolution

with the peak intensity at the half of their duration (see e.g. McCall et al. 2010; Poelhekke et al., 2016). Data used to reproduce the historic events include the time series of hindcast wind fields and 2D wave spectra time series in deep waters for the NW Mediterranean (Guedes-Soares et al., 2002; Ratsimandresy et al., 2008). Wave conditions must propagate towards the coast to properly define storm events at the study site. At the Catalan coast, the storm surge contribution to the sea surface level is one magnitude lower than the wave-induced component, and the two variables are uncorrelated (Mendoza and Jiménez, 2008). All historical events with recorded associated water levels were simulated with the real storm surge, while the synthetic storms were simulated with a storm surge of a 0.25 m constant throughout the event, as representative of the site according to the same authors.

Previous works in the area of the Lido degli Estensi-Spina case study have identified the dominant role of wave height and total water level in controlling the magnitude of storm-induced erosion and inundation (Armaroli et al 2009, 2012). Due to this, variables used to characterize the source were the maximum Hs and maximum TWL (surge+tide) during each storm event. Thus, wave period and the direction of the storms were not considered as a source characteristic variable to be discretized. The used range for each variable is shown in Table 6.1. Seven historically based events were selected from the RISC-KIT Database, and to cover all 12 possible combinations in the CUS, 5 additional synthetic events were considered. Notably, for several historic events, neither reliable nor continuous time series for waves and water levels were available from local measuring stations. To ensure consistency, both historical and synthetic events were represented based on the following methodology. Starting with the list of bulk information for each event (maximum Hs, Tp, main direction of the storm, maximum TWL or duration when available), storms following triangular-shaped evolution (e.g. Carley and Cox, 2003; Corbella and Stretch, 2012) for Hs, Tp, and surge were created. The peak of the waves was assumed to occur at the same time as the maximum surge (calculated as the difference between the TWL and maximum astronomical predicted tide). When bulk parameters were missing, the following 'worst case' assumptions were introduced: Tp at peak of 10 s, wave direction orthogonal to the shoreline, and duration based on similarity with other storms. Each storm representing a Hs-TWL combination was simulated twice, with slightly different directions, to account for potential variability on source characteristics, leading to 24 simulations in the CUS. Additional 24 simulations were performed to cover the climate change scenario.

6.3.3. Pathway: modelling multiple hazards

To simulate the pathway and obtain hazards of interest, a model chain was designed and adapted for each site (Figure 6.4, II). Any model can be used within the model chain, and results will be as good as the model is accurate. The chain must be able to reproduce all hazards to be assessed (i.e. erosion and inundation). To do this, a detailed 2D process-oriented model designed to simulate coastal storm-induced processes is used, the XBeach model which is able to provide integrated information on

inundation and erosion (see Roelvink et al., 2009 for model details). At present it is a state-of-art model on coastal systems. However, the proposed framework can work with different (simpler) models when they are able to simulate the target processes (inundation and erosion). The XBeach model was used in both study cases.

The model chain for the Tordera Delta consists of two blocks, one 'external' and one 'internal' (see deteails in Chapter 5). The external module comprises three models (HAMSOM, HIRLAM, and WAM) that supply the forcing conditions (time series of water levels, wind fields, and waves) and are run by Puertos del Estado (Spanish Ministry of Public Works). The output of these models is taken directly as an input for the internal module, which comprises the SWAN (Booij et al., 1996) and XBeach (Roelvink et al., 2009) models. SWAN was used to propagate wave conditions from deepwaters to the offshore boundary of the XBeach model (20 m depth), while XBeach was employed to assess the extension and magnitude of inundation and erosion at the study site (local scale). The model chain was validated through the St. Esteve event in 2008, obtaining a Brier Skill Score of 0,68 for the morphological response of the emerged part of the beach (Sanuy and Jiménez, 2019 – see Chapter 5). Simulation results can be considered excellent for scores over 0.6 (Sutherland et al., 2004)

The model chain for Lido degli Estensi-Spina only included the XBeach model. This simple approach was possible based on the assumption that the information derived from the RISC-KIT Database can be considered representative of the storm in the domain, as collected from different sources (e.g. offshore buoys, harbours' tide gauges, newspapers, etc.) along the Emilia-Romagna coast (Perini et al., 2011; Ciavola et al., 2018). The model was qualitatively validated using observed inundation extension and profile beach response of the February 2015 event (Perini et al., 2015; Duo et al., 2018).

6.3.4. Receptors and consequences

The methodology applied in this work individually identified receptors located at the study sites (Figure 6.4, III) (Jäger et al., 2018). First, receptors with homogeneous vulnerability characteristics were defined and separately considered. Then, for each group of receptors, polygons were drawn using a GIS-based tool to account for their exact location and size. Finally, the polygons were intersected with the cells of the 2D detailed model grid (XBeach) to assign to each receptor the nodes of the model that will affect it.

For the inundation hazard, the value of the maximum water depth inside each polygon (receptor) was used as the impact variable. Then, by using flood-damage curves for the corresponding receptor typology, inundation water depth was translated to relative damage. This was then translated into four levels of impact—none, low, medium, and high—which are case and receptor dependent (see the following sections). The chosen damage curves do not include uncertainties, and they are used as recommended by the Administration at each study site. This implies that damage ranges and damage-

hazard relations are different and therefore, final impact levels (from none to high) are site-specific. This assumption aimed to better communicate results to local stakeholders.

The magnitude of the risk associated with erosion depends on the combination of vertical erosion and distance of erosion to the receptors. This was implemented by building multiple buffers (increasing in distance) around each receptor and applying the polygon intersection formerly explained with the gridded maximum vertical erosion output from XBeach. The definition of risk categories related to erosion thresholds and distances is also site dependent, given their different morphologies.

Exposure and vulnerability in the Tordera Delta case study

The distribution of receptors for the Tordera Delta case study was derived from cartographic information of the Catalan Cartographic Institute and completed manually through orthophoto analysis (Figure 6.1, A2). The study site was divided into eight areas, of which four are located at the south of the river mouth, corresponding to the Malgrat de Mar municipality, and the other four to the north, corresponding to the Blanes municipality. These two sets of four areas were selected to enable the analysis of the impact at different bands regarding their distance to the limit of the public beach. The first band corresponds to the first 20 m of hinterland. The second band is 30 m wide and located just after the first one, i.e. 20 to 50 m from the boundary of the public domain. The third covers the range from 50 to 75 m, while the fourth band covers all the hinterland omitted between the end of the third band and the inland domain boundary. This enables an assessment of the distribution of the impacts in terms of distance to the coastline and allowed exploring setbacks as risk reduction measures. Three groups of receptors were identified to be homogeneous in terms of vulnerability, namely houses (concrete buildings), campsite elements (soft buildings and caravans), and infrastructure (promenade and road at the back of the beach). Table 6.2 shows the distribution of campsite elements and houses in the different areas. The infrastructural receptors (promenade at the north and road at the south) are only located in the first 20 m band (Areas 1 and 5).

The consequences of flooding were assessed through flood damage curves used to characterise the relative damage based only on water depth (Table 6.3). Data was obtained from the Agència Catalana de l'Aigua (ACA, 2014). The relative damage values to buildings and campsite elements were converted into the level of risk as follows: (i) no impact for 0% relative damage to buildings and campsite elements, (ii) low impact for damages below 26% to buildings and 50% for campsite elements, (iii) medium impact when damages to buildings range from 26 to 45% and damages to campsite elements range between 50 to 70%, (iv) high impact for relative damages higher than those formerly exposed for both receptors.

Table 6.2. Distribution of receptors at the Tordera Delta study site.

Area	No. of Houses	No. of Campsite Elements
Area 1 (0 to 20 m *Malgrat de Mar*)	16	45
Area 2 (20 to 50 m *Malgrat de Mar*)	10	71
Area 3 (50 to 75 m *Malgrat de Mar*)	8	169
Area 4 (> 75 m *Malgrat de Mar*)	46	509
Area 5 (0 to 20 m *Blanes*)	1	95
Area 6 (20 to 50 m *Blanes*)	4	156
Area 7 (50 to 75 m *Blanes*)	7	72
Area 8 (> 75 m *Blanes*)	51	189
Total	**143**	**1306**

Table 6.3. Vulnerability relations for houses and campsite elements at the Tordera Delta study site with and without Flood Resilience Measures (FRM). Agència Catalana de l'Aigua (ACA, 2014)

Water depth at the receptor (m)	Relative Damage (%)			
	Houses	Campsites	Houses - FRM	Campsites - FRM
0	0	0	0	0
0-0.3	18.3	50	0	0
0.3-0.6	26.5	71	18.3	50
0.6-0.9	33.2	82	18.3	50
0.9-1.5	44.7	89	26.5	71
1.5-2.1	54.1	91	33.2	82
2.1-3.0	64.5	100	44.7	89
3.0-4.0	71.2	100	54.1	91
4.0-5.0	75	100	64.5	100

The buffers defined to assess the erosion hazard at the Tordera Delta are as follows: (i) a 20 m distance was used as a threshold from 'none' to 'low' erosion risk, and corresponds to the average beach retreat at the site for a storm with a return period of 38 years (commonly used for infrastructural receptors similar to those in the Tordera Delta for a lifetime of about 25 years). (ii) The 12 m buffer (average retreat for the 10-year return period) was used as the threshold from low to 'medium' impact. Medium impact is a post-monitoring situation where receptors will be exposed to the direct impact for relatively frequent storms. (iii) Finally, the 3 m buffer was used as the threshold for 'high' impact risk, meaning

that the receptor is directly affected by erosion at the toe or impacted by waves during the storm. A buffer was considered to be affected when vertical erosion was higher than 50 cm.

Exposure and vulnerability in the Tordera Delta case study

The analysed receptors belong to the central area of the model domain at approximately 600 m from the lateral boundaries (Figure 6.1, B2). Two main types of receptors were selected: (i) the residential and commercial buildings mainly present in the towns of L. Estensi and L. Spina, and (ii) beach concessions on the beach directly facing the sea. In this study, only receptors belonging to the seafront of Lido degli Estensi and Lido di Spina were considered, as they are mainly impacted by sea storms. Receptors were extracted from a recent Regional Topographic Map (Carta Topografica Regionale, scala 1:25000, anno 2013). Table 4 summarises the identified receptors.

Table 6.4. Distribution of the receptors at Lido degli Estensi and Lido di Spina.

Area	Residential and Commercial Buildings	Concessions
Lido degli Estensi - Seafront	26	16
Lido di Spina - Seafront	47	28

The vulnerability relation for inundation hazards was defined considering a flood-damage curve from a recent study on Italian territory by Scorzini and Frank (2015). This work was based on a micro and macro-scale study of the impacts of the 2010 river flood in Veneto (Italy) on residential houses. In the current work, it was adapted and applied to the receptors of the area (see details in column A of Table 5), and relates the relative damage factor (values: 0–1) to flood depth. In particular, the worst case curve was used, which represents flood-related damages to single-family detached buildings with a basement. Although this curve is for residential buildings, it was assumed the same for commercial buildings and beach concessions, as no additional and specific information was available. The curve was modified considering the risk reduction implementation described in Section 3.5.2. The level of flood risk was defined as follows: none, when the relative damage is null, low, when the relative damage factor is higher than zero but lower than 0.1, medium, for a factor between 0.1 and 0.2, and high, for a relative damage factor higher than 0.2.

The vulnerability relation for erosion was defined for concessions only. The impacts due to the erosion hazard were defined based on a two-buffer approach for each receptor: the first buffer was the receptor limits in the ground, and the second included a corridor of 10 m around the receptor.

Erosion was considered present if >0.05m (vertical) and significant when >0.5m. The erosion risk categories for each receptor were set as follows: (i) safe: no erosion in any buffer, (ii) potential damage:

when erosion is present in the 10-m buffer and/or present but not significant in the receptor itself, and (iii) damage: when the erosion limit of 0.5 m is exceeded within the receptor limits. Notably, the threshold of 0.5 m was set considering the uncertainty of the model grid topography (±0.15 m) and assuming that the foundations of the concessions are a minimum of 0.2 m thick.

Table 6.5. Vulnerability relation for flooding adopted for the receptors at Lido degli Estensi-Spina without (A) and with Flood Resilience Measures (B).

Flood Depth [m]	Flood Relative Damage Factor [-]	
	A - adapted from Scorzini and Frank (2015)	B - modified considering the FRM
0	0	0
<0.3	<0.1	<0.1
0.3 - 0.7	0.1 - 0.2	<0.1
0.7 - 1.1	0.2 - 0.3	0.2 - 0.3
>1.1	>0.3	>0.3

6.3.5. Scenarios

To compute the analysis under climate change scenarios (CCS) and under the implementation of risk reduction measures, it was necessary to identify the variables and settings affected by each scenario, either a future projection or implementation of a measure. Therefore, an appropriate approach was selected to consider these modifications in the methodology chain.

The CCSs mainly affect the hazard and therefore, are applied in the modelling chain. The risk reduction measures can affect both hazard and vulnerability/exposure variables. In the following, the implementation of the CCSs and measures is described for each case study, emphasising the affected variables and steps of the methodology. The measures were pre-selected considering interviews with stakeholders, and were assumed to be fully implemented and completely effective (measure uptake and effectiveness: 100%) in all cases.

Climate change scenarios

Future projections of mean sea level were based on the AR5 RCP8.5 (Church et al., 2013). Other factors such as changes in storminess, wind speed, or wave height were not expected to change significantly in the NW Mediterranean (Lionello et al., 2008; Conte and Lionello, 2013), and are characterised by high uncertainty in the Northern Adriatic (IPCC, 2013). Data to include the sea level rise (SLR) in the assessment of future scenarios was provided by the EC Joint Research Centre database (for further detail,

see Vousdoukas et al., 2016). For the Tordera Delta study case, the time horizon of 2100 was chosen, while the 2050 projection was used for Lido degli Estensi-Spina, because the projections in the Adriatic are more uncertain than in the NW Mediterranean. Therefore, the 2100 horizon could yield highly unreliable results.

At the Tordera Delta, the RCP8.5 estimates an increase of 0.73 m by 2100. Therefore, all 24 simulations described in Section 3.2 were repeated with the projected future sea level. Moreover, the potential beach accommodation to SLR was modelled following Bosom (2014) and Jiménez et al. (2017). This was accomplished assuming an equilibrium coastal profile response following the Bruun rule (Bruun, 1962), resulting in landward and upward displacement of the beach profile. Dunes preserve the pre-SLR shape when there is enough accommodation space, otherwise the shape is cut. The estimated shoreline retreat due to the SLR in the area is 22 m. Thus, morphological response to SLR is included in the assessment. Finally, Casas-Prat and Sierra (2012) predicted a directional change in mean sea conditions from the current dominant (E) to the secondary direction (S). This effect was explored by assessing only eastern incoming storms in present conditions and imposing an equal frequency of eastern and southern incoming storms in future projections. Therefore, three different CCSs were explored: (i) CCS1: current situation (CUS) + SLR with the corresponding estimated beach accommodation; (ii) CCS2: CUS + effect of direction switch of incoming storms, and (iii) CCS3: assessing the contribution of both components if occurring at the same time.

In Lido degli Estensi-Spina, the combined contribution of the predicted SLR with the subsidence component (not negligible in the area, e.g. Taramelli et al., 2015) was implemented. The resulting value of relative SLR by 2050 used in the analysis is 0.30 m. The position of the MSL was changed for all forcing events, adding the predicted relative SLR by 2050 in the CCS. The morphological accommodation to the SLR was not implemented in the numerical analysis; however, the implication of this choice is discussed in Section 5.2. In total, 24 additional simulations were run for the CCS.

Risk Reduction alternatives

Three risk reduction measures were tested for the Tordera Delta zone (see Figure 6.5): (i) Receptors Setback, (ii) Flood Resilience Measures, and (iii) Nourishment + Dune.

The Receptors Setback measure affects the exposure of the receptors. It entails removing all receptors inside a defined band measured from the public domain coastal limit (the limit between the back of the beach and hinterland). Three scenarios of the setback were simulated: 20 m, 50 m, and 75 m.

The Flood Resilience Measures affect the vulnerability of receptors so that for a given water depth, the expected impact decreases when the measure is implemented. It was assumed that resilience measures such as raised electricity outlets and utilities, adapted flooring, resilient plaster, and waterproof doors

and windows were installed in all houses and campsite elements. This measure was implemented by assuming a modified damage curve as shown in Table 6.4.

Finally, the Nourishment + Dune changes the pathway and affects the inundation/erosion hazard. It includes beach nourishment at the south of the river mouth to increase the beach width by 50 m over 1 km, where the highest erosion occurs. In addition, the level at the top of the beach was increased on both sides of the river mouth, with non-erodible sandbags at the northern side, where the campsites are closer to the coastline, and a sandy dune at the southern side. At both sides, the final height of the protective measure was +4.8 m from the MSL. Since this measure affects the pathway, it had to be implemented in the XBeach grid. Thus the 48 storms (24 current MSL, 24 current MSL+SLR) were simulated again with the edited morphology arriving to the final 96 simulations.

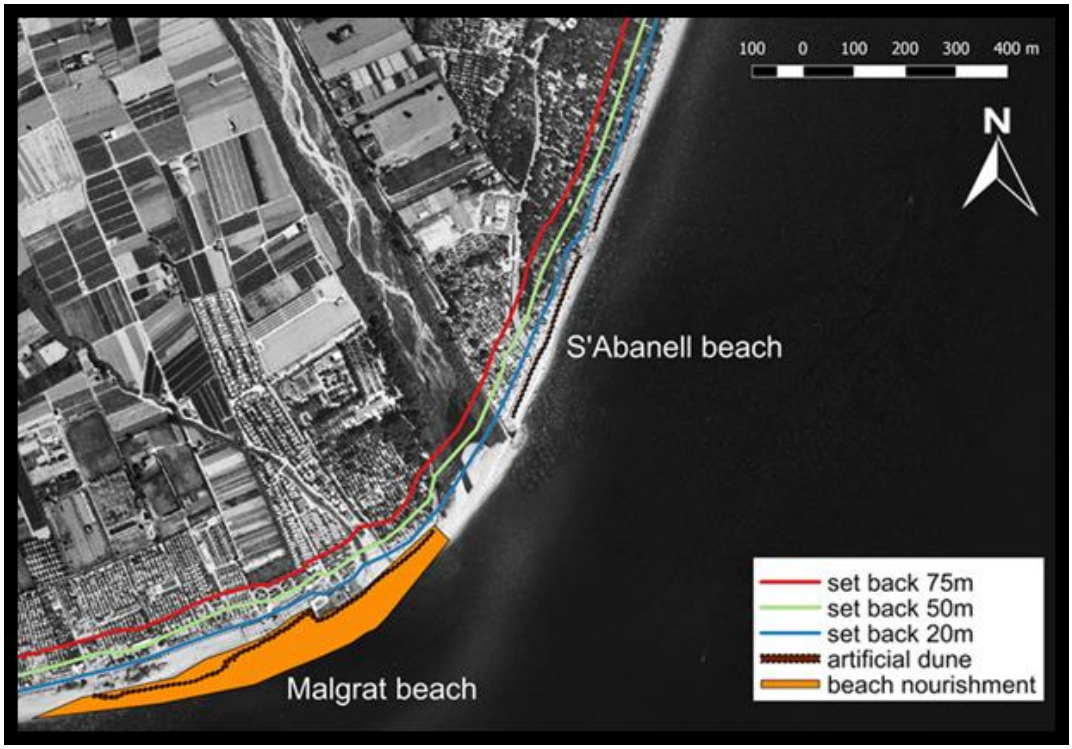

Figure 6.5. Risk reduction measures at Tordera Delta. Receptor setbacks (20, 50, and 75 m) and Nourishment + Dune (beach nourishment at Malgrat beach + artificial dune at S'Abanell and Malgrat beaches).

The selected measures tested for the Lido degli Estensi-Spina case study were: (i) a Winter Dune system, affecting both flooding and erosion impacts, and therefore the hazards modelling process; and (ii) Flood Resilience Measures, influencing the flood vulnerability relations of receptors.

The Winter Dune (see Figure 6.6) is a common risk reduction practice along the Emilia-Romagna coast, especially in the Ravenna province (Harley and Ciavola, 2013), and regularly implemented by local concessionaires without a scientifically based design criterion. It consists of a set of embankments built

on the beach in front of concessions through beach scraping or sand replenishment (less frequent option). This risk reduction measure was implemented in the XBeach model. The Winter Dune was designed as a continuous dune that protects more than one concession, introducing breaks in the continuity of the feature where natural/human obstacles or passages were located. The top of the dune was fixed at 3 m above the MSL and the width (at the top) at 10 m. The dune was integrated in the model modifying the bed levels through the Dune Maker 2.0 tool (Harley, 2014). Both the CUS and CCS were tested with this measure adding 48 additional simulations.

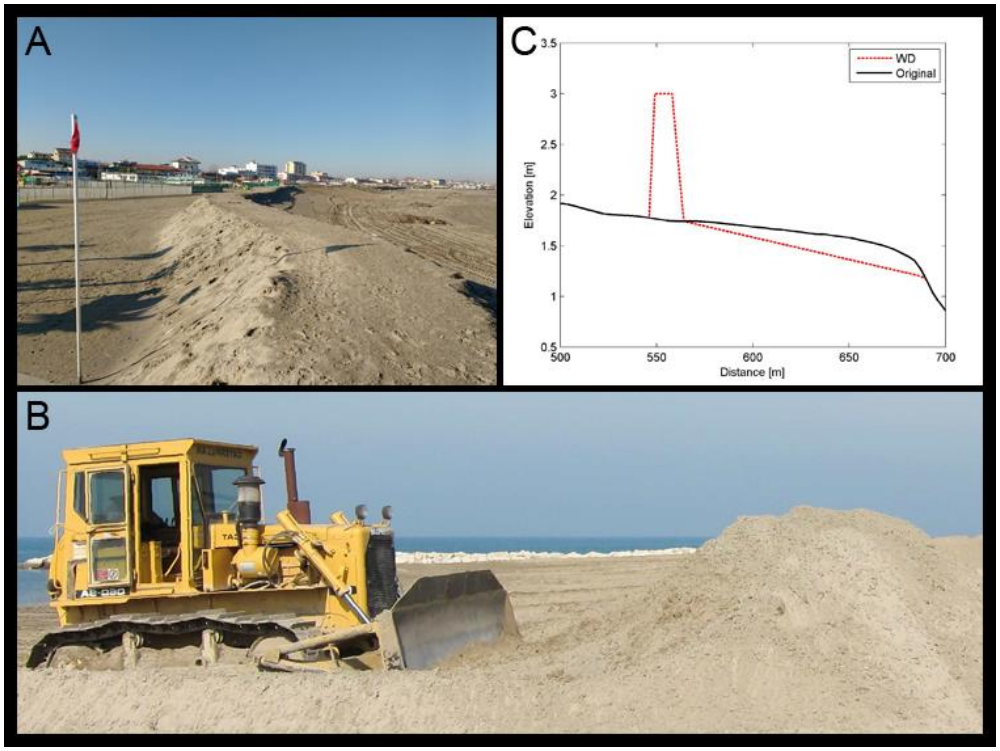

Figure 6.6. Artificial winter dunes in Emilia-Romagna: A) Winter dune in Porto Garibaldi (Comacchio, Italy); B) Building of a winter dune by beach scraping at Lido di Dante (Ravenna, Italy) (Harley, 2014); C) Representative model profiles at Lido di Spina north (original: black solid line; with winter dune measure: red dashed line).

The Flood Resilience Measures decrease the receptor's physical vulnerability to floods. It was assumed that the effective application of these measures would decrease the damages for water levels lower than a certain threshold, assumed here as 0.7 m (e.g. all electrics must be placed above the threshold). This assumption was integrated in the analysis by modifying the selected depth-damage curve, as defined in column B of Table 6.5, and included in the BN. Considering the adopted definition of flood risk levels (see Section 6.3.4), the measure results in a complete obliteration of receptors for the medium flood risk, therefore increasing the receptors at the low level and not affecting receptors at high risk.

6.3.6. The Bayesian Network

BNs use probability theory to describe the relationships between many variables, and can evaluate how the evidence of some variables influence other unobserved variables. For example, evidence could be a forecast of the source variables characterising an impending storm. On the other hand, local hazards and damages in the coastal area have not yet been observed, but can be predicted with the BN. The model can also be updated with artificial evidence to explore extreme event scenarios or investigate the potential of risk reduction plans.

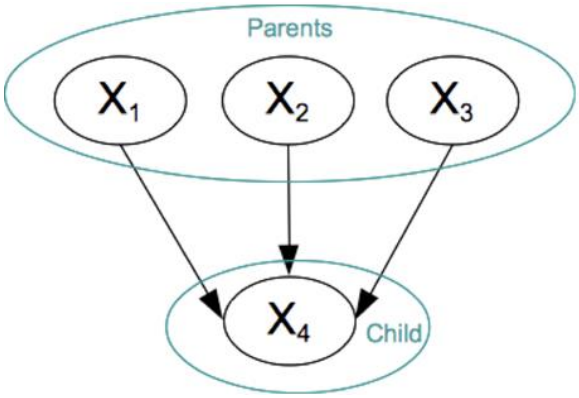

Figure 6.7. BN graph with four nodes.

A BN is based on a graph (Figure 6.7). It consists of nodes connected by arcs that represent random variables and the potential influences between them. The direction of the arcs is crucial for the probabilistic reasoning algorithm of the BN, but does not necessarily indicate causality. For any two variables connected by an arc, the influencing one is called a parent, while the one influenced is referred to as the child. Thus, in Figure 6.7, X1, X2, and X3 are the parents of X4. A simple way to parameterise a BN is to discretise continuous variables after defining their data range, and to specify conditional probability tables for each node. The authors adopted this approach. The conditional probability tables indicate how much a variable could be influenced by others. Mathematically, the graph structure and conditional probability tables define the joint distribution of all variables in the network, X1, ..., Xn, based on the factorisation of conditional probability distributions (eq.6.1):

$$p(X_1, \dots, X_n) = \prod_{i=1}^{n} p\left(X_i \middle| pa(X_i)\right), \quad (6.1)$$

where pa(Xi) are the parents of node Xi (Pearl, 1988; Jensen, 1996). Once the joint distribution has been defined, the effects of any evidence can be propagated with efficient algorithms throughout the network (Lauritzen and Spiegelhalter, 1988).

In the RISC-KIT project, a generic structure for a BN-based approach that can support decision-making in coastal risk management was proposed. This structure is based on the Source-Pathway-Receptor-Consequence and has five components (node types): source boundary condition, hazard, receptor, impact/consequence, and risk reduction measure. Typically, each component includes several variables. Panel (IV) in Figure 6.4 shows their influence on each other. In general, all boundary conditions influence all hazards. Each type of receptor (e.g. people, buildings, infrastructure, and ecosystems) is represented by a node where different areas are the different bins (proxy for the locations of receptors on the site). Hazard intensity is conditioned by the location of the receptors and the presence of measures. Consequences are conditioned by hazard intensity, receptor type and presence of measures.

Alongside the generic structure, a c++ programme that automatically creates the BN (https://github.com/openearth/coastal-dss) is also provided. As input, the programme requires variable definitions and land use data, vulnerability relationships, and a 2D gridded simulation output of numerical physical process-based models of hindcast or synthetic extreme event scenarios. Essentially, the programme extracts the values of hazard variables from the simulation output at the locations of every individual receptor so that hazard distributions for each receptor type can be obtained. Because each simulation contains the coastal response to one storm scenario under a specific set of measures, the distributions are conditional and can be stored directly as entries of the conditional probability tables associated with each hazard node. Being parents of the hazard nodes, boundary conditions, receptors' areas, and risk reduction measures define the dimensions of the conditional probability tables. In the final step, the conditional hazard distributions were transformed to conditional impact distributions with vulnerability steps. In the present application, the BN-based approach is applied assuming no prior knowledge on the statistics of the source. Thus, all source variable combinations are equally fed into the BN resulting as uniform distributions of either Hs, duration, TWL or direction. Each combination is represented by two simulations of slightly different storms to include some uncertainty due to intra-bin variability. No other uncertainty is included. Therefore, the present application is deterministic, a Bayesian-based Decision Network (BDN) which mainly uses the data assimilation capacity of the BN as principle advantage with respect to other methodologies (e.g. GIS-based assessments). Additionally, the BDN allows also reverse assessments, where output variables (i.e. consequences) can be constrained to get conditioned results on the source variables. In the Discussion sectionof the present chapter further guidance into a fully-probabilistic BN approach integrating multiple sources of uncertainty is presented. This will be implemented in Chapter 7.

BDN implementation at the case study sites

The schemes of the BDNs implemented for the Tordera Delta and Lido degli Estensi-Spina case study sites are shown in Figure 6.8 and Figure 6.9 respectively. The nodes (circles) define the variables of the network, while arcs (arrows) show the relations between the variables. The boundary conditions (blue),

and the location and distributions of the receptors (grey) affect the hazards' nodes (dark orange). The hazard is then transformed through the vulnerability relations into consequences (light orange). The measures' nodes (green) can affect different node types depending on the effect (by definition) of the measure. The structure is very flexible and can be applied at different coastal settings. The scheme can be adapted with different boundary conditions, hazards, receptors, consequences and measures depending on the needs driven by research and/or coastal management objectives. It follows that, for very similar coasts, or even for the same case study, the scheme can differ. The variables and bin ranges characterising boundary conditions are pre-selected by the user. Bins are equidistant and covering the observed values at each study site (Table 1). Additional non-observed ranges are introduced to account for SLR. The used number of intervals is a compromise between accuracy and computational effort. A total number of 96 model runs were required for the applied set-up at each case study site. As a reference, using parallel simulations with 48 threads, the ratio computation time over real storm time was ~0.2, meaning that a 40 hr storm takes ~8 hours of simulation time.

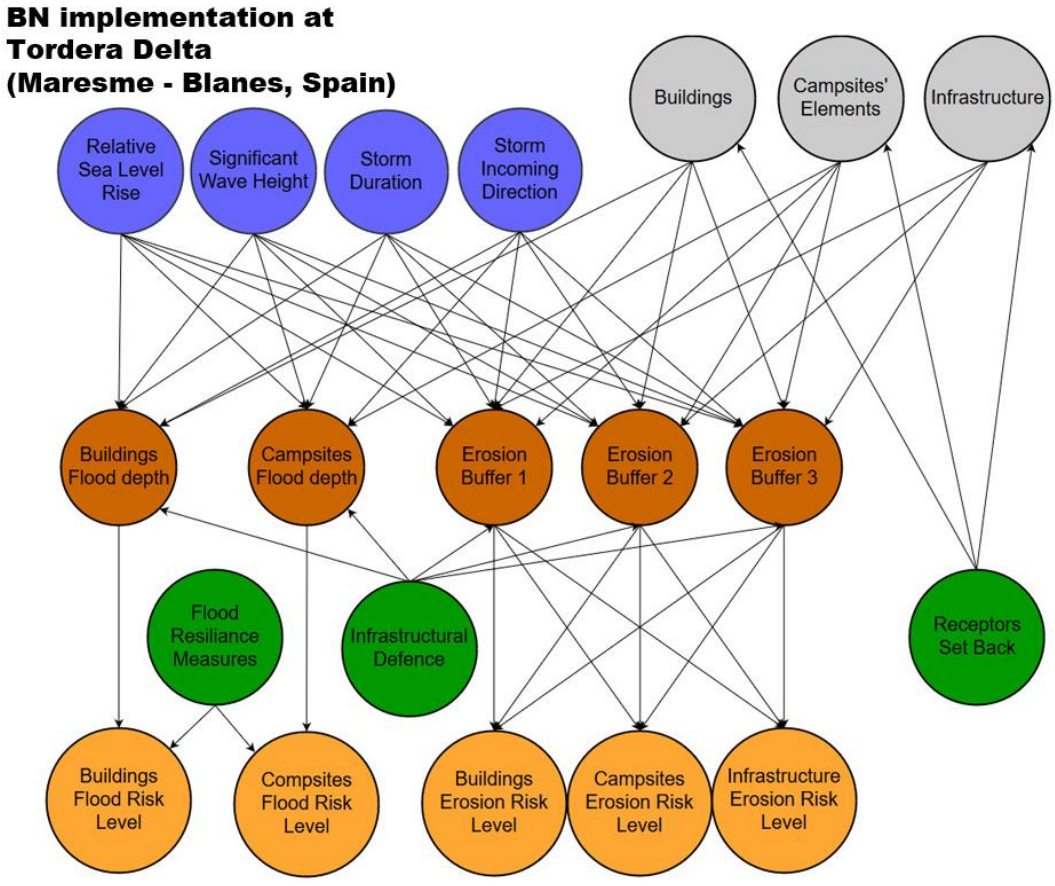

Figure 6.8. Bayesian Network scheme for the Tordera Delta site.

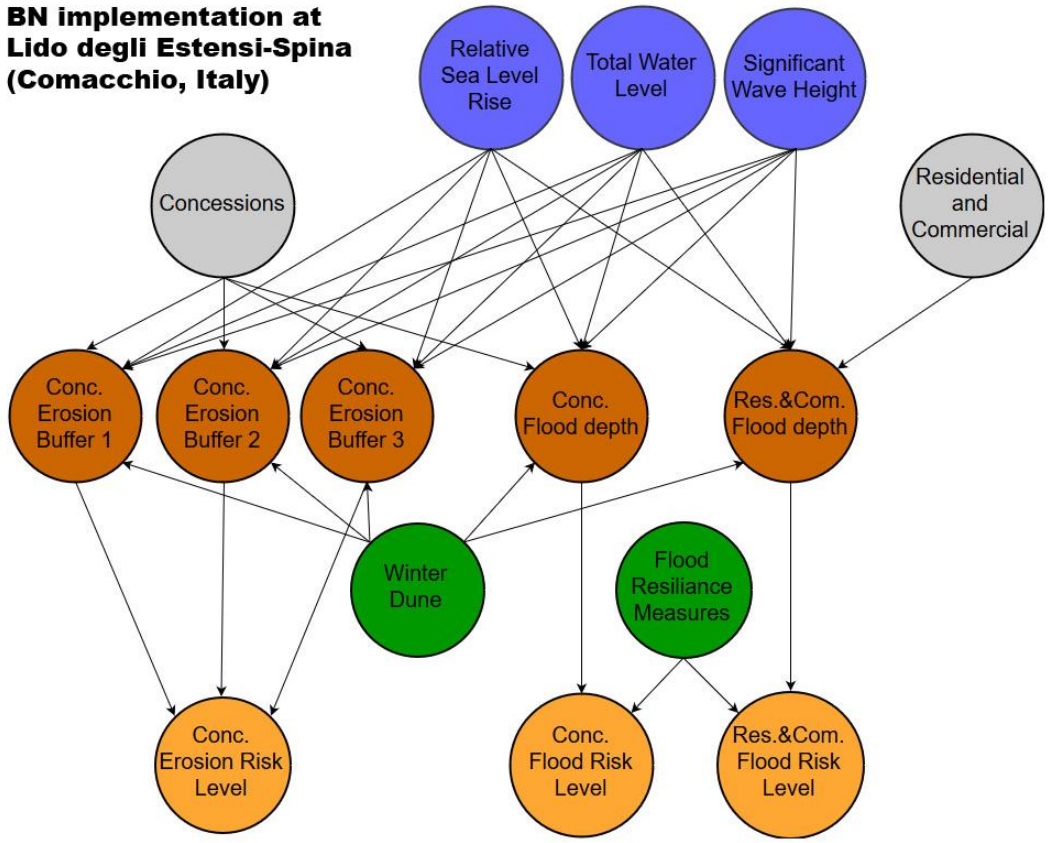

Figure 6.9. Bayesian Network scheme for the Lido degli Estensi-Spina site.

6.4. Results

The results of scenario testing are provided for each case study through an integrated comparison of percentages of receptors at each level of flooding and erosion risks. This is done by comparing the risk levels under current and climate change scenarios, with and without measures. The results of the scenarios that will be presented in the following sections are produced by integrating in subsets all 96 simulations at each study site.

Figure 6.10 shows an example of the integration of simulations at the Tordera Delta considering the CUS without measures. The figure includes 3 boxes with different level of (un)constrained boundary conditions and corresponding results in terms of erosion risk to infrastructures. In box A, both Hs and storm duration are constrained to a specific bin (in this case given by the highest values) and thus, results of two different simulations are integrated to obtain the final output. In box B, Hs is unconstrained while duration is constrained to the highest bin. In this case, the final result is produced by integrating six simulations (two per each Hs bin). Finally, in box C, both Hs and Duration are unconstrained and the output is given by integrating 12 simulations (2 per each Hs and duration bin combination) which represent the overall dataset for CUS without measures for Tordera Delta.

The current BDNs have been fed assuming no prior knowledge on the boundary conditions' distributions (i.e. any boundary condition is uniform when unconstrained). This approach is adequate to explore scenarios and to assess the efficiency of protection measures in terms of impact reduction.

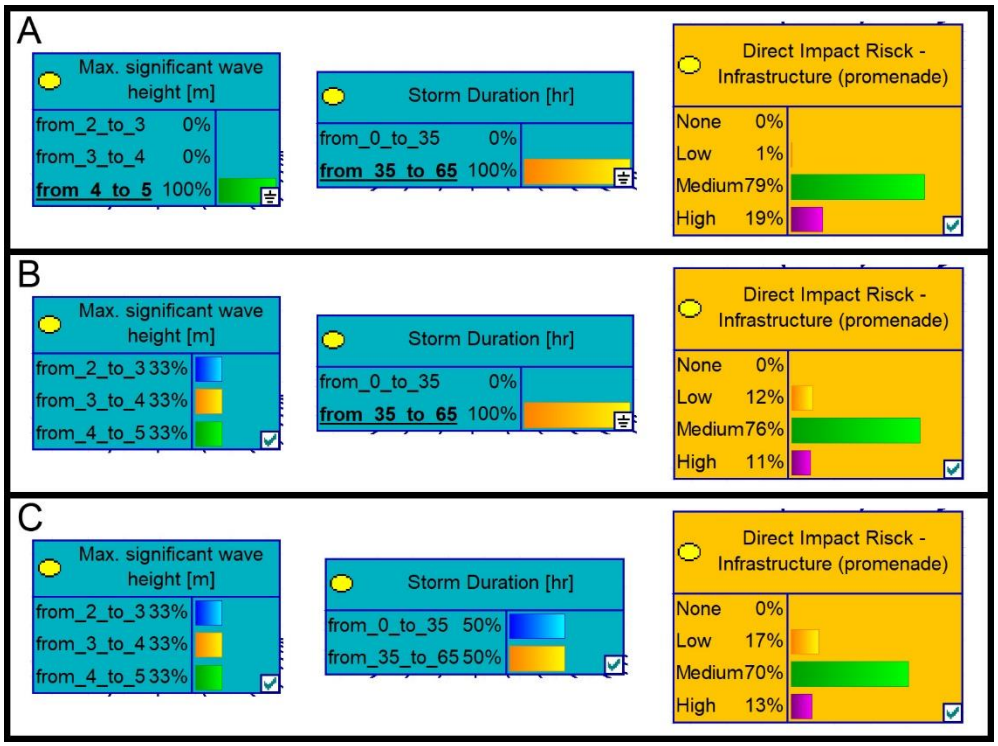

Figure 6.10. Example of result integration in the Bayesian-based Decision Network. Combinations of Hs and duration to obtain erosion risk at infrastructures in Tordera Delta. Total Water Level is constrained to "current" and direction to eastern incoming storms.

6.4.1. Tordera Delta

The results assessment was performed separately for both sides of the river at S'Abanell beach at the north and Malgrat beach at the south. The inundation impact assessment considered all receptors at the study site whereas the erosion analysis focused only on the first 20-m band of hinterland because the only receptors exposed to an erosion hazard are located in that area.

The results of the flooding impacts, here presented for campsite elements, indicate that under current conditions, receptors at both sides of the river mouth are expected to suffer the same magnitude of damages: 80–83% of elements will be safe, while only 2–3% of the elements are under high-impact risk (Figure 6.11).

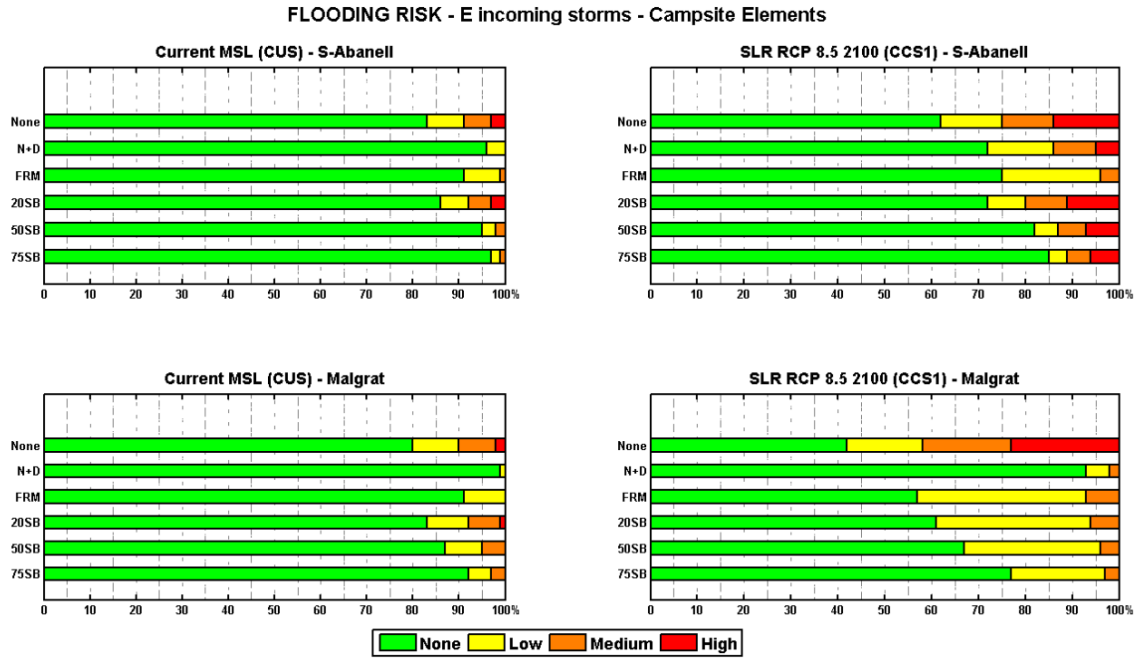

Figure 6.11. Distribution of campsite elements at every level of flooding risk. Top-left: current scenario at S'Abanell; Top-right: climate change scenario 1 (SLR) at S'Abanell; Bottom-left: current scenario at Malgrat; Bottom-right: climate change scenario 1 (SLR) at Malgrat. Each bar in a panel represents a risk reduction configuration ('None': no measure implemented; 'N+D': Nourishment and Dune; 'FRM': Flood Resilience Measures; '20SB, 50SB, and 75SB': 20, 50, and 75 m setbacks, respectively).

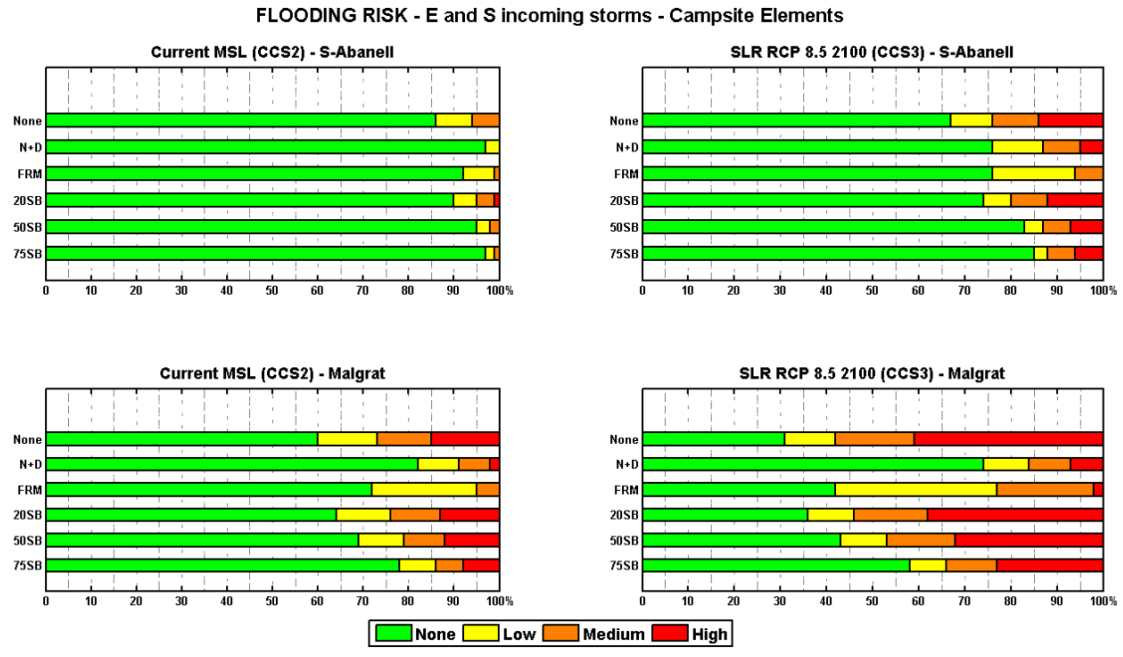

Figure 6.12. Distribution of campsite elements at every level of flooding risk. Top-left: climate change scenario 2 (50-50% east-south storms) at S'Abanell; Top-right: climate change scenario 3 (50-50% of east-south storms + SLR) at S'Abanell; Bottom-left: climate change scenario 2 (50-50% east-south storms) at Malgrat; Bottom-right: climate change scenario 3 (50-50% of east-south storms + SLR) at Malgrat. Each bar in a panel represents a risk reduction configuration ('None': no measure implemented; 'N+D': Nourishment and Dune; 'FRM': Flood Resilience Measures; '20SB, 50SB, and 75SB': 20, 50, and 75 m setbacks, respectively).

Under climate change scenarios, a different behaviour at each side of the river mouth is detected. Southwards of the river mouth, the beach is highly sensitive to both changes in storm direction and SLR (Figures 6.11 and 6.12). Thus, when CCS3 conditions are analysed in Malgrat, the BDN indicates that 69% of campsite elements are affected, with 41 % being at high risk. On the other hand, the beach at the north (S'Abanell) is highly sensitive to SLR (CCS1, Figure 6.11) but it is not affected by a potential change in storm direction (CCS2 and CCS3, Figure 12).

Comparing the effectiveness of the risk reduction measures highlights Nourishment + Dune as the most effective one against flooding under current and climate change scenarios. As expected, the effectiveness is higher in Malgrat than in S'Abanell, as beach nourishment is located only south of the river mouth whereas the dune is present on both sides. It was observed that all significant impacts (medium and high) to receptors under current scenario were removed for both sides of the river. Moreover, at Malgrat, the number of affected receptors was reduced by ~20% for the CUS, CCS1, and CCS2 scenarios, and ~40% under CCS3.

The implementation of the Flood Resilience Measures was effective in terms of preventing high impacts on any receptor, but did not significantly reduce the total number of receptors affected by some level of risk. The magnitude of reduction of receptors at risk was ~9%. It should be mentioned that this is a theoretical measure, as we assumed that it is properly designed, implemented and 100% effective for site conditions.

Finally, three Receptors Setbacks were tested: 20 m, 50 m, and 75 m. The results indicate that only the 75 m setback demonstrated a risk reduction magnitude comparable to Nourishment + Dune; however, the efficiency of the Nourishment + Dune was in general higher than the managed retreat. Only in S'Abanell, with higher topography and where the measure only consists of a dune without nourishment, a greater risk reduction was achieved through the 75 m setback.

Results for the erosion impact risk assessment showed similar results for the three analysed receptor categories and no significant differences between CUS-CC2 and CC1-CC3 respectively. For simplicity, results related to Infrastructure (Figure 6.13), for the CUS and CC1 scenarios are provided in the following.

Under the CUS, the promenade at the north of the river mouth is at significant risk (70% at medium risk and 13% at high risk), whereas the road in Malgrat is potentially safe. In the CCS1 scenario, the assessment highlights that because of the increase of sea level and corresponding morphological accommodation, the percentage of promenade under high risk and therefore direct erosion at the toe increases up to 33%, with some impact appearing on the road in Malgrat.

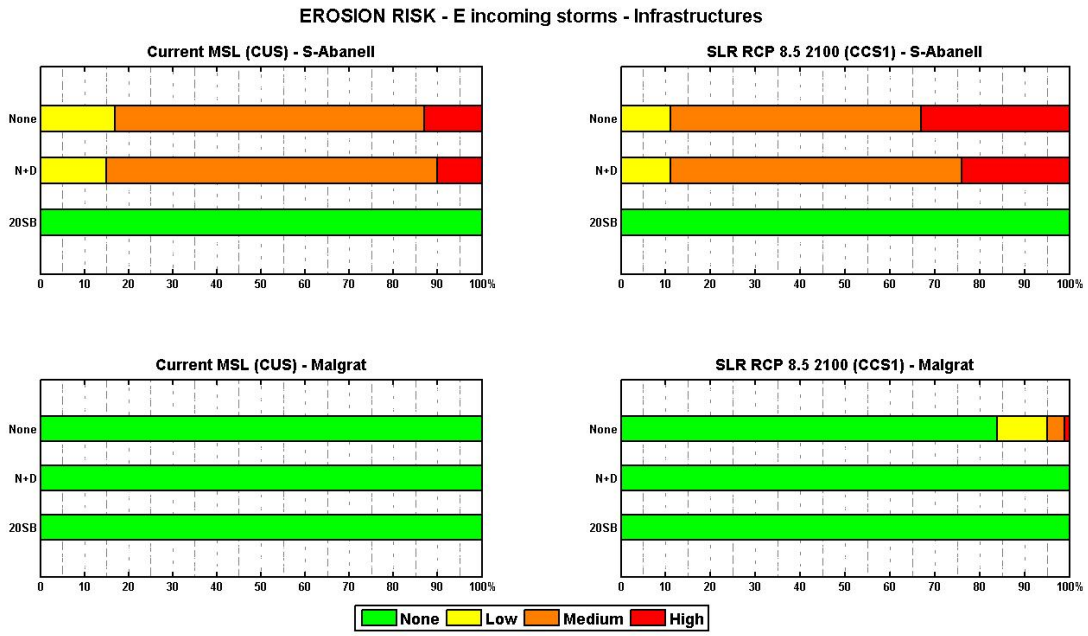

Figure 6.13. Distribution of Infrastructures at every level erosion risk. Top-left: current scenario at S'Abanell; Top-right: climate change scenario 1 (SLR) at S'Abanell; Bottom-left: current scenario at Malgrat; Bottom-right: climate change scenario 1 (SLR) at Malgrat. Each bar in a panel represents a risk reduction configuration ('"None"': no measure implemented; '"N+D"': Nourishment and Dune; '"FRM"': Flood Resilience Measures; '"20SB, 50SB, and 75SB"': 20, 50, and 75 m setbacks, respectively).

The assessment of the efficiency of the measures regarding erosion indicates that the Nourishment + Dune does not have a significant impact on reducing risk. In addition, the beach nourishment is regularly washed out in severe storm conditions. The only case where the nourishment plays some protective role is at the road in Malgrat, where the measure prevents the impact in CCS1. On the other hand, Receptor Setback is 100% effective in dealing with the impact of erosion, and a 20 m retreat (measured from beach limit in current conditions) is enough to cope with risk under the present situation and for all future projected conditions at both sides of the river mouth.

6.4.2. Lido degli Estensi-Spina

The overall results for flooding and erosion risks on concessions are shown in Figures 6.14 and 6.15. Focusing on the flooding risk (Figure 6.14), the CUS evidenced noticeable impacts, with Lido di Spina presenting the larger number of receptors at risk and with higher intensity. The presence of a climate change scenario exacerbates expected impacts.

The Winter Dune system had a positive impact in all cases, with the number of concessions at risk decreasing to 10% (only low risk) at Lido degli Estensi and 13% at low and 3% at medium risk at Lido di Spina. This measure was also effective to reduce the risk under the climate change scenario.

The Flood Resilience Measures had positive effects on impacts by moving all receptors at medium risk to the low risk category. However, by definition, it had no effect on lowering the fraction of receptors presenting, in the current situation, low and high levels of risk.

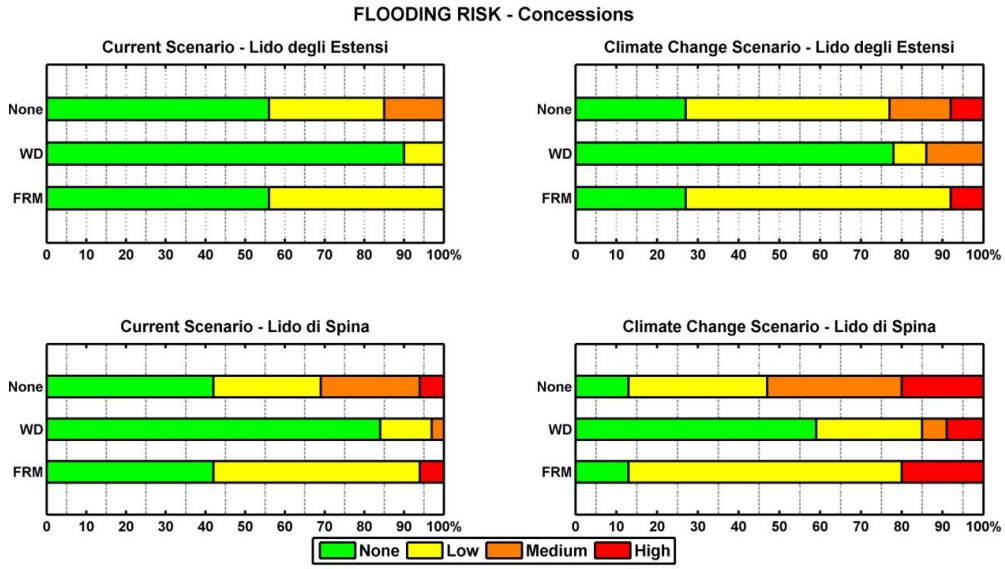

Figure 6.14. Distribution of concessions for every level of flooding risk. Top left: current scenario at Lido degli Estensi; Top right: climate change scenario at Lido degli Estensi; Bottom left: current scenario at Lido di Spina; Bottom right: climate change scenario at Lido di Spina. Each bar in a panel represents a risk reduction configuration ('None': no measure implemented; 'WD': Winter Dune; 'FRM': Flood Resilience Measures).

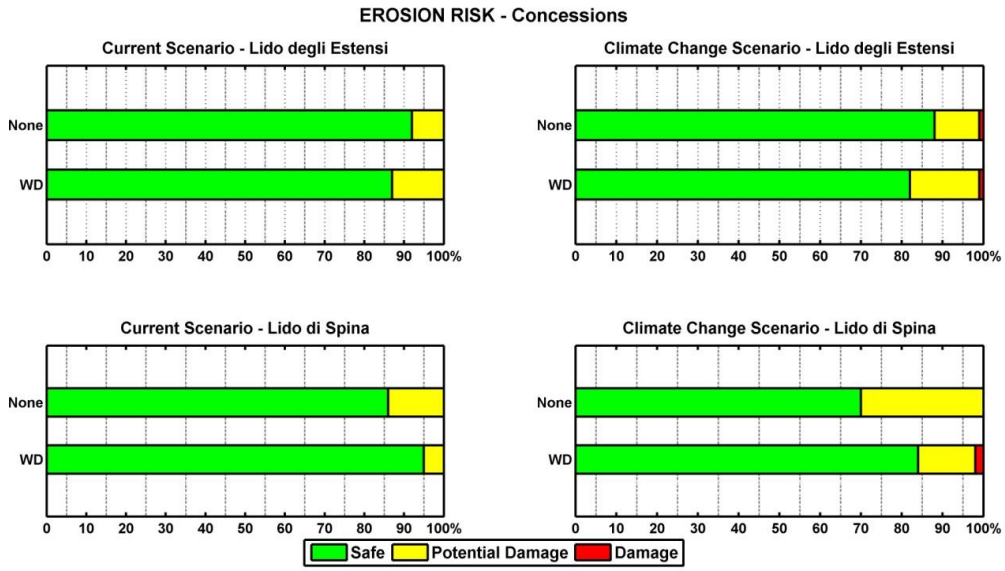

Figure 6.15. Distribution of concessions for every level of erosion risk. Top left: current scenario at Lido degli Estensi; Top right: climate change scenario at Lido degli Estensi; Bottom left: current scenario at Lido di Spina; Bottom right: climate change scenario at Lido di Spina. Each bar in a panel represents a risk reduction configuration ('None': no risk reduction implemented; 'WD': Winter Dune; 'FRM': Flood Resilience Measures).

A further step in the analysis of risk scenarios was undertaken using the BDN in reverse mode, i.e. looking at the distribution of the boundary conditions given a certain distribution of flood damage to concessions at Lido degli Estensi-Spina, both with and without Winter Dune. Flood damage to concessions is constrained in the BDN to equal fractions of low, medium and high risk. This can be understood as a qualitative scenario were all receptors suffer some damage, and the intensity of the damage is uniformly distributed. The BDN outputs the fractions of boundary conditions which are likely to produce the constrained impacts, according to the introduced data.

Notably, under current scenario and without measure, the Hs is distributed more uniformly compared to the TWL (Figure 6.16), which demonstrates a strong increasing tendency. This indicates that compared to wave conditions, the water level is the main driver for flood impacts.

The results for the Winter Dune scenario showed that the largest fraction of conditions leading to flood damages to concessions are TWL>1.45 m (93%) and Hs>4 m (4<Hs<5 m: 47%; 5<Hs<6 m: 43%). These results indicated that the Winter Dune is effective to minimise the consequences of coastal storms with TWL<1.45 m and Hs<4 m in the current situation.

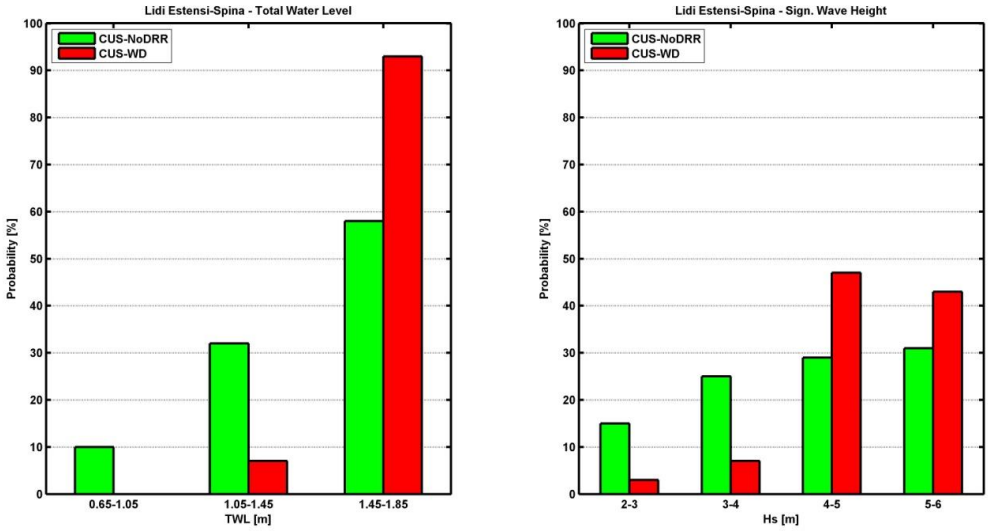

Figure 6.16. Distribution of boundary conditions (TWL on the left and Hs on the right) for constrained uniform flood damages in the current scenario for Lido degli Estensi-Spina. The configuration without measures (green bars) and for the implementation of the Winter Dune (red bars) were compared.

When the analysis was performed under the climate change scenario (Figure 6.17) the situation without measure demonstrated an even lower influence of Hs on flood consequences to concessions, since a more uniform distribution of this variable is obtained. As expected, the relative SLR (+0.3 m; RCP8.5 by 2050) increased the risk of lower intensity storms. Thus, in general, under the CCS, all storm combinations generated flood consequences to concessions.

The results for the Winter Dune in the climate change scenario showed that the influence of the dune system is less effective than in current conditions. Lower intensity storms can now lead to flood damages to concessions (TWL<1.45 m: 25%; Hs<4 m: 32%). This explains the observed decrease in effectiveness of the measure in future conditions when compared to present conditions.

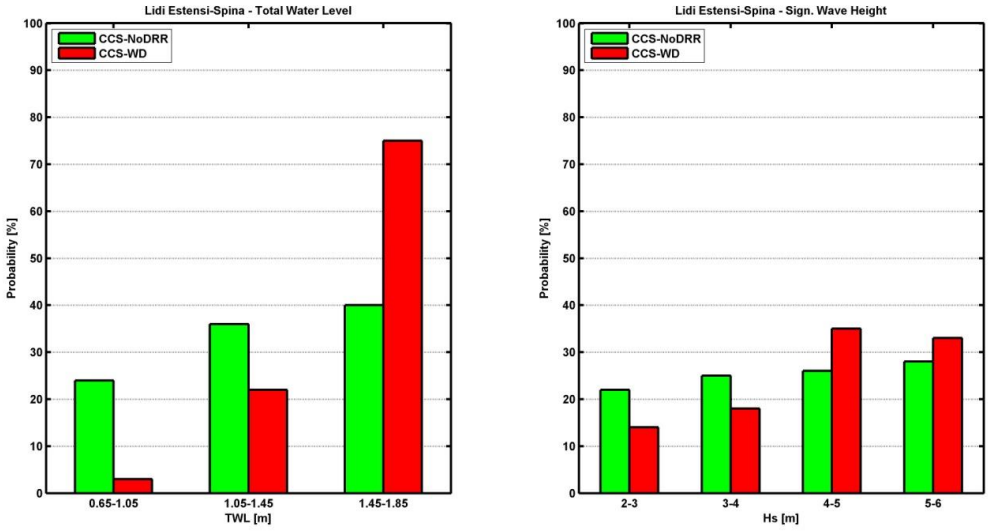

Figure 6.17. Distribution of boundary conditions (TWL on the left and Hs on the right) for constrained uniform flood damages in the climate change scenario for Lido degli Estensi-Spina. The configuration without measures (green bars) and under the implementation of the Winter Dune (red bars) were compared.

6.5. Discussion

The framework of the present study is appropriate for the prevention phase of the disaster management cycle. In this context, it has been applied to support decisions for coastal risk management by facilitating inter-comparison of risk reduction strategic alternatives. This comparison was performed for a large set of simulations, covering many (current and future) conditions and multiple hazards. The presented work is part of a larger investigatory process (see Martinez et al., 2018) where stakeholders and end-users were interviewed to select possible measures for critical coastal areas (i.e. local scale). The objective of the present work was to provide rather simple information on the efficiency of measures to be used in a participatory process (see Barquet and Cumiskey, 2018) aiming at selecting acceptable measures to be applied as part of an integrated local strategy for risk reduction. The analysis has some inherent uncertainties associated with the implementation of the steps of the Source-Pathway-Receptor-Consequence model which are identified and discussed in what follows.

With respect to the definition of sources, the Bayesian Network-based (BN) approach has been built by chosen storm variables limited to those previously identified as the most important to control the magnitude of storm-induced hazards at each site. Once identified, they were discretized in equal

intervals covering the whole range of so far observed values. A limited number of combinations has been used to cover the most important storm classes in terms of induced hazards and damages (Armaroli et al., 2009, 2012; Mendoza et al., 2011). Increasing number of variables and/or variable resolution will allow to better reproduce the inherent climate variability and to characterize better this source of uncertainty in the assessment (see e.g. Chapter 7). In spite of this, used values can be considered as representative for forcing source in both areas and, in this sense, they will allow to use the framework to assess the efficiency of tested measures to reduce inundation and erosion risks for each given condition. No prior knowledge of storm characteristic variables was assumed, representing them with uniform distributions. Thus, the current application, the Bayesian-based Decision Network (BDN) was essentially deterministic. This was enough to communicate scenarios and measure efficiencies to stakeholders by integrating the BDN in a multi-criteria analysis such as that presented in Barquet and Cumiskey (2018). In such multicriteria assessments, the BDN output is combined with information on additional elements required for decision making such as economics, endurance, ecological, stakeholders' perception, allowing for the final evaluation of alternatives. As it has been mentioned before, the next step should be to reproduce the local maritime climate to analyse this performance taking into account the relative frequency of each condition. In such a case, the BN-approach would be fully-probabilistic (see e.g. Chapter 7). In addition, using time series data on real historical events would reduce the uncertainties introduced by representing some events with synthetic design shapes (see Chapter 3).

Uncertainties associated with the pathway are related to the selection of the process-oriented models used to simulate induced hazards. In the current analysis, we have not considered this source of uncertainty since the framework is applied by using previously selected models and recommended damage curves. As it was mentioned in the method section, the selected model to simulate storm-induced hazards is XBeach (Roevilnk et al. 2009), which is currently one of the most applied at the international level. Applied model setting has been selected for each case study based on local calibrations and validations for selected storm impacts. This step must be done prior to BN development since it will control the accuracy of hazard estimation and it is also a source of uncertainty. In any case, the methodology can easily deal with this source of uncertainty if simulations from multiple models or model settings are used to feed the BN.

Another point to be considered is that this assessment framework has been designed to analyse the storm-induced coastal response. This implies that used models do not forecast the coastal morphology at a given time (where it should be necessary to couple all governing processes) but predict the expected storm-induced changes for a given coastal configuration. As storm-induced hazards depend on existing morphology at the time of the impact (e.g. Cohn and Ruggiero, 2016), the initial morphology used in the model is also a source of uncertainty. To overcome this, a long/medium term morphological model (Hanson et al. 2003; Lesser et al. 2004) could be used to forecast the future coastal morphology under a given climate scenario at a given time and then, to use it as the initial configuration to assess storm-

induced changes. This has been illustrated here by considering the change in estimated risks due to sea level rise in Tordera Delta. This approach can also be applied to assess the effects of consecutive storm impacts (Coco et al. 2014) by using estimated post-storm bed levels as pre-storm morphology for given storm combinations. Once this extra information is included in the BN, the uncertainty associated to future shoreline configurations on assessed risks can be analysed (see e.g. Chapter 7).

Regarding receptors, their location and typology have little associated uncertainty, except for future projections, where it was not considered (i.e. type and location of receptors remain constant in time). Houses, promenades and fixed elements were derived from accurate land use and cadastral data available for the sites. Moreover, campsite elements were manually located and delimited from available GIS-based tools and raster imagery. In spite of this, some uncertainty associated with the mobility of campsite elements between seasons, as well as to land-use changes or new developments, remains. In the case of temporary elements, the worst case scenario was considered, i.e. they are assumed to be present at any space allocated to them. This implies that maximum potential damage was estimated. This could be modified by considering the existing time-lag between intensive tourist use of beaches (and consequently in campsites or concessions) and storms seasonality (e.g. Valdemoro and Jiménez, 2006). The existing lag can be used to modify/reduce the exposure of this temporary elements to storm impacts.

With respect to the consequences, expected damages due to inundation have been estimated by using damage curves. Although this is a standard approach for this type of analysis (see e.g. Penning-Rowsell et al. 2013), used damage curves have been recommended by ACA (2014) and Scorzini and Frank (2015) for river flooding in Catalonia and Italy respectively. The absence of specific damage curves estimated for analyzed process and existing elements also introduces uncertainty, although in this case, it is already assumed by the corresponding administrations since they are recommending its use. The equivalent for expected damages due to erosion was set in terms of an erosion buffer, which represent the protective function of the beach against the direct impact of waves. As it was previously shown, this buffer was selected specifically for each site and, similarly to damage curves, it must be defined according to local conditions.

Regarding the inclusion of the risk reduction measures in the analysis, it is assumed that protective strategies are completely and efficiently implemented when storm events occur. In the case of flood resilience measures, this implies that all existing elements in each site (from campsites to buildings) implemented flood-proofing measures. However, local, social and economic conditions will influence its real implementation (see e.g. Bubek et al. 2013) and, in any case, this assumption clearly overestimate its efficiency.

When setback definition and retreat is the adopted strategy, the used approach to characterize the initial coastal morphology also has implications on the results consideration. This implies that the effectiveness of the retreat is just measured with respect to the storm reach. To be efficient in time, the existence of

any additional mid- long-term background erosion, as it is the case of the Tordera site (Jiménez et al. 2018 – see Chapter 4), should be included to properly define the required setback (e.g. Sano et al. 2011 and Chapter 7).

This also applies to infrastructural measures, which are considered to be implemented at the time of the storm impact. In the case of the combined nourishment-dune solution considered in the Tordera case, this would imply that to maintain its efficiency in time, the beach would have to be renourished after each storm impact to maintain the 50 m increase in beach width. This also affects the efficiency of the winter dune tested in the Italian case, which strictly depends on the beach width before the storm impact. In this sense, Harley and Ciavola (2013) indicate that the dune height and crest width required to protect the area should be designed differently for different coastal stretches along the study site. From the coastal manager standpoint, this implies that to properly assess their performance in the future, background processes must be considered to account additional losses in beach nourishment in the Tordera (e.g. Jiménez et al. 2011) or in beach width variations along the Italian case (Armaroli et al. 2012).

Assessed risks under current conditions at both locations are consistent with already observed impacts. At the Tordera site, erosion and direct wave impact problems are the main issue for campsites and existing infrastructures (Jiménez et al., 2011; 2017). At the Italian case, flooding is the dominant hazard with assessed impacts being comparable with previous observations (e.g. Perini et al., 2016).

As a result of the combination of hazard and site characteristics, a notable increase of the assessed impacts is predicted for both sites when SLR is considered. At the Tordera delta, overall results indicate a doubling of expected flooding impacts. Moreover, erosion impacts will increase even further since the induced retreat will immediately imply an increase in receptor exposure. This behaviour is similar to the observed increase in damages due to the present background erosion, where campsites located in unprotected areas have been progressively losing space at the seaward boundary, and the existing promenade has suffered frequent damages during the last decades (Jiménez et al., 2011). At the Italian case study, SLR and subsidence effects are mainly identified in flooding risk which will be significantly larger. On the other hand, although erosion risk will also increase, it will remain relatively low. This lower increase is caused by both a closer future projection compared to Tordera and by the effect of not including the morphological response to SLR since, in this case, the future scenario was only characterized by increasing the position of the MSL.

When considering SLR-induced effects on time evolution of storm-induced risks, existing uncertainties must be also taken into account. Thus, the first uncertainty is related to the magnitude of the change itself. Here the RCP8.5 SLR projection was used, but other scenarios could be possible (Church et al. 2013). The other source of uncertainty is controlled by the way in which this forcing is translated into the system. In this work the Bruun rule was assumed to be valid and it was used to generate a morphological accommodation of the Tordera Delta site to SLR. Since there is no consensus on the best

model to simulate this effect, other existing models and approaches (see e.g. Le Cozannet et al. 2014) could be tested and integrated in the BN to include this source of uncertainty. In any case, the effect of the uncertainty on the SLR projections may be larger than their associated morphological response.

In spite of the sources of uncertainty previously mentioned, this analysis has permitted to identify which are the most harmful conditions to induce storm-related inundation and erosion risks at the two study sites, to identify which are the most affected receptors and, to compare the efficiency of different risk reduction strategies. This has been done considering both hazards in a separated manner which is an advantage for the manager since damage induced by erosion and inundation differ in characteristics and they need to be afforded in a specific manner. Although this can be a valuable tool for decision making in storm-induced risk management, it must be further complemented with a similar analysis including the reproduction of the statistical structure of storms (see Chapter 7) in combination with a socio-economic valuation such as multicriteria analysis to properly make final decisions. In this sense, this analysis can be used as the first step to identify the most relevant risks and strategies to be further tested.

6.6. Conclusions

In this chapter, a methodological framework for storm-induced coastal risk management purposes developed within the framework of the RISC-KIT EU project was presented and applied in two sites in the NW Mediterranean and N Adriatic coasts. The study is based on the integration of the Source-Pathway-Receptor-Consequences model in a Bayesian Network-based (BN) approach. This was fed with a large number of numerical simulations obtained through process-oriented model chain able to simulate multiple storm-induced hazards at the receptor scale. The BN integrates impact results that individually account for all receptors in the hinterland. Once developed, the BN can be regularly updated with additional simulations and further extended with new scenarios.

The presented application, a Bayesian-based Decision Network, has been fed with storms covering the range of representative conditions at both study sites and uniform distribution of source variables. This permitted to assess in a deterministic way, the performance of different risk reduction strategies to individual hazards and under different climate scenarios.

In spite of not statistically mimicking the maritime climate, the approach demonstrated impact responses in the current situation in accordance with existing knowledge at both sites. Tordera Delta, which is characterised by quick and intense erosive responses to storms, showed greater impacts to erosion than Lido degli Estensi-Spina and they were essentially concentrated in infrastructures located just behind the beach. As expected, the flooding impact in the current situation is higher for receptors located closest to the shoreline or at the lowest elevation areas of the hinterland (i.e. concessions at Lido di Spina and campsites at Malgrat).

The estimated risk significantly increases for the climate change scenario. The morphological accommodation response to the projected MSL, which was only included at the Tordera Delta, was identified as a major process to be considered in the impact assessment to properly account for modifications in erosion and inundation hazards.

From the tested risk reduction strategies, the construction of artificial dunes was identified as very effective for inundation at both study sites, whereas its efficiency for managing erosion was lower. On the other hand, and as expected, setback definition and managed retreat seems to be the best option to tackle the impacts of erosion.

Finally, the developed framework has proven to be efficient to analyze storm-induced risks and strategies to cope with them. Moreover, a series of elements to be addressed to further improve it and to extend its applicability have been identified and discussed. In this sense, the BN approach is a versatile tool to make robust comparisons across different conditions.

CHAPTER 7.

A stochastic Bayesian Network method to characterize risk and storm-induced retreats at a local scale.

This Chapter presents a Bayesian Network (BN) methodology for hazard and risk assessments at local scale. In particular, two different applications will be presented: (i) a stochastic characterization of storm-induced risk at the Tordera Delta at present conditions and at different midterm background erosion scenarios, and (ii) a BN model for the characterization and prediction of maximum retreats in complex environments in terms of morphology and presence of beach-structure interactions.

These applications follow the schematization based on the SPRC model presented in previous Chapter 6. However, here two of the main detected limitations are tackled: (i) the use of a closed subset of storms implies a deterministic treatment of the wave climate, allowing scenario comparisons but not producing a stochastic risk characterization; and (ii) the use of synthetic triangular storms to simulate event characteristics not previously recorded, introduces large uncertainties on the estimation of storm-induced erosion and inundation (as assessed in Chapter 3).

7.1. Generalities

The general aim of the present chapter is twofold. On the one hand, to present a stochastic application of the Bayesian Network methodology for risk characterization at the local scale using all the storms from a long record of wave time series (60 years) (Section 7.2). The methodology will be applied at the Tordera Delta under present morphology and future midterm scenarios of background erosion with the objective to obtain the risk profile of the delta, its main correlations with the storm characteristics, and a probabilistic definition of receptor setbacks for the erosion and inundation hazards at different levels of risk. On the other hand, to test the Bayesian Network as predictor for storm-induced beach retreats in order to be potentially used as surrogate of simple parametric models in complex environments such as the Tordera Delta (Section 7.3). In such environments, due to the alongshore morphological variability, the different orientations of the coast and the presence of hard elements inducing beach-structure interactions, parametric models have limited applicability. The assessment aims to characterize the main variables controlling maximum beach retreats at the Tordera Delta.

The description of the study area and local storm climate has been extensively presented in Chapters 4, 5 and 6. Figure 7.1 shows the spatial divisions that will be used in Sections 7.2 and 7.3.

Coastal storms are identified using the double threshold P.O.T described in Chapter 2.The present chapter uses hindcast waves from the Downscaled Ocean Waves dataset (Camus et al., 2013) derived from the Global Ocean Waves (Reguero et al., 2012) and hindcast surge from the Global Ocean Surge dataset (Cid et al. 2014), obtained at 4 locations close the Tordera Delta at ~20 m depth (see locations in Chapter 5), covering the period from 1954-2014. The simultaneous astronomical tide is added to de GOS dataset in order to obtain the total water level.

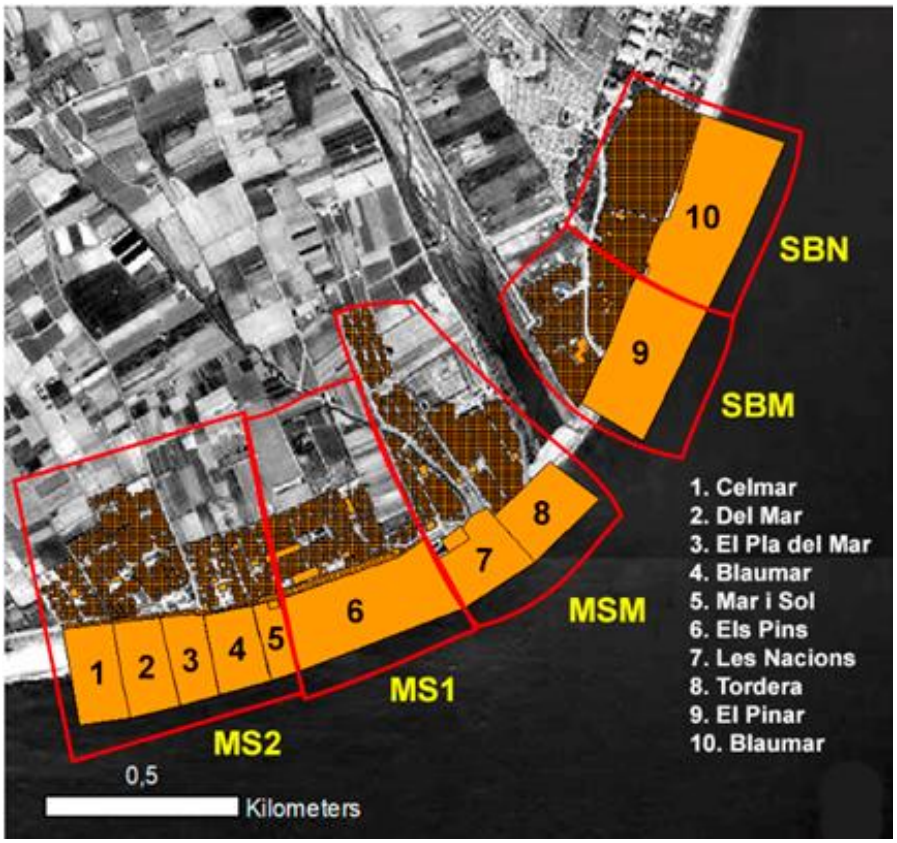

Figure 7.1. Receptors included in the risk assessment (Section 7.2). The red polygons indicate the areas used to subdivide receptors in the risk assessment (Section 7.2) and the numbers denote beach sectors for the morphologic assessment (Section 7.3). Polygons without numbers are receptors in the hinterland.

The obtained dataset is composed by 179 storms (~3 storms per year), from which the whole hourly evolution of the different wave conditions is stored, i.e. significant wave height (Hs), peak period (Tp), storm surge, wave direction and directional spreading. Of the 179 events, 43 are formed by multi-peak storms. Multiple peaks have been assessed as single storm events when the fair-weather conditions between them lasted less than 72 hours (Figure 7.2). In 12 cases, storms are formed by 3 or more peak sequences, leading to a total number of 237 individual peaks. This type of storms is relatively common in the NW Mediterranean (Mendoza et al., 2011), and its related to cyclogenesis meteorological conditions (see e.g., Trigo et al., 2002). Multi-peak storms are of particular interest due to their associated coastal response (Mendoza et al., 2011).

The XBeach model of the Tordera Delta is used in Section 7.2 and 7.3 to simulate storm-induced erosion and inundation for each of the individual storm peaks. See Chapter 5 for further detail on model-grid (and corresponding source data) and model set-up and validation.

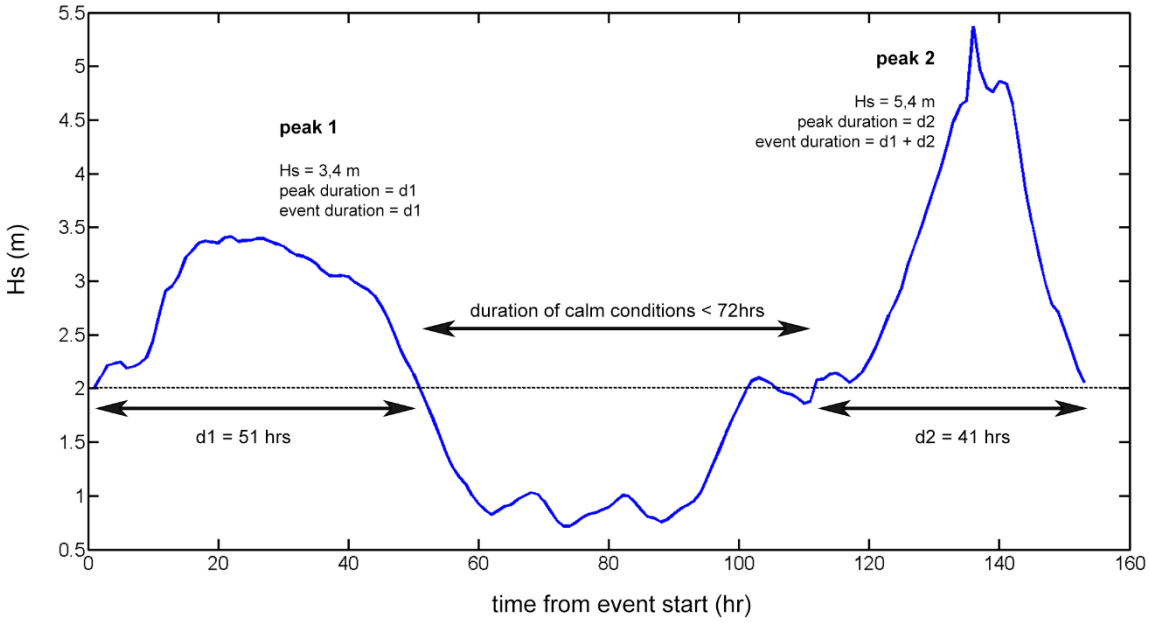

Figure 7.2. Storm peak characterization in a multi-peak event. The case of the November 2001 storm.

7.2. BN-based risk characterization at local scale

7.2.1. Introduction

The motivation and contexts behind local scale risks assessments has largely been presented in Chapter 6. The aim of this Section 7.2 is to present a fully stochastic application of the BN-based SPRC scheme to characterize coastal risks at local scale. Risks related to storm –induced erosion and inundation will be assessed, for a current morphology and for future configurations. For that purpose, all available storms derived from a long dataset (60 years) of wave time series will be simulated and the induced hazards analysed. Receptor characterization will be individually performed as in Chapter 6. The inundation risk will be assessed in terms of relative damage to structures and risk to life, while the erosion risk will be assessed as a function of the loss of protective capacity of the coast in front of the receptors.

The inclusion in the BN of simulation results from a long dataset of storms allows a fully stochastic assessment in terms of wave climate characterization. This can be considered as a novelty with respect to existing studies that only use a subset of events to describe the source (e.g. Van Verseveld et al., 2015; Plomaritis et al., 2018; Ferreira et al. 2019; Chapter 6). In addition, such an approach follows the idea behind the response approach (Garrity et al., 2006, and Chapter 2) and simulates the storms using their real shapes (i.e. the storm evolution with time), avoiding the uncertainties introduced by the use of a synthetic representation of the events (Chapter 3).

7.2.2. Methodology

Receptors and risk characterization

This application follows the methododology used in Chapter 6. However, key points are also given here for clarity and better readability. Receptors are individually considered by their footprint polygons obtained by means of a GIS-based tool, accounting for their exact position and dimensions. These polygons are intersected with the XBeach model mesh assigning to each receptor the model nodes directly affecting them. The coordinates of the receptor corners are also known, which allows calculating the distance from the receptor to both the public domain limit (boundary between beach and hinterland) and to the closest eroded cells in the XBeach simulations. Receptors with different vulnerability characteristics were defined and separately considered. As in Chapter 6, considered receptors comprise hard constructions, such as houses and infrastructures, and softer elements such as campsite elements (e.g. bungalows). Receptors are grouped in 5 different areas (Figure 7.1) in the alongshore direction, aiming to capture the effects of the morphological variabilities and different orientations at both sides of the river mouth. Thus, SBN and SBM (Figure 7.1) are two areas defined at the north side of the river mouth with SBM closest to the river and SBN further to the north and limited at the back by the existing promenade. On the other hand, areas located south of the river are divided in three (Figure 7.1): MSM

being closest to the mouth; MS1 following MSM and located south of a coastal revetment with associated flanking effects and MS2 located furthest to the south, with wider beaches and sheltered due to its orientation against eastern incoming storms.

Table 7.1. Flood damage curves to obtain relative damage to structures using simulated inundation depth as input (Agència Catalana de l'Aigua, ACA, 2014).

Inundation depth (m)	Relative damage (%)	
	Hard structures (Road, promenade, houses)	Soft structures (campsite elements)
0	0	0
0 – 0.3	18.3	50
0.3 – 0.6	26.5	71
0.6 – 0.9	33.2	82
0.9 – 1.5	44.7	89
1.5 – 2.1	54.9	91
> 2.1	64.5	100

Table 7.2. Risk to life calculated as a function of the product between water depth and flow velocity (Priest et al. 2007).

Flood depth-velocity (m2/s)	Risk to Life
0 – 0.25	None
0.25 – 0.5	Low
0.5 – 1.1	Medium
> 1.1	High

Table 7.3. Erosion risk as a function of the distance from the receptors to erosion magnitudes greater than 0.25m of bed level change. A distance of 7.5 m corresponds to the expected retreat for the 10-year return period (Jiménez et al., 2018).

Erosion risk level	Distance to receptor (m)
None	> 30
Very Low	22.5 - 30
Low	15 – 22.5
Moderate	7.5 - 15
High	3 – 7.5
Extreme	0 - 3

For the inundation hazard, relative damage to receptors is calculated by means of flood-damage curves (Table 7.1) using the maximum modelled water depth within the receptor polygon. No specific damage curves exist for the Catalan coast, and the chosen curves are assumed to be representative for the inundation risk as they are used by the Catalan Water Agency (ACA, 2014) for the development of the inundation plans. Additionally, risk to life is also included in the assessment, using as input the water-depth-velocity product (Table 7.2, Priest et al., 2007) within the receptors boundaries.

For the erosion hazard, the magnitude of the associated risk is based on the distance from the significantly eroded XBeach nodes to the receptors. Significant erosion was set to 25 cm of vertical bed

level change, assumed as common minimum depth for light structure foundations The closest distance from the receptor corners to that erosion level is compared with the erosion risk thresholds in Chapter 4 (Table 7.3).

Background erosion

In this study, midterm background erosion along the sandy beach sectors has been estimated by analysing shoreline position changes from aerial photographs available at different time frequencies that cover the last 25-30 years. The estimated average retreat for the 3 sandy beach sectors are 1.1 m/y at SBN and SBM, 4 m/y at MSM and MS1, and 1.9 m/y at MS2 (Jiménez and Valdemoro, 2019; see Figure 7.1 for locations). In this application is assumed that the observed trends remain constant during the analysed timeframe. However, this can be substituted by time-varying evolution provided this should be the case.

To account for this background response, the framework is applied to different base morphologies assumed representative of a given time horizon. The baseline morphology is the one described in Section 7.1.2 (and Figure 7.1) which was directly measured. The morphologies corresponding to different time horizons (i.e. +5, +10 and +20 years) are built by retreating all profiles (cross-shore nodes of the XBeach grid) from -10m depth to the subaerial beach according to the erosion rates at the different areas, using linear transitions between sectors affected by different retreat rates to ensure smoothness alongshore. The result of DEM re-interpolation to the XBeach grid is shown in Figure 7.3, along with example profiles at locations under the 3 different levels of background retreat. When there is not enough accommodation space because of the existence of hard structures at the hinterland, profile retreat is adapted to that factor: e.g. +20 years in P1, Figure 7.2 lacks the dune because the profile arrives at the road, and +10 and +20 years in P2 are limited by the presence of the promenade.

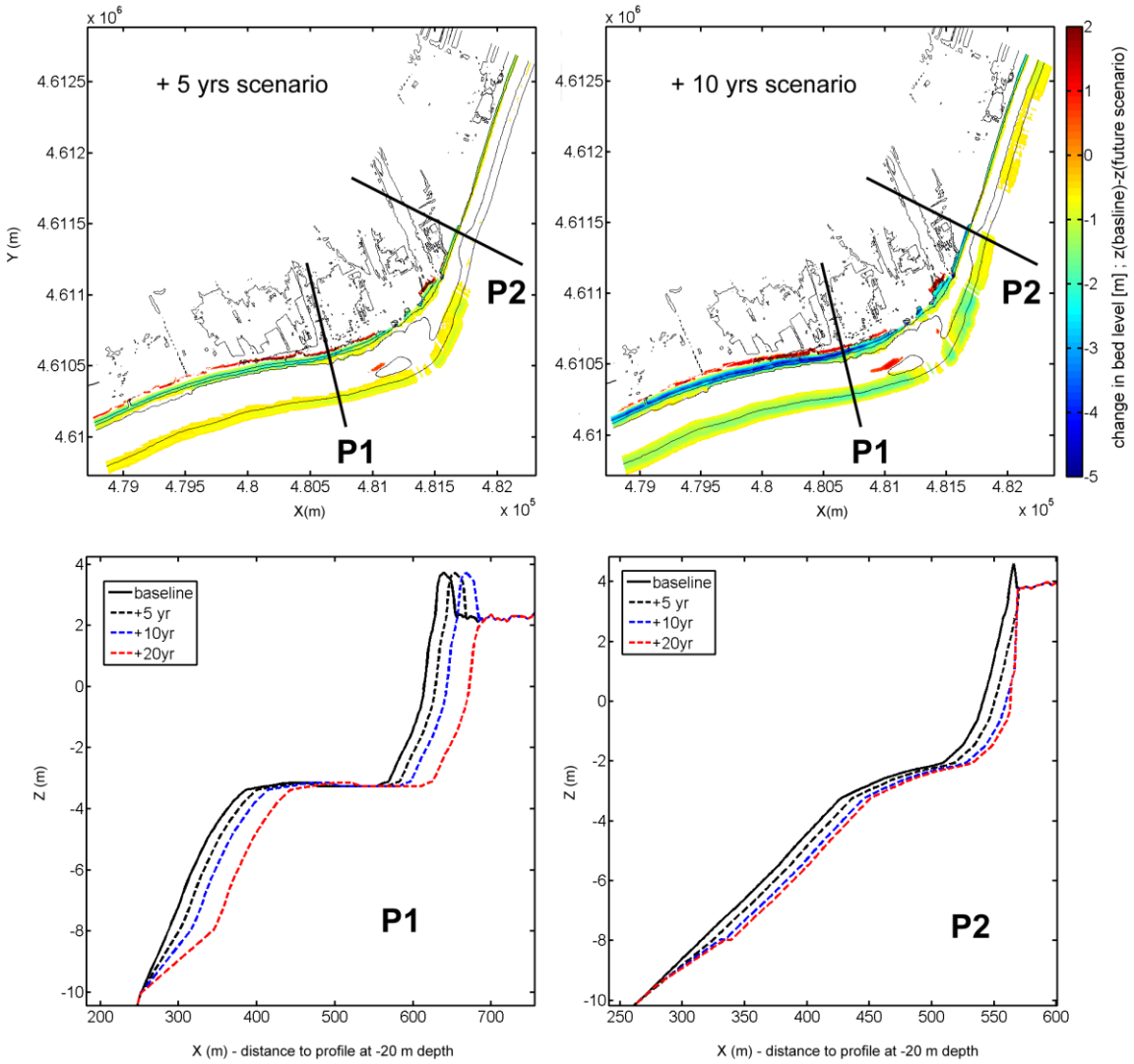

Figure 7.3. Changes in the bed level grid for the future scenarios. Difference between baseline bed level and scenario bed level (upper). Profile retreat at both sides of the river mouth at the different time horizons (lower).

Storm subsets and validation

In order to statistically compare the risk response of the study site under the baseline morphology and each of the three midterm structural erosion horizons, the whole set of 179 storms (237 storm peaks) should be simulated 4 times, one for each configuration.

In order to reduce the computational effort, a storm subset is derived aiming to maintain statistical representativeness while avoiding repetition of simulations of strongly similar storm conditions. The followed procedure was dividing the main 4 storm variables (i.e. Hs, Tp, duration and direction) in homogeneous intervals covering their whole range as shown in Table 7.4. Then, storms are classified according to these characteristic peak variables.

Table 7.4. Subset characteristics compare to the original storm dataset. Source variable combinations used to classify storms and select the subset events.

Original dataset characteristics			
179 storms	136 single-peak	43 multi-peak	237 storm peaks
Subset characteristics			
69 storms	26 single-peak	43 multi-peak	127 storm peaks
Source variable combinations to produce subsets			
Hs (m)	Tp (s)	Duration (hr)	Direction (ºN)
< 3	< 9	< 20	> 110
3 – 3.5	9 – 11	20 – 40	110 – 150
3.5 – 4	> 11	40 – 60	> 155
4 – 4.5		> 60	
> 4.5			

To produce the subset, only one storm is selected for each combination of variables. Later, using multiplicity factors, the Bayesian Network can be trained taking into account the total number of events that belong to each source combination. Multi-peak storms are a common phenomenon in the NW Mediterranean (Mendoza et al., 2011; Figure 7.2) with specific coastal response due to the accumulation of peak impacts. Thus, all of them were simulated, saving the simulation output after each individual peak. The simulation of each multi peak event was representative of two types of storms: (i) the multi-peak event itself and (ii) the single-peak storms with properties matching the first peak of the simulated event. The result was a subset of 69 storms, preserving the 43 multi-peak storm events (Table 7.4). Note that de division of variables is here more refined than in the Bayesian Network bins (subsection 7.2.2.4), to later ensure intra-bin variability during the training.

In order to test the statistical representativeness of the subset with respect to the whole storm dataset, the methodology to compare histograms proposed in Bityukov et al. 2013 is used here. The method assumes the values at each bin of the histogram follow a normal distribution with expected value $n_{i,k}$ and variance $\sigma^2_{i,k}$ (with "i" representing the bin and "k" the histogram). Then, significance is defined as:

$$\hat{S}_i = \frac{\hat{n}_{i,1} - \hat{n}_{i,2}}{\sqrt{\hat{\sigma}_{i,1} + \hat{\sigma}_{i,2}}} \qquad (7.1)$$

Where $\hat{n}_{i,k}$ is an observed value at bin "i" of histogram k, and $\hat{\sigma}_{i,k} = \hat{n}_{i,k}$. Then, we consider the RMS of the distribution of significances:

$$RMS = \sqrt{\frac{\sum_{i=1}^{M} \hat{S}_i - \bar{S}}{M}} \quad (7.2)$$

Where $\bar{S}$ is the mean value of $\hat{S}_i$ and M is the number of bins of the histogram. The RMS represents a distance measure with the following interpretation: RMS = 0 both histograms are identical; RMS =0~1 both histograms are obtained from the same parent population; RMS >> 1 histograms are obtained from different parent distributions.

Bayesian Networks

Here, two BN configurations are used to characterize system response to the impact of extreme events. This is done to optimize the BN structure limiting the number of variables per network, while solving the different parts of the SPRC framework. In practice, one BN solves the source-consequences relationships (BN-A) and the other the receptor-consequences spatial distribution, giving complementary information on the local risk profile (BN-B).

BN-A (Figure 7.4) links storm-related variables (i.e. Hs, Tp, duration, direction, and water level) between them and to the obtained impacts at the receptors (i.e. erosion impact, risk to life and structural relative damage). The central variable of the network is used to perform conditioned assessments and it is one of three depending on the analysis: (i) total number of affected receptors by inundation within a storm event; (ii) total number of affected receptors by erosion within a storm event and (iii) receptor area (i.e, SBN, SBM, MSM, MS1 and MS2). The total number of affected receptors has been included to account for the spatial extension of the impacts. For the inundation impact, after each storm-simulation all receptors presenting a relative damage different than 0% or a risk to life different than None are counted and used as an additional storm characteristic variable. Similarly, all receptors presenting an erosion impact level different than None after the storm event are counted in the total number of affected receptors by erosion variable. This means that generally, storms will present a larger number of affected receptors by erosion as Very Low to Moderate erosion risks represent loss of beach protection function without direct wave impact to the receptors, while inundation-related impacts are associated to presence of water at the receptors. This has to be taken in consideration when interpreting obtained results.

BN-B (Figure 7.5) links the simulated receptor impacts to the area where they are located and to their distance to the public domain (i.e., limit between the beach and the hinterland). Additionally, two variables accounting for the number of erosion or inundation impacts per receptor are included. These variables are aimed to give additional insight on the system response, since obtained distributions with the Bayesian Network merge storm-climate variability with the spatial distribution of receptors. Therefore, knowing the proportion of receptors with a given number of impacts for the entire storm record is an important additional source of information. For the inundation risk, the number of damage

impacts different than 0% and/or risk to life impacts different than None are counted at each receptor. Similarly, all erosion impacts different than None are counted per receptor. This means that a receptor can have multiple erosion impacts and not a single inundation impact, as Very Low to Moderate erosion risks represent loss of beach protection function without direct wave impact to the receptors, while inundation-related impacts are associated to presence of water at the receptors. Similarly to the previous case, this has to be taken into account when interpreting obtained results.

It must be noted that from all receptors displayed in Figure 7.1, only those presenting at least 1 impact for the entire dataset either by inundation or erosion have been included in the BN training. Otherwise, the choice of receptor population to include in the assessment would be arbitrary and so affecting the obtained distributions.

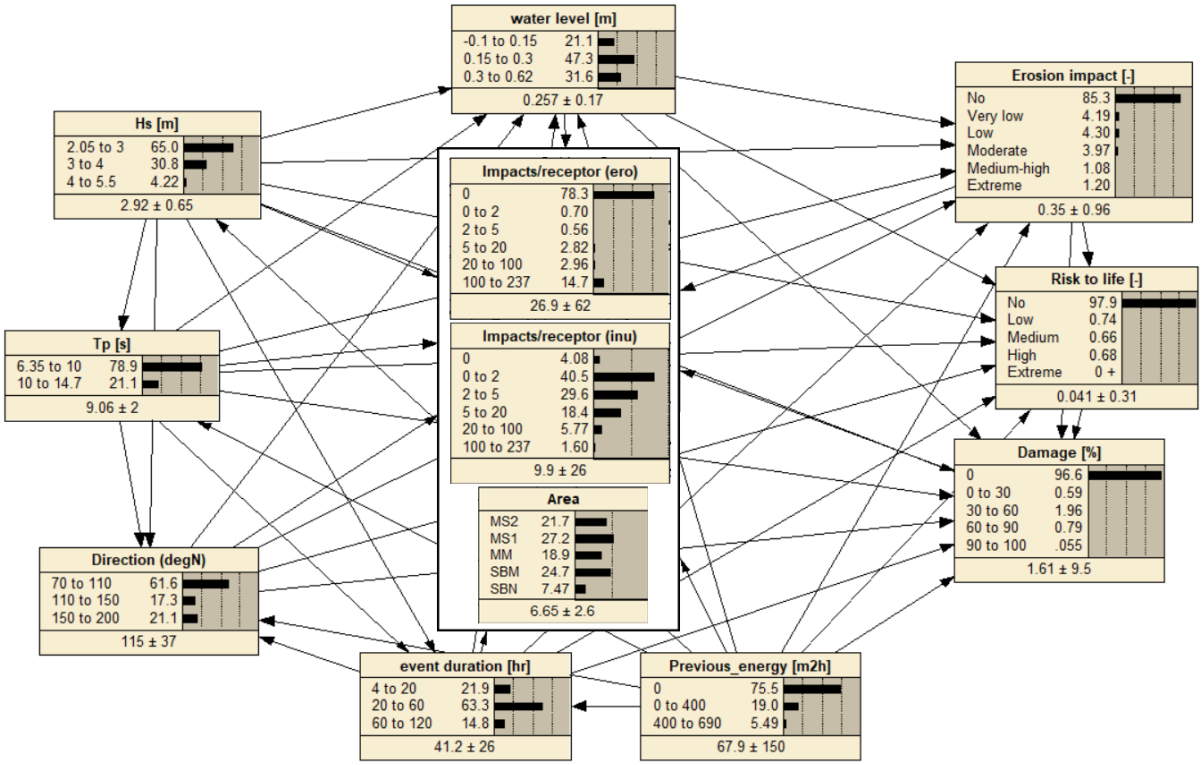

Figure 7.4. BN-A, linking source variables to consequences. Central variable is used for conditioned assessments and it is one of three: (i) total number of affected receptors by inundation within a storm event; (ii) total number of affected receptors by erosion within a storm event and (iii) receptor area (i.e, SBN, SBM, MSM, MS1 and MS2).

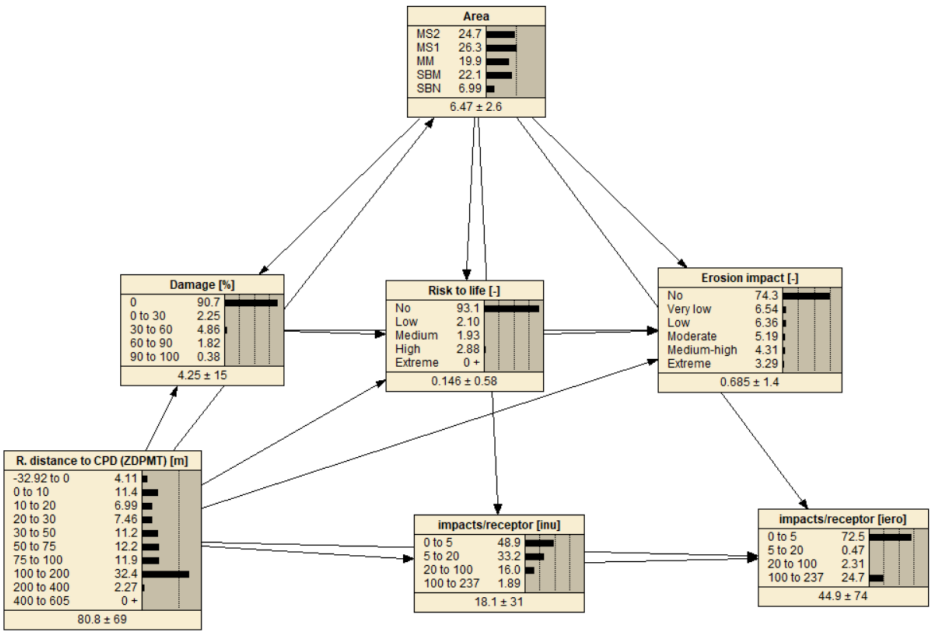

Figure 7.5. BN-B, linking consequences to receptors spatial distribution.

Different discretization methods exist in order to represent continuous variables in environmental BN applications, such as manual discretization (used in this work) or supervised and unsupervised automatic methods (Beuzen et al. 2018a). The presented BN-model is designed for application to a well-known coastal hotspot (Chapter 4) were expert knowledge on storm climate and coastal response is abundant. This fits the use of manual discretization (Figures 7.4 and 7.5) as it has better accuracy than automatic unsupervised methods and close accuracy to supervised discretization with less associated variability on model performance (Beuzen et al. 2018a).

7.2.3. Results

Subset verification

Results for the midterm future horizons will be obtained by feeding the BN with the selected subset of storms. Due to this, the first step consisted in comparing for the current configuration results using the subset and the complete dataset. Table 5 shows obtained statistics comparing the histograms of the discrete PDFs of the global system response and conditioned probabilities both related with dependencies to source characteristics and spatial receptor distribution to risk. Results of global system response represent the general discrete PDF distributions without any constriction in the BNs. System response conditioned to storm characteristics corresponds to Hs, duration direction and water level distributions obtained after constraining the BN to certain cases. The spatial distribution of risk profile corresponds to the PDFs of risk related variables conditioned to spatial variables.

Table 7.5. Results of the histogram comparison between the original dataset and the storm subset for the baseline scenario.

Verification case	$\bar{S}$	RMS
Global system response		
Prior probabilities on risk variables (Table 7.6)	-0.009±0.006	0.04±0.05
System response conditioned to storm characteristics		
Storm variables conditioned to number of affected receptors per storm (Figure 7.7)	0.013±0.03	0.1±0.07
Storm variables conditioned to high risk levels and area (Figure 7.8)	0.0006±0.02	0.05±0.03
Spatial distribution of the risk profile		
Risk distributions conditions to area and distance to beach limit (Figures 7.9 to 7.13)	0.0041±0.02	0.04±0.08

All obtained values of the mean significance $\bar{S}$ and its RMS are close to 0, and thus, from the perspective of the obtained results, it can be assumed that obtained distributions by training the BNs with the subset represent almost identically the same source population to that of feeding with the complete dataset. This is true both for global distributions and also for conditioned discrete PDFs.

Global system response and associated storm characteristics

The so-called prior (unconstrained) probabilities of the different risk-related variables represent the expected frequency of the different risk levels. Obtained probabilities combine the variability of the source (storm climate) with the spatial distribution and extent of the impacts. Table 6 shows obtained probability levels under the baseline morphology and for the midterm horizons.

Table 7.6. Unconstrained probabilities for different risk levels under the different scenarios

Risk variable	baseline	+ 5 yrs	+10 yrs	+ 20 yrs
Inundation risk				
% storms affecting ≥ 200 receptors	4 %	16 %	20 %	40 %
Probability of Damages ≥ 30%	3 %	5 %	5 %	7 %
Probability of Damages ≥ 60%	1 %	2 %	1 %	2 %
Probability of risk to life ≥ Medium	2 %	3 %	3 %	5 %
Probability of risk to life ≥ High	1 %	2 %	2 %	3 %
Erosion risk				
% storms affecting ≥ 450 receptors	4 %	66 %	100 %	100 %
Probability of risk ≥ Medium	5 %	9 %	13 %	13 %
Probability of risk ≥ High	2 %	4 %	8 %	8 %

As it can be observed, the expected increase in probability of the inundation damages and the risk to life is lower than the associated to erosion. The probabilities of medium-high erosion risks in the baseline are larger, as erosion generally affects a larger number of receptors per storm event. The larger increase of the erosion risk is associated to the sharper increase of the frequency in which storm events causes the highest-class number of affected receptors by any level of risk as it is more directly affected by the shoreline retreat. Here it is important to remember that the erosion risk is not only related to direct impact but also to loss of protection function, while inundation risk implies that water is directly affecting the receptor. Direct erosion affecting the receptor physical limits corresponds to the High erosion risk, which has a similar behaviour to that of low to severe inundation damages.

The BNs also output the spatial distributions across the 5 areas of the receptors impacted by any level of risk (Figure 7.6). Results show how areas more commonly affected by erosion (north) differ from those impacted by inundation (south) in the baseline scenario. The general spatial distribution of receptors receiving impacts changes when looking at future scenarios, which is associated to the fact that the midterm shoreline evolution at the site is not homogeneous, and neither the existing topography. As a consequence, the erosion and inundation impacts in future scenarios increase proportionally more in MS2 than in other areas.

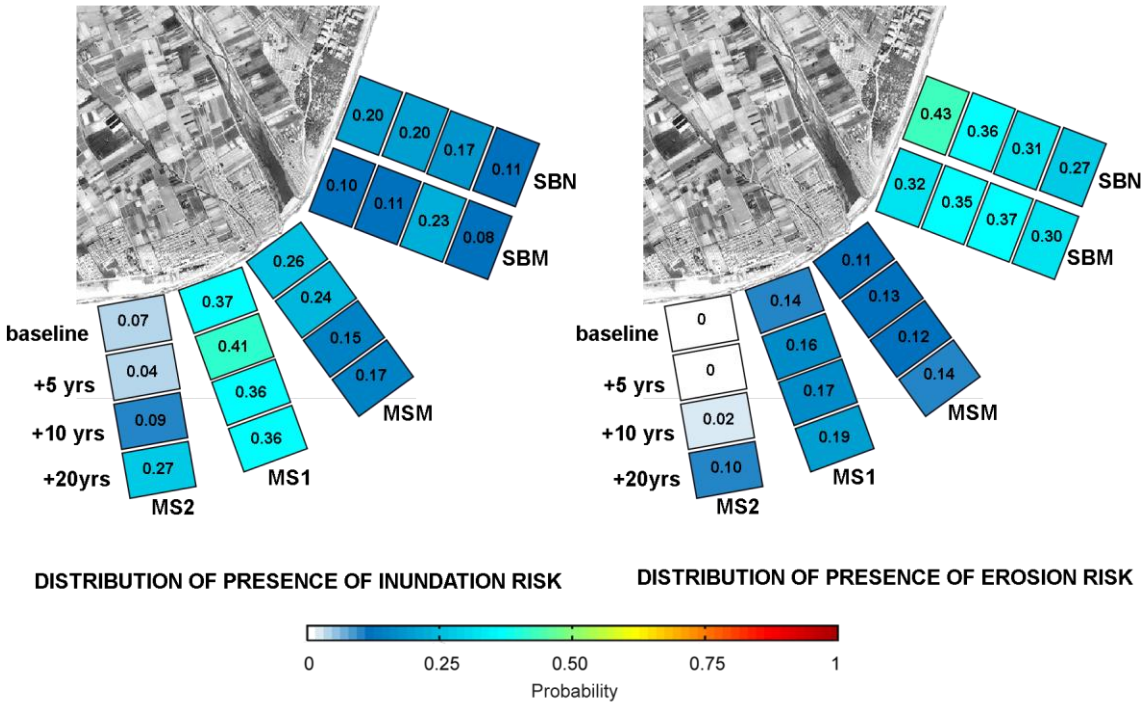

Figure 7.6. Global Spatial distribution of receptors receiving impacts (presence of any level of risk) in baseline and future scenarios for the erosion and inundation hazards.

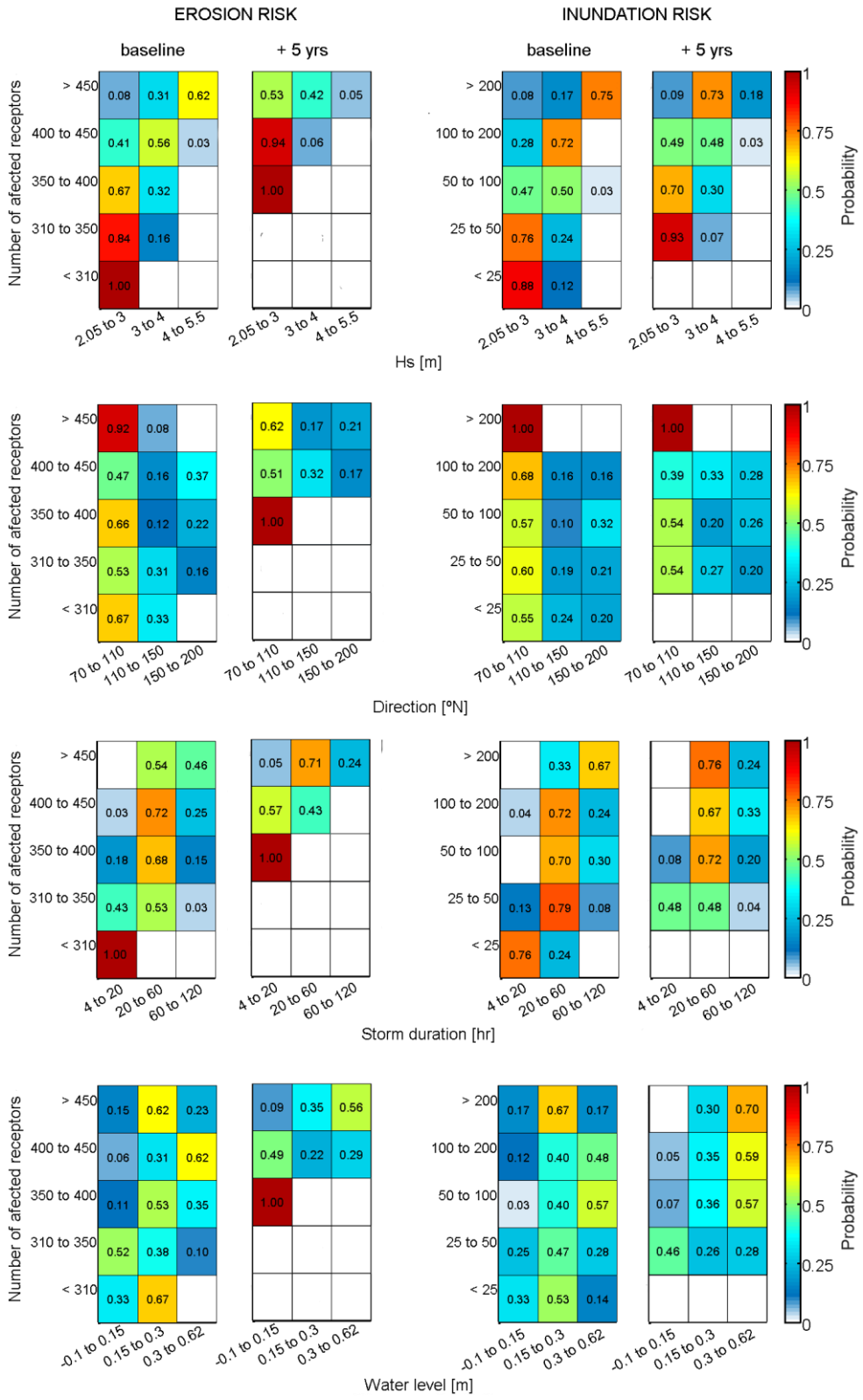

Figure 7.7. Storm characteristics conditioned to different levels of number of affecter receptors for the erosion and inundation hazards. Baseline scenario compared to +5-year time horizon.

BN-A is used to analyse the changes between scenarios in the characteristics of the storms associated with induced risks by conditioning the storm-related variables (Hs, direction, duration and water level)

to the different classes of number of impacted receptors per storm (Figure 7.7). Here the baseline scenario is compared to the future horizons, and the +5-year scenario.

Results show that under baseline morphology, storm characteristics associated with the largest number of affected receptors (>450) by erosion start beign significant for Hs ≥ 3 m, eastern incoming direction and durations over 20 hours. Lower Hs and southern incoming storms are associated with lower extensions of affected receptors and the water level does not show a particular correlation with the erosion risks. When analysing the +5-year scenario, important changes on the conditional probabilities are observed. Notably, the minim class of number of affected receptors increases, and no storms are associated with less than 350 affected receptors. Additionally, a 53% of storms causing high extension of impacts will be of Hs < 3m, and a 21% will be of southern direction. Water levels over 0.3 m also show a more important role in the future horizon than they do in the baseline. In other words, as a consequence of the shoreline retreat, forcings with lower Hs or southern incoming direction will be more associated with risks, and the role of high water levels will be more important.

Regarding the inundation impacts, similar baseline situation and trends to the +5-year horizon are obtained. In this case, the largest extent of affected receptors (>200) is also associated with Hs ≥3 m, eastern direction and durations over 20 hours, but with a stronger association with H s≥ 4 m (75%) and duration over 60 hrs (67%). Thus, storm characteristics associated with the inundation impact are more extreme than for the erosion risk in the baseline. In +5-year scenario, risk associated storm characteristics move to lower Hs and lower durations, and Hs < 3m and southern incoming storms become more frequently responsible of impacts of lower extension (i.e. 50 – 200 receptors). The same effect is observed with the water levels, as storms with high water allow storms of lower intensities to induce inundation risks as the shoreline retreats due to the background erosion.

BN-A is also used to better characterize the conditioned probabilities of storm characteristics with highest-intensity risks, and to assess whether these probabilities are also affected by location (Figure 7.8). In this case, the +10-year and +20-year scenarios are also presented, and the interest is on the fraction of receptors under the highest risk levels for each hazard, i.e. high to extreme for the erosion risk and medium to high inundation risk (risk to life ≥ medium and damages ≥ 60 %). Extreme risk to life and damages over 90% are not present at the study site. Figure 7.8 focuses on the Hs and direction variables as water levels and durations follow for the whole study site a similar trend to that showed in figure 7.7).

For the *erosion risk* under baseline conditions, high-extreme impacts are associated mainly to low Hs and eastern storms, as much of these impacts happen in areas where receptors are closest to the shoreline (i.e. SBN and MSM and MS1). Storms inducing erosion risk at SBM are more frequently characterized by larger Hs and eastern direction with very little affection by southern components. This singularity of the SBM areas is observed to blend out when assessing the midterm scenarios along with a general increase on the association of extreme impacts with lowest Hs. Notably, for the SBM area, this increase

is from 33 % in the baseline to 66 % at the +20-year horizon. Another particular case is that of MS2, where no high-extreme erosion impacts are expected in the baseline scenario. They start appearing in +5-year scenario, characterized as eastern incoming events with medium-high Hs. As the time horizon increases, and as a consequence, the shoreline retreat, storm characteristics associated with significant risks are also observed to expand, ending at the +20-year case with similar directional distributions as in other areas and slightly higher Hs.

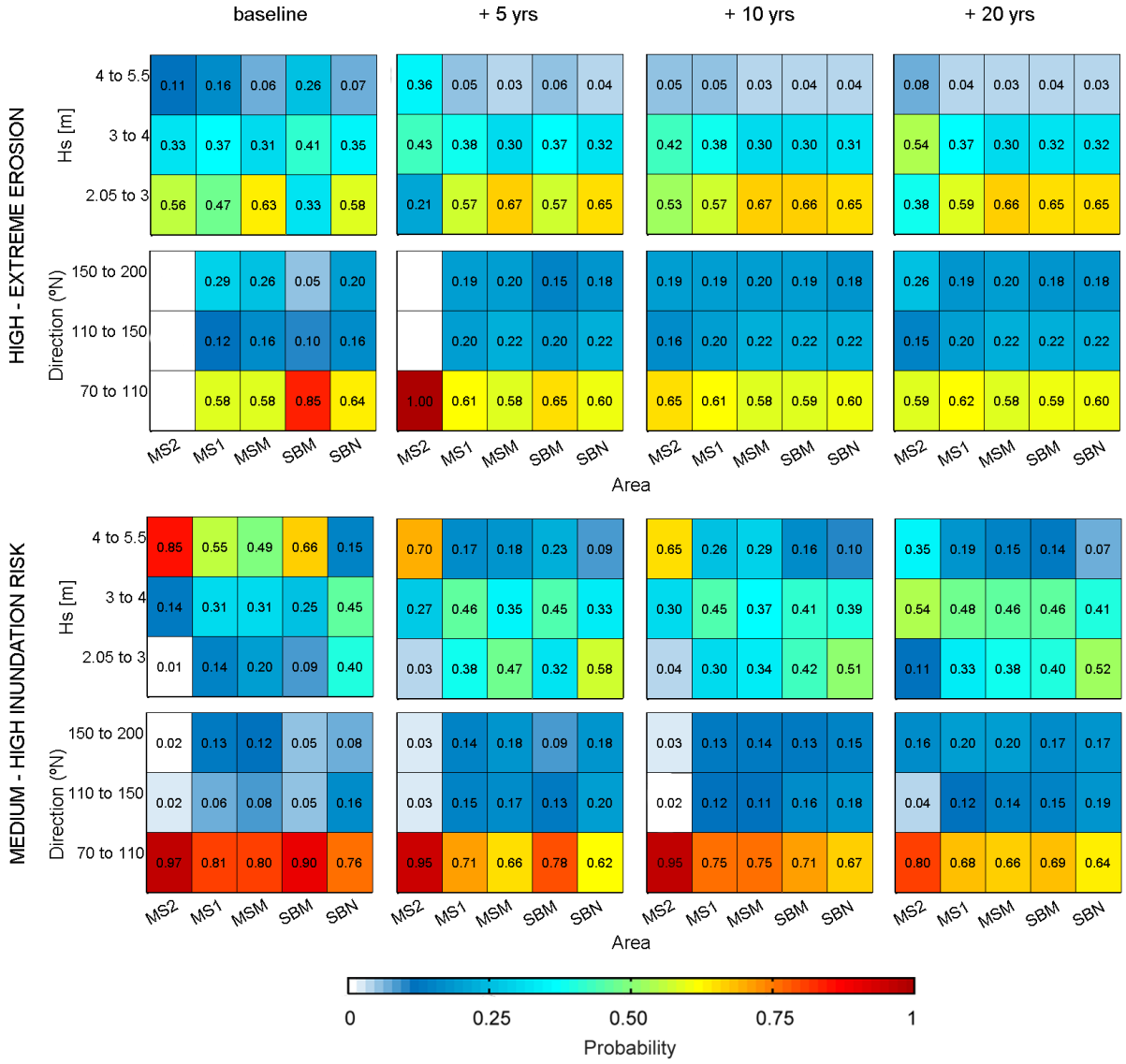

Figure 7.8. Storm characteristics conditioned to the area and associated to highest intensity risk, i.e. erosion risk high to extreme and inundation risk causes by risk to life ≥ medium and damages ≥ 60 %. Extreme risk to life and damages over 90% are not present at the study site

When analysing the *inundation risk*, storm characteristics with Hs ≥ 4 m and eastern direction are more strongly related with high risk in all areas. The only exception is SBN where the promenade is so close to the shoreline that lower Hs can induce inundation damages. As shoreline retreats, a larger variety of forcing characteristics will be associated with risks, and lower Hs and southern incoming directions will

be able to induce medium-high inundation risks. High inundation risks in the baseline configuration are more associated with large Hs in areas to the south, beaches are wider. In future horizons this characteristic homogenizes for MS1, MSM and SBM and remains stronger for MS2, as this area inundates from indirect flow that penetrates the hinterland through MS1.

Spatial risk profile

BN-B is used to assess the spatial distribution of expected impacts accounting for the distance of the receptors to the beach (i.e. limit between beach and hinterland). This allows a detailed spatial characterization to inform decision-making. Baseline results can be compared to those obtained in midterm scenarios to analyse whether significant changes in spatial distributions exist. Here, the results obtained for the baseline and the +20-year scenarios are compared.

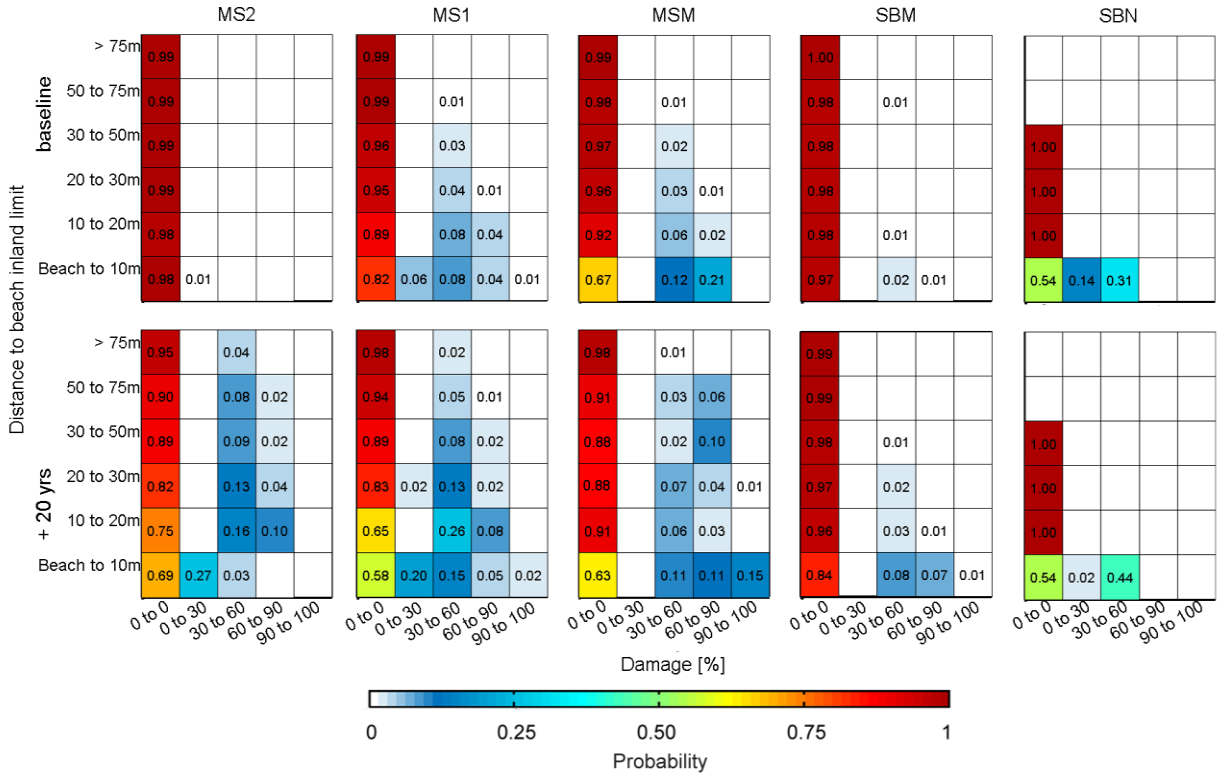

Figure 7.9. Probability distributions of the relative damage by inundation conditioned to the different subareas (see Figure 7.1 for locations) and the distance to the inner limit of the beach. Baseline scenario and +20-year time horizon of background shoreline retreat.

Under the baseline conditions, no structural *damages*>90% (Figure 7.10) nor extreme risk to life (Figure 7.11) are present. *Damages* > 60% are mainly concentrated at MSM at the beach and first 10m of hinterland (21%) followed by MS1 (8%). The probability of larger distances of risk penetration into the

hinterland is also the highest at MSM and MS1. SBN presents an important probability of *damages* > 30% (31%) mainly due to the location of the promenade at the inner beach limit. Regarding *risk to life*, a similar pattern for the baseline case is observed, with MSM showing the largest probability of high risk (20%) at the beach and first 10 meters, but in this case with SBN following with (12%) at the promenade and MS1 only showing a residual 4%. At higher distances to the beach limit, only medium and low risk values are found at MSM and MS1. Observed results are a consequence of the lower topographies with narrower beaches on MSM and MS1 and the promenade located close to the shoreline in SBN. Notably, SBM with narrow beach but higher topography without promenade and MS2 with low topography but wider beaches are the areas where the lowest risks are obtained.

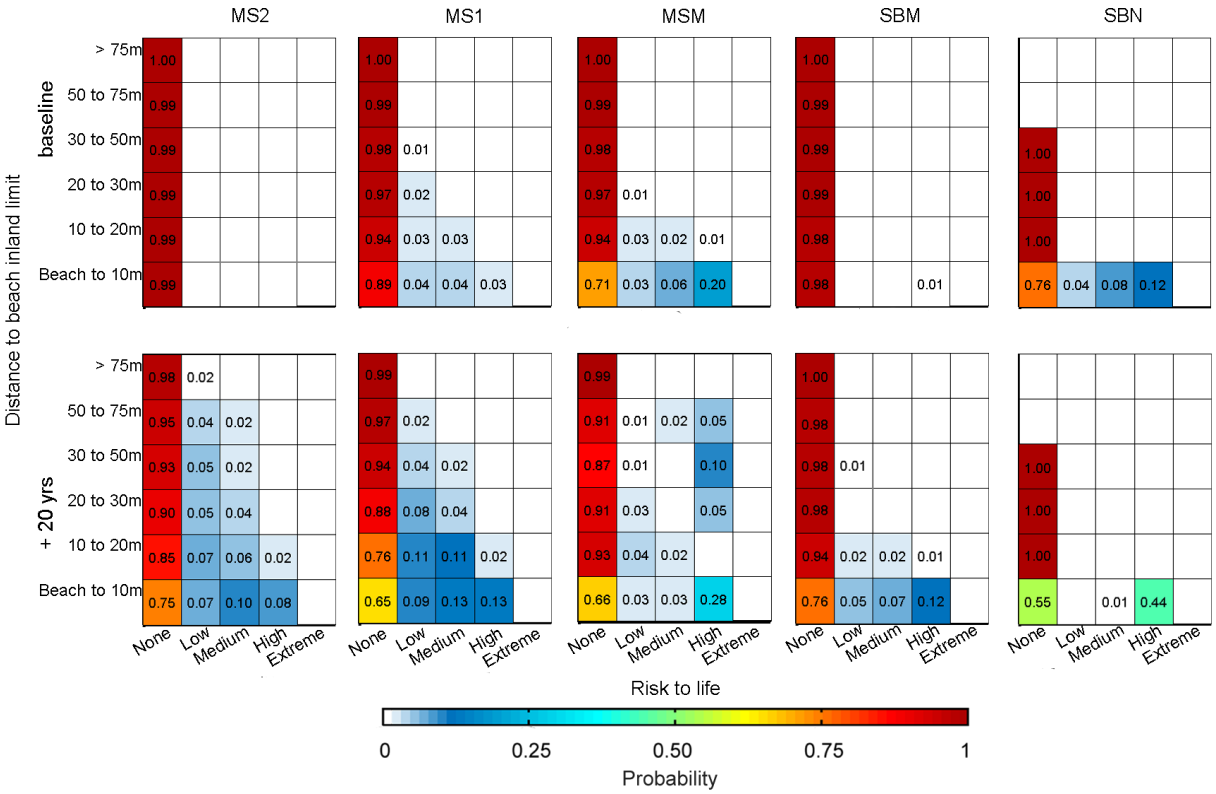

Figure 7.10. Probability distributions of the risk to life by inundation conditioned to the different subareas (see Figure 7.1 for locations) and the distance to the inner limit of the beach. Baseline scenario and +20-year time horizon of background shoreline retreat.

Under the +20-year horizon notable changes are observed. Notably, as a consequences of the beach narrowing due to background erosion, the MS2 area which did not show any significant probability of risk in the baseline, presents a 10% probability of *damages* > 60% at 10 to 20 m from the beach limit and a 4% at 20 to 30m. High *risk to life* is also obtained (8%) at the beach and first 10 meters. Risks at MS2 show similar penetration into the hinterland of that of MSM and MS1. A 12% of high *risk to life* accompanied by a 7% of *damages* >60% also appear at SBM. *Damages* beyond 90% appear at MSM (15%) and MS1 (2%) at the beach and first 10 meters. *Damages* >60% and high risk to life also show a

larger incursion into the hinterland. At SBN high *risk to life* at the promenade increases from 12% to 44%, as the beach completely disappears.

Regarding the *erosion risk* (Figure 7.11), SBN shows the largest probability of extreme impacts at the promenade (54%) in the baseline configuration, increasing to 79% at the +20-year horizon. As the promenade acts as physical boundary for erosion (both background and storm-induced) at SBN, the distribution of risk levels into the hinterland shows a linear pattern. In the baseline scenario, *erosion risks* ≥ high are present at MSM (20%), SBM (9%) and MS1 (7%), in all cases concentrated in the beach and first 10 meters of hinterland. The penetration of lower risk levels into the hinterland is largest in MSM and SBM where there is no physical boundary to limit erosion, whereas in MS1, the existing road limits this effect. These three areas also show an increase in extreme erosion probability and penetration of *erosion risks* for the +20-year scenario. Notably, SBN increases its probability of risk ≥ high to 81% at the beach and first 10 m, with all remaining receptor in that zone being affected by moderate risk. Similarly, MSM presents a 76% of risk ≥ high at the area closest to the shoreline and shows also probability of penetration of high and extreme risks up to the 20 to 50m distances. Finally, MS1 increases from 7% to 29% its probability of high and extreme erosion impacts.

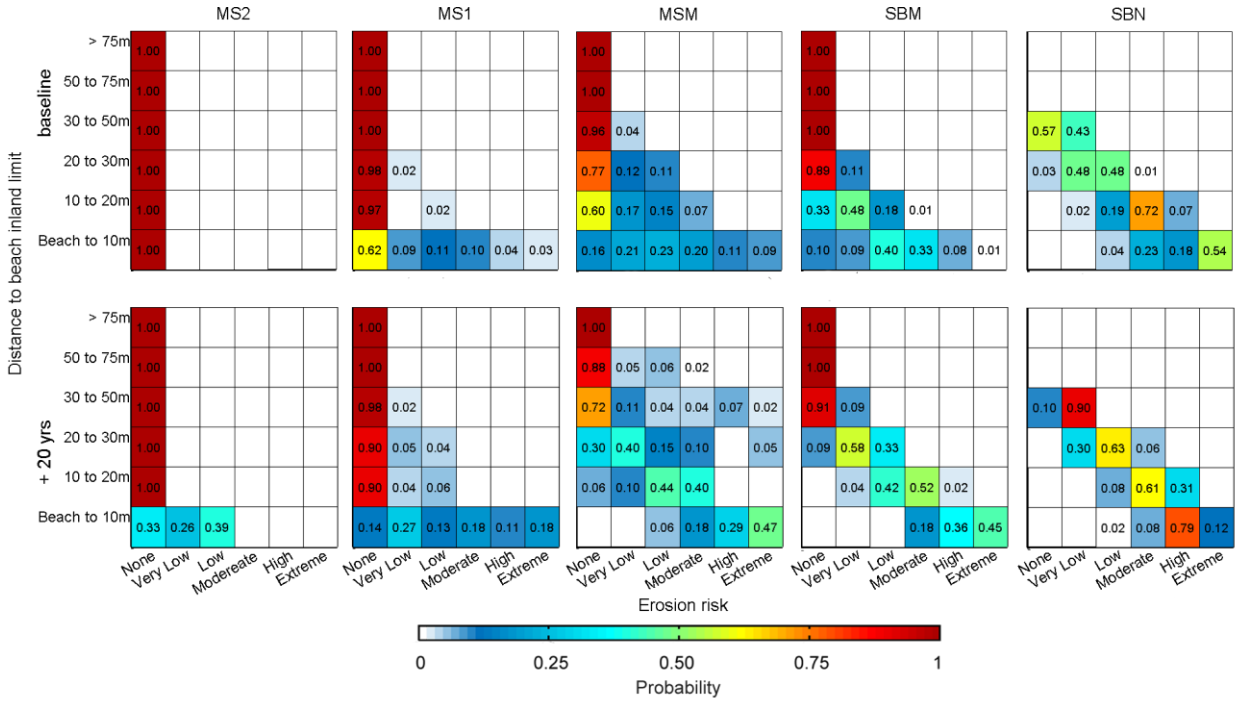

Figure 7.11. Probability distributions of the erosion risk conditioned to the different subareas (see Figure 7.1 for locations) and the distance to the inner limit of the beach. Baseline scenario and +20-year time horizon of background shoreline retreat.

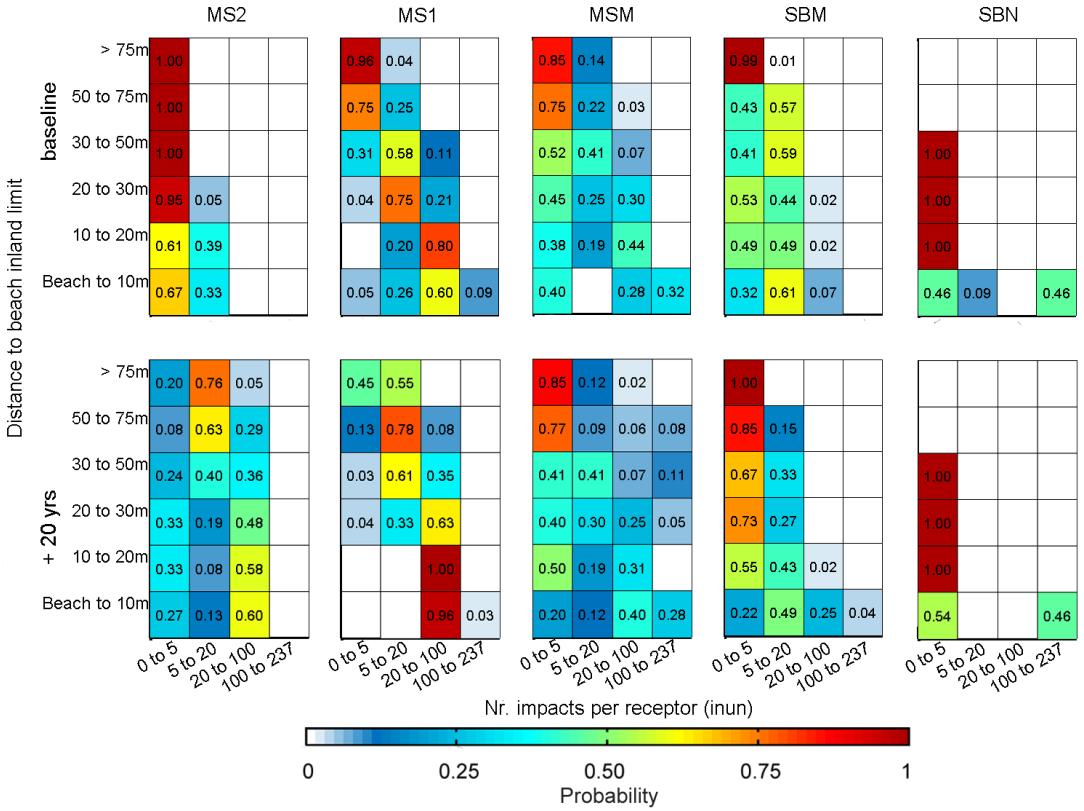

Figure 7.12. Distribution of number of inundation impacts per individual receptor at each area and conditioned to the distance to the beach inner limit. Baseline scenario and +20-year time horizon of background shoreline retreat.

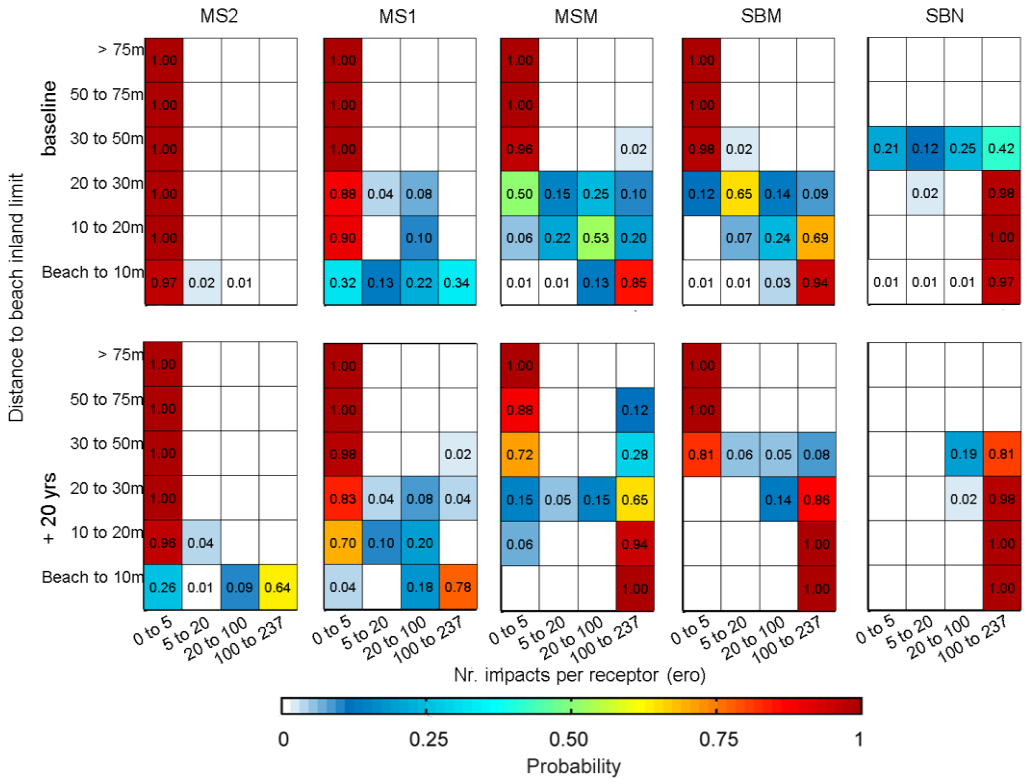

Figure 7.13. Distribution of number of erosion impacts per individual receptor at each area and conditioned to the distance to the beach inner limit. Baseline scenario and +20-year time horizon of background shoreline retreat.

In addition to previously obtained results, an extra variable is assessed to capture the frequency in which individual receptors are impacted at any level of risk. Note that here all impacts different than none are counted per receptor. Figures 7.12 and 7.13 show the results of such an assessment for the inundation and erosion hazards respectively, where the baseline and the +20-year time horizon are again compared.

For the *inundation hazard*, a 46% of the promenade at SBN and 32% of receptors at the beach at MSM are affected by impacts for many of the assessed storms (i.e. > 100 impacts). Although this fraction remains almost unaltered at the +20-year scenario, the proportion of receptors affected by 20 to 100 impacts significantly increases at all areas but SBN. Results also show significant increases of impacts per receptor at inland locations for all areas but SBN (which is physically limited by the promenade).

Regarding the *erosion hazard*, results show how the whole beach area the Tordera Delta study site is under some impact for most of the storm events specially at SBN, SBM and MSM in the baseline scenario and adding also MS1 and MS2 at the +20-year horizon. Thus, the lack of protection function of the coast is evident. Penetration to the hinterland for erosion is less intense than for inundation as it is more directly correlated with the background shoreline retreat and limited by physical hard-structures. Therefore, the largest proportion of impacts per receptor at inland locations happen in MSM and SBM where no physical boundaries exist.

Results obtained in Figures 7.12 and 7.13 help characterizing how the risk increases obtained in Figures 7.9 to 7.11 from the baseline to the +20-year horizon are not only the result of an increase of the extent of the affected receptors by the storms but also the consequence of an important increase in the frequency in which individual receptors are impacted. This is in accordance with previously obtained results where it was evidenced that the number of storms with the capacity to induce impacts in future scenarios is expected to increase.

7.2.4. Discussion and conclusions

Differently from the previous application (Chapter 6), this section presented a fully probabilistic characterization of the source as it uses all available storms in a 60-year long wave time-series hindcast.

The methodology was successful in identifying the storm characteristics with higher probabilities to induce given risk levels for different hazards (inundation and erosion), and how these storm characteristics are expected to change with time under given future scenarios of shoreline retreat due to background erosion. In this sense, the obtained correlation in the baseline scenario of erosion and inundation risks with storm direction, Hs and duration depict the general characteristics of storm-induced hazards in the study area (Mendoza et al. 2011). The lack of correlation with water levels is also agrees in agreement with the already known independency between surges and waves in the area (Mendoza and Jiménez, 2008). In the midterm scenarios, a larger population of storms will be responsible of induced impacts, and higher risks will be associated with lower Hs or southern incoming

events. This effect is associated to the shoreline retreat and the known sensitivity of the area to southern incoming storms (Chapter 5)

The method allows performing the assessment for different subareas within the study site, giving insight on characteristic responses that might be related to different morphological characteristics, beach orientations and the presence of hard structures. In this sense local responses affected by the presence of the promenade at S'Abanell and the revetment in Malgrat North where indentified in the BN.

Table 7.7. Characterization of setbacks for different hazards and risk levels at the Tordera Delta. Baseline scenario and +20-year time horizon using two approaches: (i) total probability, i.e. natural variability of the storm climate with the spatial variability of the impacted receptors and (ii) risk presence, i.e. focusing only on the spatial distribution of receptors under that level.

Area	Setbacks (m)				
	Damage > 30%	**Medium Risk to Life**	**High Risk to life**	**Low Erosion Risk**	**High Erosion Risk**
Baseline - based on total probability					
MS1	10	10	0	10	5
MSM	10	10	10	30	10
SBM	0	0	0	25	8
SBN	10	10	10	50	15
Baseline - based on risk presence					
MS1	98	43	9	8	7
MSM	196	110	19	38	9
SBM	150	71	41	23	9
SBN	10	10	10	44	16
+ 20 years - based on total probability					
MS1	50	20	10	25	10
MSM	55	50	10	75	50
SBM	10	10	10	40	10
SBN	10	10	10	50	20
+ 20 years - based only risk presence					
MS1	137	49	10	24	5
MSM	130	98	71	69	44
SBM	111	109	29	38	10
SBN	10	10	10	47	18

It also permits the definition of probabilistic setbacks at the study site, as it outputs the probabilistic distributions of the different risk levels and impacts per receptor at each subarea and conditioned to different distances to the beach inner limit. As an example, Table 7.7 shows the definition of buffer zones or setbacks for coastal management, both in the baseline scenario and for the future time horizons. The setbacks can be derived for given levels of risk of interest. Since the BN output combines the natural variability of the storm climate with the spatial variability of the impacted receptors, the setbacks can be defined from these (total probability) or by assuming that the presence of a given risk level must be completely tackled, focusing then only on the spatial distribution of receptors under that level. As it can

be observed in Figures 7.12 and 7.13 there are impacts to some receptors at a greater inland distance to that shown by probabilistic distributions in Figures 7.9 to 7.11. Thus, the second approach will give more conservative buffers. Table 7.7 shows buffer distances derived with both perspectives. Setbacks obtained accounting for total probabilities can be used as proposal for managed retreats, as they reflect also the areas with a high number of impacts per receptor, while the setbacks defined by presence of a given risk level can be used to inform self-preparedness against risk, as it highlights zones were the existence of risk is possible but highly infrequent. It must be noted that al scenarios have been simulated without any assumption on receptor re-allocation, and therefore, hard limits to erosion remain homogeneous across scenarios. Therefore, the presented distances in table 7.7 must be interpreted as the evolution of the currenet setbacks at diferent horizons in a business-as-unsual framework.

The approach is based on the response (see e.g. Chapter 2) as it produces probabilities on how the hazards (erosion and inundation) affect the receptors in each of the storm events derived from a long dataset of 60 years. It does not allow to extrapolate to storm conditions different than the ones registered in such dataset. However, this allows simulating all the storm events with their real shapes (time evolutions) without introducing in the assessment the large uncertainty in hazard estimation associated with the use of triangular synthetic storms commonly used to define the time evolution of a statistically extrapolated storm event (see e.g. Chapter 3).

The XBeach model setup has been calibrated with an event representative for extreme conditions at the study site (see Chapter 5) as it was the only storm in which detailed pre- and post-event morphologies where available. In order to improve model performance in such a statistical approach as presented here, model calibration would need to be preferably performed over a set of storm events covering a wider range of storm conditions at the study site (see Callaghan et. al 2013). Additionally, model uncertainty can be introduced in the analysis by using results from different models or model setups to train the BN. Uncertainty on the characterization of risk levels from hazard results can be similarly introduced by using multiple damage curves or hazard-impact relations from different sources and applicable to the study site conditions. The data assimilation capacity of the BN is useful to perform this exercise of model assembling to explicitly include uncertainties

Future scenarios based on shoreline retreat due to background erosion where assessed by assuming that measured rates in Jiménez and Valdemoro (2019) for the last 25 years are completely representative for the following 20 years, and by assuming that existing hard elements in the baseline morphology remain unaltered with time. This could be complemented by using midterm morphological simulations under different hypothesis of presence of structures.

The BN capacity to characterize risk, and its spatial distribution, conditioned to source conditions (storm characteristics) can be exploited as a preliminary early warning system (EWS) similarly to Ferreira et al. (2019). Additionally, the measurements needed to properly validate the EWS during its operational

phase can be included in the BN training, progressively switching from simulation results to measurements, and improving its performance with time.

The BN methodology is flexible and can be furtherly complemented with the inclusion of model uncertainties and measurements to extend the data training, improving the results while testing at the same time its predictive capacity.

7.3. A BN-model to characterize and predict storm-induced retreat at local scale

7.3.1. Introduction

The estimation of storm induced coastal erosion and its association with probabilities of occurrence or return periods its of key importance for coastal managers. It is one of the main components to be assessed when designing coastal plans, along with the chronic coastline retreat due to e.g. sea level rise or gradients in the longshore sediment transport (see e.g. ICZM, UNEP/MAP/PAP, 2008). Different methods exist in literature to estimate this short-term component, of varying complexity regarding the statistical treatment of the available data or the type of model used to estimate coastal response to given storm forcing.

Regarding the statistical or empirical treatment of the data, the simplest option is to use a reference extreme event to calculate its induced coastal response assuming it is representative for management purposes. This reference event can be either an historical extreme episode (e.g. Xynthia in Bertin et al., 2014; hurricane Sandy in Van Verseveld et al., 2015) or the result of statistical extreme value analysis performed on the forcing component (i.e. the event approach in Chapter 2, applied e.g. at the Emilia Romagna coast in Armaroli and Duo, 2018; hurricane levels in Stockdon et al., 2007). This approach is simple but departs from physical reality since leaves out processes that effect beach erosion estimation (e.g. the importance of storm duration, direction and storm sequencing). An alternative to overcome this issue is to perform the response approach, i.e. statistical assessment on the hazard variable (e.g. beach retreat) after calculating the storm-induced coastal response. This uses measured, hindcasted or even simulated long records of storm events (see e.g. Callaghan et al. 2008, Li et al. 2014). With this statistical approach, the natural variability of the storm characteristics is preserved and thus, its influence to the processes that need to be taken into account.

Since long records of storm induced beach retreat are not usually available, this must be estimated from data on the forcing by means of models. The simplest option is to use structural functions (i.e. parametric models, e.g. Kriebel and Dean, 1993; Mendoza and Jiménez, 2008; Yates et al., 2009 and 2011) which allow the estimation of the coastal response given some storm-related parameters and beach characteristics. This approach often implies the calibration of the function to specific cite characteristics, and even when properly calibrated, these models often stop short of accounting for some processes such as alongshore transport gradients due to strong alongshore variability or erosion effects due to beach-structure interactions (e.g. flanking). Process-based numerical models are an alternative to overcome this limitation, and the number of processes that can included in the coastal response assessment will depend on the model used and the way they schematize the coast. As an example, 1-D models (e.g. SBEACH Larson and Kraus 1989 or XBEACH-1D Roelvink et al. 2009) can be used to better include the effects of cross-shore features such as bars and 2DH or 3D models (e.g. XBEACH-2DH Roelvink

et al. 2009) can be calibrated to estimate processes which depend on alongshore variability and beach-structure interactions.

Therefore, the number of choices to solve the problem is abundant and the choice of model to estimate storm-induced erosion is usually conditioned to the statistical treatment of the assessment due to computational effort limitations. As an example, time consuming 2DH and 3D models are difficult to use in assessments that require a large number of simulations, such as the ones needed to assess long records (~1000 year) of statistically derived storm characteristics (e.g. Callaghan et al 2008). Thus, such robust and complex statistical approaches are more feasibly applied in combination with beach response estimations based on parametric models (Callaghan et al., 2008; Ranashingue et al., 2012; Li et al., 2014). In the context of complex study cases, such as curvilinear coastal configurations with alongshore morphologic variability and presence of structures, the capacity of 2DH-3D models to simulate all involved processes is needed. Bayesian Networks (BNs) can be used to learn variable dependencies from such simulations aiming to characterize the coastal response and predict maximum retreats as surrogate to simple parametric models. BNs can be designed to model storm induced coastal erosion by learning from different data sources (e.g. simulations and/or observations). The data training fills the conditional probability tables that are defined from the chosen variables and dependency links of the network. As an example, some applications to assess storm-induced coastal response, mainly on straight natural coasts, can be found in Hapke and Plant (2010), Poelhekke et al., (2015), Plant (2016) or Beuzen et al (2018b).

In this work, a BN designed to characterize the coastal response in terms of maximum beach retreat is presented. The network is tested as surrogate to storm-induced erosion parametric models used to quickly estimate maximum retreats. The aim is to use the descriptive capacity of the BN to characterize conditional dependencies between system variables, and assess the influence of multiple-peak storms, wave direction and beach-structure interactions to the storm-induced retreat. Later, the potential of the BN to perform as surrogate of parametric functions in environments where main processes involved deeply depart from simple cross-shore sediment transport will be analysed. The BN is used to characterize and predict the system response of the Tordera Delta, which has a configuration in agreement with the context formerly presented, i.e., different coastal orientations with strong alongshore morphological variability combined with the presence of a promenade, a road and an embankment close enough to the shoreline to interact with the storm dynamics. Multi-peak events are relatively abundant in NW Mediterranean conditions (Trigo et al. 2002). The chosen study site is a well-known coastal hotspot for both ephemeral and long term coastal erosion (e.g. Chapters 4 and 5). The BN is fed with results from a long dataset (60 years, 179 storms events; 237 storm peaks) of XBeach-2DH simulations.

7.3.2. Methodology

Characterization of the beach response

The area has been divided in 10 different beach sectors (Figure 7.1) in the alongshore direction, in order to capture the spatial variability of the storm induced coastal response. Due to its morphology and configuration, the Tordera Delta presents differentiated responses alongshore, which are at the same time sensitive to the incoming storm direction and affected by the presence of existing structures (Chapters 4 and 5). Areas 1 to 5 (Figure 7.1) are far from existing structures and oriented to the south, while areas 6 and 7 and 8 start orienting towards SE. In areas 1 to 6 there is a road at the beach inner limit. Between areas 6 and 7 there is a coastal embankment inducing flanking effects. Areas 9 and 10 are characterized by an ESE orientation with area 10 presenting a promenade at the inner beach limit with a narrow beach in front.

The storm-induced maximum beach retreat is assessed at the end of each storm peak and at each location (Figure 7.14). This is calculated as the maximum horizontal displacement outputted by the model within the location boundaries at any height of the sub-aerial beach (Figure 7.14). In multi-peak storms, the values of the maximum retreat are derived from the simulations after each individual peak, allowing the analysis of the cumulative effect over the coast.

In order to associate return periods to retreat values at each location, the empirical CDFs at each area are calculated by means of eq.7.3 and the obtained probabilities are transformed to return periods using eq.7.4. For each location, the maximum retreats induced by each of the 179 events are sorted being x_1 lowest and x_n the highest.

$$F_X = P(X \leq x) = \frac{1}{N}\sum_{n=1}^{N} I(x_n \leq x) \tag{7.3}$$

$$T_R = 1 - \frac{1}{\lambda F_X} \tag{7.4}$$

Fx is the empirical CDF and I(·) is a function that evaluates 1 if the condition in the parenthesis is satisfied and 0 otherwise. The parameter λ stands for the annual event density which is nearly 3 events/year in the present study. This corresponds to an empirical application of the response approach (Chapter 2) as computed probabilities are based on the target hazard variable.

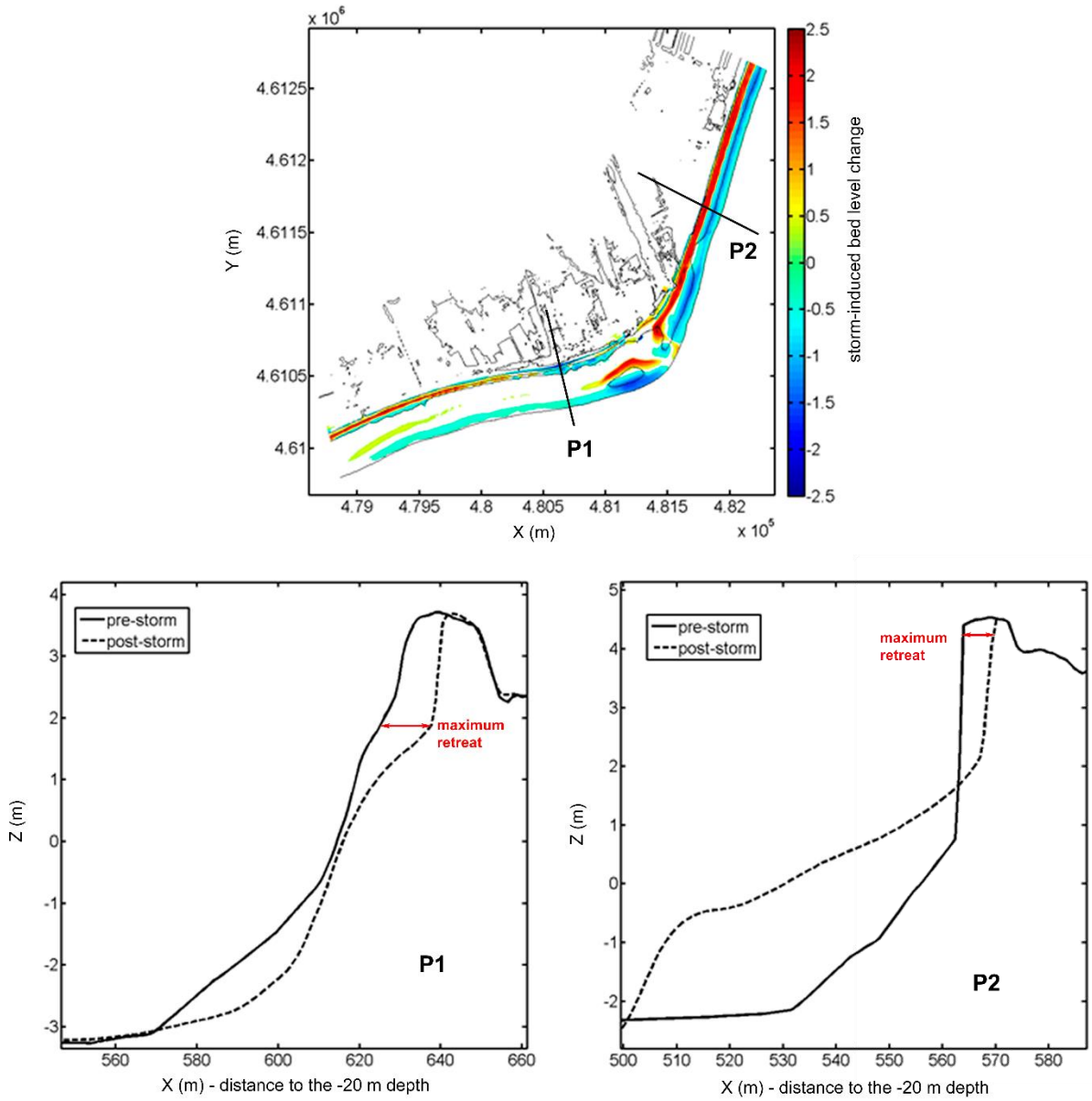

Figure 7.14. Definition of maximum beach retreats. P1 shows maxim retreat for the example event in area 6. P2 shows maximum retreat for the example event in area 10.

The Bayesian Network

The BN-model developed to assess the storm-induced beach retreat conditioned to the storm characteristics at the Tordera Delta is shown in Figure 7.15.

The variables included in the BN were chosen based on common dependencies observed in existing parametric models (e.g. Hs at the peak of the event, event duration, event energy) extended to properly describe the incidence of storm direction (directly included as a variable) and storms with multiple peaks (e.g. previous energy and peak duration). All these are linked to the maximum retreat and return periods which are also dependent on the assessment area. A detailed description of the variables is given as follows, taking as reference to the storm definition shown in Figure 7.2

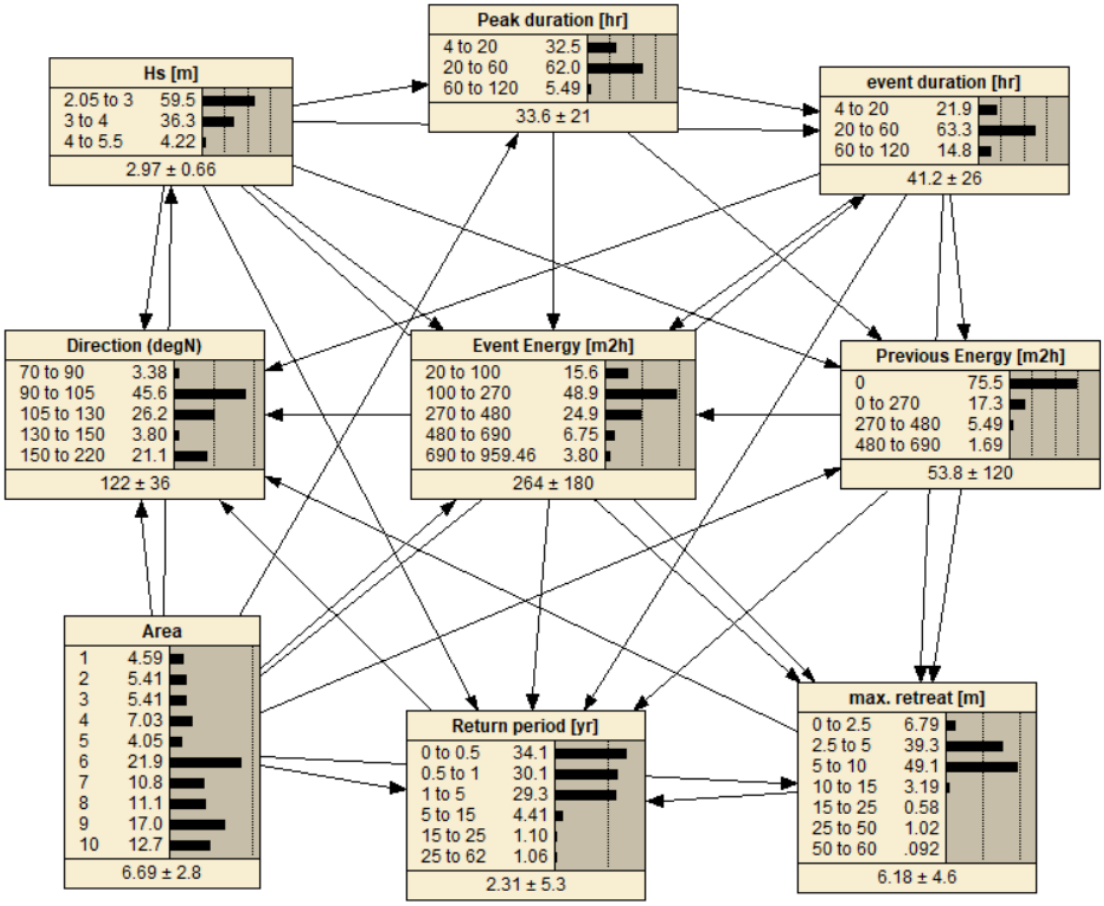

Figure 7.15. Bayesian Network used in the present study with prior (unconstrained) probabilities of the whole dataset

Hs (m): Maximum significant wave height reached during the storm event until the current peak. E.g. in Figure 7.2 two peaks are assessed, and Hs after peak 1 is 3.4m and Hs after peak 2 is 5.4m.

Direction (ºN): mean incoming direction during the storm (single peak events) or during the currently assessed storm peak (storm clusters).

Peak duration (h): duration of the currently assessed peak. E.g. in Figure 7.2. peak duration of peak 1 is d1 and of peak 2 is d2.

Event duration (h): duration of the storm, i.e. cumulative peak duration until the end of the currently assessed peak. In Figure 7.2 event duration is d1 for peak 1 and d1 + d2 for peak 2.

Previous energy (m^2h): Storm energy calculated as the integration of $Hs^2 \cdot dt$ of the event time series prior to the currently assessed storm peak. Thus, single peak storms have always previous energy of 0 m^2h. In Figure 7.2, peak 1 has previous energy of 0 m^2h while peak 2 has previous energy of $Hs^2 \cdot dt$ integrated over d1.

Event energy (m^2h): Storm energy calculated as the integration of $Hs^2 \cdot dt$ during the event. In Figure 7.2, peak 1 has event energy of $Hs^2 \cdot dt$ integrated over d1 while peak 2 has event energy of $Hs^2 \cdot dt$ integrated over d1+d2

Area: Identifies the location of the simulated maximum beach retreats. It indirectly captures the effects of local structures.

Max. retreat (m): Maximum retreat assessed at each location and after each storm peak as described in former sections.

Return period (yr): Return period (TR) associated to the magnitude of the maximum retreat at the specific location calculated empirically as described in former section.

Similar to section 7.2, this case fits the use of manual discratization (Beuzen et al., 2018a), and thus, this was the discretization method used here (Figure 7.15).

Testing the predictive skill of the Bayesian Network

When using the BN-model to predict maximum beach retreats, the predictions given as probabilities of the value falling within each of the variable bins (Figure 7.15). In order to compare with individual values from the dataset (simulations with XBeach for each peak and location), the mean and standard deviation of the BN prediction must be calculated. Then, the skill of the model is calculated by means of eq.7.5, where msr is the mean-square of residuals of the linear regression between the Bayesian-mean value and the data, and msd is the mean-square of the data.

$$Skill = 1 - \frac{mrs}{msd} \tag{7.5}$$

The standard deviation of the prediction can be used as a weight such that predictions that are uncertain (high standard deviation) weight less than confident outputs (e.g, Plant et al., 2016). Thus, a wrong prediction but with large standard deviation will be considered more skilful than a confident and wrong answer, as in the first case the BN correctly outputs a large uncertainty on its output.

In order to test the BN performance outside the training dataset, the k-fold cross-validation approach developed by Fienen and Plant (2015) is followed. The dataset is divided into k number of folds (subsets) and the BN is trained with all subsets but one. The model performance is tested against the training data (descriptive skill or calibration) and then against the 1 withheld partition (prediction skill or validation). This is done for different values of k (i.e., 2, 3, 5 and 10) to assess the effect of the training dataset length to the model performance. For further detail on the distinction between descriptive and predictive BN applications in coastal engineering the reader is referred to Beuzen et al. 2018b.

7.3.3. Results

Characterization of the coastal response

Results show a clear spatial variability of coastal response in terms of maximum storm-induced beach retreats (Figure 7.16), as expected by the different orientation of the areas with respect to the storms main incoming directions and the existence of hard structures. The empirical return period distributions calculated at each area compared to the BN output of maximum retreat distributions across the study site are shown in Figure 7.16.

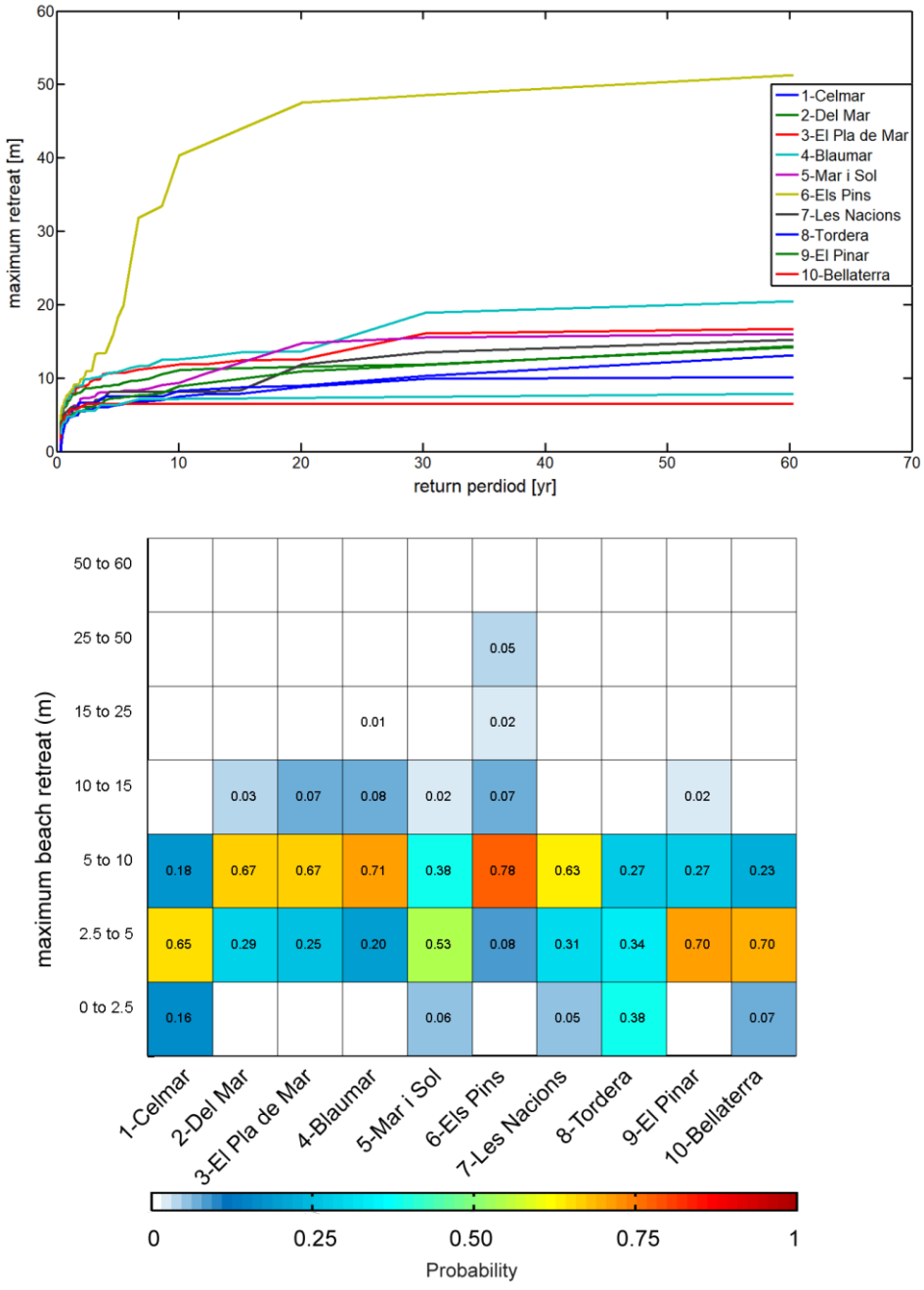

Figure 7.16. TR vs maximum retreat at each location from calculated CDFs (left) and distribution of maximum retreat magnitudes per area outputted by the BN (right)

Going from north to south (10 to 1 in Figure 16) the BellaTerra sector presents a maximum retreat distribution mainly centred to 2.5 to 5 m with no values >10 m. The response of this area is physically limited by the existence of a promenade. Moving closer to the river mouth, El Pinar is no longer affected by that physical limit allowing retreats in the range of 10 to 15 meters. South of the river mouth, the first sector, Tordera, presents a lower retreat as it receives sediment from the northern half of the domain during NE to E incoming events and its orientation starts providing sheltering to those directions. The following three sectors, Les Nacions, Els Pins and Mar i Sol, are affected by the local processes induced by the existing coastal revetment between the first two. Notably, Els Pins presents the highest retreat magnitudes due to the flanking effect of the revetment, which at the same time limits the magnitude of the response at Mai i Sol. Generally, southernmost areas are affected by larger retreats than northern sectors. Moving to the south (i.e. Blaumar, El pla del Mar, Del Mar and Celmar), sectors are more sheltered to NE-E storms and thus, probabilities of experiencing retreats greater than 10 m decrease, disappearing when arriving to Celmar.

Taking into account the sensitivity of the study area to storm direction (Chapters 5 and 6) and the relative abundance of multi-peak storms in NW Mediterranean conditions due the atmorpherical phenomena (Trigo et al. 2002) and the known effect that this may cause in the storm-induced response (Mendoza et al., 2011), the BN can be used to characterize maximum beach retreat conditioned to dominant direction during the storm and peak energy sequencing. For that purpose, Figure 7.17 shows the probability distributions of return periods associated to simulated maximum retreats, Hs, direction and energy sequencing, conditioned to the latter two. Figure 7.18 shows the distributions of the return periods conditioned to the different directions and areas Figure 7.19 shows the same distributions conditioned to different levels of peak energy sequencing. Distributions on Figures 7.18 and 7.19 must be read carefully, as they are relative to the unconstrained distributions of the input variables in Figure 7.15 (given in the titles as percentages). It must be noted that the assessment has been intentionally performed in such a way that an individual storm peak may have different associated return periods at different areas.

Storms with directions from 90ºN to 130ºN are the main responsible for largest retreats which are associated with long return periods (Figure 7.17,a). This is related to the fact that these directions are also associated with highest Hs and largest energy sequencing (Figure 7.17,b). Moreover, 90ºN to 130ºN can cause the largest responses across the entire study site, except for the southern end which corresponds to the most sheltered area to these directions (Figure 7.18). Southern storms (150ºN to 220ºN) have some associated probability to cause the largest responses to the southern end (Figure 7.18). Notably, this directional bin has some associated probability of Hs exceeding 4 m and large energy sequencing (Figure 7.17,b,c). The 70 to 90ºN and 130 to 150ºN storm directions are the least erosive ones (Figure 7.18) and, at the same time, are the two incoming directions with least associated probability of peak sequencing and maximum wave height (Figure 7.17,b,c).

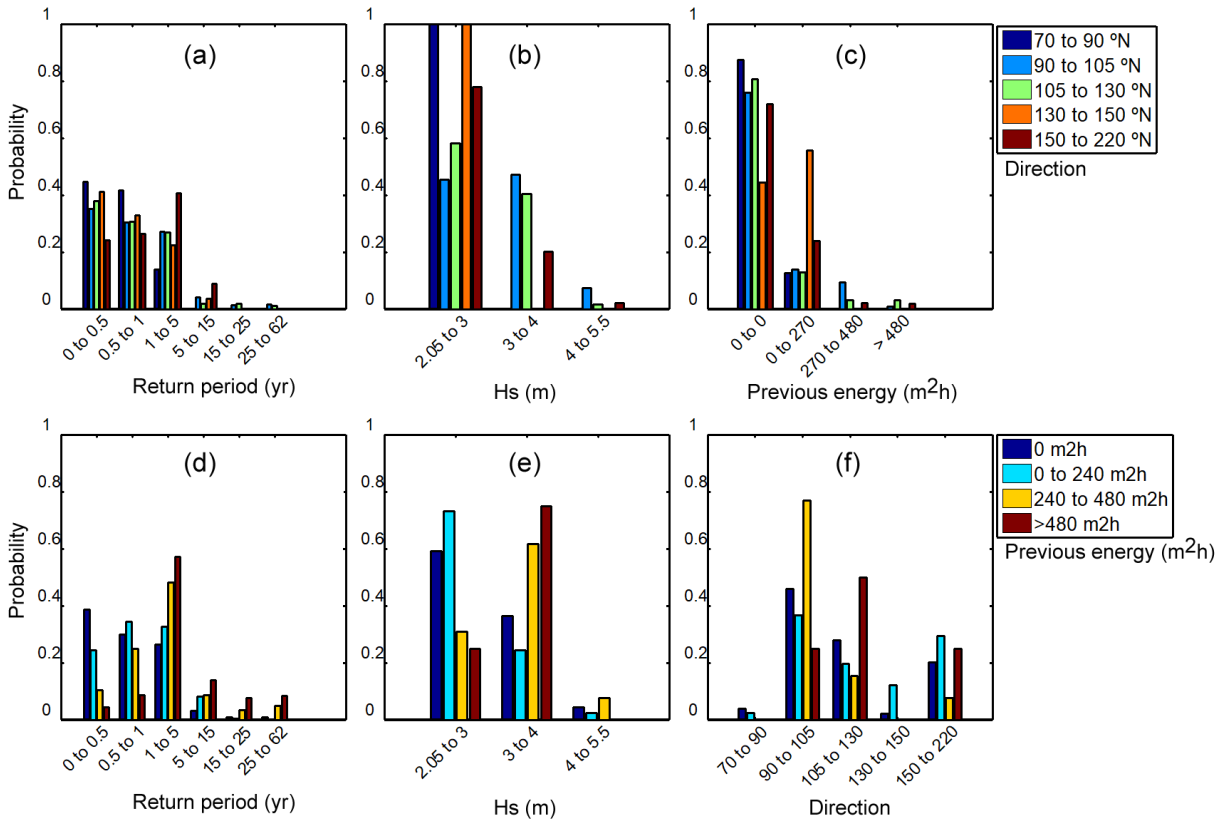

Figure 7.17. Probability distributions of max retreat return periods and Hs conditioned to storm direction (top) and storm cluster previous energy (bottom). Conditioned probabilities between directions and cluster energies are shown at the right.

Regarding the storm peak energy sequencing, longest return periods are also associated with the two largest classes of previous energy (Figure 7.17,d). Peaks following prior large energy (previous energy > 480 m^2h) are associated with Hs lower than 4 meters (Figure 7.17,e). Nevertheless, this type of peaks causes the maximum response at the southern half of the domain (Figure 7.19). Peaks following after previous energy between 240 and 480 m^2h have also deep impact across the whole study site (Figure 7.19). Single-peak events (previous energy = 0 m^2h) can cause also large return periods across the domain with main incidence being north of the river mouth, since single peaks with high Hs are mainly correlated with NE-E direction. They can also significantly affect "El Pins" due to the flanking effect (Figure 7.19). Therefore, this indicated that peak sequencing is a key component to extreme beach response, and permits storms with lower Hs to be associated with longer return periods. In addition, it is mainly correlated with only some directional bins (Figure 7.17,c,f). These are the same directional bins presenting greater impacts across the study site and the location of such impacts will highly depend on the specific direction of the storm.

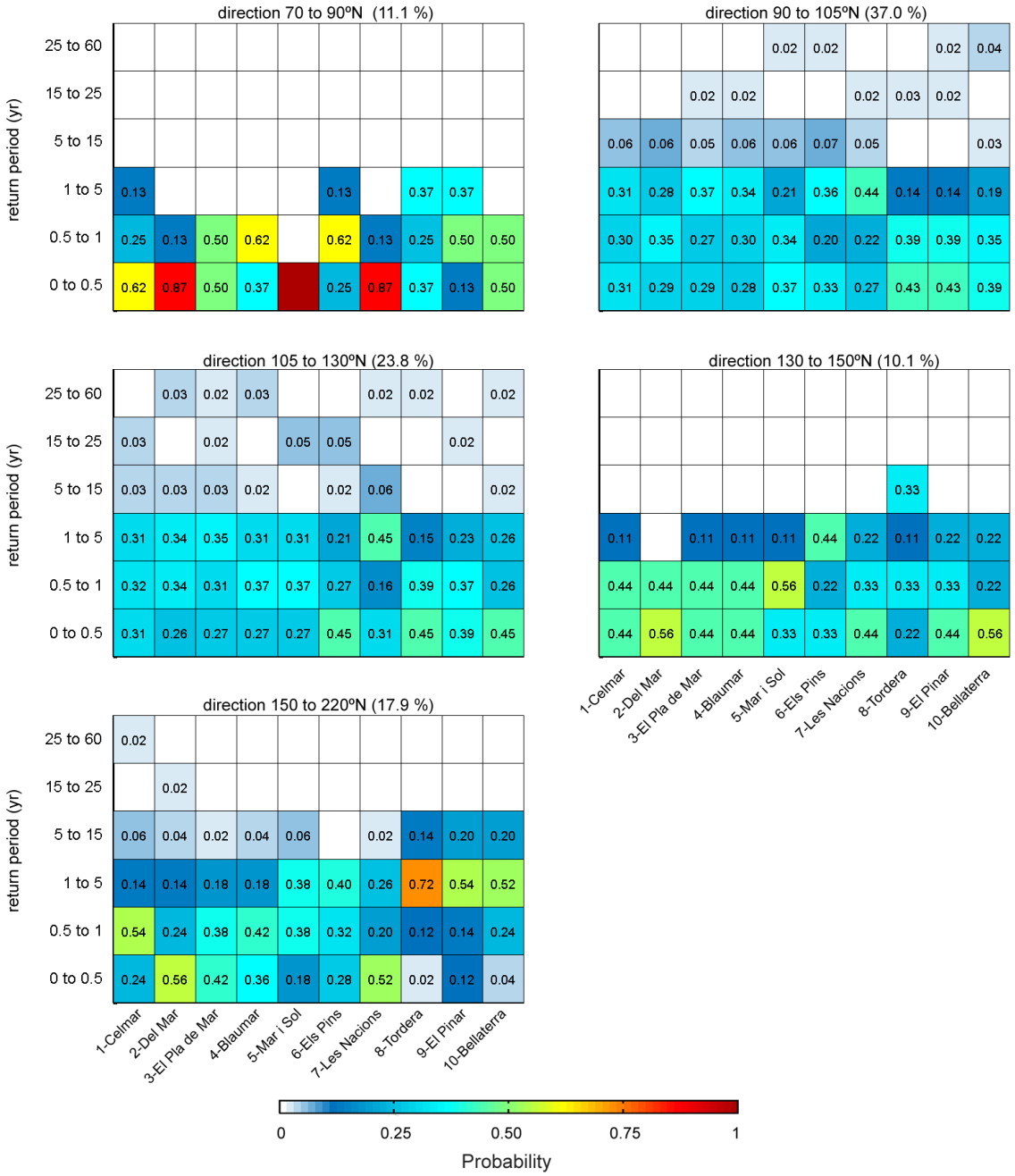

Figure 7.18. Distribution of TRs associated with maximum storm induced retreat across the study site conditioned to storm incoming direction. See Figure 7.1 for locations, they are ordered from south to north. The river mouth is located between 8 and 9. The frequency of each directional class is given in the title as a percentage.

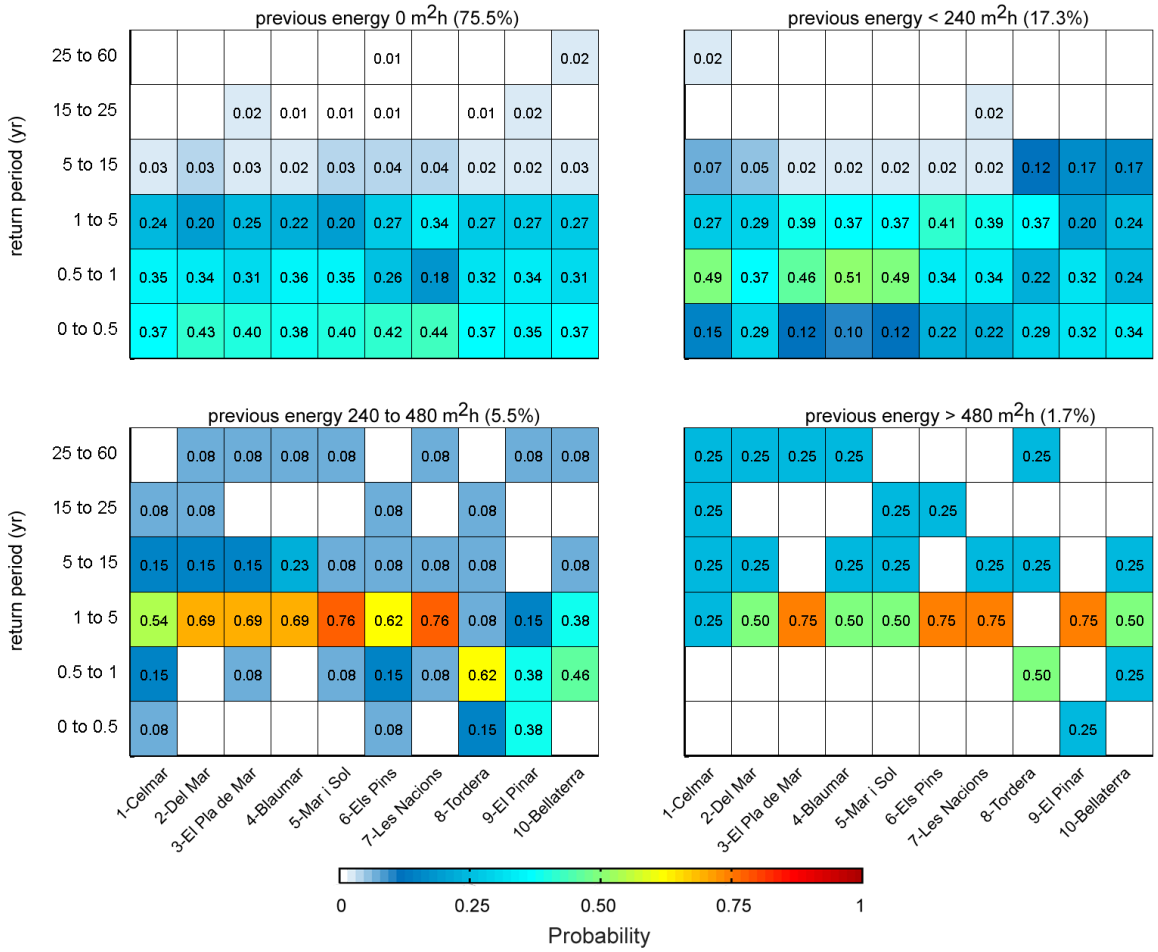

Figure 7.19. Distribution of TRs associated with maximum storm induced retreat across the study site conditioned to storm incoming direction. See Figure 7.1 for locations, they are ordered from south to north. The river mouth is located between 8 and 9. The frequency of each peak sequencing class is given in the title as a percentage.

BN descriptive skill and predictive potential

At the light of the previously shown results, it is evidenced that any model trying to accurately predict maximum storm induced beach retreat at the study site needs to include information on storm directions and storm clustering. Moreover, it will need to be locally calibrated to properly include the effects of beach orientation, morphology and existing hard structures. The presented BN, once fed with all the model simulations, has the ability to perform as such a model. In Figure 7.20, the BN prediction of maximum retreat for all the cases formed by the 273 storm peaks acting at the 10 location (2730 cases) are compared to the XBeach simulations. The comparison is presented both case by case showing the uncertainty of the BN output and also as a scatterplot of the mean BN output versus the XBeach simulations The BN shows weighted and unweighted skills of 0.99 and 0.86 respectively and predicts beach retreats with a mean RSME of 1.31 m.

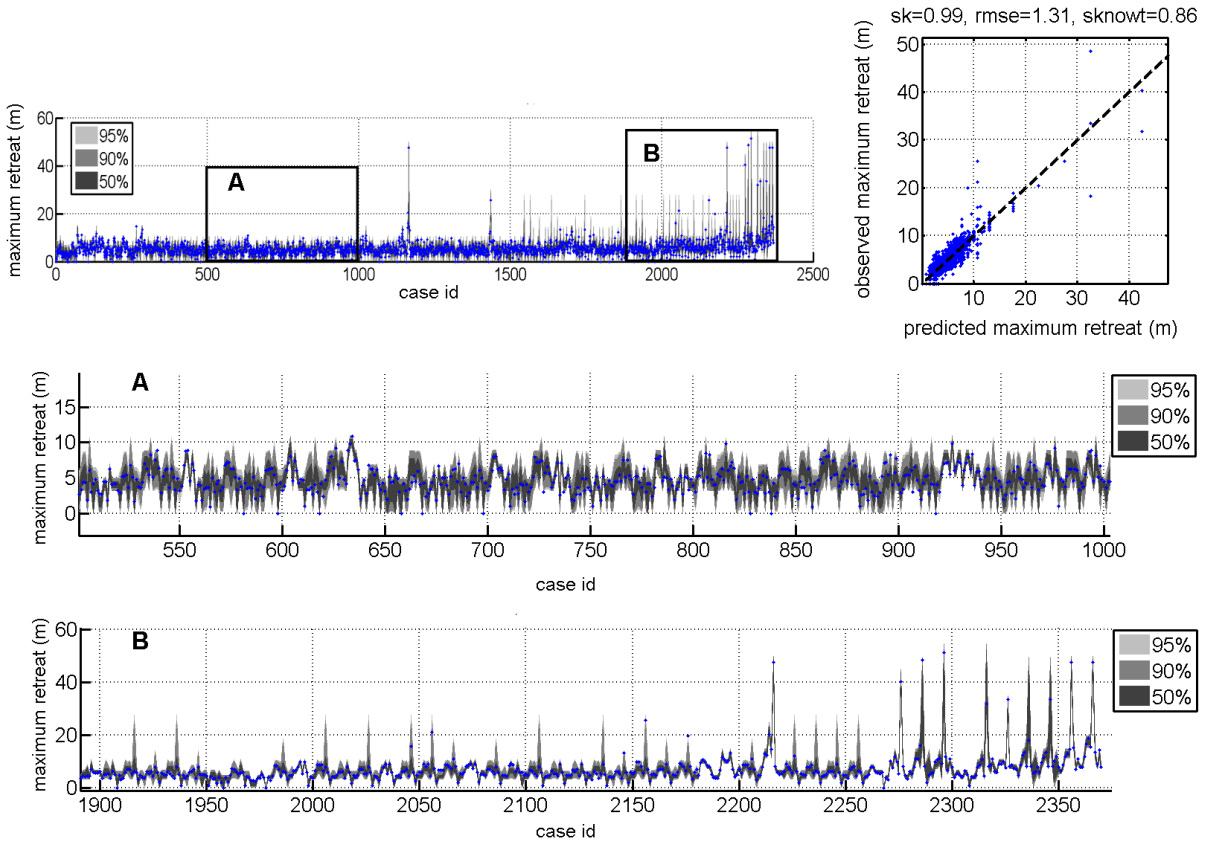

Figure 7.20. BN output versus maximum retreats derived from the XBeach simulations at each location. The case id corresponds to each of the 273 peaks acting on each of the 10 locations (i.e. id = 1,…,2730). A and B are windows to cases with low and high associated retreats respectively and BN output is characterised by the 50%, 90% and 90% confidence ranges. The scatterplot represents the direct comparison of the predicted values (BN output mean) versus the observed (XBeach simulations).

The obtained weighted skill indicates that in those cases where the BN prediction (the mean of the output distribution) has a larger associated error, it also has higher associated uncertainty (standard deviation of the output distribution), correctly indicating those input variable combinations with largest associated variability in terms of beach retreat (e.g. Figure 7.20,A-B). In order to assess the relative importance of input variables on model skill and prediction RMSE, different sets of predictions have been calculated, using specific combinations of input variables (Table 7.8). Results show that Area is the most important variable controlling the BN performance. The magnitude of the hazard (beach retreat) is deeply controlled by the location along the coast due to the varying coastal orientations and morphology, and the local effect of existing structures. Notably, predicting maximum retreat only with the total event energy gives a model skill of 0.22, or using all forcing variables without Area only improves it to 0.30. Alternatively, if the information on storm direction and peak sequencing is not included (i.e. total energy + area + Hs) the skill improves with respect to former cases to 0.67, but still represents a significant drop compared to the base case. Therefore, the combined information on storm directions and peak sequencing has great importance for the prediction of storm-induced retreat at the study site.

Table 7.8. BN skills for different combinations of input variables.

Variables included	weighted skill	unweighted skill	RSME (m)
All forcing variables	0.99	0.86	1.31
All varibles without Area	0.30	0.30	3.03
Event energy	0.22	0.22	3.16
Event energy + Area	0.58	0.56	2.34
Event energy + Area + Hs	0.67	0.66	2.02

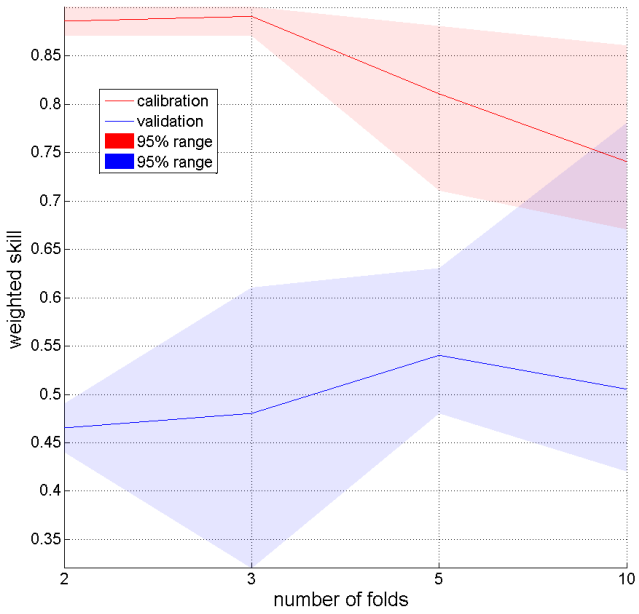

Figure 7.21. BN predictive skill, i.e. when used to predict cases outside the training dataset. Data is divided in k-folds, and one fold withheld from the training process. Calibration skill: descriptive performance of the BN on the training data. Validation skill: performance of the BN on the 1-fold outside the training.

Figure 7.21 shows obtained calibration (descriptive) and validation (predictive) skills for different number of folds. As more data is included in the training (i.e., higher number of folds) the skill of the BN to predict data outside the training improves, although with a large variability on its performance. This is the consequence of the existence of relatively unfrequent cases (i.e. largest events and specific combinations of clustering and directions affecting different areas) that are either be included or left out of the training during the fold classification. It must be noted that a 60-year record is in the limit of what may be considered statistically sufficient to represent a storm wave climate in terms of extreme events. As an example, only 1.7% (i.e. 4 peaks out of 273) correspond to cases with previous energy > 480 m^2h, and these specific cases are responsible of maximum responses in southernmost areas. Therefore, this relatively low predictive skills obtained applying the k-fold analysis are not unexpected, and indicate that the whole dataset is needed to produce reasonable outputs at the study site. The observed drop in

calibration skill for higher number of folds is associated to the fact that the BN cannot explain the increasing amount of observed detail when some key pieces of information are missing from the training dataset (see also Gutierrez et al. 2015).

7.3.4. Discussion and conclusions

The presented BN-model produced useful results to characterize the site's response and its correlation to different event characteristics. The location along the coastline was found to be the most important variable to predict maximum beach retreat. Due to the existing morphological variability and beach structures, it has been found that the beach response correlates locally (i.e. intra-study site sectors) with different forcing characteristics. In this sense, and as a consequence, the relative combined importance of storm direction and storm-peak clustering in a place such as the Tordera Delta has been proved significant.

Obtained results are consistent with previous analysis of energetic content of storms in the Catalan Sea (Mendoza and Jiménez, 2008) as well as their potential hazard intensity (Mendoza et al., 2011) and correctly depict the main hazardous directions and correlations between waves and peak sequencing (Mendoza et al., 2011). Results furtherly show how peak sequencing is correlated with specific directions (90ºN to 130ºN and 150ºN to 220ºN) and can induce retreats associated to long return periods with lower Hs. Moreover, spatial distribution of retreats is sensitive to storm direction, in agreement with results showed in Chapter 5.

The proposed BN-model can perform as maximum retreat predictor once fed with a representative long record of storms (60 years, 179 storms). It can perform as surrogate of simple parametric models at locations where involved processes are complex, with weighted and unweighted skills of 0.99 and 0.86 respectively and an average RSME of 1.31 m. This can be of special interest when methodologies involving large number of storm simulataions (~1000 years, e.g., Callaghan 2008; Ranashingue et al 2012 or Li et al. 2014) are to be applied. However, when the 60-year record is partitioned ro assess predictive skill, some unfrequent conditions are always left out of the training directly affecting the obtained results. Longer records or combined records from different study sties would be needed to perform a robust predictive test. Therefore, the applicability of the method is restricted to study sites with available long records (>50 years) of storms. According to Beuzen et al 2018b, the current BN is more a descriptive than a predictive model, with interesting prediction potential.

The training data are the result of XBeach model simulations, and therefore are affected by the uncertainty associated to the model. The Tordera Xbeach model (see Chapter 5) has been calibrated using a specific extreme storm event. This is a limitation given that when simulations are to be used for statistical assessments, the model set-up should preferably be the result of a calibration process using multiple events covering the storm characteristics of the site (Callaghan et al., 2013). However, even if

affected by errors, obtained XBeach results can be considered representative to describe site response. Moreover, XBeach model accuracy is independent to the BN skill as surrogate of the model. The BN has shown great skill predicting the training data and thus, the reliability of the BN prediction will be directly linked to the reliability of the training dataset. In this context, long records of coastal response measurements would be the ideal option to train the model.

The current BN set-up has local application, as it relies on the Area variable. Specific sector characteristics such as presence of structures, nearshore morphology, beach height and width or grainsize could be included in order to make the tool applicable at larger scales (i.e. generalizing the Area variable by using a number of substitutive descriptive variables, either quantitative or qualitative). However, this would require a much more intense data training and thus longer datasets properly covering all interest conditions. In such a case, manual variable discretization might no longer be the best option and automated supervised methodologies should also be explored (Beuzen et al. 2018a), along with different options in the machine learning field.

CHAPTER 8.

A Bayesian Network methodology for coastal hazard assessments on a regional scale.

Adapted from: Sanuy, M., Jiménez, J.A., Plant, N. n.d. A Bayesian Network model for coastal hazard assessments on a regional scale: the BN-CRAF. Coastal Engineering (in review).

This chapter presents the development of a BN methodology to extend and improve the CRAF phase 1 approach (Chapter 4) with the inclusion of intrasector morphological variability and the explicit consideration of model errors in the hazard assessment. It is applied at two coastal sectors (Cabrera de Mar and Tordera Delta) in the Maresme coast (NW Meditarranean). The work, which combines the use of a BN with Monte-Carlo simulations on hazard estimations, represents the first step towards future works taking advantage of data assimilation and machine learning approaches to coastal risk management problems at regional scale.

8.1. Introduction

The problem to be solved in coastal hotspot identification is complex due to its multidimensionality (both in terms of multiple and interdependent hazards and vulnerabilities) and their multiscale nature (both in space and time). Moreover, hazard estimation comes with a number of associated uncertainties that can become especially large when dealing with future projections (Vousdoukas et al., 2018b).

As already presented in chapters 6 and 7, a widely used approach in risk assessment is the Source-Pathway-Receptor-Consequences (SPRC) model (Sayers et al., 2002; Narayan et al., 2014). However, the implementation of a suite of complex numerical models at a high resolution (e.g., 1~10 m spatially, 1 s ~ 1 h temporally) at the regional scale (e.g., hundreds of km) may not be feasible or time/cost efficient. Furthermore, the probabilistic definition of the hazard component should preferably be performed based on the response (Garrity et al. 2006; Callaghan et al. 2008; Chapter 2) due to the nonlinear and multidimensional dependencies involved in the driving processes (see e.g., Hawkes et al., 2002; Masina et al., 2015; Lin-Ye et al., 2016). This implies the simulation of the erosion and inundation induced by a large set of conditions characterizing the existing storm climate. Additionally, model error is an important source of uncertainty that should be included in the assessment. Simple parametric models which use only bulk information on the source (e.g. peak Hs, Tp, direction and duration) and the pathway (e.g., slope, grain size, or beach height and width) can be a suitable option to generate sufficient hazard estimations at a reduced computational expense (e.g., Stockdon et al., 2006; Mendoza and Jiménez, 2006). The drawback is the simplification of the storm characteristics to a set of parameters and the simplification of the morphology to the bulk definition of a 1-D cross-shore profile. When a long coastal stretch (~1km) is represented by the bulk characteristics of a single profile, the pathway is treated deterministically, as neither spatial (alongshore) nor temporal (seasonal) variabilities are included in the assessment.

All this makes that any robust methodology for hazard assessments needs both to account for the existing variability in source and pathway and to tackle model uncertainties. However, this has to be done in a reasonable cost-effective manner, and it is in this aspect where Bayesian Networks (BNs) have demonstrated their versatility and utility in efficiently combining multiple variables to predict system behaviour (see references in Chapters 1, 6 and 7). Notably, they can be used to represent the SPR scheme

through the dependency relations that physically, or even psychologically, exist between the different steps (e.g., Straub 2005, Jäger et al. 2018, Chapters 6 and 7) and thus, they can be adapted to assess many kinds of natural hazards and impacts on many kinds of receptors.

The general aim of this chapter is to develop a methodology for the assessment of storm-induced erosion and inundation at regional scale with the purpose of hotspot identification and characterization under present conditions and future scenarios. Within this context, the development and implementation of a BN-based hazard assessment methodology is presented. It is based on the CRAF phase 1 methodology (Viavattene et al., 2018), which has been validated and applied across different study sites within the RISC-KIT project (Van Dongeren et al. 2018; Ferreira et al. 2018), and outlined in Chapter 4. The CRAF combines a probabilistic treatment of the source (storms) with a deterministic treatment of the pathway (coastal morphology), without including model error uncertainties. The here presented new methodology is able to deal with the small-scale variability of coastal morphology (20-30 profiles per kilometre) and with model uncertainties by using Monte-Carlo simulations based on known model errors. The method is applied under current conditions and given scenarios defined in terms of SLR and background erosion projections, where Monte-Carlo simulations are used to incorporate their associated variability. The proposed methodology, while maintaining a relatively simple structure, represents an advantage with respect to other existing approaches where the treatment of the source is deterministic or do not properly include hazards statistics (e.g., use of hurricane categories as levels, Stockdon et al., 2007; use of event approach in Chapter 2, e.g., Villatoro et al., 2014; Armaroli and Duo, 2018; use of a homogenous representation of the source Poelhekke et al. 2016). Moreover, by accounting for the spatial variability of the coastal morphology, it also represents an improvement with respect to existing methodologies adopting a deterministic treatment of the pathway (Callaghan, 2008; Bosom and Jimenez, 2011; Ballesteros et al. 2018, Viavattene et al., 2018). Notably, none of the referenced works included model errors in the analysis.

This methodology is applied at two sectors of the Catalan coast (NW Mediterranean), and obtained results are compared to those of the semideterministic CRAF phase 1 (Chapter 4). One sector is a 2 km long fully rigidized coastline composed by a rip-rap revetment protecting a coastal railway. The other one is a 3 km long sandy coastal fringe protecting a low lying deltaic area with campsites in the hinterland. Both locations have been identified as coastal hotspots to storm impacts in Chapter 4)

The structure of the chapter is as follows: (i) the second section describes the data used, (ii) the third section presents the BN- based proposed methodology, (iii) the fourth section shows and example of the application of the method, followed by (iv) the discussion and comparison with CRAF phase 1 and (v) the main conclusions.

8.2. Data

To perform this analysis, data on waves and water levels to characterize the forcing, and on coastal morphology to characterize the pathway, are required. The assessment of coastal inundation and erosion hazards requires a long-term series of wave conditions and water levels that have the appropriate spatial and temporal coverage. This work uses hindcast waves from the Downscaled Ocean Waves dataset (Camus et al., 2013) derived from the Global Ocean Waves (Reguero et al., 2012) and hindcast surges from the Global Ocean Surge dataset (Cid et al. 2014), which were obtained at a node located in front of the Tordera Delta at ~20 m depth and cover the period 1950-2014. Simultaneous mean water levels were available at the same resolution of the GOS dataset.

The coastal morphology has been represented by using LIDAR-derived topography from the Institut Cartogràfic i Geológic de Catalunya. The data were provided as high-resolution digital elevation models (DEMs) with 1m x 1m grid cells and a vertical precision of 2-3 cm (Ruiz et al. 2009). This was complemented with data obtained from a topo-bathymetric survey provided by the Ministry of Agriculture, Fish, Food and Environment. Data up to 1.5 m water depth were obtained by total station topographic surveying and, data down to 50 m water depth were recorded with a dual-frequency echosounder with a nominal accuracy of 7 cm.

The long-term shoreline evolution is obtained from a 25-year shoreline dataset (Jiménez and Valdemoro, 2019) and the SLR projections correspond to the RCP8.5 IPCC (2014).

8.3. The BN-CRAF methodology

8.3.1. The general scheme

As previously introduced, the general methodological scheme follows CRAF phase 1 (Viavattene et al., 2008) which was applied to the Catalan coast in Chapter 4.

In CRAF phase 1 (Figure 8.1A), the source is characterized by identifying all the storms in a long (e.g. 60 years) time series of waves and water levels. The pathway (morphology) is characterized by a single cross-shore profile for each ~1km coastal sector. This sector-characteristic profile can be calculated by simple beach profile averaging, or by choosing the worst-case profile (e.g. lowest dune and narrowest beach). The second option was applied in Chapter 4. Then, parametric models are used to estimate hazard magnitudes (e.g. total water level at the coast for inundation, and shoreline retreat for erosion) for each storm. Obtained hazard values are fitted by an extreme probability distribution, and finally, erosion and inundation magnitudes associated with selected probabilities/return periods are transformed to hazard indicators (see e.g. Ferreira et al., 2017) within a scale ranging from 0 to 5, being 0 no hazard and 5 the most hazardous situation. These indicators combine information of the hazard magnitude with basic information on the relative exposure of the hinterland to each hazard (e.g. beach width for erosion

and, dune/berm height for inundation). The final output is, thus, a single intensity value per sector for each hazard associated with a given return period.

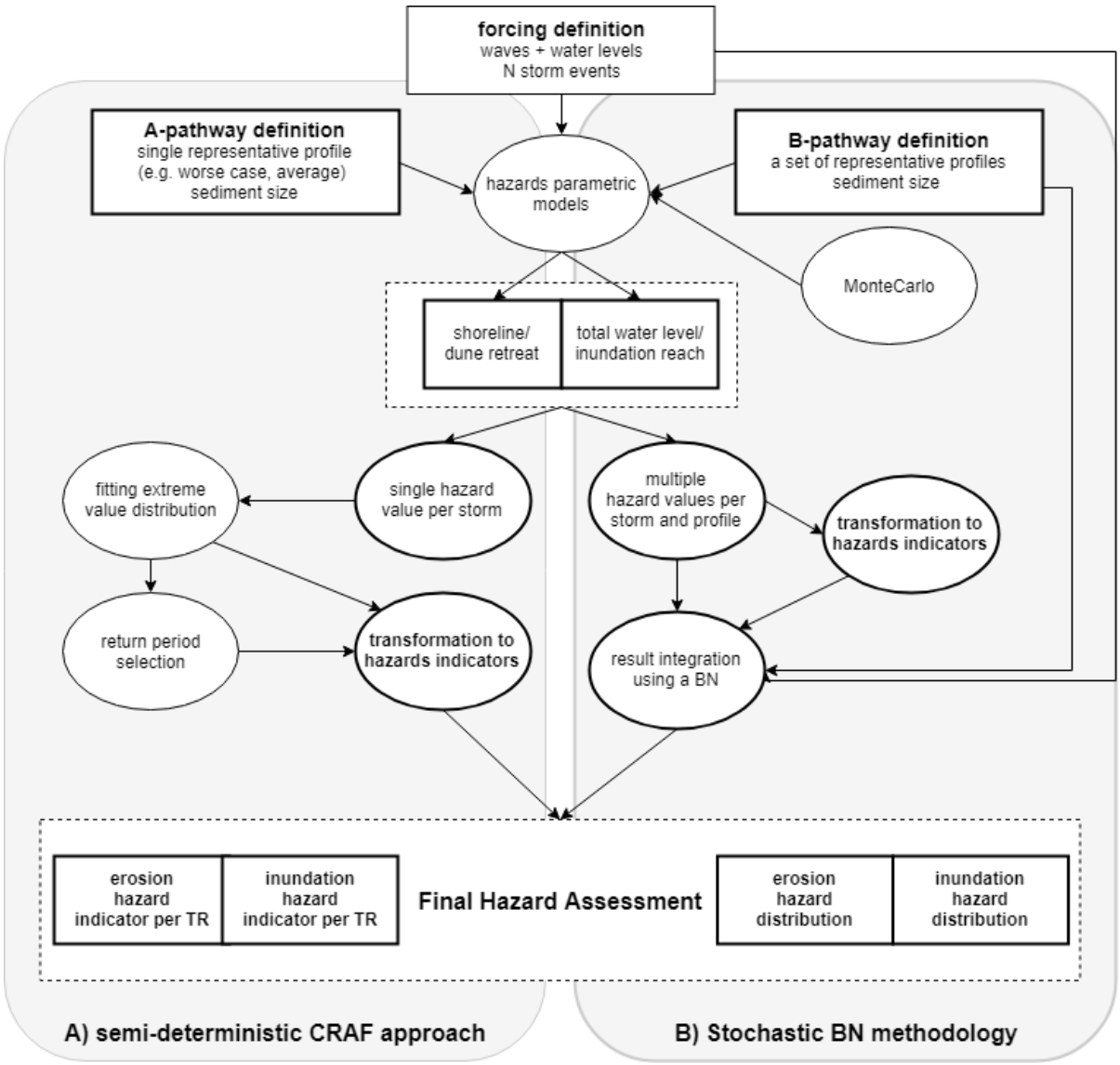

Figure 8.1. Conceptual scheme of the CRAF-phase 1 approach, Chapter 4 (A), compared to the BN-based methodology (B).

In the here presented BN-based methodology (Figure 8.1B), the source is characterized as in CRAF phase 1 (Chapter 4), but the pathway is characterized by using a set of profiles (~10-30, Figure 2) to properly capture the existing morphological variability within each sector. Hazards magnitude is computed by means of parametric models for each storm and profile. To account for the uncertainty associated with model errors, Monte-Carlo simulations (Hastings, 1970) are used. Thus, for each profile and storm, multiple erosion and inundation hazard values are calculated, which are later transformed to hazard indicators using the same scale as in CRAF phase 1. These hazard estimations together their corresponding source (storm characteristics) and pathway (profile characteristics) data are used to train

the BN. The final output are probabilistic distributions of the different erosion and inundation hazard levels at each sector, which consider model uncertainties and preserve the information on conditional dependencies with source and pathway.

In addition to detecting hotspots along the coast, the BN methodology is used to assess hazard values under given scenarios associated with future SLR and background erosion projections, where the Monte-Carlo approach is also applied to simulate multiple conditions per scenario.

8.3.2. Source and pathway characterization

For comparison purposes, the areas to be studied are divided into ~1 km sectors, with the same spatial division as in the CRAF-phase1 application (Chapter 4). Each sector is represented by a number of profiles (Figure 8.2). Profile selection is aimed to capture the existing morphological variability in each sector, in terms of slope, beach height (i.e. dune or upper berm or embankment height), and beach width (Figure 8.3b). The shape of the first part of the hinterland is also taken into account for profile selection. Notably, rigidized coastal sectors such as Cabrera South (CS) and Cabrera North (CN) require a lower number of profiles (16 and 9 respectively) than natural beach sectors with larger variability such as Malgrat North (MN) and S'Abanell (SB) with 20 and 32 profiles respectively. Malgrat South is more homogeneous and was characterized with 15 profiles.

Coastal storms have been identified in the dataset (see location of the node in Figure 8.2) by means of a double threshold P.O.T analysis as in Chapter 2. Figure 8.3a shows scatterplots of the main characteristics of the dataset.

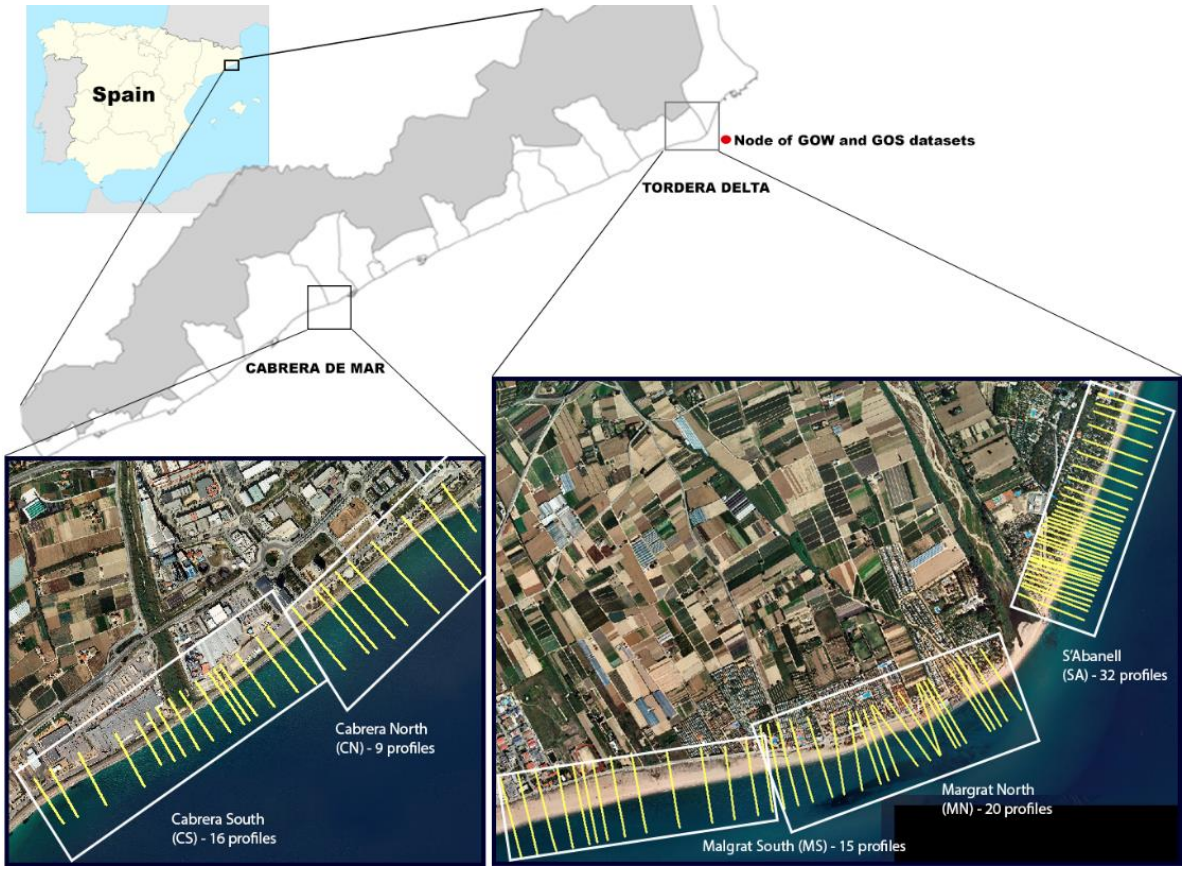

Figure 8.2. Locations of the wave and surge data nodes used in this work. Sector limits and used profiles are indicated. The red dot highlights the location of the numerical node for wave and surge data.

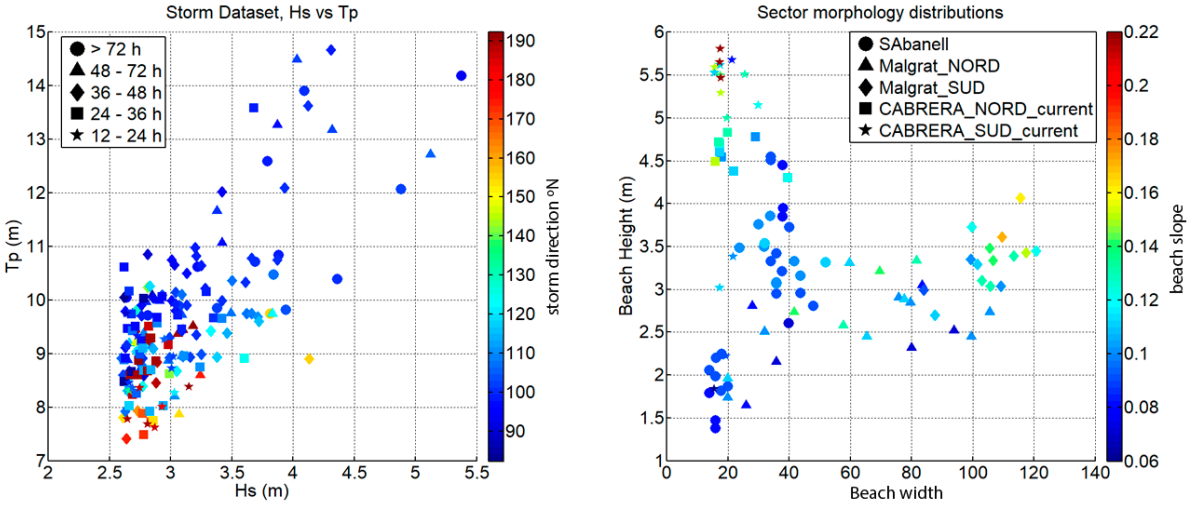

Figure 8.3. Dataset characteristics. Storm bulk parameters (left) Hs vs Tp, colored by storm duration, and markers by storm duration. Main morphological features (right), beach height vs beach width, colored by beach slope and markers by sector.

8.3.3. Hazard indicators

In this work, the inundation hazard is estimated similarly to that of Bosom and Jiménez (2011) and was also similarly applied in Chapater. The inundation potential is calculated using, as proxy, the total water level at the coast (TWL), characterized by the wave-induced run-up and the surge level. The run-up models used are the Stockton et al. 2006 model [eq.8.1] for sectors composed of sandy beaches and the EuroTop model (Pullen et al., 2007) [eq.8.2] for rigidized sectors with protected revetments. These models use significant wave height in deepwaters (Hs) or breaking conditions (Hb), wave length in deepwaters (Lo) and beach slope (tanβ) to estimate the vertical level potentially reached by waves at the coast. The EurOtop model (Pullen et al., 2007) also includes factors accounting for wave directionality (γ_β) and surface friction (γ_f).

$$Ru = 1.1\left(0.35\tan\beta\,(Hs\,Lo)^{1/2} + \frac{\left[Hs\,Lo\,(0.563\tan\beta^2 + 0.004)\right]^{1/2}}{2}\right) * \gamma_\beta\,, \tag{8.1}$$

$$Ru = 1.65 * Hb * \gamma_f * \gamma_\beta * \frac{\tan\beta}{\sqrt{\frac{Hs}{Lo}}}, \tag{8.2}$$

The erosion hazard has been estimated by using the Mendoza and Jimenez (2006) model, which has been widely applied to estimate storm-induced erosion potential (see e.g., Armaroli and Duo, 2018; Silva, 2019). The model is given by the following:

$$\Delta V = 7{,}9 * JA * duration + 3.6\,, \quad with \quad JA = \left|4 - \frac{Hs}{Tp * w_f}\right| * tan\beta\ , \tag{8.3}$$

where ΔV is the eroded volume at the beach face (Figure 8.4), Tp is the wave period at the peak and wf is the sediment fall velocity.

$$\Delta X = \frac{\Delta V}{ZB + d^*}\quad , \tag{8.4}$$

where ΔX is the beach retreat calculated as a function of the eroded volume, the beach heigh (ZB) and the pivot point depth (d*), (Figure 8.4).

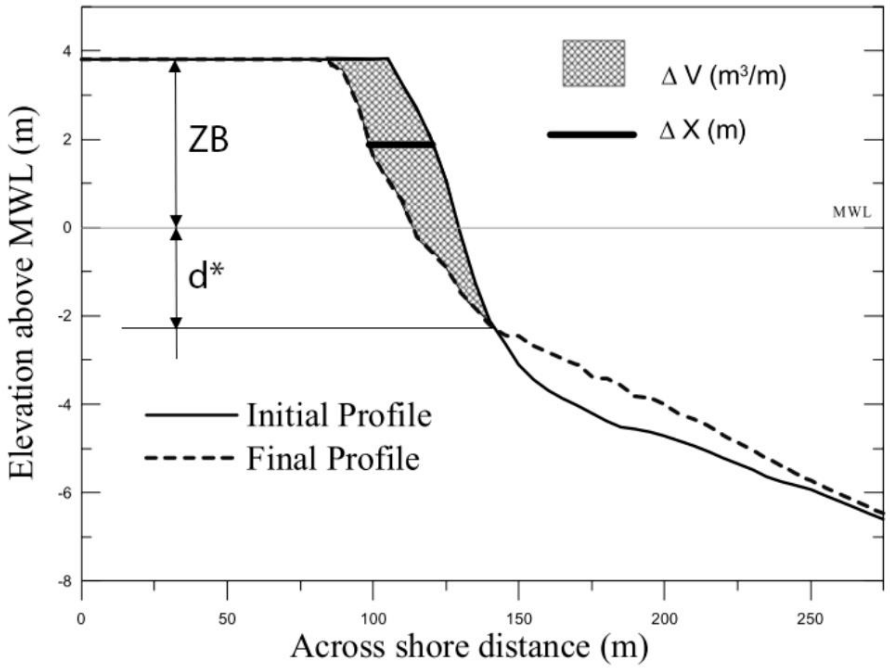

Figure 8.4. Profile erosion schematization used to derive beach retreat from eroded volume adapted from Mendoza and Jiménez, 2006).

Table 8.1. The hazard indicator levels as a function of the beach width (BW) against inundation reach or beach retreat. All units are in meters, and ΔX_{10} stands for average profile retreat associated with TR=10 years for the site, which has a value of 7.5 m.

Hazard indicator level	Inundation	Erosion
0	Reach < 0.5*BW	BW – Retreat >4 ΔX_{10}
1	0.5* BW <Reach< BW	4 ΔX_{10}< BW – Retreat <3 ΔX_{10}
2	0 < Reach – BW < 20	3 ΔX_{10}< BW – Retreat <2 ΔX_{10}
3	20 < Reach – BW < 40	2 ΔX_{10}< BW – Retreat < ΔX_{10}
4	40 < Reach – BW < 60	ΔX_{10}< BW – Retreat <0
5	Reach > BW + 60	BW – Retreat ≤ 0

Finally, hazard estimations are converted into a 0-5 hazard intensity scale, as in Chapter 4 (Table 8.1). For the inundation hazard, the TWL is compared against the profile to obtain the potential reach of the flooding by means of the bathtub approach. This magnitude is then compared with the beach width (BW) to derive the hazard index (Table 8.1). The erosion index, in a different manner, is derived by comparing the resulting postevent BW (i.e., the pre-event BW subtracting the storm-induced retreat) with a reference width. Following Chapter 4, the reference width of the different levels is based on the average beach retreat for the 10-year return period at the study site ΔX10, with a value of 7.5 meters (Table 8.1).

8.3.4. Future scenarios

The assessment of the possible evolution of hazards requires having information on morphology (pathway) and forcing (source) in future conditions. In the present application, this is done by estimating how such elements will vary under a given scenario by a given time horizon. As an example, to assess how hazard will evolve at mid-term scale (from years to few decades), we have considered the current decadal-scale coastline evolution to build the future morphology (beach width) at selected time horizons. When the analysis is extended at the long-term scale (several decades to centuries), we have to consider potential changes in forcing conditions. If storminess is not expected to change significantly (see e.g., Somot et al. (2019) for the Mediterranean basin or Bender et al. (2010) for Atlantic hurricanes), the main variable affecting analysed hazards is the long-term change in sea level. In such a case, this is done by considering the future mean sea level under a given SLR scenario by the selected time horizons. In the case that long-term changes in storminess are expected, storm properties must be modified accordingly.

In this study, mid-term background erosion along the sandy beach sectors has been estimated by analysing shoreline position changes from aerial photographs available at different time frequencies that cover the last 25-30 years. The estimated average retreat for the 3 sandy beach sectors are 1.1 m/y at S'Abanell, 4 m/y at Malgrat North and 1.9 m/y at Malgrat South (Jiménez and Valdemoro, 2019; see Figure 2 for locations). This corresponds to a 1-D version of the mid-term assessment in Chapter 7.

To introduce SLR-induced effects, the IPCC (2014) RCP8.5 scenario was considered in this study, which accounts to 0.30 m and 0.60 m of global mean SLR by the years 2050 and 2100, respectively, with respect to the period 1986-2005.

8.3.5. Monte carlo approach

All hazard models and future projections are affected by errors and uncertainties. The available knowledge on these errors, or reasonable assumptions on the uncertainties, may be included in this hazard assessment. Known model root mean squared error (RMSE), and confidence ranges (Table 8.2) have been included in hazard estimations by means of Monte-Carlo simulations (Hastings, 1970). Other existing uncertainties may also be included following a similar procedure.

Uncertainty in the run-up has been estimated as follows. For the Stockdon (2006) model, we use the RSME of the formula as an estimator of the standard deviation of the variable (Plant et al. 2014). It is assumed that the variable follows a normal distribution with the mean calculated by [eq 1] and a standard deviation equal to the model RSME (0.32 m). For the EurOtop (Pullen et al., 2007) model, the knowledge of the standard deviation of the coefficient in [eq.8.2] (Table 8.2) is included in the assessment along with an estimation of the uncertainty of the actual value of the revetment friction coefficient.

Uncertainty of erosion potential (ΔV) has been similarly estimated. First, the RMSE of the eroded volume of the Mendoza and Jiménez (2006) model. Then, the uncertainty on the real height of the eroded profile (i.e., distance from submerged pivot point to beach top) is included by assessing the variability of the pivot point position assessed from simulations with XBeach 1D under different storm intensities (d*, Table 8.2).

Table 8.2. Ranges of the uncertain variables included in the assessment. Note that total number of cases is always 100 for hazard variables and 20 for future scenario variables The total number of cases can be the result of the simulation of a single variable or of the combination of simulations from 2 variables.

Tordera Delta- S'Abanell (SB), Malgrat North (MN) and South (MS)			
Variable	**Mean and std. dev.**	**Monte-Carlo simulations**	**Total number of Cases**
Ru on [eq 1]	[eq 1] ± 0.32 (m)	100	100 (Ru)
ΔV on [eq 3]	[eq 3] ± 10 m^3	10	100 (ΔX)
d* on [eq 4]	0.8 ± 0.15 m	10	
Retreat trends	SB: 1.1 ± 0.8 m/yr MN: 4.0 ± 0.5 m/yr MS: 1.9 ± 2.1 m/yr	20	20 (BW)
Cabrera de Mar North (CN) and South (CS)			
Variable	**Mean and std. dev.**	**Monte-Carlo simulations**	**Total number of Cases**
Coef. (1.65) on [eq 2]	1.65 ± 0.10	10	100 (Ru)
γ_f on [eq 2]	0.65 ± 0.10	10	
SLR	2050: 0.30 ± 0.04 (m) 2100: 0.63 ± 0.10 (m)	20	20 (MSL)

Confidence ranges on projected conditions under future scenarios are included in the assessment. In this case, the 95% confidence interval of the SLR estimates (IPCC, 2014) is used to derive the standard deviation of the variable, assuming a normal distribution. The standard deviation of shoreline evolution rates within each sector (Jiménez and Valdemoro, 2019) was used to simulate multiple values of beach width per future scenario (Table 8.2).

Therefore, following the Monte-Carlo example, normally distributed values of the uncertain variables for each combination of storm and profile characteristics are simulated. This extends uniformly to the dataset maintaining the natural variability of the storm climate (source) and the morphology (pathway). The total number of cases introduced in the BN training is 100 values of erosion and inundation hazards per profile and storm combined with 20 values of MSL or beach width per future scenario.

8.3.6. Bayesian Network

As already presented before, Bayesian Networks (BN) are probabilistic models based on acyclic graphs (see see Chapters 6 and 7 and references therein). They use Bayes' probability theory [eq.8.5] to describe the relationships between different variables.

$$p[Oi|Pi] = p[Pi|Oi]*p[Oi]/p[Pi] \quad (8.5)$$

In this chapter, Oi represents the hazard-estimators, such as inundation reach or beach retreat, and Pi represents the parent conditions for such hazard's results. Basically, Pi is a set of variables containing the storm and scenario morphological characteristics, e.g., Hs, duration, direction, surge, period, slope, beach height and beach width. By this method, the hazard outputs at each profile are mapped through the conditional probability tables to their parent inputs in the BN, and the sector results are obtained by weighting each profile according to their contribution length over the sector. Source variables, which are known to present interdependencies can also be interconnected in the BN, e.g., establishing Hs, Tp, direction and duration as parents of storm surge. Figure 8.5 shows the BN structure used in this work. Arrows denote dependency relations between the variables. The forcing and morphologic variables are parents of the preliminary hazard output (i.e., Ru, and eroded volume). Ru, eroded volume, and morphology are parents of the main hazard outputs (i.e., inundation reach and beach retreat). Finally, these hazards are combined with beach width to obtain the final hazard index.

As previously mentioned, the uncertainties on a number of variables are included in the BN by means of Monte-Carlo simulations. Figure 8.6 shows a graphical example of how this information goes into the BN and propagates to the output. Simulated variables are assumed to be Gaussian. For each profile, storm and scenario, the BN hazard output is a discretized probability distribution accounting for the considered uncertainties (see the cases in Table 8.2). The total number of cases is a function of the number of profiles, number of storms, number of uncertain variables considered, and number of simulations per uncertain variable. As an example, a sector with 20 profiles and 150 storms would have 100 Monte-Carlo outputs of TWL for each specific profile, storm and MSL condition. Since each future SLR scenario is defined with 20 Monte-Carlo values of MSL, this leads to a total number of $6*10^6$ cases per time projection to feed the BN.

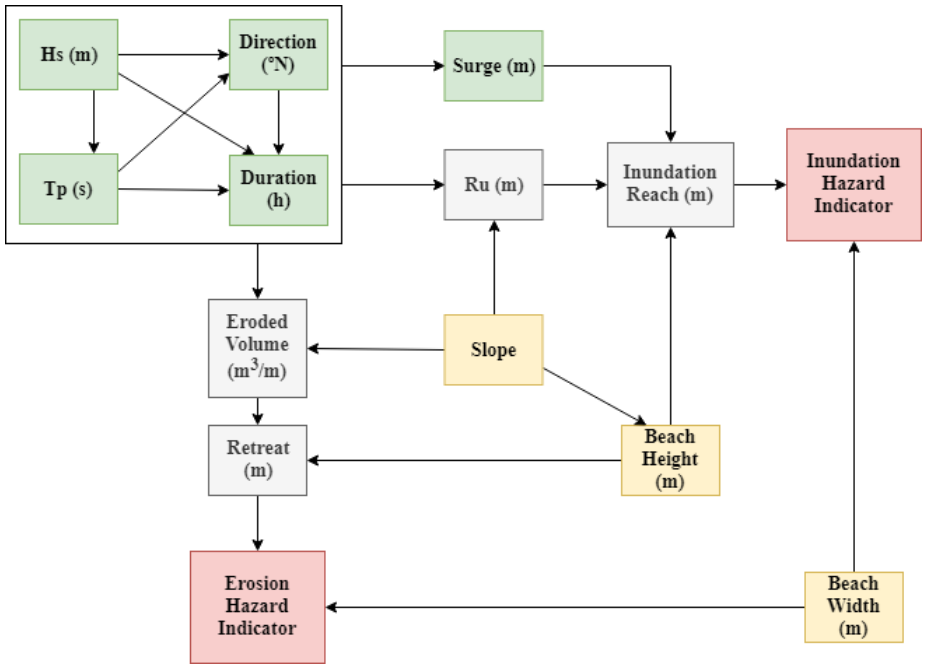

Figure 8.5. The BN structure used in the present work. Source variables are highlighted in green, pathway variables in orange, primary hazard variables in grey and final hazard indexes are in red.

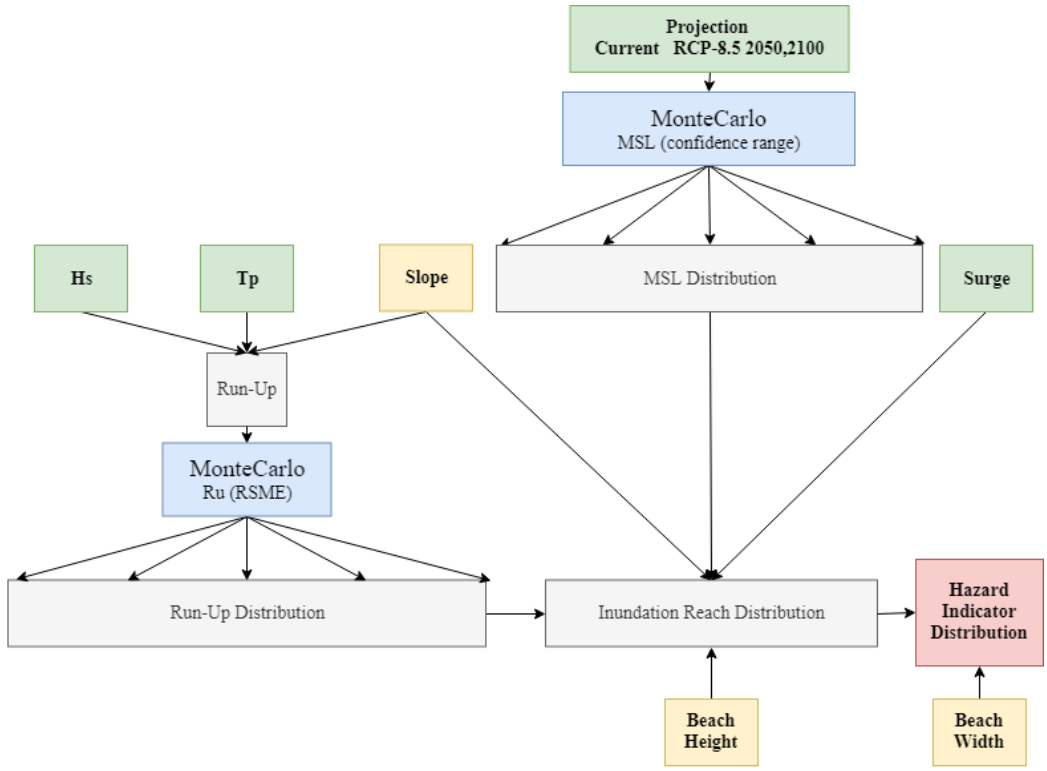

Figure 8.6. Graphical description of inclusion and propagation of Monte-Carlo simulations in the BN. Example on inundation hazard estimation.

8.4. Application of the methodology

8.4.1. Current state hazard profile

The first direct result produced by the BN is the unconstrained distribution of all the variables. Data training fills the conditional probability tables with all simulated cases, being each case a set of the source (waves and water level parameters), pathway (beach characteristics) and hazard variables (Figure 8.5). When no conditioning is applied to the BN, it shows the prior probabilities, i.e. the marginal distributions of each variable without information on the other variables [eq.8.5].

The distributions of the calculated hazard indexes (Figure 8.7-B) represent the probabilities of each hazard level at each sector, both considering the variability of the source (storms) and the variability of the sector morphology. This consideration allows a more representative and detailed sector intercomparison than from the semideterministic approaches (Figure 8.7-A), which aims for a single hazard level for the sector associated with a given return period (e.g., Chapter 4). Note that results are presented here with the same sector definition (~1 km) as in Chapter 4 for comparison purposes, but the framework allows integration at any scale.

The percentages in the hazard profile results can be interpreted in two ways. For example, looking at the erosion distribution at S'Abanell as follows: (i) from the perspective of an incoming event of unknown characteristics, there is a 6% probability of a Level 5 hazard intensity occurrence at some location within the sector, or (ii) from the perspective of an average incoming event, 6% of the total length of the sector is estimated to be affected by an intensity 5 erosion hazard. This dual interpretation is a consequence of the combination in the BN of the storm-climate and the morphological variabilities which allows comparing differences between sectors under the same storm-climate with similar representative profiles but with different morphological variability, which in the case of a deterministic treatment of the pathway would produce the same result.

Focusing on the inundation hazard in Tordera Delta, both Malgrat North and South sectors present percentages > 5% (a typical threshold for statistical significance) of Level 5 intensity, although they show different distributions. In S'Abanell, where the topography is higher, the maximum inundations are less frequent but intermediate hazard levels present higher probabilities, which is a consequence of its narrow beach. In Malgrat North the response is the opposite due to its morphology, characterized by wider beaches and a lower hinterland. Since the inundation reach is approximated by using the bathtub approach, when water exceeds the berm height a large extension is potentially inundated, and therefore, hazard level jumps from low (0-1) to extreme values (5). This dual state behaviour is reinforced in Malgrat South as a consequence of its even wider and more homogeneous beaches. Identifying the different hazard responses is of key importance if a hazard profile is to be combined with vulnerability data to obtain a risk profile. In Cabrera de Mar, both sectors have similar inundation hazard distributions, while the semideterministic approach (Figure 8.7-A) showed a different level between the sectors because of its representation by single-transect and no inclusion of uncertainties. Notably, using a single

transect fixes a single beach height and hinterland shape, and the inundation reach upon the profile chosen for Cabrera South for the TR=100 yr was higher than 40 m and lower than 60 m. However, an even higher profile but with lower hinterland topography may exist, which combined with the inclusion of model errors in the analysis (higher run-ups) may result in the possibility of inundation reaches higher than 60 m leading to a level 5 inundation hazard. A similar effect can be observed comparing CRAF 1 results with the BN-based distributions for inundation in Malgrat South.

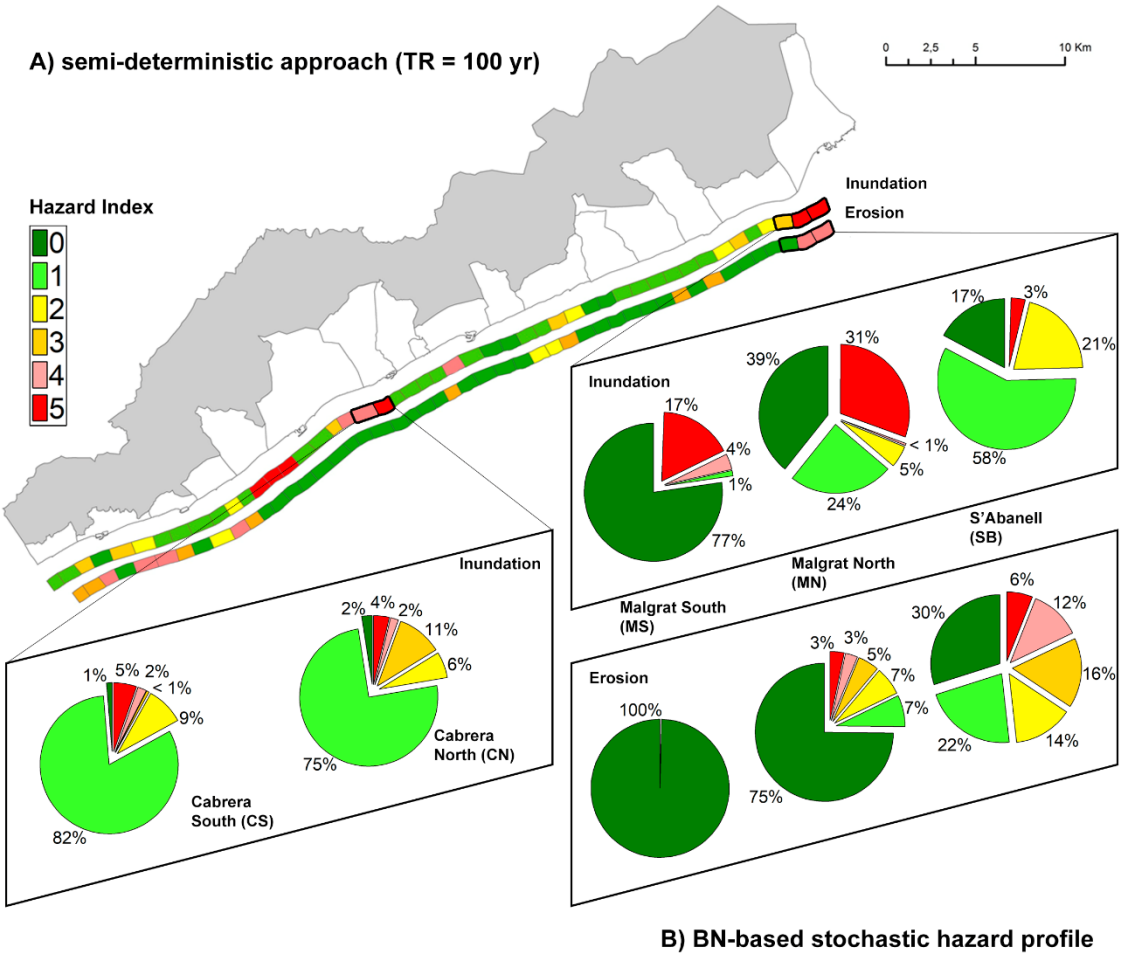

Figure 8.7. Results for a current state hazard-profile. A) semi deterministic results according to Chapter 4. B) stochastic results obtained with the BN-based approach.

Moving to the erosion result at Tordera Delta (Figure 8.7-B), it can be observed how the hazard intensity decreases from north (SB) to south (MS). In addition, the use of multiple profiles and the inclusion of model errors shows that Level 5 erosion is actually probable at SB (6%), whereas it was not shown in the semideterministic approach (Figure 8.7-A). In addition, SB and MN show a quite different profile, whereas in Figure 8.7-A they appear as equivalent sectors. SB shows a generalized vulnerability to erosion, having significant probabilities throughout all intensity levels. Meanwhile, MN has a large

probability of no-hazard at 75%, and the remaining probabilities are mainly at medium intensity levels, with some residual probability of occurrence of a top-level erosion episode. This outcome is a consequence of S'Abanell having narrower and more uniform beaches along the costal stretch while MN has various areas (wide and narrow) that behave differently, which are also detectable with the BN (see results on backward propagation and hazard source below).

8.4.2. Identification of hazard sources

One of the main advantages of using BN is its capacity to assess correlations between variables by means of the information stored in the conditional probability tables. Thus, the BN can also be used to answer questions about the sector behaviour because conditional probability tables are built preserving the relationships between variables connected in Figure 8.5. By means of backpropagation, i.e. imposing values in output variables (hazards) and assessing the distributions obtained in their parent variables (source and pathway), the BN can assess storm or morphological characteristics associated with induced hazard levels of interest.

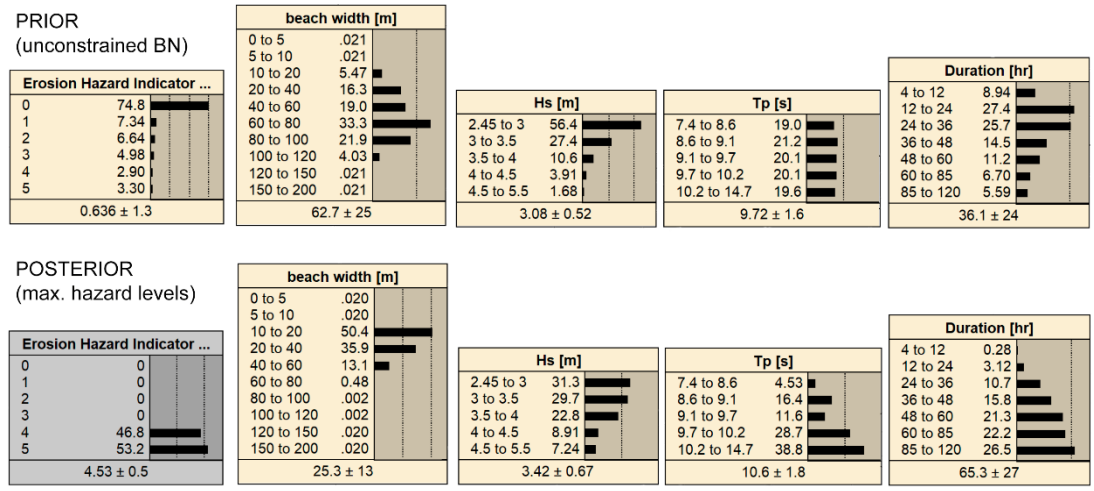

Figure 8.8. Results of hazard source identification at Malgrat North. The prior shows unconstrained dataset probabilities. The posterior shows probabilities conditioned to Level 4 and 5 erosion indexes. Number at the left side of the boxes represent the ranges in which each variable is discretized while numbers next to black bars represent the discretised probability density at each bin.

To illustrate the potential of BNs in this aspect, the case of the erosion hazard at MN is presented in Figure 8.8, where the number at the left side of the boxes represent the ranges in which each variable is discretized, and numbers next to black bars represent the discretised probability density at each bin. This case shows a probability of hazard at ≥ 4 of 6%, with a residual of 3% associated to a Level 5. The prior distributions represent unconstrained probabilities of some variables of the sector. As an example, the

beach width distribution shows a sector mainly with a 40-100-m wide beach, with some extension (~22%) of a relatively narrower coast.

The BN can be constrained to show how the source and the morphological variables change, e.g. when constraining the maximum erosion hazard levels (i.e., 4 and 5), obtaining the conditional probabilities related to that specific case (posterior distributions) and identifying the combination of variables that result in such hazard values. As observed, sectors that have a beach width between 10 to 40 meters (representing only ~22% of the sector's locations) concentrate the ~86% of the probability of getting a 4 to 5 erosion intensity.

Focusing on the hydrodynamic variables, it can be observed how the duration of the event is the main driver of high intensity erosion episodes at the sector (Figure 8.8, posterior). Higher Hs and Tp also favor a large erosion but the changes between prior and posterior are less intense.

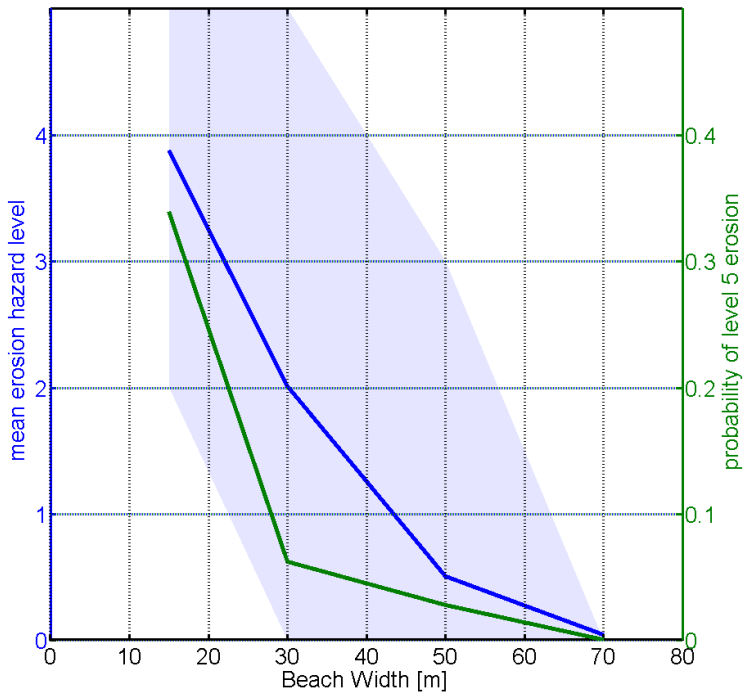

Figure 8.9. Beach Width (BW) against mean erosion hazard level (blue) and probability of Level 5 erosion (green) at Malgrat North. The shaded area represents the 95% confidence interval of the mean erosion level. Obtained probabilities are assessed at the erosion hazard variable after constraining the beach width variable to its different levels.

Since the erosion hazard is quite sensitive to the beach width in the analysed sector, the BN can be used to statistically assess the expected erosion hazard for existing width values along the area. Thus, Figure 8.9 shows the mean erosion hazard level and its 95% confidence range, together the probability of occurrence of an erosion hazard level 5 by constraining beach widths to a range between 15 and 70 m.

As it can be observed, a minimum width of 40 m is needed in Malgrat North to fully avoid an erosion level 4 to 5 (probability of level 5 < 0.05 and confidence interval out of levels 4 to 5). With a value of BW of 70 m or more, all erosion hazard levels are prevented, which is also important information for other uses of the coast, such as the recreational use of the beach. Note that the results presented in Figure 9 are for current conditions and do not yet include information on the temporal evolution of the study site.

8.4.3. Hazard assessment at future scenarios

When the scenario-datasets are introduced in the BN, the hazard profile at different time horizons is obtained. Semideterministic indexes (Figure 8.7-A) in future scenarios will only show the changes in the sector hazard's single-level, and once it reaches its maximum (index 5), it will stop showing changes unless new levels are created. Alternatively, the BN-approach allows the evaluation of changes in the probabilities of the different hazard intensities at different time horizons. To illustrate this, two main results are presented: erosion hazard mid-term horizons due to background erosion in the Tordera Delta assuming that past shoreline trends remain in the future (Figure 8.10), and long-term horizons of the inundation hazard due to SLR at Cabrera de Mar (Figure 8.11).

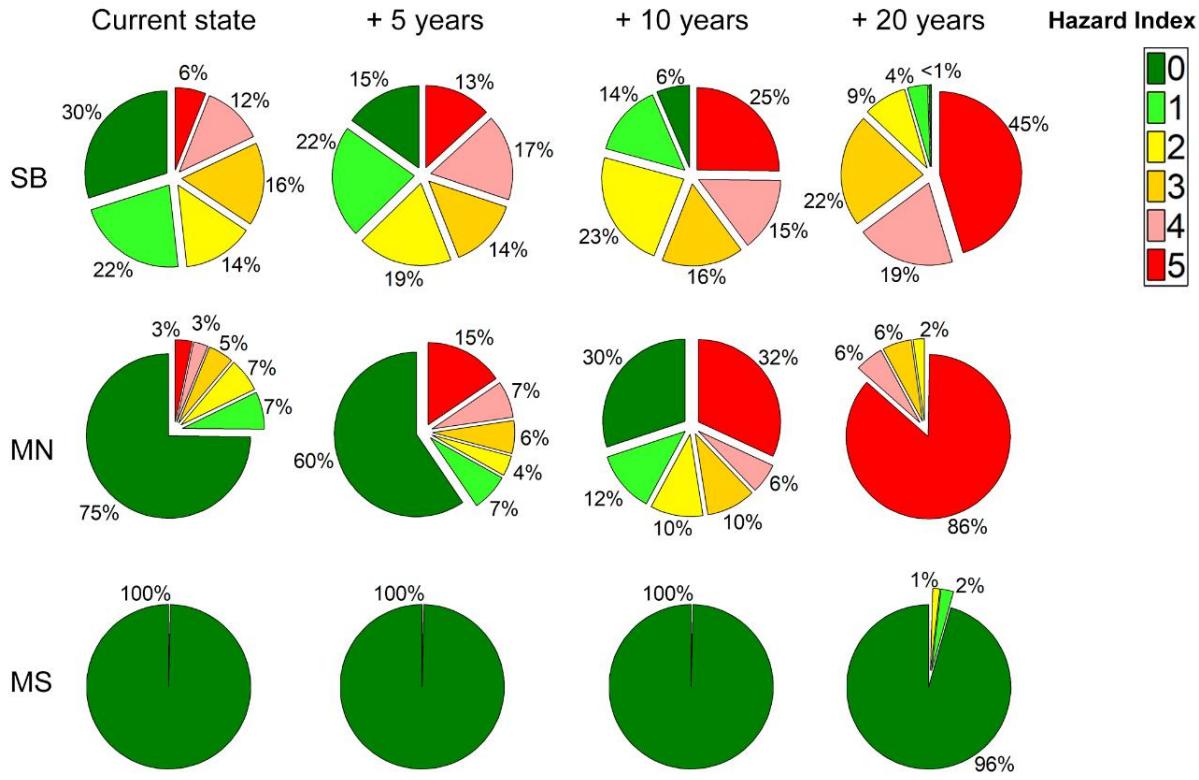

Figure 8.10. Changes in erosion hazard-profiles at Tordera Delta at different time horizons due to background shoreline retreat. S'Abanell (SB), Malgrat North (MN) and Malgrat South (MS) at current scenario, and +5, +10 and +20-year horizons, assuming past measured shoreline trends remain unchanged in the future.

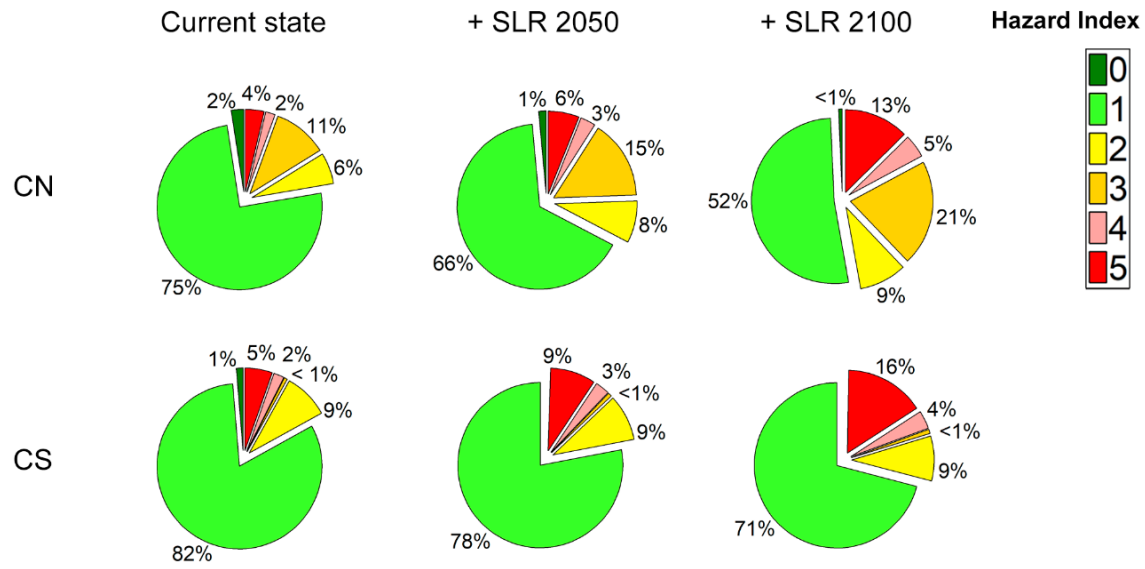

Figure 8.11. Changes in inundation hazard-profiles as at different time horizons under RCP 8.5 SLR. Cabrera de Mar North (CN) and South (CS) at current state, 2050 and 2100.

In the Tordera Delta, SB is the sector showing the current highest level of the erosion hazard, but MN shows a faster progression towards intense erosion events in future scenarios. Notably, in 5 years, SB still shows a general situation with larger frequencies of medium-high erosion episodes, but MN reaches a similar frequency for hazard index 5. At the 10-year horizon, MN is clearly in a worse situation than SB for Level 5 frequencies but still better for probabilities of 0 to 4 erosion intensities. At the 20-year horizon, MN is the most vulnerable sector to erosion with almost all events causing at least a Level 3 situation, with 86% frequencies of Level 5. In contrast, MS remains unaltered across scenarios showing a no-impact profile. (Figure 8.10).

In Cabrera de Mar, both CN and CS show similar responses to SLR at the 2050 and the 2100 RCP 8.5 scenarios. CN shows a higher increase in frequency of medium-intensity events whereas CS keeps on showing slightly larger probabilities of Level 5 situations. In this case, this distinction is crucial, since Level 3 intensities already reach the infrastructure behind the revetment also causing significant disruptions which makes the northern sector more vulnerable (in general terms) than the southern one (Figure 8.11).

8.5. Discussion

In this work, a Bayesian Network-based methodology for regional storm induced hazard assessment has been presented and applied at two sectors on the Catalan coast to illustrate its potential.

Obtained results highlight the benefits of estimating a hazard probability distribution for each sector. The explicit inclusion of uncertainties and extensive coverage of the morphological characteristics showed potential highest-intensity hazards not detected in Chapter 4 - CRAF phase 1 (e.g., erosion at S'Abanell or inundation at Cabrera South, Figure 8.7). In other words, the framework has been successful in hotspot identification, as Chapter 4, but allowing detailed sector intercomparison and reducing hazard underprediction due to uncertainty omissions. In order to illustrate this, Figure 8.12 shows an additional comparison between results obtained here and those using CRAF phase 1. The BN-method outputs the complete curve of Ru vs the hazard index, obtained by constraining the BN at different Ru levels and assessing the distribution of the hazard indicator. On the other hand, the application of CRAF 1 results in a single hazard level value associated to a given return period (illustrated by a point in the graph). At Malgrat North, both results are equivalent (see also Figure 7) and the BN output allocates the Ru associated to TR = 100 yr to a hazard level 5 with a ~95% of probability. At Cabrera South, the CRAF phase 1 output is a hazard level 4 for TR=100 yr (which has a 0% probability of reaching level 5 for the associated Ru, which corresponds to 5.6m), while the BN-method outputs some probability of having level 5. This difference between both approaches is due to the configuration of the area, which is controlled by the embankment height and the topography of the hinterland. The consequence is the existence of an abrupt increase in the expected mean hazard levels and the probability of occurrence of hazard level 5 (and associated 95% confidence ranges) for Ru values higher than 5.5 m. The inclusion of model uncertainty in the BN assessment produces values for Ru up to 6.5 meters which will fall into the level 5 category. This explains the difference in hazard levels obtained using both methods showed in Figure 8.7. In both cases, it can be observed how the BN-method gives more detailed information on the relation between Ru values and expected hazard levels (Figure 8.12) than the CRAF phase 1 single value, showing explicitly the expected variability due to the morphology and model uncertainties.

This is especially important when performing mid-term and long-term hazard assessments. When assessing hazards at future horizons, changes in the frequencies of low-intermediate hazard levels can be as important as those of the extreme (large TR) intensities (Figures 8.10 and 8.11). Thus, obtained changes in the hazard distributions give complete information about the sector response. This allows a better identification of tipping points for coastal adaptation, as information of intermediate hazard levels at different time horizons is also needed for such purpose. This also allows identification of sectors with different responses over time but with nearly the same current hazard profile (Figure 8.11). Mid-term and long-term scenarios are based on modelled projections with associated uncertainties that are often estimated with a given error or expected range (e.g., expected SLR for a given horizon and the associated 95% confidence range). This is included in hazard assessment, which should be considered for sector intercomparison since it prevents hazard underprediction that may arise from single-value future estimations.

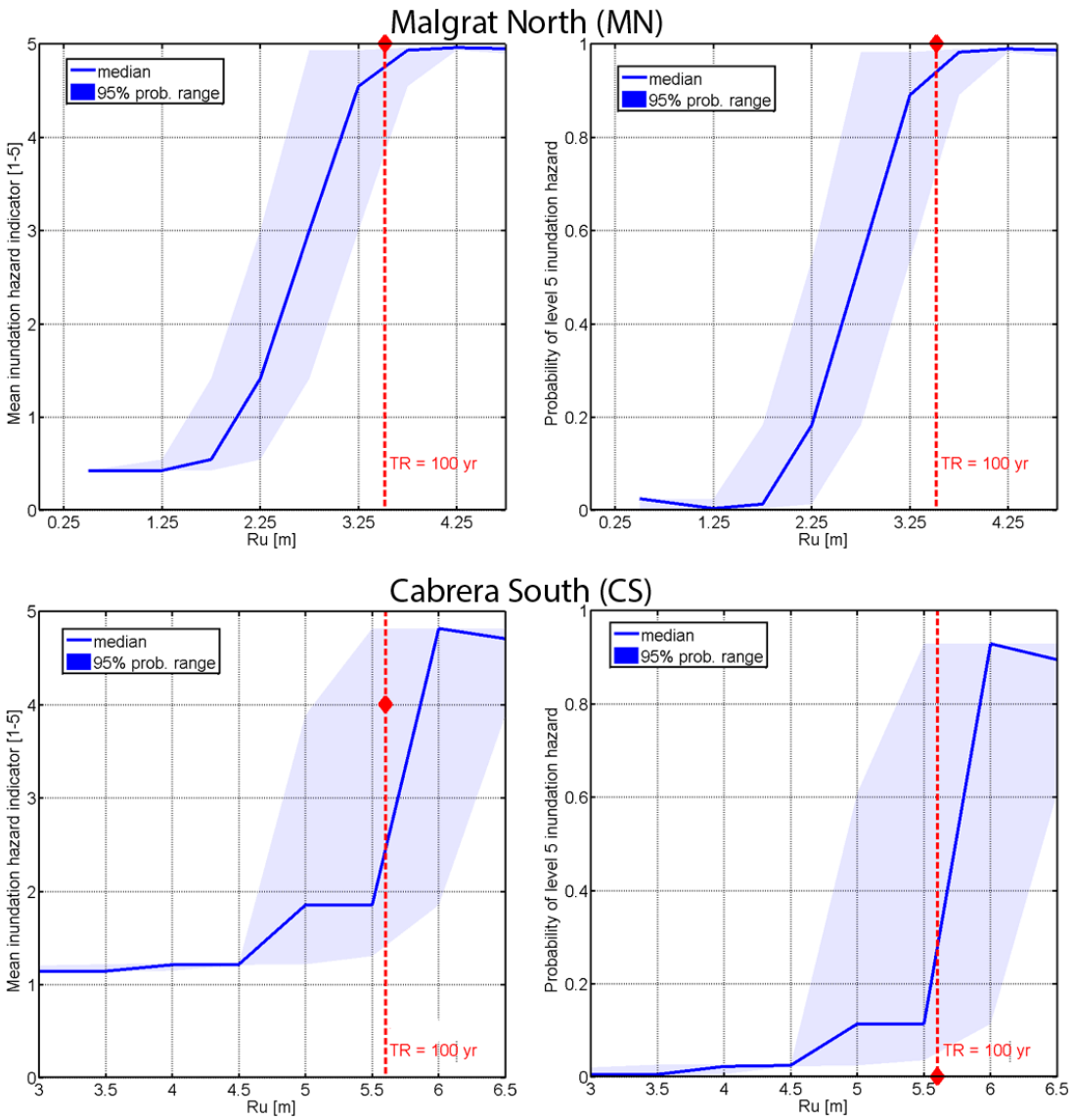

Figure 8.12. Run-up vs mean inundation hazard indicator (left) and probability of Level 5 inundation hazard (right) at Malgrat North (top) and Cabrera South (bottom). The BN results are in blue and Jimenez et al. (2018) hazard value for TR = 100 yr is in red (see chapter 4).

The methodology can also produce results of sector morphology and forcing characteristics conditioned to a given hazard intensity (Figures 8.8 and 8.9). Thus, the BN, through back-propagation, indicates the potential causes of given hazard levels, giving insights into which processes are important or even to what remediation measures could be effective. Moreover, the BN can produce hazard distributions conditioned to specific storm conditions (i.e., known values of Hs, Tp, duration, direction and surge) in real time. Thus, since these variables are produced by operational hydrodynamic forecasting systems, the tool can perform as a preliminary regional early warning system (EWS) without the need of time-consuming, detailed, morphodynamic, process-based modeling.

In this work, we have applied the developed methodology by integrating hazards at ~1 km spatial units. This was done mainly for comparison purposes with the results obtained in Chapter 4. However, the BN

can integrate results at any spatial and scale depending on the physical-process or management questions to be addressed.

One limitation of the presented methodology is that a long record of storms is needed to produce robust results. As opposed to CRAF phase 1, no extreme analysis is done and therefore, no extrapolation of storm conditions is performed to consider possible future events of higher magnitude than recorded ones. However, as highlighted in Figure 8.12 and from the direct comparison of obtained results, for the analysed record length (60 years), this seems to have a smaller impact than not accounting for model errors and morphological variability in the sense that CRAF phase 1 results associated to a TR =100yr underestimate hazard levels when compared to the BN-CRAF using 60 years of storm events.

In the current application, some assumptions have been imposed for the sake of simplicity and test the output. However, they are independent of the method, and they could easily be substituted by other choices. Thus, future scenarios due to background shoreline retreat have been built assuming that measured past trends will keep unchanged in the future. However, they could be substituted by using shoreline using time-varying rates or results from long term morphodynamic models. Moreover, process-based models (e.g., 1D-Xbeach, Roelvink et al. 2009; SBeach, Larson and Kraus 1989; LISFLOOD, Bates and de Roo, 2000; Bates et al., 2005) could be used to quantify erosion and inundation hazards instead of simple parametric models. The uncertainty associated with numerical modeling can be included through an ensemble of simulation outputs from different parametrizations or different models, similar to model ensembles that assess the uncertainties in future projections (Purvis et al. 2008). Following this concept, many different sources of uncertainty (e.g., seasonality of the coast morphology), which were omitted in the present chapter, could be included with the only consequence being an increase in the size of the case-dataset feeding the BN. The current analysis was executed on a regular laptop, meaning that there is still room, computationally speaking, to explore new elements to include in the analysis. In this sense, the approach could also be extended with socioeconomic data in order to translate hazard profiles into impact profiles.

8.6. Conclusions

A BN-based methodology for storm-induced hazards assessment at regional scale has been developed. It has successfully identified coastal erosion and inundation hotspots in two sectors of the Catalan coast (NW Mediterranean) similarly to what was previously done in Chapter 4 with the CRAF-phase 1 method while giving further information.

The method accounts for the contribution of different sources of uncertainty characterising the variability in storms and coastal morphology, as well as taking into account that associated with used models. As a result, instead of resulting in a single value, the BN-based method provides hazard distributions which will indicate the probability of occurrence of hazards at any level.

The method can be easily used to forecast changes in storm-induced hazard levels by applying it under given future scenarios, based on changes in morphology and/or storm properties. In such a case, the method will predict the expected change in the probability of occurrence for the entire range of hazard levels.

The inherent capability of BN's capability to assess the interdependence between variables is used to identify source (storms) and pathway (beach morphology) characteristics responsible for given hazard distributions. When this is applied under different scenarios permit to identify harmful combinations taking place at specific locations and at given time horizons. From the management standpoint this will provide essential information for making decisions on selecting coastal adaptation alternatives.

CHAPTER 9.

Conclusions

9.1. SUMMARY OF THESIS MAIN FINDINGS AND CONCLUSIONS

The following section wraps up all main concluding remarks derived from chapters 2 to 8, which stablish the baseline for future research. This thesis had the main objective of studying and proposing methodologies around the main core topic about the identification and characterization of coastal hotspots to the impact of extreme events for managing purposes.

The present work started investigating the effects on hazard estimation of two sources of uncertainty involved in common practice of coastal risk and hazard assessments related to storm-induced inundation and erosion.

Chapter 2 analysed the expected differences on flooding estimates when associating probabilities or return periods to different variable-indicators by the event or response approaches. The assessment concluded that differences between methods are location dependent and thus, affected by local wave climate conditions. The preferred method is the response approach as it takes into account natural variabilities of wave conditions affecting the inundation process. Notably, differences with the event approach, which bases the probability of the hazard on the probability of a single wave parameter (significant wave height), become unacceptable as inundation variable-estimates are closer to the final inundation maps. E.g., differences in Ru are of less magnitude than differences in inundation water volumes or simulated inundation surface. This is attributed also to the fact that the event approach must use one of the common assumptions in coastal engineering hazard-modelling, which is the use of the triangular shape to represent storm events given its peak significant wave height and its total duration.

Chapter 3 explores in detail the effects of such an assumption when modelling inundation and erosion hazards. The analysis of an extensive dataset of storm conditions at two Mediterranean sub-basins (NW Mediterranean and N Adriatic), and related storm-induced effects over both dissipative and reflective conditions, highlighted that erosion and inundation hazards were not properly reproduced in most of cases and tended to be under-predicted with synthetic triangular storms. Evidences showed that differences in the real and synthetic forcing generated considerable differences in terms of total energy, energy at the peak and timing of the peak. The energy of the storms, the breaker conditions, the local storm climate and the mean sea level did not consistently influence the differences between the synthetic- and real-based output, and obtained differences were considerable in all analysed cases. Therefore, detailed hazard estimations should be preferably based on real storm shapes given the large uncertainty on the results that may be induced by using synthetic triangular simplifications.

Then, the thesis followed with the methodologies proposed at regional and local scales for hazard and risk assessments to support coastal management to storm-induced impacts under multiple scenarios.

Chapter 4 presented the regional methodology developed in RISC-KIT and applied to the Maresme coast (NW Mediterranean). The methodology, based on simple parametric hazard models, used the response approach (Chapter 2) for a proper assignation of hazard return periods, and successfully

identified erosion and inundation hotspots along the studied coastal stretch. Notably, severe hazards associated to given probabilities are not necessarily coincident, due to spatial variability of the coastal resilience and different dependencies of the hazards with the storm characteristics. Few areas behaved as hotspots to both erosion and inundation at the same time. The Tordera Delta was identified as the most sensitive sector to both storm induced hazards. Existing values at exposure in the identified hotspot, have been significantly affected during the past decades, with most of the damages affecting campsite installations (tourist use). The main limitations of the method were the spatial simplification of 1km coastal sectors to a single beach profile, and the direct application of the hazard models without considering their uncertainties.

Bayesian Network (BN) models can conceptualize the RISC-KIT regional tool while including explicitly hazard model errors, future projection uncertainties and the morphological variability within the 1km sectors (Chapter 8). The performed analysis with the BN-model proved that not accounting for all these factors can lead to an undesired underestimation of storm-induced hazards. Additionally, the tool outputs hazard-intensity distributions at each sector that give more insight on sector response than a single value associated to a given reference return period. This is especially useful when different tipping points for coastal adaptation need to be considered, and sector response at different time horizons need to be estimated. Finally, the BN capability in representing conditional dependencies between variables showed to be very useful to identify key causality relations between site morphological characteristics or storm conditions and the obtained hazard levels.

Moving to hazard and risk characterization at local scale, the first step was building a model train which based hazard simulation on the XBeach process based model. The model was first tested (Chapter 5) and later intensively applied (Chapters 6, and 7) at the Tordera Delta hotspot.

The validation exercise performed in Chapter 5 was conducted by using the largest historical event ever recorded at the site, representative of extreme conditions of large return periods (the Sant Esteve 2008 storm). The final set-up represented with great accuracy the morphological changes at the emerged part of the beach, with better reproduction at the northern half of the domain were incoming conditions have a more orthogonal incidence. The study area is a highly curvilinear coastline with coarse sediment and steep nearshore slope, and some parameter adjustments were needed to improve simulation results with the XBeach model. These, included the limitation of avalanching and sediment mobility processes, the inclusion of groundwater effects and the increase of wave asymmetry and skewness. The validation was performed on that single storm event as it was the only where data on sub-aerial beach morphology was available pre- and post-storm. Thus, this event was used as reference to test the sensitivity to different incoming storm directions, while keeping all other storm characteristics unchanged. The analysis highlighted that storm-induced hazards along a highly curvilinear coast are extremely sensitive to changes in wave direction. This means that even under a climate scenario of relatively steady storminess (wave power and frequency), a potential shift in wave direction may significantly change hazard conditions and, in consequence, need to be accounted for in robust damage risk assessments.

The XBeach model was then used to simulate a wide range of storm conditions to be used in the local scale RISC-KIT tool. Simulation results were coupled with receptor georeferenced polygons to feed a BN-model built to conceptualize the source-pathway-receptors-consequences framework to test risk reduction measures under different scenarios (Chapter 6). In addition to SLR, changes in future storm direction where included in the assessment as a consequence of findings in Chapter 5 and existing literature about its likelihood in the NW Mediterranean basin (Cases-Prat and Sierra 2012, 2013).

The approach concluded that from all tested measures, increasing beach height by means of a dune was the most effective against inundation, with little improvement by creating a beach nourishment in front due to the morphological feedback processes during the storms. Receptor set-back was the only effective measure against erosion, as beach nourishments were found to wash out very fast. The analysis of future projections showed that the study site is equally sensitive to a 50% of storm shifting towards southern incoming conditions than to SLR plus corresponding beach accommodation under the RCP 8.5 scenario by 2100. The RISC-KIT local tool was successful for scenario comparison purposes and had great impact in communicating results to stakeholders as the analysis considers a large dataset of hazard simulations accounting for receptors individually, but using a model scheme (BN) that is easy to interpret and follow by non-technical and non-expert users.

However, it had some inherent limitations that made it not applicable for risk characterization out of scenario comparisons. It was semi-deterministic as it used a wide range of storm conditions but not accounting for their actual probability of occurrence (i.e. event approach in Chapter 2), and it filled the gaps of storm characteristics that were never recorder with synthetic triangular events, which induce important errors in hazard estimations (Chapter 3).

This was addressed in Chapter 7 were the BN-framework was used with all existing hindcast storms in a 60-year dataset (response approach), maintaining their real shapes and considering the effect of multiple-peak events. This resulted in a fully probabilistic risk characterization of the Tordera Delta in present conditions and future horizons considering the effect of background shoreline retreat (Section 7.2). As a first step towards future works, Section 7.3 explored the BN capability as predictive model for maximum retreat in such a complex study site as the Tordera Delta

In Section 7.2, the BN-framework proved useful in identifying and quantifying source characteristics related with intense hazard extension and magnitude, and its local conditioning to sub-sector areas. It also allowed studying quantitatively the evolution of such relations at different short-midterm time horizons, highlighting and increase in the number of storms that will be able to cause important impacts and therefore and increase on the diversity of impacting storm characteristics, e.g. lower Hs storms and southern incoming events will have deeper impacts in the future due to the existing trends of background shoreline retreats.

It also proved useful in characterising the probabilistic spatial distribution of risks along and across the study site, allowing a probabilistic definition of receptor setbacks associated to different risk intensities and the evolution of such setbacks in short and midterm projections of future conditions.

Finally, Section 7.3 showed the relative and combined importance of storm direction and multi-peak events for proper response prediction, along with the critical importance of local effects caused by existing hard structures such as flanking or physical limits at the hinterland. The BN-model used in Section 7.3 showed great descriptive skill and acceptable predictive skill given the short length in statistical terms of existing records. This highlights the promising future of this type of predictive models as surrogate for simple parametric models (chapters 4 and 8) that cannot be directly used to properly reproduce all the involved complexity under study site conditions similar to those in the Tordera Delta.

9.2. FUTURE RESEARCH

After the development of this PhD, a number of future research questions are detected which would continue to improve the current state of the art on the assessment of storm induced impacts in present and future conditions.

In order to reduce uncertainties associated with the use of triangular synthetic events, the present work highlighted the need of further studies to better correlate local meteorological conditions with storm shapes, with the final objective of defining synthetic storms with the ability to represent the induced hazards under a given storm climate. This will be especially useful in combination with storm climate simulation technics based on statistical simulations and data mining (e.g., Callaghan 2008; Ranashingue 2016; Antolínez et al., 2016), currently used to enlarge datasets of forcing conditions and projecting wave cliamtes into the future. These are based on bulk storm characteristics and will need the estimation of storm shapes in order to properly simulate the induced hazards.

Regarding future research in regional BN-frameworks for coastal risk assessment, the first natural step would be the completion of the work developed here, i.e. first, its full application to the whole Catalan coast and second, the inclusion of the vulnerability and exposure component with explicit treatment of its associated uncertainties in the network. An additional step would be including in the framework additional sources of uncertainty not yet included in the presented version, such as the morphological state of the coast.

This is also true for the local (hotspot) BN-framework where this component was only indirectly considered by assessing multi-peak storms. The local BN-framework relies on model results that have been validated using a single storm event. Further research is needed (and also new measurements to properly conduct it) in order to see the performance of the current model set-up under other storm characteristics, as model calibrations for its use in statistical approaches should be preferably performed with different storm conditions covering the wave climate ranges (Callaghan et al., 2013).

In both cases (regional and local) BN-frameworks would favour the use of measurements to complement and gradually substitute model results. BNs can merge both data sources giving more weight to measurements and keeping some underlying information on model results while the first source is still scarce. Additionally, both frameworks can perform as preliminary offline Early Warning Systems (EWS) giving immediate predictions on storm-induced impacts prior to the output of detailed online model based systems. The validation of the frameworks as EWS also needs measurements on actual system response, which at the same time can be used to feed the BNs and improve the frameworks with time.

Therefore, there is a clear need of further research activity on beach monitoring both at regional scale and local scale in the case of hotspots and highly dynamic study sites. New approaches that come associated with up-to-date technologies such as the assessment of shoreline positions (e.g. Sánchez-Garcia, 2019) and nearshore bathymetries (Caballero and Stumpf, 2019) at subpixel scale derived from satellite data or detailed and fast local surveys allowed by UAVs and drones (e.g. Duo et al., 2018) can be used for such purposes and improve the overall performance of BN-frameworks for coastal risk assessments.

Finally, on the use of BNs for predictive purposes in order to perform as surrogates of hazard estimation models, more research is needed in order to generalise its application, and larger datasets should be analysed in order to properly quantify prediction capabilities. During the stay in the USGS the PhD candidate also started a research on the use of the BN to generally predict annual shoreline trends, that gave preliminary promising results although still incomplete and not strong enough to be included in the present tesis. This research needs to be furtherly explored with additional data and processings to properly test and adjust the tool.

Additional methodologies in the field of machine learning, and other artificial intelligence-related approaches should be explored in combination with (or as an alternative to) the BN frameworks for all purposes presented here. The increasing amounts of data at hand allows the inclusion of these technics in coastal engineering and particularly on the study of storm-induced effects. Remote sensing sciences and the increasing philosophy of open data and international collaborations also increases the potential success of these fields in applications related to the topics discussed in the present PhD thesis.

References

ACA, 2014: Pla especial d'emergències per inundacions (INUNCAT). Agència Catalana de l'Aigua

Alvarez-Ellacuria, A., Orfila, A., Olabarrieta, M., Gomez-Pujol, L., Medina, R., Tintoré, J., 2009. An alert system for beach hazard ´ management in the Balearic Islands. Coastal Management 37(6), 569– 584.

Antolínez, J.A.A., Méndez, F.J., Camus, P., Vitousek, S., González, E.M., Ruggeiro, P., Barnard, P., 2016. A multiscale emulator for longterm morphodynamics (MUSCLEmorpho), Journal of Geophysical Research: Oceans, 121, 1-16. doi:10.1002/2015JC011107.

Apel, H., Thieken, A.H., Merz, B., Blöschl, G., 2004. Flood risk assessment and associated uncertainty. Nat. Hazards Earth Syst. Sci., 4, 295-308.

Arcement, G., Schneider, V., 1989. Guide for selecting Manning's roughness coefficients for natural channel and floodplains. Technical Report WSP2339, U.S. Geological Survey.

Armaroli, C. and Duo, E., 2018. Validation of the coastal storm risk assessment framework along the EmiliaRomagna coast. Coast. Eng. 134, 159–167. doi:10.1016/j.coastaleng.2017.08.014

Armaroli, C., Ciavola, P., Masina, M., Perini, L., 2009: Run-up computation behind emerged breakwaters for marine storm risk assessment, J. Coast. Res., SI 56, 1612–1616.

Armaroli, C., Ciavola, P., Perini, L., Calabrese, L., Lorito, S., Valentini, A., Masina, M., 2012. Critical storm thresholds for significant morphological changes and damage along the Emilia- Romagna coastline, Italy. Geomorphology 143-144, 34-51, doi.org/10.1016/j.geomorph.2011.09.006.

Arns, A., Wahl, T., Haigh, I. D., Jensen, J. and Pattiaratchi, C., 2013. Estimating extreme water level probabilities: A comparison of the direct methods and recommendations for best practise Coast. Eng., 81, 51–66, doi:10.1016/j.coastaleng.2013.07.003.

Ballesteros, C., 2017. The coastal risk landscape application on the Catalan coast. Universitat Politècnica de Catalunya. PhD Thesis. 154 p. http://hdl.handle.net/10803/456811

Ballesteros, C., Jiménez, J.A., Viavattene, C., 2018. A multi-component flood risk assessment in the Maresme coast (NW Mediterranean). Nat. Hazards 90, 265–292. doi.org/10.1007/s11069-017-3042-9.

Barnard, P.L., Allan, J., Hansen, J.E., Kaminsky, G.M., Ruggiero, P., Doria, A., 2011. The impact of the 2009-10 El Niño Modoki on U.S. West Coast beaches. Geophys. Res. Lett., 38, doi:10.1029/2011GL047707.

Barquet, Cumiskey, 2018. Using participatory Multi-Criteria Assessments for assessing disaster risk reduction measures. Coast. Eng., 134, 93-102, doi.org/10.1016/j.coastaleng.2017.08.006.

Bates, P.D., Dawson, R.J., Hall, J.W., Horritt, M.S., Nicholls, R.J., Wicks, J., Hassan, M.A.A.M., 2005. Simplified two-dimensional numerical modeling of coastal flooding and example applications. Coast. Eng., 52, 793-810.

Bates, P.D., De Roo, A.P.J., 2000. A simple raster-based model for floodplain inundation. Journal of Hydrology 236, 54-77.

Benavente, J., Del Río, L., Gracia, F.J., Martínez-del-Pozo, J.A., 2006. Coastal flooding hazard related to storms and coastal evolution in Valdelagrana spit (Cadiz Bay Natural Park, SW Spain). Cont. Shelf Res., 26, 1061–1076. doi.org/10.1016/J.CSR.2005.12.015

Bender, M. A., T. R. Knutson, R. E. Tuleya, J. J. Sirutis, G. A. Vecchi, S. T. Garner, and I. M. Held, 2010. Modeled Impact of Anthropogenic Warming on the Frequency of Intense Atlantic hurricanes, Science, 327, 454.

Bertin, X., Bruneau, N., Breilh, J. F., Fortunato, A. B. and Karpytchev, M., 2012. Importance of wave age and resonance in storm surges: The case Xynthia, Bay of Biscay, Ocean Model., 42, 16–30, doi:10.1016/j.ocemod.2011.11.001,.

Bertin, X., Li, K., Roland, A., Zhang, Y.J., Breilh, J.F., Chaumillon, E., 2014. A modeling-based analysis of the flooding associated with Xynthia, central Bay of Biscay. Coast. Eng., 94, 80–89, doi:10.1016/j.coastaleng.2014.08.013.

Bertoni, D., Armaroli, C., Ciavola, P., 2015. Fast retreat of a barrier system due to reduced sediment supply (Bellocchio, Northern Adriatic Sea, Italy), in Coastal and Maritime Mediterranean Conference, Edition 3, Ferrara, Italy, pp. 7–10.

Beuzen, T., Marshall, L., Splinter, K.D., 2018a. A comparison of methods for discretizing continuous variables in Bayesian Networks. Environ. Model. Softw. 108, 61–66. doi.org/10.1016/j.envsoft.2018.07.007.

Beuzen, T., Splinter, K.D., Marshall, L.A., Turner, I.L., Harley, M.D., Palmsten, M.L., 2018b. Bayesian Networks in coastal engineering: Distinguishing descriptive and predictive applications. Coast. Eng. 135, 16–30. doi.org/10.1016/j.coastaleng.2018.01.005.

Beven II, J. L., Avila, L. A., Blake, E. S., Brown, D. P., Franklin, J. L., Knabb, R. D., Pasch, R. J., Rhome, J. R. and Stewart, S. R., 2008. Atlantic Hurricane Season of 2005, Mon. Weather Rev., 136(3), 1109–1173, doi:10.1175/2007MWR2074.1.

Billi, P., Rinaldi, M., 1997. Human impact on sediment yield and channel dynamics in the Arno River basin (central Italy), in Human Impact on Erosion and Sedimentation (Proceedings of Rabat Symposium S6, April 1997), pp. 301–311, IAHS Press, Institute of Hydrology, Wallingford, Oxfordshire, UK.

Bird, E.C.F. 2000. Coastal geomorphology: an introduction. John Wiley, Chichester, UK.

Bityukov, S., Krasnikov, N., Nikitenko, A., Smirnova, V.V., 2013. On the distinguishability of histograms. Eur. Phys. J. Plus, 128(11), 143. doi.org/10.1140/epjp/i2013-13143-8

Bolaños, R., 2004. Tormentas de Oleaje en el Mediterráneo: Física y Predicción. Ph.D. Thesis, Universitat Politecnica de Catalunya, Barcelona, Spain.

Bolaños, R., Jorda, G., Cateura, J., Lopez, J., Puigdefabregas, J., Gomez, J., Espino, M., 2009. The XIOM: 20 years of a regional coastal observatory in the Spanish Catalan coast. J. Mar. Syst., 77, 237–260, doi:10.1016/j.jmarsys.2007.12.018.

Booij, N., Holthuijsen, L. H. and Ris, R. C., 1996. The SWAN wave model for shallow water, in Proc. 25th Int. Conf. Coastal Eng., pp. 668–676, Orlando, Florida, USA..

Booij, N., Ris, R.C., Holthuijsen, L.H., 1999. A third-generation wave model for coastal regions. I-Model description and validation. J. Geophys. Res., 104, 7649–7666, doi:10.1029/98jc02622.

Bosom, E., Jiménez, J.A., 2011. Probabilistic Coastal vulnerability assessment to storms at regional scale. Application to Catalan beaches (NW Mediterranean). Natural Hazards & Earth System Sciences 11, 475-484. doi.org/10.5194/nhess-11-475-2011

Bosom, E., 2014. Coastal vulnerability to storms at different time scales: application to the Catalan coast, Universitat Politècnica de Catalunya. PhD Thesis. 203 p. http://hdl.handle.net/10803/277381

Bruun, P., 1962. Sea-level rise as a cause of shore erosion, J. Waterw. Harb. Div., 88(1), 117–132.

Bubeck, P., Botzen, W. J. W., Kreibich, H., & Aerts, J. C. J. H., 2013. Detailed insights into the influence of flood-coping appraisals on mitigation behaviour. Global Environmental Change, 23(5), 1327-1338.

Caballero, I., Stumpf, R.P., 2019. Retrieval of nearshore bathymetry from Sentinel-2A and 2B satellites in South Florida coastal waters. Estuar. Coast. Shelf Sci. 226, 106277. doi.org/10.1016/J.ECSS.2019.106277

Callaghan, D.P., Nielsen, P., Short, A., Ranasinghe, R., 2008. Statistical simulation of wave climate and extreme beach erosion. Coast. Eng. 55, 375–390. doi.org/10.1016/j.coastaleng.2007.12.003

Callaghan, D.P., Ranasinghe, R., Andrew, S., 2009. Quantifying the storm erosion hazard for coastal planning. Coast. Eng. 56, 90–93. doi.org/10.1016/j.coastaleng.2008.10.003

Callaghan, D.P., Ranasinghe, R., Roelvink, D., 2013. Probabilistic estimation of storm erosion using analytical, semi-empirical, and process based storm erosion models. Coast. Eng. 82, 64–75. doi.org/10.1016/j.coastaleng.2013.08.007

Camus, P., Mendez, F.J., Medina, R., Tomas, A., Izaguirre, C., 2013. High resolution downscaled ocean waves (DOW) reanalysis in coastal areas. Coast. Eng. 72, 56–68. doi.org/10.1016/j.coastaleng.2012.09.002

Carley, J.T., Cox, R.J., 2003. A methodology for utilising time-dependent beach erosion models for design events, in: Kench, P.S., Hume, T.M. (Eds.), Coasts & Ports 2003 Australasian Conference: Proceedings of the 16th Australasian Coastal and Ocean Engineering Conference, the 9th Australasian Port and Harbour Conference and the Annual New Zealand Coastal Society Conference, Auckland, New Zealand, 9-1. Institution of Engineers, Australia, pp. 587–595.

Carrier, W.D., 2003. Goodbye, Hazen, Hello, Kozeny-Carman. J. Geotech. Geoenviron. Eng., 129, 1054–1056, doi:10.1061/(ASCE)1090-0241(2003)129:11(1054).

Casas-Prat, M., Sierra, J.P., 2010. Trend analysis of wave storminess: wave direction and its impact on harbour agitation. Natural Hazards and Earth System Sciences 10, 2327-2340.

Casas-Prat, M., Sierra, J.P. 2013. Projected future wave climate in the NW Mediterranean Sea. Journal of Geophysical Research - Oceans 118.7, 3548-3568. doi: 10.1002/jgrc.20233

Casas-Prat, M., Sierra, J.P., 2012. Trend analysis of wave direction and associated impacts on the Catalan coast. Clim. Chang., 115, 667–691, doi:10.1007/s10584-012-0466-9.

Chini, N., Stansby, P. K., 2012. Extreme values of coastal wave overtopping accounting for climate change and sea level rise, Coast. Eng., 65, 27–37, doi:10.1016/j.coastaleng.2012.02.009.

Church, J. A., Clark, P. U., Cazenave, A., Gregory, J. M., Jevrejeva, S., Levermann, A., Merrifield, M. A., Milne, G. A., Nerem, R. S., Nunn, P. D., Payne, A. J., Pfeffer, W. T., 2013: Sea-Level Rise by 2100, Science (80-.)., 342(6165), 1445, doi:10.1126/science.342.6165.1445-a.

Ciavola, P., Armaroli, C., Chiggiato, J., Valentini, A., Deserti, M., Perini, L., Luciani, P., 2007. Impact of storms along the coastline of Emilia-Romagna: the morphological signature on the Ravenna coastline (Italy), J. Coast. Res., SI 50, 540–544.

Ciavola, P., Ferreira, O., Haerens, P., Van Koningsveld, M., Armaroli, C., 2011a. Storm impacts along European coastlines. Part 2: Lessons learned from the MICORE project, Environ. Sci. Policy, 14(7), 924–933, doi:10.1016/j.envsci.2011.05.009.

Ciavola, P., Ferreira, O., Haerens, P., Van Koningsveld, M., Armaroli, C., Lequeux, Q., 2011b. Storm impacts along European coastlines. Part 1: The joint effort of the MICORE and ConHaz Projects, Environ. Sci. Policy, 14(7), 912–923, doi:10.1016/j.envsci.2011.05.011.

Ciavola, P., Harley, M. D., den Heijer, C., 2018: The RISC-KIT storm impact database: a new tool in support of DRR, Coast. Eng., 134, 24-32, doi.org/10.1016/j.coastaleng.2017.08.016.

Cid, A., Castanedo, S., Abascal, A. J., Menéndez, M., Medina, R., 2014. A high resolution hindcast of the meteorological sea level component for Southern Europe: the GOS dataset, Clim Dyn, 43:2167-2184.

CIIRC, 2010. Estat de la zona costanera a Catalunya. International Centre for Coastal Resources Research, Barcelona.

Cirella, G. T., Semenzin, E., Critto, A., Marcomini, A. 2014. Natural hazard risk assessment and management methodologies review: Europe. In: Linkof, I. (Ed.), Sustainable Cities and Military Installations. Springer, pp. 329-358.

Coco, G., Senechal, N., Rejas, A., Bryan, K. R., Capo, S., Parisot, J. P.,, MacMahan, J. H., 2014. Beach response to a sequence of extreme storms. Geomorphology, 204, 493-50.

Cohn N, Ruggiero P., 2016. The influence of seasonal to interannual nearshore profile variability on extreme water levels: Modeling wave runup on dissipative beaches. Coastal Engineering, 115:79-92.

Coles, S.G., 2001. An introduction to statistical modelling of extreme values. Springer, London.

Conte, D. Lionello, P., 2013. Characteristics of large positive and negative surges in the Mediterranean Sea and their attenuation in future climate scenarios, Glob. Planet. Change, 111, 159–173, doi:10.1016/j.gloplacha.2013.09.006.

Corbella, S., Stretch, D.D., 2012. Predicting coastal erosion trends using non-stationary statistics and process-based models. Coast. Eng. 70, 40–49. doi.org/10.1016/j.coastaleng.2012.06.004

Cunge, J.A., Holly, F.M., Verwey, A., 1980. Practical aspects of computational river hydraulics. Pitman Advanced Publishing Program, Boston, 420 p.

Davison, A.C., Smith, R. L., 1990. Models for exceedances over high thresholds (with discussion). Journal of the Royal Statistical Society: Series B 52, 393–442.

de Moel, H., Asselman, N.E.M., Aerts, J.C.J.H., 2012. Uncertainty and sensitivity analysis of coastal flood damage estimates in the west of the Netherlands. Nat. Hazards Earth Syst. Sci 12, 1045-1058.

de Winter, R.C., Ruessink, B.G., 2017. Sensitivity analysis of climate change impacts on dune erosion: Case study for the Dutch Holland coast. Clim. Chang., 141, 685–701, doi:10.1007/s10584-017-1922-3.

Dissanayake, P., Brown, J., Karunarathna, H., 2014. Modelling storm-induced beach/dune evolution: Sefton coast, Liverpool Bay, UK. Mar. Geol., 357, 225–242, doi:10.1016/j.margeo.2014.07.013.

Divoky, D., McDougal, W.G., 2006. Response-based coastal flood analysis, Proc.30th Int. Conf. on Coastal Engineering, ASCE, 5291-5301.

Duo, E., Trembanis, A. C., Dohner, S., Grottoli, E., Ciavola, P., 2018. Local-scale post-event assessments with GPS and UAV-based quick-response surveys: a pilot case from the Emilia–Romagna (Italy) coast. Nat. Hazards Earth Syst. Sci. 18, 2969-2989. doi:10.5194/nhess-18-2969-2018

Dupuis, D.J., 1998. Exceedances over high thresholds: a guide to threshold selection. Extremes 1 (3), 251–261.

Durán, R., Guillén, J., Ruiz, A., Jiménez, J.A., Sagristá, E., 2016. Morphological changes, beach inundation and overwash caused by an extreme storm on a low-lying embayed beach bounded by a dune system (NW Mediterranean). Geomorphology 274, 129-142, doi:10.1016/J.GEOMORPH.2016.09.012.

EC, 2007. Directive 2007/60/EC of the European Parliament and of the Council of 23 October 2007 on the assessment and management of flood risks. Official Journal of the European Union L 288 , 06/11/2007, 27-34. http://data.europa.eu/eli/dir/2007/60/oj

Egozcue, J. J., Pawlowsky-Glahn, V., Ortego, M. I. and Tolosana-Delgado, R., 2006. The effect of scale in daily precipitation hazard assessment, Nat. Hazards Earth Syst. Sci., 6(3), 459–470, doi:10.5194/nhess-6-459-2006.

Elsayed, S.M., Oumeraci, H., 2017. Effect of beach slope and grain-stabilization on coastal sediment transport: An attempt to overcome the erosion overestimation by XBeach. Coast. Eng., 121, 179–196, doi:10.1016/j.coastaleng.2016.12.009.

European Commission, 2004. Living with coastal erosion in Europe. Part I. Major Findings and Policy Recommendations of the EUROSION Project. Office for Official Publications of the European Communities, Luxembourg, 54 pp.

Ferreira, J.C., 2004. Coastal Zone Vulnerability and Risk Evaluation. A Tool For Decision-Making (An Example in the Caparica Littoral - Portugal). Journal of Coastal Research SI 39, 1590-1593.

Ferreira, Ó., Plomaritis, T.A., Costas, S., 2019. Effectiveness assessment of risk reduction measures at coastal areas using a decision support system: Findings from Emma storm. Sci. Total Environ. 657, 124–135. doi.org/10.1016/j.scitotenv.2018.11.478

Ferreira, Ó., Plomaritis, T.A., Costas, S., 2017. Process-based indicators to assess storm induced coastal hazards. Earth-Science Rev. 173, 159–167. doi.org/10.1016/J.EARSCIREV.2017.07.010

Ferreira, Ó., Viavattene, C., Jiménez, J. A., Bolle, A., Das Neves, L., Plomaritis, T. A., McCall, R., Van Dongeren, A. R., 2018. Storm-induced risk assessment: Evaluation of two tools at the regional and hotspot scale. Coastal Engineering, 134, 241-253, doi: 10.1016/j.coastaleng.2017.10.005.

Fienen, M.N., Masterson, J.P., Plant, N.G., Gutierrez, B.T., Thieler, E.R., 2013. Bridging groundwater models and decision support with a Bayesian network. Water Resour. Res. 49, 6459–6473. doi.org/10.1002/wrcr.20496

Fienen, M.N., Plant, N.G., 2015. A cross-validation package driving Netica with python. Environ. Model. Softw. 63, 14–23. doi.org/10.1016/J.ENVSOFT.2014.09.007

FLOODsite, 2009: Language of risk: Project Definitions, edited by P. Samuels and B. Gouldby, Wallingford, Oxfordshire, UK. (http:// floodsite.net/ html/partner_area /project_docs/ T32_04_01_FLOODsite_Language_of_Risk_D32_2_v5_2_P1.pdf, accessed 31 August 2017),.

Gallien, T.W., Kalligeris, N., Delisle, M.-P.C., Tang, B.-X., Lucey, J.T.D., Winters, M.A., 2018. Coastal flood modeling challenges in defended urban backshores. Geosciences, 8, 450. doi.org/10.3390/geosciences8120450

Garrity, N.J., Battalio, R., Hawkes, P.J., Roupe, D., 2006. Evaluation of the event and response approaches to estimate the 100-year coastal flood for Pacific coast sheltered waters. Proc. 30th Int. Conf. on Coastal Engineering, ASCE, 1651-1663.

General Bathymetric Chart of the Oceans (GEBCO). 2014. Available online: https://www.gebco.net (accessed on 10th February 2019).

Genest, C., Favre, A-C., 2007. Everything you always wanted to know about copula modeling but were afraid to ask. Journal of Hydrologic Engineering 12(4), 347-368.

Gieder, K.D., Karpanty, S.M., Fraser, J.D., Catlin, D.H., Gutierrez, B.T., Plant, N.G., Turecek, A.M., Robert Thieler, E., 2014. A Bayesian network approach to predicting nest presence of the federally-threatened piping plover (Charadrius melodus) using barrier island features. Ecol. Modell. 276, 38–50. doi.org/10.1016/j.ecolmodel.2014.01.005

Gomis, D., Ruiz, S., Sotillo, M. G., Alvarez-Fanjul, E., Terradas, J., 2008. Low frequency Mediterranean sea level variability: The contribution of atmospheric pressure and wind. Global Planetary Change 63, 215–229.

Guedes-Soares, C., Weisse, R., Carretero, J.C., Alvarez, E. 2002. A 40 years hindcast of wind, sea level and waves in European waters. Proc. of the 21st Int. Conf. on Offshore Mechanics and Arctic Engineering, 669–675.

Guillen, J. 2008. Els riscos litorals a Catalunya. En: Els riscos naturals a Catalunya (RISKCAT). CADS, Generalitat de Catalunya. Barcelona.

Gutierrez, B. T., Plant, N. G., Thieler, E. R., 2011. A Bayesian network to predict coastal vulnerability to sea level rise, J. Geophys. Res. Earth Surf., 116(2), 1–15, doi:10.1029/2010JF001891.

Gutierrez, B.T., Plant, N.G., Thieler, E.R., Turecek, A., 2015. Journal of Geophysical Research : Earth Surface geomorphologic characteristics 2452–2475, doi.org/10.1002/2015JF003671

Hall, J., Solomatine, D., 2008. A framework for uncertainty analysis in flood risk management decisions. International Journal of River Basin Management 6 (2), 85–98.

Hallegatte, C. Green, R.J. Nicholls, J. Corfee-Morlot, 2013. Future flood losses in major coastal cities, Nat. Clim. Chang. 3, 802–806.

Hanson, H., Aarninkhof, S., Capobianco, M., Jiménez, J.A., Larson, M., Nicholls, R.J., Plant, N.G., Southgate, H.N., Steetzel, H.J., Stive, M.J.F., de Vriend, H.J., 2003. Modelling of coastal evolution on yearly to decadal time scales. J. Coastal Research, 19, 790-811.

Hapke, C., Plant, N., 2010. Predicting coastal cliff erosion using a Bayesian probabilistic model. Mar. Geol. 278, 140–149, doi.org/10.1016/j.margeo.2010.10.001

Harley, M., Ciavola, P., 2013. Managing local coastal inundation risk using real-time forecasts and artificial dune placements, Coast. Eng., 77, 77–90, doi:10.1016/j.coastaleng.2013.02.006.

Harley, M., Armaroli, C., Ciavola, P., 2011. Evaluation of XBeach predictions for a real-time warning system in Emilia-Romagna, Northern Italy, J. Coast. Res., 64(64),

Harley, M., Valentini, A., Armaroli, C., Perini, L., Calabrese, L., Ciavola, P., 2016. Can an early-warning system help minimize the impacts of coastal storms? A case study of the 2012 Halloween storm, northern Italy, Nat. Hazards Earth Syst. Sci., 16(1), 209–222, doi:10.5194/nhess-16-209-2016.

Harley, M., 2014. DuneMaker 2.0: A MATLAB tool to simulate artificial dunes using XBeach, Unpublished, doi:10.13140/2.1.3941.7120.

Harley, M., Turner, I.L., Middleton, J.H., Kinsela, M.A., Hanslow, D., Splinter, K.D., Mumford, P., 2017. Observations of Beach Recovery in SE Australia Following the June 2016 East Coast Low, In proceedings of Australasian Coasts & Ports 2017: Working with Nature. p. 559, Australia, Cairns, 21-23 June.

Harter, C., Figlus, J., 2017. Numerical modeling of the morphodynamic response of a low-lying barrier island beach and foredune system inundated during Hurricane Ike using XBeach and CSHORE. Coast. Eng., 120, 64–74, doi:10.1016/j.coastaleng.2016.11.005.

Hastings, W. K., 1970. Monte Carlo sampling methods using Markov chains and their applications, Biometrika, Volume 57, Issue 1, Pages 97–109, doi.org/10.1093/biomet/57.1.97

Hawkes, P.J., Gouldby, B.P., Tawn, J.A., Owen, M.W., 2002. The joint probability of waves and water levels in coastal engineering design. J. Hydraul. Res. 40, 241–251. doi.org/10.1080/00221680209499940

Hedges, T.S., Reis, M.T., 1998. Random wave overtopping of simple seawalls: anew regression model, Proc. ICE Water, Maritime and Energy 130, 1-10.

Hinkel, J., Lincke, D., Vafeidis, A. T., Perrette, M., Nicholls, R. J., Tol, R. S., Marzeion, B., Fettweis, X., Ionescu, C., Levermann, A., 2014. Coastal flood damage and adaptation costs under 21st century sea-level rise. Proceedings of the National Academy of Sciences, 111(9), 3292-3297.

Hinkel, J., Jaeger, C., Nicholls, R.J., Lowe, J., Renn, O., Peijun, S., 2015. Sea-level rise scenarios and coastal risk management. Nat. Clim. Chang., 5, 188, doi:10.1038/nclimate2505.

Ibàñez, J.J., Burriel, J.A., 2010. Mapa de cubiertas del suelo de Cataluña: características de la tercera edición y relación con SIOSE. Tecnologías de la Información Geográfica: La Información Geográfica al servicio de los ciudadanos 3, 179–198.

IDESCAT, 2014. Anuari Estadístic de Catalunya. Generalitat de Catalunya.

IDROSER, 1996. Progetto di Piano per la difesa del mare e la riqualificazione ambientale del litorale della Regione Emilia-Romagna, Bologna, Italy.

IPCC, 2012: Climate Change 2012. Managing the risks of extreme events and disasters to advance climate change adaptation. A Special Report of Working Groups I and II of the Intergovernmental Panel on Climate Change, edited by C. B. Field, V. Barros, T. F. Stocker, D. Qin, D. J. Dokken, K. L. Ebi, M. D. Mastrandrea, K. J. Mach, G.-K. Plattner, S. K. Allen, M. Tignor, P. M. Midgley, Cambridge University Press, Cambridge, UK and New York, NY, USA., 2012.

IPCC, 2013: Climate Change 2013. The Physical Science Basis. Contribution of Working Group I to the Fifth Assessment Report of the Intergovernmental Panel on Climate Change, edited by T. F. Stocker, D. Qin, G.-K. Plattner, M. Tignor, S. K. Allen, J. Boschung, A. Nauels, Y. Xia, V. Bex, P. M. Midgley, Cambridge University Press, Cambridge, United Kingdom and New York, NY, USA., 2013.

IPCC, 2014: Climate Change 2014. Synthesis Report. Contribution of Working Groups I, II and III to the Fifth Assessment Report of the Intergovernmental Panel on Climate Change [Core Writing Team, R.K. Pachauri, L.A. Meyer (eds.)]. IPCC, Geneva, Switzerland, 151 pp.

Jäger, W. S., Christie, E. K., Hanea, A. M., den Heijer, C., Spencer, T., 2018. A Bayesian network approach for coastal risk analysis and decision making, Coast. Eng., 134, 48-61, doi:10.1016/j.coastaleng.2017.05.004.

Jensen, F. V., 1996. An introduction to Bayesian networks, UCL Press, London, UK.

Jiménez, J. A., Gracia, V., Valdemoro, H. I., Mendoza, E. T., Sánchez-Arcilla, A., 2011. Managing erosion-induced problems in NW Mediterranean urban beaches, Ocean Coast. Manag., 54(12), 907–918, doi:10.1016/j.ocecoaman.2011.05.003.

Jiménez, J. A., Sancho-García, A., Bosom, E., Valdemoro, H. I., Guillén, J., 2012. Storm-induced damages along the Catalan coast (NW Mediterranean) during the period 1958–2008, Geomorphology, 143–144, 24–33, doi:10.1016/j.geomorph.2011.07.034, 2012.

Jiménez, J. A., Sanuy, M., Ballesteros, C., Valdemoro, H. I., 2018. The Tordera Delta, a hotspot to storm impacts in the coast northwards of Barcelona (NW Mediterranean). Coast. Eng. 134, 148-158. doi:10.1016/j.coastaleng.2017.08.012, 2018.

Jiménez, J. A., Valdemoro, H. I., Bosom, E., Sánchez-Arcilla, A., Nicholls, R. J., 2017. Impacts of sea-level rise-induced erosion on the Catalan coast, Reg. Environ. Chang., 17(2), 593–603, doi:10.1007/s10113-016-1052-x.

Jiménez, J. A. 2012. Characterizing Sant Esteve's storm (26th December 2008) along the Catalan coast (NW Mediterranean). In: Mateo M, Garcia-Rubies A (Eds). Assessment of the ecological impact of the extreme storm of Sant Esteve's Day (26 December 2008) on the littoral ecosystems of the north Mediterranean Spanish coasts. Final Report (PIEC 200430E599) Centro de Estudios Avanzados de Blanes, CSIC, Blanes, 31–44.

Jiménez, J.A., Valdemoro, H.I., 2019. Shoreline evolution and its management implications in beaches along the Catalan coast. In: Morales, J.A. (ed), The Spanish Coastal Systems Dynamic Processes, Sediments and Management, Springer, 745-764.

Jiménez, J. A., Valdemoro, H.I., Sánchez-Arcilla, A. 2016. Medidas de protección en la costa del Delta de la Tordera – Malgrat de Mar-. Technical Report, Laboratori d'Enginyeria Marítima, Barcelona.

Jiménez, J. A., Plana, A., Sanuy, M., Ruiz, A., 2014. Morphodynamic impact of an extreme storm on a cuspate deltaic shoreline. In Proceedings of the 34th International Costal Engineering Conference (2014 ASCE), Seoul, Korea, 15–20 June.

Johnson, J.M., Moore, L.J., Ells, K., Murray, A.B., Adams, P.N., MacKenzie, R.A., III, Jaeger, J.M., MacKenzie, R.A., Jaeger, J.M., 2015. Recent shifts in coastline change and shoreline stabilization linked to storm climate change. Earth Surf. Process. Landf., 40, 569–585, doi:10.1002/esp.3650.

Jongman, B., Ward, P. J., & Aerts, J. C., 2012. Global exposure to river and coastal flooding: Long term trends and changes. Global Environmental Change, 22(4), 823-835.

Kolen, B., Slomp, R., Jonkman, S. N., 2013. The impacts of storm Xynthia February 27-28, 2010 in France: Lessons for flood risk management, J. Flood Risk Manag., 6(3), 261–278, doi:10.1111/jfr3.12011.

Komen, G.J., Hasselmann, K., Hasselmann, K., 1984. On the Existence of a Fully Developed Wind-Sea Spectrum. J. Phys. Oceanogr., 14, 1271–1285, doi:10.1175/1520-0485(1984)014<1271:OTEOAF>2.0.CO,2.

Kraus, N.C., McDougal, W.G., 1996. The Effects of Seawalls on the Beach: Part I, an Updated Literature Review. J. Coast. Res., 12, 691–701.

Kriebel, D.L., Dean, R.G., 1993. Convolution method for time-dependent beach-profile response. Journal of Waterway, Port, Coastal, and Ocean Engineering, 119(2), pp.204-226. doi.org/10.1061/(ASCE)0733-950X(1993)119:2(204)

Kron, W. 2013. Coasts: the high-risk areas of the world. Natural Hazards 66, 1363–1382. doi:10.1007/s11069-012-0215-4

Kunz, M., Mühr, B., Kunz-Plapp, T., Daniell, J. E., Khazai, B., Wenzel, F., Vannieuwenhuyse, M., Comes, T., Elmer, F., Schröter, K., Fohringer, J., Münzberg, T., Lucas, C., Zschau, J., 2013. Investigation of superstorm Sandy 2012 in a multi-disciplinary approach, Nat. Hazards Earth Syst. Sci., 13(10), 2579–2598, doi:10.5194/nhess-13-2579-2013.

La Caixa. 2013. Anuario Económico de España, Caja de Ahorros y Pensiones de Barcelona, Barcelona.

Larson, M., Kraus, N.C., 1989. SBEACH. Numerical model for simulating storm-induced beach change, Report 1: Empirical foundation and model development. Tech. Rep. CERC (US Army Eng. Waterw. Exp. Stn. Coast. Eng. Res. Center). https://apps.dtic.mil/dtic/tr/fulltext/u2/a212212.pdf

Laudier, N.A., Thornton, E.B., MacMahan, J., 2011. Measured and modeled wave overtopping on a natural beach. Coast. Eng., 58, 815-825.

Lauritzen, S. L., Spiegelhalter, D. J., 1988. Local Computations with Probabilities on Graphical Structures and Their Application to Expert Systems, J. R. Stat. Soc. B, 50(2), 157–224.

Le Cozannet G, Garcin M, Yates M, Idier D, Meyssignac B, 2014. Approaches to evaluate the recent impacts of sea-level rise on shoreline changes. Earth Sci Rev, 138: 47-60. doi:10.1016/j.earscirev.2014.08.005

Lesser, G. R., Roelvink, J. V., Van Kester, J. A. T. M., Stelling, G. S., 2004. Development and validation of a three-dimensional morphological model. Coastal engineering, 51(8-9), 883-915.

Li, F., Gelder, P.H.A.J.M. va., Vrijling, J.K., Callaghan, D.P., Jongejan, R.B., Ranasinghe, R., 2014. Probabilistic estimation of coastal dune erosion and recession by statistical simulation of storm events. Appl. Ocean Res. 47, 53–62. doi.org/10.1016/j.apor.2014.01.002

Lin-Ye, J., Garcia-Leon, M., Gracia, V., Sanchez-Arcilla, A., 2016. A multivariate statistical model of extreme events: An application to the Catalan coast. Coast. Eng. 117, 138–156. doi.org/10.1016/j.coastaleng.2016.08.002

Lionello, P., Boldrin, U., Giorgi, F., 2008. Future changes in cyclone climatology over Europe as inferred from a regional climate simulation, Clim. Dyn., 30(6), 657–671, doi:10.1007/s00382-007-0315-0.

López-Dóriga, U., Jiménez, J.A., Bisaro, A., Hinkel, J., 2019. Financing and implementation of adaptation measures to climate change along the Spanish coast (in review).

López Royo, M., Ranasinghe, R., Jiménez, J.A., opez Royo, M., 2016. A Rapid, Low-Cost Approach to Coastal Vulnerability Assessment at a National Level. Source J. Coast. Res. 32, 932–945. doi.org/10.2112/JCOASTRES-D-14-00217.1

Luijendijk, A., Hagenaars, G., Ranasinghe, R., Baart, F., Donchyts, G., Aarninkhof, S., 2018. The state of the world's beaches. Scientific reports, 8(1), 6641.

Marcos, M., Chust, G., Jordà, G., Caballero, A., 2012. Effect of sea level extremes on the western Basque coast during the 21st century. Climate Research, 51(3), 237-248.

Martinez, G., Armaroli, C., Costas, S., Harley, M. D. Paolisso, M., 2018. Experiences and results from interdisciplinary collaboration: Utilizing qualitative information to formulate disaster risk reduction measures for coastal regions, Coast. Eng., 134, 62-72, doi:10.1016/j.coastaleng.2017.09.010.

Martín-Vide, J., Llasat, M.C., 2000. Las Precipitaciones Torrenciales en Cataluña. Serie Geográfica, Volume 9, pp. 17–26.

Masina, M., Lamberti, A., Archetti, R., 2015. Coastal flooding: A copula based approach for estimating the joint probability of water levels and waves. Coast. Eng. 97, 37–52. doi.org/10.1016/j.coastaleng.2014.12.010

Mather, A., Stretch, D., Garland, G., 2011. Predicting extreme wave run-up on natural beaches for coastal planning and management. Coast. Eng .53(2), 87-109.

Mathiesen, M., Goda, Y., Hawkes, P. J., Mansard, E., Martín, M. J., Peltier, E., Thompson, E. F. and Van Vledder, G., 1994. Recommended practice for extreme wave analysis. J. Hydraul. Res. 32(6), 803–814. doi:10.1080/00221689409498691

McCall, R.T., Van Thiel de Vries, J.S.M., Plant, N.G., Van Dongeren, A.R., Roelvink, J.A., Thompson, D.M., Reniers, A.J.H.M., 2010. Two-dimensional time dependent hurricane overwash and erosion modeling at Santa Rosa Island. Coast. Eng. 57, 668–683. doi.org/10.1016/j.coastaleng.2010.02.006

Mendoza, E.T., 2008. Coastal vulnerability to storms in the Catalan coast. Universitat Politècninca de Catalunya, PhD thesis.,150p. http://www.tdx.cat/TDX-0414108-122517/

Mendoza, E.T., Jiménez, J.A., 2008. Clasificación de tormentas costeras para el litoral catalán (Mediterráneo NO), Ing. Hidr. en México, (2), 23–34.

Mendoza, E.T., Jiménez, J.A. 2006. Storm-Induced Beach Erosion Potential on the Catalonian Coast. Journal of Coastal Research SI 48, 81-88.

Mendoza, E.T., Jiménez, J.A., Mateo, J., 2011. A coastal storms intensity scale for the Catalan sea (NW Mediterranean). Nat. Hazards Earth Syst. Sci. 11, 2453–2462. doi.org/10.5194/nhess-11-2453-2011

Menéndez, M., García-Díez, M., Fita, L., Fernández, J., Méndez, F. J., Gutiérrez, J. M., 2014. High-resolution sea winds hindcasts over the Mediterranean area, Clim Dyn, 42(7-8):1857-1872.

Merz, B., Thieken, A., Gocht, M., 2007.Flood Risk Mapping at the Local Scale: Concepts and Challenges. In Flood Risk Management in Europe. Advances in Natural and Technological Hazards Research, Begum, S., Stive, M.J.F., Hall, J.W., Eds., Springer: Dordrecht, The Netherlands, Volume 25, doi:10.1007/978-1-4020-4200-3_13.

Mortlock, T.R., Goodwin, I.D., McAneney, J.K., Roche, K., 2017. The June 2016 Australian East Coast Low: Importance of wave direction for coastal erosion assessment. Water, 9, 121, doi:10.3390/w9020121.

Musić, S., Nicković, S. 2008. 44-year wave hindcast for the Eastern Mediterranean. Coastal Engineering 55, 872–880.

Narayan, S., Nicholls, R. J., Clarke, D., Hanson, S., Reeve, D., Horrillo-Caraballo, J., le Cozannet, G., Hissel, F., Kowalska, B., Parda, R., Willems, P., Ohle, N., Zanuttigh, B., Losada, I., Ge, J., Trifonova, E., Penning-Rowsell, E., Vanderlinden, J. P., 2014. The SPR systems model as a conceptual foundation for rapid integrated risk appraisals: Lessons from Europe, Coast. Eng., 87, 15–31, doi:10.1016/j.coastaleng.2013.10.021.

Nielsen, A.F., Adamantidis, C.A., 2007. Defining the Storm Erosion Hazard for Beaches. Aust. J. Civ. Eng. 3, 39–50. doi.org/10.1080/14488353.2007.11463920

Nordstrom, K. F., Armaroli, C., Jackson, N. L., Ciavola, P., 2015. Opportunities and constraints for managed retreat on exposed sandy shores: Examples from Emilia-Romagna, Italy, Ocean Coast. Manag., 104, 11–21, doi:10.1016/j.ocecoaman.2014.11.010.

Oumeraci, H., Kortenhaus, A., Burzel, A., Naulin, M., Dassanayake, D. R., Jensen, J., Wahl, T., Mudersbach, C., Gönnert, G., Gerkensmeier, B., Fröhle, P., Ujeyl, G., 2015. XtremRisK — Integrated Flood Risk Analysis for Extreme Storm Surges at Open Coasts and in Estuaries: Methodology, Key Results and Lessons Learned, Coast. Eng. J., 57(1), 1540001, doi:10.1142/S057856341540001X.

Pagès, J.F., Gera, A., Romero, J., Farina, S., Garcia-Rubies, A., Hereu, B., Alcoverro, T., 2013. The Mediterranean Benthic Herbivores Show Diverse Responses to Extreme Storm Disturbances. PLoS ONE, 8, e62719, doi:10.1371/journal.pone.0062719.

Pallares, E., Sánchez-Arcilla, A., Espino, M., 2014. Wave energy balance in wave models (SWAN) for semi-enclosed domains-Application to the Catalan coast. Cont. Shelf Res., 87, 41–53, doi:10.1016/j.csr.2014.03.008.

Palmsten, M.L., Todd Holland, K., Plant, N.G., 2013. Velocity estimation using a Bayesian network in a critical-habitat reach of the Kootenai River, Idaho. Water Resour. Res. 49, 5865–5879. doi.org/10.1002/wrcr.20361

Passeri, D.L., Bilskie, M.V., Plant, N.G., Long, J.W., Hagen, S.C., 2018. Dynamic modeling of barrier island response to hurricane storm surge under future sea level rise. Climatic Change 149(3-4), 413-425. doi.org/10.1007/s10584-018-2245-8

Pearl, J., 1988. Probabilistic reasoning in intelligent systems: networks of plausible inference, Morgan Kaufmann, San Francisco, California, USA.

Penning-Rowsell, E. C., De Vries, W. S., Parker, D. J., Zanuttigh, B., Simmonds, D., Trifonova, E., Hissel, F., Monbaliu, J., Lendzion, J., Ohle, N., Diaz, P. Bouma, T., 2014. Innovation in coastal risk management: An exploratory analysis of risk governance issues at eight THESEUS study sites, Coast. Eng., 87, 210–217, doi:10.1016/j.coastaleng.2013.12.005.

Penning-Rowsell, E. C., Priest, S. J., Parker, D. J., Morris, J., Tunstall, S. M., Viavattene, C., Chatterton, J., Owen, D., 2013. Flood and coastal erosion risk management: a manual for economic appraisal. Routledge, Taylor & Francis, London.

Perini, L., Calabrese, L., Deserti, M., Valentini, A., Ciavola, P., Armaroli, C., 2011. Le mareggiate e gli impatti sulla costa in Emilia-Romagna 1946-2010, ARPA Emilia-Romagna, Bologna, Italy.

Perini, L., Calabrese, L., Lorito, S., Luciani, P., 2015. Costal flood risk in Emilia-Romagna (Italy): the sea storm of February 2015, in Coastal and Maritime Mediterranean Conference, Edition 3, Ferrara, Italy (2015), pp. 225–230.

Perini, L., Calabrese, L., Salerno, G., Ciavola, P., Armaroli, C., 2016. Evaluation of coastal vulnerability to flooding: comparison of two different methodologies adopted by the Emilia-Romagna region (Italy), Nat. Hazards Earth Syst. Sci., 16(1), 181–194, doi:10.5194/nhess-16-181-2016.

Plana-Casado, A., 2013. Storm-Induced Changes in the Catalan Coast Using Lidar: The St. Esteve Storm (26/12/2008) Case. Master's Thesis, Faculty of Civil Engineering, Universitat Politècnica de Catalunya, Barcelona, Spain. Available online: http://hdl.handle.net/2099.1/23343 (accessed on 5th December 2016).

Plant, N. G., J. Flocks, H. F. Stockdon, J. W. Long, K. K. Guy, D. M. Thompson, J. M. Cormier, C. G. Smith, J. L. Miselis,, P. S. Dalyander, 2014. Predictions of barrier island berm evolution in a time-varying storm climatology, Journal of Geophysical Research F: Earth Surface, 119(2), 300-316.

Plant, N. G., Robert Thieler, E., & Passeri, D. L.., 2016. Coupling centennial-scale shoreline change to sea-level rise and coastal morphology in the Gulf of Mexico using a Bayesian network. Earth's Future, 4(5), 143-158.

Plant, N.G., Stockdon, H.F., 2015. How well can wave runup be predicted? Comment on Laudier et al. (2011) and Stockdon et al. (2006). Coast. Eng. 102, 44–48. doi.org/10.1016/j.coastaleng.2015.05.001

Plomaritis, T.A., Costas, S., Ferreira, Ó., 2018. Use of a Bayesian Network for coastal hazards, impact and disaster risk reduction assessment at a coastal barrier (Ria Formosa, Portugal). Coast. Eng. 134, 134–147. doi.org/10.1016/j.coastaleng.2017.07.003

Poelhekke, L., Jäger, W.S., van Dongeren, A., Plomaritis, T.A., McCall, R., Ferreira, Ó., 2016. Predicting coastal hazards for sandy coasts with a Bayesian Network. Coast. Eng. 118, 21–34. doi.org/10.1016/j.coastaleng.2016.08.011

Preciso, E., Salemi, E., Billi, P., 2012. Land use changes, torrent control works and sediment mining: Effects on channel morphology and sediment flux, case study of the Reno River (Northern Italy), Hydrol. Process., 26(8), 1134–1148, doi:10.1002/hyp.8202.

Priest, S., Wilson, T., Tapsell, S., Penning-Rowsell, E., Viavattene, C., Fernandez-Bilbao, A., 2007. Building a Model to Estimate Risk to Life for European Flood Events – Final Report, FLOODsite project report T10-07-10, HR Wallingford, UK.

Prime, T., Brown, J. M., Plater, A. J., 2016. Flood inundation uncertainty: The case of a 0.5% annual probability flood event, Environ. Sci. Policy, 59, 1–9, doi:10.1016/j.envsci.2016.01.018,.

Puertos del Estado, 2006. Extremos Máximos de Oleaje (Altura Significante). Boya de Palamós. Available online: http://www.puertos.es/es-es/oceanografia/Paginas/portus.aspx (accessed on 8th February 2019). Madrid.

Pullen, T., Allsop, N.W.H., Bruce, T., Kortenhaus, A., Schüttrumpf, H., van der Meer, J.W. 2007. EurOtop. Wave overtopping of sea defences and related structures: Assessment manual. www.overtopping-manual.com.

Purvis, M.J., Bates, P.D., Hayes, C.M., 2008. A probabilistic methodology to estimate future coastal flood risk due to sea level rise. Coast. Eng. 55, 1062–1073. doi.org/10.1016/j.coastaleng.2008.04.008

Ranasinghe, R., 2016. Assessing climate change impacts on open sandy coasts: A review. Earth-Sci. Rev, 160, 320–332, doi:10.1016/j.earscirev.2016.07.011.

Ranasinghe, R., Callaghan, D., 2017. Assessing Storm Erosion Hazards, in: Ciavola, P., Coco, G. (Eds.), Coastal Storms: Processes and Impacts. John Wiley & Sons Ltd., pp. 241–256.

Ranasinghe, R., Callaghan, D., Stive, M.J.F., 2012. Estimating coastal recession due to sea level rise: beyond the Bruun rule. Clim. Change 110, 561–574. doi.org/10.1007/s10584-011-0107-8

Rangel-Buitrago, N., Anfuso, G. 2015. Review of the Existing Risk Assessment Methods. In: Risk Assessment of Storms in Coastal Zones: Case Studies from Cartagena (Colombia) and Cadiz (Spain), Springer International Publishing, pp. 7-13.

Ratsimandresy, A.W., Sotillo, M.G., Carretero Albiach, J.C., Álvarez Fanjul, E., Hajji, H. 2008. A 44-year high-resolution ocean and atmospheric hindcast for the Mediterranean Basin developed within the HIPOCAS Project. Coastal Engineering 55, 827-842.

Regione Emilia-Romagna, 2010. Servizio Geologico Sismico e dei Suoli: Il sistema mare-costa dell'Emilia-Romagna, edited by: Perini, L., Calabrese, L., Pendragon Monographies, Bologna, 240 pp.

Reguero, B. G., Menéndez, M., Méndez, F. J., Mínguez, R., Losada, I. J., 2012. A Global Ocean wave (GOW) calibrated reanalysis from 1948 onwards, Coast Eng 65:38-55. doi.org/10.1016/j.coastaleng.2012.03.003

Reis, M.T., Hu, K., Hedges, T.S., Mase, H., 2008. A comparison of empirical, semi empirical, and numerical wave overtopping models. Journal of Coastal Research 24, 250–262. doi.org/10.2112/05-0592.1

Reyes, J. L., Martins, J. T., Benavente, J., Ferreira, O., Gracia, F. J., Alveirinho-Dias, J. M., & López-Aguayo, F., 1999. Gulf of Cadiz beaches: a comparative response to storm events. Boletín-Instituto Español de Oceanografía, 15(1/4), 221-228.

Ris, R.C., Holthuijsen, L.H., Booij, N., 1999 A third-generation wave model for coastal regions: Verification. J. Geophys. Res., 104, 7667–7681, doi:10.1029/1998JC900123.

Rodrıguez-Ramırez, A., Ruiz, F., Cáceres, L. M., Vidal, J. R., Pino, R., & Muñoz, J. M., 2003. Analysis of the recent storm record in the southwestern Spanish coast: implications for littoral management. Science of the Total Environment, 303(3), 189-201.

Roelvink, D., Reniers, A., 2012. A guide to modeling coastal morphology. World Scientific Publishing Co. Pte. Ltd. doi.org/10.1142/9789814304269

Roelvink, D., Reniers, A., van Dongeren, A., van Thiel de Vries, J., McCall, R., Lescinski, J., 2009. Modelling storm impacts on beaches, dunes and barrier islands. Coast. Eng. 56, 1133–1152. doi.org/10.1016/j.coastaleng.2009.08.006

Roelvink, D., Stelling, G., Hoonhout, B., Risandi, J., Jacobs, W., Merli, D., 2012. Development and Field Validation of a 2Dh Curvilinear Storm Impact Model. Coast. Eng., 1, 120, doi:10.9753/icce.v33.sediment.120.

Ruggiero, P., Holman, R. A., Beach, R. A., 2004. Wave run-up on a high-energy dissipative beach, J. Geophys. Res., 109(C6), C06025, doi:10.1029/2003JC002160.

Ruiz, A., Kornus, W., Talaya, J., 2009. Coastal applications of Lidar in Catalonia. In Proceedings of the 6th European Congress on Regional Geoscientific Cartography and Information Systems, Munich, Germany, 9–12 June.

Sallenger, A.H., 2000. Storm impact scale for Barrier Islands. Journal of coastal research, 16(3), pp.890-895.

Sánchez-Arcilla, A., Mendoza, E.T., Jiménez, J.A., Peña, C., Galofré, J., Novoa, M., 2009. Beach Erosion and Storm Parameters: Uncertainties for the Spanish Mediterranean., in: McKee Smith, J. (Ed.), Coastal Engineering 2008 Proceedings of the 31st International Conference Hamburg, Germany, 31 August – 5 September 2008. World Scientific, pp. 2352–2362. doi.org/10.1142/9789814277426_0194

Sánchez-Arcilla, A., González-Marco, D., Bolaños, R., 2008. A review of wave climate and prediction along the Spanish Mediterranean coast. Nat. Hazards Earth Syst. Sci. 2008, 8, 1217–1228, doi:10.5194/nhess-8-1217-.

Sánchez-García E., 2019. Phtogrammetry and image processing techniques for beach monitoring. Universitat Politècnicna de València, PhD Thesis (April 2019).

Sánchez-Vidal, A., Canals, M., Calafat, A.M., Lastras, G., Pedrosa-Pàmies, R., Menéndez, M., Medina, R., Hereu, B., Romero, J., Alcoverro, T. 2012. Impacts on the deep-sea ecosystem by a severe coastal storm. PLoS One 7(1), p.e30395.

Sano, M., Jiménez, J.A., Medina, R., Stanica, A., S-Arcilla, A., Trumbic, I. 2011. The role of coastal setbacks in the context of coastal erosion and climate change. Ocean & Coastal Management 54, 943-950.

Sanuy, M., Jiménez, J.A., 2019. Sensitivity of Storm-Induced Hazards in a Highly Curvilinear Coastline to Changing Storm Directions. The Tordera Delta Case (NW Mediterranean). Water, 11, 747.

Sanuy, M., Duo, E., Jäger, W.S., Ciavola, P., Jiménez, J.A., 2018. Linking source with consequences of coastal storm impacts for climate change and risk reduction scenarios for Mediterranean sandy beaches. Nat. Hazards Earth Syst. Sci. 18, 1825–1847. doi.org/10.5194/nhess-18-1825-2018

Sanuy M, Jiménez JA, Ortego MI, Toimil A., 2019. Differences in assigning probabilities to coastal inundation hazard estimators: Event versus response approaches. J Flood Risk Management, e12557. doi.org/10.1111/jfr3.12557

Sardá, R., Conde, R., Casadesús, M., Sánchez, A., Pablo, J., 2013. Erosión en las playas y gestión desintegrada: la problemática actual de la playa de S'Abanell, in Hacia un nuevo modelo integral de gestión de playas, pp. 51–71, Documenta Universitaria, Girona.

Sardá, R., Valls, J.F., Pintó, J., Ariza, E., Lozoya, J.P., Fraguell, R.M., Martí, C., Rucabado, J., Ramis, J., Jiménez, J.A. 2015. Towards a new integrated beach management system: The Ecosystem-Based Management System for beaches. Ocean & Coastal Management 118, 167-177.

Sayers, P.B., Gouldby, B.P., Simm, J.D., Meadowcroft, I., Hall, J., 2003. Risk, Performance and Uncertainty in Flood and Coastal Defence – A Review. Defra R&D Technical Report FD2302/TR1.

Sayers, P.B., Hall, J.W., Meadowcroft, I.C., 2002. Towards risk-based flood hazard management in the UK. Proc. Inst. Civ. Eng. - Civ. Eng. 150, 36–42. doi.org/10.1680/cien.2002.150.5.36

Scorzini, A. R., Frank, E., 2015. Flood damage curves: New insights from the 2010 flood in Veneto, Italy, J. Flood Risk Manag., 1–12, doi:10.1111/jfr3.12163.

Silva, 2019. Coastal Hazard Assessments for Sandy Coasts: Appraisal of Five Methodologies. J. Coast. Res. doi.org/10.2112/JCOASTRES-D-18-00083.1

Simmons, J.A., Harley, M.D., Marshall, L.A., Turner, I.L., Splinter, K.D., Cox, R.J., 2017. Calibrating and assessing uncertainty in coastal numerical models. Coast. Eng. 125, 28–41. doi.org/10.1016/J.COASTALENG.2017.04.005

Slott, J.M., Murray, A.B., Ashton, A.D., 2006. Crowley, T.J. Coastline responses to changing storm patterns. Geophys. Res. Lett., 33, 1–6, doi:10.1029/2006GL027445.

Somot, S., Jordà, G., Harzallah, A., Darmaraki, S., 2019. Sub-chapter 1.2.3. The Mediterranean Sea in the future climate projections In : The Mediterranean region under climate change : A scientific update [en ligne]. Marseille : IRD Éditions, 2016 (généré le 27 mars 2019). Disponible sur Internet : <http://books.openedition.org/irdeditions/23100>. ISBN : 9782709922203. DOI : 10.4000/books.irdeditions.23100.

Sotillo, M. G., Ratsimandresy, A. W., Carretero, J. C., Bentamy, A., Valero, F., Gonzalez-Rouco, F. 2005. A high-resolution 44-year atmospheric hindcast for the Mediterranean Basin: contribution to the regional improvement of global reanalysis. Climate Dynamics 25, 219–236.

Soulsby, R.L., 1997. Dynamics of Marine Sands, Thomas Telford: London, UK.

Spencer, T., Brooks, S. M., Evans, B. R., Tempest, J. A., Möller, I., 2015. Southern North Sea storm surge event of 5 December 2013: Water levels, waves and coastal impacts, Earth-Science Rev., 146, 120–145, doi:10.1016/j.earscirev.2015.04.002.

Stephens, M. A., 1977. Goodness of fit for the extreme value distribution, Biometrika, Volume 64, Issue 3, Pages 583–588, doi.org/10.1093/biomet/64.3.583

Stockdon, H. F., Sallenger, A. H., Holman, R. A., Howd, P. A., 2007. A simple model for the spatially-variable coastal response to hurricanes, Mar. Geol., 238(1–4), 1–20, doi:10.1016/J.MARGEO.2006.11.004.

Stockdon, H.F., Holman, R.A., Howd, P.A., Sallenger, A.H., 2006. Empirical parameterization of setup, swash, and runup. Coast. Eng. 53, 573–588. doi.org/10.1016/j.coastaleng.2005.12.005

Straub, D., 2005. Natural hazards risk assessment using Bayesian networks. 9th Int. Conf. Struct. Saf. Reliab. ICOSSAR 05 Rome Italy 2509–2516.

Sutherland, J., Peet, A., Soulsby, R. 2004. Evaluating the performance of morphological models. Coastal Engineering 51(8), 917-939. doi:10.1016/j.coastaleng.2004.07.015.

Sytnik, O., Stecchi, F., 2014. Disappearing coastal dunes: tourism development and future challenges, a case-study from Ravenna, Italy, J. Coast. Conserv., 19(5), 715–727, doi:10.1007/s11852-014-0353-9.

Tapsell, S.M., Penning-Rowsell, E.C., Tunstall, S.M., Wilson, T.L. 2002. Vulnerability to flooding: health and social dimensions. Phil Trans R Soc Lond A 360, 1511-1525.

Taramelli, A., Di Matteo, L., Ciavola, P., Guadagnano, F., Tolomei, C., 2015. Temporal evolution of patterns and processes related to subsidence of the coastal area surrounding the Bevano River mouth (Northern Adriatic) - Italy, Ocean Coast. Manag., 108, 74–88, doi:10.1016/j.ocecoaman.2014.06.021.

Tarantola, A., 2006. Elements for physics: Quantities, qualities, and intrinsic theories, Springer-Verlag, Berlin Heidelberg, doi:10.1007/978-3-540-31107-2.

Teixidó, N., Casas, E., Cebrián, E., Linares, C., Garrabou, J., 2013. Impacts on Coralligenous Outcrop Biodiversity of a Dramatic Coastal Storm. PLoS ONE, 8, e53742, doi:10.1371/journal.pone.0053742.

Toimil, A., Losada, I. J., Díaz-Simal, P., Izaguirre, C., Camus, P., 2017. Multi-sectoral, high-resolution assessment of climate change consequences of coastal flooding, Clim Change 145:431-444.

Tolman, H., Balasubramaniyan, B., Burroughs, L., Chalikov, D., Chao, Y., Chen, H., Gerald, V., 2002. Development and implementation of wind generated ocean surface wave models at NCEP. Weather and Forecasting 17, 311–333.

Tomás, A., Méndez, F. J., Medina, R., Jaime, F. F., Higuera, P., Lara, J. L., Ortiz, M. D., Álvarez de Eulate, M. F., 2016. A methodology to estimate wave-induced coastal flooding hazard maps in Spain, J. Flood Risk Manag., 9(3), 289–305, doi:10.1111/jfr3.12198.

Trigo, I. F., Bigg, G. R., Davies, T. D., 2002. Climatology of Cyclogenesis Mechanisms in the Mediterranean, Mon. Weather Rev., 130(3), 549–569, doi:10.1175/1520-0493(2002)130<0549:COCMIT>2.0.CO,2.

TU Delft, 2016. SWAN Simulating Waves Nearshore. Available online: http://www.swan.tudelft.nl/ (accessed on 13th April 2016).

UNEP/MAP/PAP, 2008. Protocol on Integrated Coastal Zone Management in the Mediterranean. Priority Actions Programme, Split.

Uusitalo, L., 2007. Advantages and challenges of Bayesian networks in environmental modelling. Ecol. Modell. 203, 312–318. doi.org/10.1016/j.ecolmodel.2006.11.033

Valchev, N., Eftimova, P., Andreeva, N., 2018. Implementation and validation of a multi-domain coastal hazard forecasting system in an open bay. Coast. Eng., 134, 212–228, doi:10.1016/j.coastaleng.2017.08.008.

Valdemoro, H.I., Jiménez, J.A., 2016. The Influence of Shoreline Dynamics on the Use and Exploitation of Mediterranean Tourist Beaches. Coastal Management, 34, 405-423.

Van Dongeren, A., Ciavola, P., Martinez, G., Viavattene, C., Bogaard, T., Ferreira, O., Higgins, R., McCall, R., 2018. Introduction to RISC-KIT: Resilience-increasing strategies for coasts. Coastal Engineering 134, 2-9, doi.org/10.1016/j.coastaleng.2017.10.007.

Van Dongeren, A., Roelvink, D., McCall, R., Neferhoff, K., van Rooijen, A., 2017. Modeling the morphological impacats of coastal storms. In Coastal Storms, Ciavola, P., Coco, G., Eds., John Wiley & Sons Ltd.: Hoboken, NJ, USA, pp. 195–216.

Van Verseveld, H. C. W., Van Dongeren, A. R., Plant, N. G., Jäger, W. S., den Heijer, C., 2015. Modelling multi-hazard hurricane damages on an urbanized coast with a Bayesian Network approach, Coast. Eng., 103, 1–14, doi:10.1016/j.coastaleng.2015.05.006.

Viavattene, C., Jiménez, J.A., Ferreira, O., Priest, S., Owen, D., McCall, R., 2018. Selecting coastal hotspots to storm impacts at the regional scale: a Coastal Risk Assessment Framework. Coast. Eng. 134, 33–47. doi.org/10.1016/j.coastaleng.2017.09.002

Vila, I., Serra, J., 2015. Tordera River Delta system build up (NE Iberian Peninsula): Sedimentary sequences and offshore correlation. Sci. Mar., 79, 305–317, doi:10.3989/scimar.04188.07A.

Villatoro, M., Silva, R., Méndez, F.J., Zanuttigh, B., Pan, S., Trifonova, E., Losada, I.J., Izaguirre, C., Simmonds, D., Reeve, D.E., Mendoza, E., Martinelli, L., Formentin, S.M., Galiatsatou, P., Eftimova, P., 2014. An approach to assess flooding and erosion risk for open beaches in a changing climate. Coast. Eng. 87, 50–76. doi.org/10.1016/j.coastaleng.2013.11.009

Vojinovic, Z., Abebe, Y., Sanchez, A., Medina Pena, N., Nikolic, I., Monojlovic, N., Makropoulos, C., Pelling, M., Abbott, M., 2014. Holistic flood risk assessment in coastal areas - the PEARL approach, in 11th International Conference on Hydroinformatics, pp. 1–8, CUNY Academic Works, New York City, USA..

Vousdoukas, M. I., Mentaschi, L., Voukouvalas, E., Verlaan, M., Jevrejeva, S., Jackson, L. P., & Feyen, L., 2018a. Global probabilistic projections of extreme sea levels show intensification of coastal flood hazard. Nature communications, 9(1), 2360.

Vousdoukas, M. I., Voukouvalas, E., Annunziato, A., Giardino, A., Feyen, L., 2016. Projections of extreme storm surge levels along Europe, Clim. Dyn., 1–20, doi:10.1007/s00382-016-3019-5.

Vousdoukas, M.I., Bouziotas, D., Giardino, A., Bouwer, L.M., Mentaschi, L., Voukouvalas, E., Feyen, L., 2018b. Understanding epistemic uncertainty in large-scale coastal flood risk assessment for present and future climates. Nat. Hazards Earth Syst. Sci. 18, 2127–2142. doi.org/10.5194/nhess-18-2127-2018

Vousdoukas, M.I., Ferreira, Ó., Almeida, L.P., Pacheco, A., 2012. Toward reliable storm-hazard forecasts: XBeach calibration and its potential application in an operational early-warning system. Ocean Dynamics 62(7), 1001-1015. doi.org/10.1007/s10236-012-0544-6

Vousdoukas, M.I., Almeida, L.P., Ferreira, Ó., 2011. Modelling storm-induced beach morphological change in a meso-tidal, reflective beach using XBeach. J. Coast. Res., 64, 1916–1920.

Williams, J.J., Esteves, L.S., Rochford, L.A., 2015. Modelling storm responses on a high-energy coastline with XBeach. Model. Earth Syst. Environ. 1:3. doi.org/10.1007/s40808-015-0003-8

Winter, B., Schneeberger, K., Huttenlau, M., Stötter, J., 2018. Sources of uncertainty in a probabilistic flood risk model. Nat. Hazards 91, 431–446. doi.org/10.1007/s11069-017-3135-5.

Wong, P.P. et al. 2014. Coastal systems and low-lying areas Climate. In: Field, C.B. et al (Eds), Change 2014: Impacts,Adaptation, and Vulnerability. Part A: Global and Sectoral Aspects. Contribution of Working Group II to the Fifth Assessment Report of the Intergovernmental Panel on Climate Change. Cambridge University Press, Cambridge, 361–409.

Wright, L.D., Short, A.D., 1984. Morphodynamic variability of surf zones and beaches: A synthesis. Mar. Geol., 56, 93–118, doi:10.1016/0025-3227(84)90008-2.

Yates, M.L., Guza, R.T. and O'reilly, W.C., 2009. Equilibrium shoreline response: Observations and modeling. Journal of Geophysical Research: Oceans, 114(C9). doi.org/10.1029/2009JC005359

Yates, M. L., Guza, R. T., O'Reilly, W. C., Hansen, J. E., Barnard, P. L., 2011. Equilibrium shoreline response of a high wave energy beach. J. Geophys. Res. 116, C04014, doi:10.1029/2010JC006681

Zanuttigh, B., Simcic, D., Bagli, S., Bozzeda, F., Pietrantoni, L., Zagonari, F., Hoggart, S., Nicholls, R. J., 2014. THESEUS decision support system for coastal risk management, Coast. Eng., 87, 218–239, doi:10.1016/j.coastaleng.2013.11.013.

Zhang, K., Douglas, B.C., Leatherman, S.P., 2000. Twentieth-Century Storm Activity along the U.S. East Coast. Journal of Climate 13, 1748-1761.

Research activity

Publications in international journals

Jiménez, J.A., **Sanuy, M.**, Ballesteros, C., Valdemoro, H.I., 2018. The Tordera Delta, a hotspot to storm impacts in the coast northwards of Barcelona (NW Mediterranean). Coast. Eng. 134, 148–158. doi.org/10.1016/j.coastaleng.2017.08.012

Sanuy, M., Duo, E., Jäger, W.S., Ciavola, P., Jiménez, J.A., 2018. Linking source with consequences of coastal storm impacts for climate change and risk reduction scenarios for Mediterranean sandy beaches. Nat. Hazards Earth Syst. Sci. 18, 1825–1847. doi.org/10.5194/nhess-18-1825-2018

Sanuy, M., Jiménez, J.A., 2019. Sensitivity of Storm-Induced Hazards in a Highly Curvilinear Coastline to Changing Storm Directions. The Tordera Delta Case (NW Mediterranean). Water, 11, 747. doi.org/10.3390/w11040747

Sanuy M., Jiménez J.A., Ortego MI, Toimil A., 2019. Differences in assigning probabilities to coastal inundation hazard estimators: Event versus response approaches. J Flood Risk Management, e12557. doi.org/10.1111/jfr3.12557

Currently under review

Sanuy, M., Jiménez J.A., Plant N., (n.d.). A Bayesian Network model for coastal hazard assessments on a regional scale: the BN-CRAF. Coastal Engineering, in review

Duo, E.., **Sanuy, M.**, Jiménez J.A., Ciavola, P., (n.d.). On the Ability of Symmetric Triangular Synthetic Storms to Represent Real Events for Coastal Hazard Modelling. Coastal Engineering, in review

Communications in conferences

Jiménez, J. A., Plana, A., **Sanuy, M.**, Ruiz, A., 2014. Morphodynamic impact of an extreme storm on a cuspate deltaic shoreline. In Proceedings of the 34th International Costal Engineering Conference (2014 ASCE), Seoul, Korea, 15–20 June (Oral by Jiménez, J.A.).

Sanuy, M., Ballesteros, C., Jiménez, J.A., 2017. Assessing coastal risk impacts at regional level - Application to the Maresme (Spain) coast. Risks and hazards in natural and urban environaments under múltiple stress factors, including climate change. Riederalp, Switzerland, 21-25 March 2017 (Oral).

Sanuy, M., Jiménez, J.A., 2017. Modelling the Catalan Coast. Risc-KIT End User Conference. Deltares, Delft, The Netherlands, 7-10 April 2017 (Oral).

Sanuy, M., Jiménez, J.A., 2017. A Bayesian Network based analysis of alternatives to manage storm-induced risks at the Catalan coast. SCARC 2017. IH-Cantabria, Santander, Spain, 3-6 October 2017 (Oral). **Communication awarded as best presentation in the conference, with free registration for SCARC 2019**

Sanuy, M., Jiménez, J.A., 2017. Understanding the response to extreme events in a deltaic curvilinear sensitive coast. XBeachX Conference. Deltares, Delft, The Netherlands, 1-3 November 2017 (Oral).

Duo, E., **Sanuy, M.,** 2017. Bayesian Network approach for climate change and DRR scenarios' testing – pilot cases from Italy and Spain. XBeachX Conference. Deltares, Delft, The Netherlands, 1-3 November 2017 (Oral).

Sanuy, M., Jiménez J.A., 2018. A Bayesian Network framework for coastal risk assessment. Dealing with multiple hazards, vulnerabilities and measures under varying scenarios. INQUIMUS 2018. Università Ca'Foscari, Venice, Italy, 3-5 December 2018 (Poster).

Sanuy, M., Jiménez J.A., Plant, N., 2018. A Bayesian Network framework for coastal risk assessment. Dealing with multiple hazards, vulnerabilities and measures under varying scenarios. EGU 2019. Vienna, Austria, 11-12 April 2018 (Oral).

Sanuy, M., Jiménez, J.A., 2018. A Bayesian Network framework for coastal risk assessment. Dealing with multiple hazards, vulnerabilities and measures under varying scenarios. XV Jornadas de Puertos y Costas. Málaga, Spain, 8-9 May 2018 (Oral).

Participation in national and international projects

Resilience-Increasing Strategies for Coasts – toolKIT (**RISC-KIT**). EU-FP7 International project (FP7-603458-RISC-KIT, 5.999.692 €). November 2013 – April 2017. Project Coordinator: Ap van Dongeren (Deltares). Project lider in Spain: Jose A. Jiménez (UPC). 50 investigators involved.

El Paisaje del Riesgo Costero en el litoral catalán La influencia del cambio climático (**PairisClima**). MINECO National Project (CGL2014-55387-R, 54.450,00 €). January 2015- April 2018. Project Coordinator: José A. Jiménez (UPC). 22 investigators involved.

Rutas de adaptación al Cambio Climático en la zona costera Mediterránea. Superando los límites de la adaptabilidad (**M-CostAdapt**). MINECO National Project (CTM2017-83655-C2-1-R, 133.100,00 €). January 2018- December 2020. Project Coordinators: José A. Jiménez (UPC) and Maria del Carmen Llasat (UB). 9 investigators involved.

Project reports

RISC-KIT, 2016a. Storm Impact Database for the Case Study Sites (in English), official URL: http://risckit.cloudapp.net/risckit/#/map (accessed: April 2016) [WWW Document]. URL http://risckit.cloudapp.net/risckit/#/map

RISC-KIT, 2016b. Resilience-Increasing Strategies for Coasts – Toolkit. Structure of the EWS/DSS, WP5, Task 5.4 (D5.3).

RISC-KIT, 2016c. Resilience-Increasing Strategies for Coasts – Toolkit. Testing proposed strategic DRR measures using historic and climate-change scenarios, WP5, Task 5.3 (D5.2).

RISC-KIT, 2014. Resilience-Increasing Strategies for Coasts – Toolkit. Synthesis of data collection consultations organized at local level, WP1, Task 1.2 (D1.2), 242pp

RISK-KIT, 2015. Resilience-Increasing Strategies for Coasts – Toolkit. Coastal Hazard Assessment Module, WP2, Task 2.1 (D2.1) 113pp

Project international meetings and workshops

RISC-KIT 2ND GENERAL ASSEMBLY MEETING. University of Cambridge. Cambridge, United Kingdom, 7-9 May 2014

RISC-KIT 1ST MODEL CONFIGURATION TRAINING INTERNAL WORKSHOP. Deltares. Delft, The Netherlands, 7-11 July 2014

RISC-KIT 2ND MODEL CONFIGURATION TRAINING INTERNAL WORKSHOP. Deltares. Delft, The Netherlands, 29 Sptember -3 October 2014

RISC-KIT 3RD GENERAL ASSEMBLY MEETING. Consorzio Ferrara Ricerche (CFR), Bologna, Italia, 4-7 November 2014.

RISC-KIT 3RD MODEL CONFIGURATION TRAINING INTERNAL WORKSHOP. IMDC. Antwerp, Belgium, 20-21 April 2015

RISC-KIT 4TH GENERAL ASSEMBLY MEETING. Ecologic Institute EU, Berlin, Germany, 16-19 June 2015.

RISC-KIT 5TH GENERAL ASSEMBLY MEETING. EurOcean, Brussels, Belgium, 13-16 October 2015.

RISC-KIT 6TH GENERAL ASSEMBLY MEETING. Universidade do Algarve (UALG), Faro, Portugal, 20-22 April 2016.

RISC-KIT 7TH GENERAL ASSEMBLY MEETING. Institute of Oceanology – Bulgarian Academy of Sciences (IO-BAS), Varna, Bulgaria, 28-30 September 2016.

RISC-KIT 8TH GENERAL ASSEMBLY MEETING Deltares. Delft, The Netherlands, 5-7 April 2017.

International internships

16-23 March 2017 (2 weeks): University of Ferrara (UNIFE) and Consorzio Futuro in Ricerca (CFR), Ferrara, Italy. Prof. Paolo Ciavola and Dr. Enrico Duo. Analysis and processing for the common work published as Sanuy et al. 2018 (NHESS).

5 May- 31 July 2017 (3 months): United States Geological Survey (USGS). Florida, United States. Dr. Nathaniel Plant. Learning and unsing Bayesian Networks as predictive models for coastal dynamics. Development of a shoreline evolution predictive BN. Adquisition of technical knowledge for the design of BN models in general.

25 August -7 September 2017 (2 weeks): University of Ferrara (UNIFE) and Consorzio Futuro in Ricerca (CFR), Ferrara, Italy. Prof. Paolo Ciavola and Dr. Enrico Duo. Writing phase of thework published as Sanuy et al. 2018 (NHESS), and conceptual design of the uncertainty analysis on hazard stimation by triangular design storms.

15 April – 26 June 2018 (2.5 months): University of Ferrara (UNIFE) and Consorzio Futuro in Ricerca (CFR), Ferrara, Italy. Prof. Paolo Ciavola and Dr. Enrico Duo. Development of the uncertainty analysis on hazard stimation by triangular design storms. Learning how the plan and perform field surveys to derive detailed topography by using drons and UAV technology. Learning field post-processing thorugh photogrammetry.

Obtained grants

2014. Ayudas para contratos predoctorales de Formación del Profesorado Universitario FPU2014. MINECO. 2015-2019 (4 years).

2017. Ayudas para Estancias Breves para contratos predoctorales de Formación del Profesorado Universitario EEBB-FPU. MINECO. 4 April – 31 July 2017 (3 months). 4.800€.

2018. Beca de estancia de doctorado programa Erasmus+ KA103. EU. 15 April – 26 June 2018 (2.5 months). 900€.